Novel mediators in phosphate homeostasis: noncoding RNAs and the microbiome

Hany Saber Khalaf Zinad

BVMS, MSc

Biosciences Institute

Faculty of Medical Sciences

Newcastle University

Thesis submitted for the degree of Doctor in Philosophy at Newcastle University

Abstract

Phosphate is an essential nutrient and its level in the blood is tightly regulated by well-studied hormonal and non-hormonal factors. The renal sodium phosphate cotransporter (SLC34A1) is essential to maintaining Pi homeostasis. Recently two novel factors have emerged that potentially modulate phosphate body levels; a non-coding SLC34A1-antisense transcript and the gut microbiome.

The first part of this study aimed to understand the coordination between *SLC34A1*-sense/antisense transcripts in the human renal epithelial cell lines HEK293 and HKC8. In both cell lines *SLC34A1*-sense/antisense RNAs are expressed at very low levels. Transcription of *SLC34A1* was stimulated using the epigenetic modifiers Zebularine (Zeb) and dexamethasone (Dex) and its coordinated expression was assessed by RT-qPCR. HKC8 cells treated with Zeb showed that *SLC34A1*-sense/antisense transcripts are positively correlated, i.e. concordantly upregulated. A similar expression pattern was recorded in HEK293 cells following Dex treatment. The expression changes were paralleled by a reduction in DNA methylation of the sense/antisense promoter regions. In addition a significant increase in histone acetylation (H3K27Ac) at the sense promoter and a decrease in H3K4Me3 at the antisense promoter were detected after 5 days of Dex treatment.

After establishing a system to induce *SLC34A1*-sense/antisense expression with the aid of Zeb and Dex, we sought to experimentally manipulate SLC34A1 locus expression by introducing polyadenylation signals using CRISPR/Cas9 to silence sense or antisense transcription, respectively. Sense- antisense expression was quantified by RT-qPCR using different primer sites up- and downstream of the insertion site. Unexpectedly, termination was incomplete and read-through transcripts were generated. Again, *SLC34A1*-sense/antisense transcripts were concordantly upregulated regardless of the orientation of the read-through transcript.

From a functional perspective, both strategies -hormonal induction and read-through transcription- led to an increase in SLC34A1 protein expression as determined by western blot and ^{32}Pi uptake experiments.

The second part of the thesis aimed to determine the impact of a high/low Pi diet on the human gut microbiome. The experimental strategy included a dietary intervention in two healthy groups of volunteers followed by stool sampling, DNA extraction and sequencing. Alpha and beta diversity examination indicated that both high and low Pi regimens resulted in only minor alterations in bacterial compositions. However, a focus on the relative abundance of bacterial phyla and species demonstrated a reduction in *Bacteroidetes* among probands with reduced Pi intake suggesting potential involvement of this bacterial species in Pi homeostasis.

To summarise, this PhD investigated two novel aspects in the field of microbiology of Pi homeostasis; noncoding RNAs and the microbiome. The concordant expression of *SLC34A1*-sense/antisense transcripts confirms the impact and biological importance of the antisense transcript on *SLC34A1*-sense expression, potentially affecting renal Pi reabsorption. On the other hand, consuming a high or low Pi diet may have an impact on the abundance of certain bacterial species, but only insignificant effects on the overall composition of the microbiome. A potential link between the affected bacterial groups and Pi homeostasis remains to be investigated in depth.

Acknowledgments

First and foremost, I would like to express my sincere gratitude to my supervisors, Dr Andreas Werner (Andi) and Dr Anjam Khan for their encouragement and commitment as my mentors throughout this work. Under various difficulties that were faced during my study, Andi has gone out of his way to help and guide me, and for that I am eternally grateful.

I would like to thank all the supportive staff in the Faculty of Medical Sciences; Dr Alison Tyson-Capper and Dr Tim Cheek, who have been there to dissolve any difficulties. As well, I cannot forget Louise Campbell and Stuart Davison for answering all my questions!

I would also like to thank all my colleagues and collaborators because their help made this thesis possible. A big thanks goes to Prof Carsten Wagner and Dr Nati Hernando (Zurich University, Switzerland), Dr Lindsay Hall and Shabhonam Caim (University of East Anglia, UK), Prof Jelena Mann and Dr Christopher Stewart (Newcastle University, UK), for providing samples, helping in analysing data, advising me, sharing views and letting me use their lab facilities whenever needed.

This project was funded by Higher Committee for Education Development in Iraq (HCED) and Baghdad University. The non-coding RNA, microbiome fields and I are thankful for your generosity.

My friends both in- and- outside of Newcastle: Angela Petrocchi, Benjamin Allison, Leon Müller, Verena Mather, Janis Meiβner, Gerhard Hütter, Olivia Paddeson and Monica Renn; I couldn’t have asked for better friends, thank you for the emotional support and listening to me and providing a sound of logic no matter how tired, grumpy or asocial my mood was.

My deepest thanks goes to my family; the soul of my beloved Dad (Saber), my beloved Mom (Majeeda), my brothers and sisters; Dr Yasser, Dr Dhafer, Omar, Dr Younis, Dr Huda and Asmaa; without your support, prayers and patience, I would not be where I am today. Words cannot describe how thankful I am to have such wonderful family…

Table of Contents

List of Figures

Chapter 1.

Chapter 2.

Chapter 3.

Chapter 4.

Chapter 5.

Chapter 6.

List of Tables

Chapter 1.

Chapter 2.

Chapter 3.

Chapter 6.

Abbreviations

ADP	Adenosine diphosphate
ATP	Adenosine triphosphate
Bp	Base pair
Ct	Cycle threshold
ChIP	Chromatin immunoprecipitation
DNA	Deoxyribonucleic acid
DNMTs	DNA methyl transferases
DsRNA	Double stranded RNA
Endo-siRNA	Endogenous small interfering RNA
ELISA	Enzyme linked immunosorbent assay
GI	Gastro intestinal tract
GAPDH	Glyceraldehyde 3-phosphate dehydrogenase
Hpf	Hours post fertilization
HDAC	Histone deacetylase
HDR	Homologues direct repair
HAT	Histone acetyl transferase
NaCl	Sodium chloride
NaOH	Sodium hydroxide
NAT	Natural antisense transcript
NcRNA	Non-coding RNA
Nt	Nucleotide
NGS	Next generation sequencing
NHEJ	Non-homologues end joining
PBS	Phosphate buffered saline
PCR	Polymerase chain reaction
RNA	Ribonucleic acid
RNAi	RNA interference
Pi	Inorganic phosphate
Puro	Puromycin
RT	Reverse transcription
SgRNA	Single guide RNA

SiRNA	Small interfering RNA
SSC	Saline sodium citrate
SsRNA	Single stranded ribonucleic acid
TI	Transcriptional interference
UTR	Untranslated region

Chapter 1: Literature review

Phosphorous is a pivotal element abundantly distributed in all cells and tissues of living organisms. In the human body phosphorus is present in two forms, organic and inorganic phosphate. Organic phosphate was found in combination with lipids, carbohydrates, proteins and accounts for two-thirds of total serum phosphate. Inorganic phosphate (Pi), which is routinely measured in clinical laboratories in blood and urine, is combined with calcium, magnesium or sodium ions (Sabbagh *et al.*, 2011).

1.1. Physiological functions of Pi

Pi plays a critical role in a wide range of biological structures and processes such as intracellular signalling, bioenergetics (ATP and ADP), metabolic regulation (glycolysis or oxidative phosphorylation), cell membrane structure and function (phospholipids) and nucleic acids (DNA and RNA). In adults, about 85 % of total body phosphate is deposited in the skeleton and teeth complexed with calcium in the form of hydroxyapatite crystals, $Ca_5(PO_4)_3(OH)$. Adequate mineralization of bone is essential in providing physical support (Amini *et al.*, 2012). In the plasma, urine, and extracellular fluid, Pi is found in the form of protein-bound structures and 10-15 % of circulating Pi is present in the form of monovalent (H_2PO_4-) or divalent anions (HPO_4^{2-}). Because of its pKa in the physiological range, Pi is considered as titrable buffer with an essential role in maintaining acid-base balance (McNamara and Worthley, 2001; Alizadeh Naderi and Reilly, 2010). The important physiological functions of Pi and its disposition to form precipitates with divalent cations (Ca^{2+}) require tight control of Pi homeostasis.

1.2. Pi homeostasis

The diet represents the sole source of Pi to the body. Studies showed that the recommended average daily intake of phosphate in adults ranges between 500 and 700 mg (Brown and Razzaque, 2015). Organic phosphate is available from animal and plant sources whereas free Pi is found either in food additives or released after hydrolysis by phosphatases of gastrointestinal tract bacteria which also compete with the host for Pi (Knöpfel *et al.*, 2017). Two main mechanisms have been established for Pi uptake in the digestive tract (Wagner *et al.*, 2014): first, the para cellular route, which is poorly characterised but is thought to be based on passive diffusion and accounts for most of the Pi uptake under normal conditions (Knopfel *et al.*, 2017). Second, the transcellular uptake via the sodium phosphate cotransporters (SLC34A2 and SLC20). SLC20 is reported to play a housekeeping role in fulfilling the cellular requirements for Pi (Forster *et al.*, 2013) whereas SLC34A2 plays an important role in whole body Pi absorption . The daily average rate of Pi absorption by the intestinal sodium-phosphate cotransporters (SLC34A2) in adult human is in the range of 10-12 mg/kg, yet the absorption ratio depends on physiological status, sex, race, and geographical factors (Quann *et al.*, 2015).

Individual age was also shown to have a most significant impact on intestinal Pi uptake ratio. For instance, the concentration of plasma Pi in newborn was found to be two-fold higher than in adults due to high Pi requirement during growth (newborn 4.5-9.0 mg Pi/dL, children 4.5-5.5 mg Pi/dL and adults 2.7-4.5 mg Pi/dL)(Fischbach and Dunning, 2009).

In adults, 20-30 % of body Pi contributes to biological processes intracellularly, in blood and interstitium (Pi pool in Figure 1.1). Only 60-70 % is stored in bones, and the remaining 20 % is excreted by the kidneys in a tightly controlled process. The renal sodium-phosphate cotransporters (SLC34A1 and SLC34A3) are considered the main regulators of Pi homeostasis (Figure 1.1) (Berndt and Kumar, 2009) (Segawa *et al.*, 2015).

Accordingly, several hormones known to balance Pi levels such as parathyroid hormones (PTH), vitamin D3, FGF23 and growth hormone as well as metabolic factors (blood Pi levels, pH) influence the expression level and activity of SLC34A cotransporters (Berndt and Kumar, 2009) (discussed in detail in 1.4).

Body Pi concentration is tightly controlled, both under- and over-supply have deleterious consequences predominantly on skeleton and the cardiovascular system (Ghezzi *et al.*, 2011). Bone deformities such as osteoporosis and rickets are related to hypophosphatemia (Pi in plasma is < 2.7 mg/dL). On the other hand, hyperphosphatemia results in renal complications such as kidney stones as well as to cardiovascular disease such as vascular calcification and atherosclerosis. Importantly, hyperphosphataemia is a major complication in patients with later stage chronic kidney disease (CKD) (Tonelli *et al.*, 2009; Tonelli, 2013). Furthermore, other pathological conditions that affect the kidney and bones induce a dysregulation of entire body Pi levels (Kendrick *et al.*, 2011; Lederer, 2014).

In order to obtain a comprehensive image of the mechanisms which maintain body Pi levels, it is essential to understand the regulatory factors that affect the absorption/excretion rate of Pi.

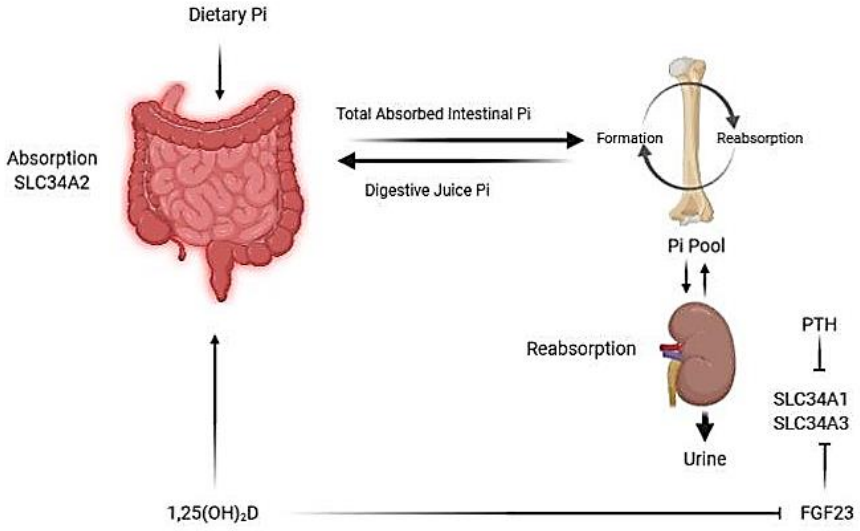

Figure 1. 1: Factors that contribute to Pi homeostasis. Pi is absorbed in the intestine via SLC34A2 and via paracellular paths. From the plasma Pi is transported into cells or stored in bones. Pi excretion occurs in the kidneys by controlled tubular reabsorption via SLC34A1 and SLC34A3. The main factors that regulate Pi levels in the body such as parathyroid hormone (PTH), Vitamin D3 (1,25(OH)2D) and FGF23 are indicated. Figure adopted from (Segawa *et al.*, 2015).

1.3. SLC34 family of sodium-dependent phosphate co-transporters

The solute transporter family SLC34A (or NaPi-II), is essential for maintaining Pi homeostasis in the body. The protein family consists of three members which are classified according to their phylogeny into SLC34A1, SLC34A2 and SLC34A3. SLC34A1 (NaPi-IIa) and SLC34A3 (NaPi-IIc) are both located in renal proximal tubular cells whereas SLC34A2 (NaPi-IIb) is mainly expressed in intestine and lung. The level of expression of these transporters is dependent on the body Pi demand and the dietary phosphate levels. Many studies using genetically modified mice have confirmed the physiological importance of Slc34a in maintaining Pi levels (Hediger *et al.*, 2004). To avoid confusion, SLC34A terminology will be used in the thesis.

1.4.1 Renal SLC34A1 and SLC34A3

Human *SLC34A1* was first cloned by functional expression of a human cDNA library in *Xenopus laevis* oocytes (Magagnin *et al.*, 1993; Capuano *et al.*, 2007). It is almost exclusively expressed at the brush border membrane (BBM) of the early convoluted proximal tubule, though immunohistochemistry studies have reported staining in the late proximal tubules (Custer *et al.*, 1994a; Levi *et al.*, 1994; Bergwitz *et al.*, 2006).

Human SLC34A1 is localised on chromosome 5q35.3, is 13 kb in length and composed of 13 exons and 12 introns. A shorter isoform contains 9 exons and 8 introns encompassing 6.1kb, though there is no evidence that this form displays any function. The SLC34A1 protein consists of 639 amino acids and, depending on the glycosylation status, the functional protein migrates between 75–90 kDa as determined by western blots experiments (Hartmann *et al.*, 1996; de la Horra *et al.*, 2001). SLC34A1 is electrogenic as manifested by voltage-dependent cotransporter activity with a 3:1 ratio of
Na^+: HPO_4^{2-}. On the other hand, transporter activity is highest at neutral pH and decreases significantly under acidic conditions (Fenollar-Ferrer *et al.*, 2015a).

Mice lacking Slc34a1 transporters suffered from hyperphosphaturia and increased levels of vitamin D_3 and Ca^+ in their serum. Moreover, experiments with mutant mice revealed that a mutation in Slc34a1 led to accumulation of the protein inside the cell with cytotoxic effects which contribute to the development of Fanconi syndrome (Magen *et al.*, 2010).

In contrast to SLC34A1, SLC34A3 is localized predominantly at the apical membrane of proximal tubules of deep nephrons. SLC34A3 is found on chromosome 9q34 with 5.8 kb in length and the gene contains 13 exons. The gene encodes a protein of 599 amino acids with an apparent molecular weight of 75 kDa (Bergwitz *et al.*, 2006).

Functional analysis of SLC34A3 using *Xenopus laevis* oocytes revealed electroneutral activity (2Na/1Pi stoichiometry) with optimal function at alkaline pH (pH 8.5) (Bergwitz *et al.*, 2006; Yamamoto *et al.*, 2007). Clinical studies linked mutations found in the SLC34A3 transporter gene in humans to the development of hypophosphatemic rickets with hypercalciuria (HRHH) (Lorenz-Depiereux *et al.*, 2006).

Conversely, in mice mutations of *Slc34a3* had no effect on plasma and urine Pi levels but elevated serum Ca^{+} and vitamin D_3 were recorded (Beck *et al.*, 1998; Jones *et al.*, 2001; Bergwitz *et al.*, 2006; Segawa *et al.*, 2009b; Dasgupta *et al.*, 2014). Studies by Myakala *et al.*, confirmed that knock-out (KO) of *Slc34a3* did not have a significant effect on the renal Pi reabsorption/excretion rate. Pi homeostasis appeared unaffected suggesting that Slc34a3 transporters are not essential for maintaining Pi balance in mice (Myakala *et al.*, 2014).

1.4.2 Intestinal Pi transporter: SLC34A2

SLC34A2 was first discovered as an expressed sequence tags (EST) clone from alveolar tissue (Hilfiker *et al.*, 1998b). The transporter is located in the brush border of enterocytes in the small intestine, at the apical membrane of mammary gland ducts, in hepatocytes, lung and testis (Lesser *et al.*, 2019). The chromosomal location of SLC34A2 is 4p15, the gene is 14.25 kb in length divided into 13 exons. The primary structure of SLC34A2 is slightly different from other family members as it has 690 amino acids and includes a cluster of cysteine residues at the C-terminus.

On western blots, the protein is detected between 77-108 kDa depending on the glycosylation status. SLC34A2 has electrogenic activity and transports 3 Na^{+} ions together with one HPO_4^{2-} ion. Transport is pH dependent and most active at acidic pH (Hilfiker *et al.*, 1998a).

Homozygous *Slc34a2*-KO mice show a high rate of embryonic lethality whereas milder mutations cause respiratory complications such as pulmonary alveolar microlithiasis (PAM) and testicular microlithiasis (TM) (Corut *et al.*, 2006; Huqun *et al.*, 2007).

In *Slc34a*-KO mice, an essential component of the regulatory system that controls Pi balance is removed. This affects blood parameters including hormones, metabolic factors and electrolytes related to Pi homeostasis. The major changes are listed below in table 1.1.

Table 1. 1: Physiological parameters of Slc34a transporter knock-out mice. Low plasma Pi levels with high rates in renal Pi excretion and bone deformities have been noticed mainly in *Slc34a1* (or in combination with *Slc34a3*) -KO mice.

Parameter	***Slc34a1*-KO mice (Beck *et al.*, 1998)**	***Slc34a2*-KO mice (Sabbagh *et al.*, 2011)**	***Slc34a3*-KO mice (Segawa *et al.*, 2009b)**	***Slc34a1/Slc34a3* double KO mice (Segawa *et al.*, 2009a)**
Plasma Pi	Low	Low/normal	Normal	Low
Pi excretion	High	Low	Normal	High
Vitamin D3	High	High/normal	High	High
FGF23	Low	Low/normal	Low	Low
Linked disordered	Skeletal abnormalities	Pulmonary alveolar microlithiasis	---	Osteoporosis and rickets

All Slc34a isoforms have comparable primary amino acid sequence. This suggest a common protein structure, however no crystal structure of a Slc34a transporter has yet been solved. Instead, a homology 3D model has been proposed based on a related crystal structure of VcINDY a bacterial Na^+ dependent dicarboxylate transporter, as presented in figure 1.2.

Further conformation analysis has been performed on the suggested model by mutating predicted key residues with functional consequences (Fenollar-Ferrer *et al.*, 2014a; Fenollar-Ferrer *et al.*, 2015b; Patti *et al.*, 2016).

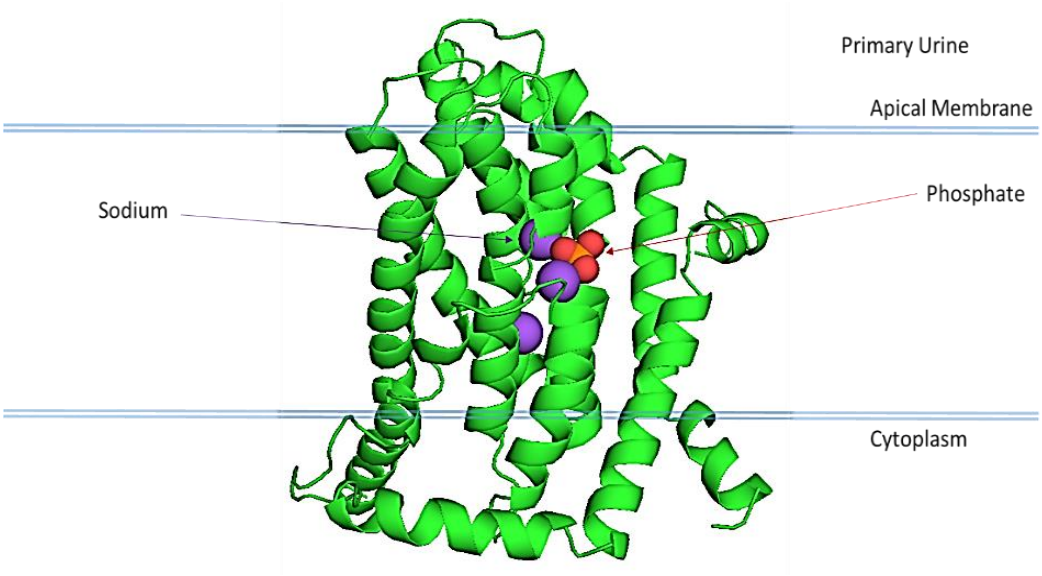

Figure 1. 2: Proposed model of the human SLC34A isoform based on the VcINDY crystal structure. The purple spheres represent Na^+ ions, the yellow/red spheres represent Pi. Adopted from (Fenollar-Ferrer *et al.*, 2014b).

1.4. Regulators of Pi homeostasis

Many factors have been identified that help to maintain Pi levels in the body. These factors have been studied extensively and their physiological importance in regulating Pi levels are well documented (Prasad and Bhadauria, 2013). The main factors include parathyroid hormone (PTH), vitamin D_3 ($vitD_3$) and fibroblast growth factor (FGF-23), which will be described in detail below.

1.4.1. Parathyroid hormone (PTH)

PTH or parathyrin is synthesised by chief cells in the parathyroid gland and plays an important role in controlling blood Ca^{2+}, Pi and $vitD_3$. PTH is released into the blood after the stimulation of calcium-sensing receptors (CaSR) in the parathyroid gland in response to hypocalcemia, decreased serum $vitD_3$ and/or hyperphosphatemia. PTH exhibits its main effects on bones and kidneys- and to a lesser extent on intestine- as shown in figure 1.3.A (Kumar and Thompson, 2011).

In bones, PTH contributes to bone remodelling and osteoclast proliferation and, importantly, enhances bone resorption and the release of Ca^{2+} and Pi from osteoclasts (Talmage and Mobley, 2008). Whereas in kidney, PTH controls the reabsorption/excretion threshold of calcium and phosphate in opposite manner to keep the solubility product of Ca^{2+} and Pi low.

While it upregulates Ca^{2+} reuptake, PTH decreases renal Pi reabsorption by inducing the retrieval of the Pi cotransporter SLC34A1 from the apical membrane (Figure 1.3.B) (Kempson *et al.*, 1995; Picard *et al.*, 2010). The inhibition of renal cotransporter activity was linked to both protein kinase C (PKC) and protein kinase A (PKA) mediated phosphorylation (Bacic *et al.*, 2006).

Direct phosphorylation of SLC34A1 has not been demonstrated, the sodium-hydrogen exchanger regulatory factor (NHRF-1) which also binds to SLC34A1 is a likely target instead. This leads to the internalization of the Pi transporter and its degradation in lysosomes (Pfister *et al.*, 1998). Furthermore, PTH has a stimulatory effect on $vitD_3$ hydroxylation in the proximal renal tubule (as described below). Consequently, PTH indirectly induces the expression of the intestinal Pi transporter (*SLC34A2*) via the elevation of plasma $vitD_3$ levels (Figure 1.3.B).

Pathological disorders that cause an excess secretion of PTH from the parathyroid gland severely influence Ca^{2+} and Pi metabolism. The bones and kidney are mainly affected, in addition, debilitating complications including cardiovascular disease are observed. Likewise, patients with secondary hyperparathyroidism (SHPT) often exhibit signs of reduced kidney function manifested by hyperphosphaturia, hypophosphatemia, high plasma Ca^{2+} and low $vitD_3$ levels (Tomasello, 2008).

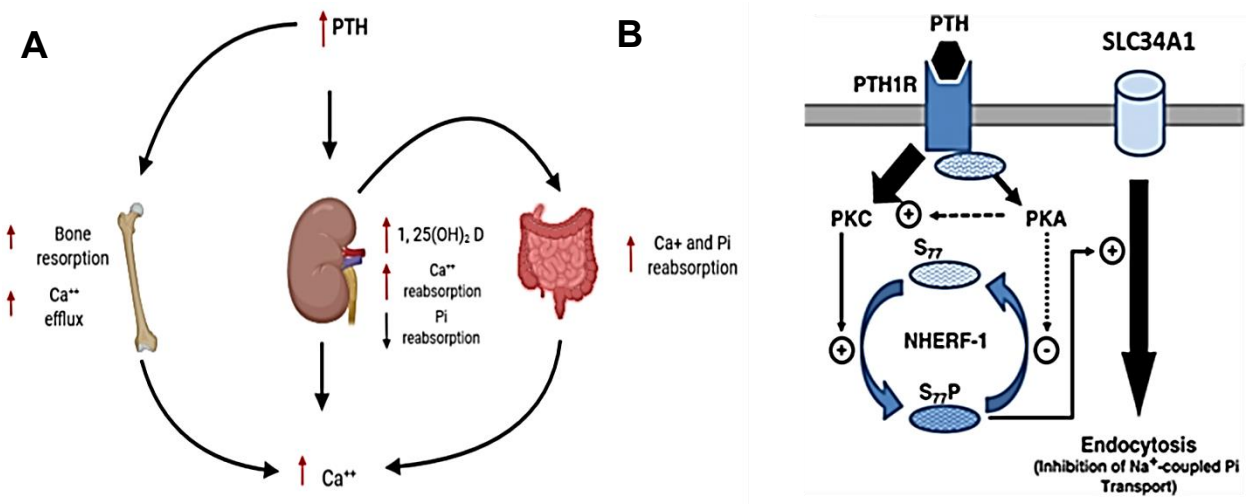

Figure 1. 3: The physiological role of PTH on the different organs in the body. A) PTH targets bone, kidneys and indirectly intestine. In bone, PTH induces bone resorption which increases Ca^{2+} and Pi in the plasma whereas in kidney PTH induces Pi excretion and Ca^{2+} retention. The action of PTH in intestine is indirect via vitamin D3. B) Proposed inhibitory mechanism of PTH on SLC34A1 transporter in renal cells. PTH binds to its receptor (PTH1-R) and triggers NHERF-1 phosphorylation by PKC and PKA which leads to the endocytosis of SLC34A1, figures adopted from (Hinson A.M.; Jacquillet and Unwin, 2019).

1.4.2. Vitamin D3 (vitD3)

Vitamin D_3 is an essential Pi regulator. Organs that contribute to maintaining Pi homeostasis such as kidneys and bones are also involved in vitD_3 synthesis. The synthesis process starts in skin where 7-dehydrocholestol (ergosterol) is transformed into cholecalciferol in the presence of UV-light. Cholecalciferol is then hydroxylated in the liver by CYP2R1 which converts cholecalciferol into 25-hydroxycholecalciferol 25(OH)vitD. The active form of vitD_3 is produced in proximal renal tubular cells which convert 25-dihydroxycholecalciferol to 1,25-dihydroxycholecalciferol 1,25$(OH)_2$D by the 1α-hydroxylase (CYP27B1).

In vivo and *in vitro* investigations showed that vitD$_3$ induces an upregulation of the intestinal sodium phosphate cotransporter, reduces FGF-23 and PTH secretion (Figure 1.4).

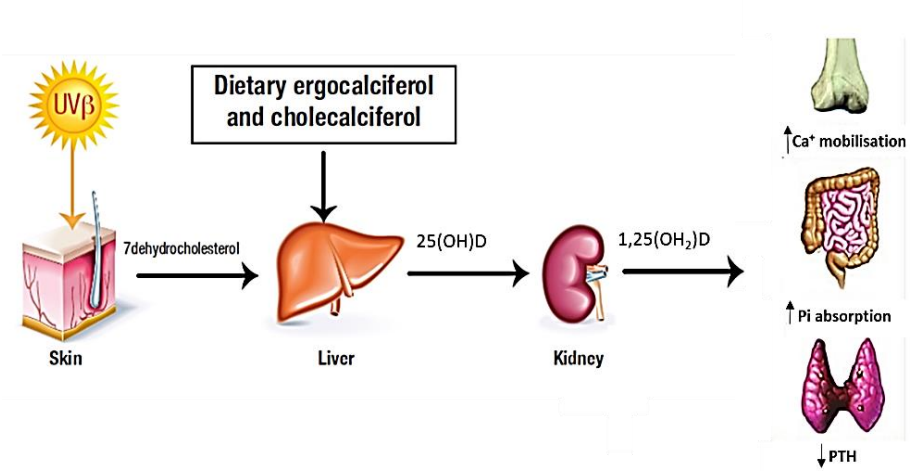

Figure 1. 4: Synthesis of vitamin D3 and target organs. Following sun exposure and dietary intake of ergocalciferol and cholecalciferol synthesis in liver, the active form of vitD3; 1,25(OH)$_2$D is produced in renal proximal tubules. 1,25(OH)$_2$D induces bone resorption and the release of Ca^{2+} and FGF-23. In the intestine, vitD3 increases Pi uptake by the intestinal SLC34A2 transporter. Moreover, 1,25(OH)$_2$D causes a decrease in PTH secretion by parathyroid glands. The figure is adapted from (Raubenheimer and Noffke, 2011; Boudal and Attar, 2012).

KO-mice lacking the vitD3 receptor (VDR) suffer from low intestinal Pi uptake (because of *Slc34A2* downregulation), hypophosphatemia and shorter life span (Kato *et al.*, 1999). Another report found VDR knock out caused upregulation of the renal Pi cotransporters (*Slc34a1* and *Slc34a3*) to compensate the Pi wasting (Marks *et al.*, 2010). Conversely, vitD$_3$ injection in healthy mice caused an upregulation of *Slc34a2* expression, which was attributed to transcriptional stimulation of *Slc34a2* by vitD$_3$ (Hattenhauer *et al.*, 1999).

1.4.3. Fibroblast growth factor (FGF-23)

The FGF protein family plays an important role in various biological processes during embryonic development, wound repair and tissues regeneration (Yamashita *et al.*,

2000; Yoshiko *et al.*, 2007). FGF-23 is the latest member in the family and is characterised by an endocrine-like function. FGF-23 is triggered in response to high levels of plasma Pi, PTH, and vitD_3 (Itoh and Ornitz, 2011). FGF-23 is expressed mainly in osteoblasts and osteoclasts, in addition to other organs such as heart, parathyroid gland, small intestine and thymus. In kidney, FGF-23 binds predominantly to cell-surface receptors-1 (FGF-23 receptor-1, FGFR1).

Activation of FGFR1 by FGF-23 results in the formation of a tertiary complex in the presence of α-Klotho enzyme causing a reduction of SLC34A1 and SLC34A3 cotransporters in the membrane (Ruta *et al.*, 1989; Powers *et al.*, 2000; Ranch *et al.*, 2011; Martin *et al.*, 2012). Moreover, FGF-23 plays an important feedback role in 25-hydroxycholecalciferol to 1, 25-dihydroxycholecalciferol hydroxylation by inhibiting 1α-hydroxylase (CYP27B1) via the ERK1/2 pathway (extracellular signal-regulated protein kinases 1 and 2) (Perwad *et al.*, 2007). FGF-23 was also reported to decrease SLC34A2 transporter abundance in intestine as a result of reduced vitD_3 synthesis (Figure 1.5) (Miyamoto *et al.*, 2005).

In addition to the PTH, vitD3 and FGF-23 a number of other factors affect both renal and intestinal sodium/phosphate cotransporters (i.e. *SLC3434A1*/*SLC34A3* and *SLC34A2*), listed in table 1.2.

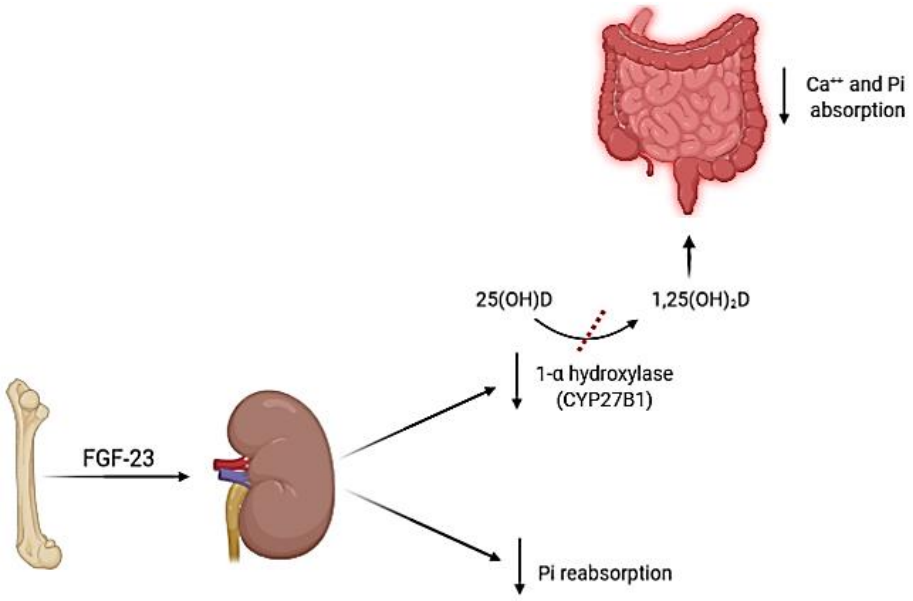

Figure 1. 5: Regulatory role of FGF-23 in Pi homeostasis. FGF-23 is secreted mainly by bone cells and decreases renal Pi reabsorption via *SLC34A1* and *SLC34A3*. Intestinal absorption of Pi by SLC34A2 is also decreased due to the inhibitory effect of FGF-23 on 1α-hydroxylase reducing vitD3 synthesis. Figure adopted from (Beck-Nielsen, 2012).

Despite the many established hormones and metabolites that affect Pi balance, novel mediators have recently emerged that potentially influence *SLC34A* expression, for example Natural Antisense Transcripts (NATs) or the microbiome. These factors are not well-established and will be discussed in more details later in this chapter and throughout the thesis.

Table 1. 2: Regulators of Pi homeostasis. Hormonal and non-hormonal factors that influence body Pi balance. Most of these factors affect the expression of *SLC34A* cotransporters in the renal and intestinal epithelium (Knöpfel, 2016). Red arrows refer to an increase and black arrows to a decrease in transporter expression.

Regulator (s)	Cotransporter	Mechanism of action
Dietary Pi	↓↑ *SLC34A1, A2 and A3*	The expression of *SLC34A2* decreases significantly in response to high Pi diet. In contrast, with low Pi diet, all *SLC34A* transporters are increased (Wen *et al.*, 1978).
Growth hormone (Insulin growth factor-1, IGF-1)	↑ *SLC34A1/A3*	IGF-1 is produced in kidney and has a stimulatory effect on the transporter activity by activating phospholipase C (Hammerman *et al.*, 1980; Rogers and Hammerman, 1989; Caverzasio *et al.*, 1990).
Glucocorticoids	↓↑ *SLC34A1/A3*	The effect of steroids depends on dose, time and experimental conditions. Diverse effects on transporter activity and protein abundance including *SLC34A1/A3* have been reported (Noronha-Blob and Sacktor, 1986; Ambühl *et al.*, 1998). The potential molecular mechanism of action will be discussed extensively elsewhere in this thesis.
Thyroid hormone	↑ *SLC34A1*	Rats administrated parenterally with T4 showed a significant increase in BBM *SLC34A1* (Beers and Dousa, 1993).
Calcitonin	↓ *SLC34A1/A3*	Calcitonin increases cytoplasmic levels of Ca^{2+} in renal BBM vesicles and inhibits Pi reabsorption (Berndt and Knox, 1984).
Glucagon	↓ *SLC34A1/A3*	Glucagon induces phosphaturia (Ahloulay *et al.*, 1996).
Phosphatonins	↓ *SLC34A1/A3*	The best-studied Phosphatonins such as sFRP-4 reduce vitD3 by inhibition of 1-α-hydroxylase (Masi, 2011).
Prostaglandins	↑ *SLC34A1, A2 and A3*	PGE2 produced in the kidney act to antagonise PTH action (Dominguez *et al.*, 1984).
Blood calcium	↓ *SLC34A1, A2 and A3*	In vivo studies showed that high blood Ca^{2+} levels result in a decrease in SLC34A1/A3 activity in renal BBM (Rouse and Suki, 1985; Caverzasio and Bonjour, 1988).
Insulin	↑ *SLC34A1, A2 and A3*	Insulin induces renal Pi reabsorption and antagonises PTH action (Hammerman and Rogers, 1987).

Gene expression is a tightly controlled process that involves a wide range of factors at both transcriptional and/or post-transcriptional levels. The process starts with a reduction in chromatin compaction, unwinding of the DNA helix, recruiting of transcriptional factors and RNA polymerases at specific regulatory sites such as enhancer and promoter sequences.

In eukaryotes, a generic promoter sequence consisted of two parts (i) the TATA box located at 25-30 nucleotides upstream of the transcription start site (TSS) and (ii) the CAAT box which located at 60-100 nucleotides upstream of the TSS and contains the consensus sequence 5'-GGCCAATCT-3'. Alternatively, CpG islands act as frequent promoters, generally associated with housekeeping and developmentally regulated genes (Deaton and Bird, 2011).

On the other hand enhancers promote transcription from distant sites often several kilobases up- or downstream of the TSS. The distant regulation is achieved when a protein or a complex of proteins simultaneously binds to enhancer elements and proximal regulatory elements forming DNA loops. Once transcription factors bind to enhancer and promoter sequences, the transcription machinery is assembled, RNA pol II is recruited and the transcription process begins in 5' to 3' direction (Schoenfelder and Fraser, 2019).

RNA Pol II slows down over the termination sequence at the 3' end of the gene due to recruitment of cleavage and polyadenylation specificity factors (CPSF) that recognise the AAUAAA motif at nascent transcripts. A further reduction in Pol II speed is observed when nascent transcripts invade the DNA duplex resulting in R loop structures. Eventhough CPSF promote the detachment of mRNA from chromatin, Pol II continues to transcribe the DNA template. The resulting transcripts are short-lived due to the activity of the exonuclease Xrn2 that degrades the transcript from its 5′ end and eventually displaces Pol II from the DNA (torpedo mechanism) (Platt, 1986; Proudfoot, 2016).

Transcription termination is a critical step, read-through or incomplete termination have been reported particularly in cells exposed to stress factors such as osmotic- or heat shock, viral infection or cancer-inducing mutations (Nielsen *et al.*, 2013).

1.5. Non-coding RNA (ncRNA)

The Human Genome Project revealed that approximately 2 % of the entire human genome are transcribed into mRNA and translated into proteins (Djebali *et al.*, 2012b). The vast majority of the transcriptional output is non-coding and was often considered as transcriptional noise and referred to as “dark matter’’ of the genome (Kiyosawa *et al.*, 2003).

The various ncRNAs make up a heterogeneous group of RNAs and many share common characteristics with mRNAs such as transcription by RNA polymerase II, the splicing process, polyA tailing and the cap-structure. However, unlike mRNAs, ncRNAs lacks of long protein coding potential, nonetheless experimental studies have shown that many of these transcripts are biologically active. Various approaches have been used to identify ncRNAs including large-scale sequencing (Mercer and Mattick, 2013), hybridization techniques and bioinformatic analyses (Wang *et al.*, 2005). These techniques resulted in identification of a wide range of noncoding transcripts with different characteristics.

Based on experimental considerations an initial classification of ‘long’ and ‘short’ noncoding RNAs was introduced. A length of 200 nucleotides was considered as cut off between short and long noncoding transcripts (the latter bind to the column matrix whereas the former remain in the flow through in column-based RNA purification kits).

The short RNA group includes; miRNA (microRNA) snoRNA (small nucleolar RNA), snRNA (small nuclear RNA), piRNA (Piwi-interacting RNA), endogenous siRNA (endo-siRNA) and tRNA (transfer RNA), though these short RNAs are not the focus of this thesis. The long noncoding RNA family includes; NATs (natural antisense transcripts), eRNA (enhancer ncRNA), intergenic ncRNA (lincRNA) and pseudogene gene derived ncRNA, as listed in table 1.3 (Kowalczyk *et al.*, 2012a).

Some studies focusing on lncRNAs have classified noncoding transcripts according to their genomic localisation, related to the closest neighbouring protein coding gene. For instance, a lncRNA which is localised in an intergenic region is known as intervening lncRNA or lincRNA. In contrast, those lncRNA which are exonic, intronic

or fully overlapping with a protein coding gene are referred to as genic ncRNA (Derrien *et al.*, 2012; Aprea and Calegari, 2015).

Table 1. 3: Classification of ncRNA and their biological roles in mammals. The transcript length is referred to in nucleotides (nt). The approximate number of transcripts in the human genome is also given as well as a summary of features and functions.

ncRNA	number of genes	Features and function
Short RNAs (<200 nt)		
miRNA	>2500	- 21–23 nt, - transcribed by polymerase II & III, - bind to 3' untranslated region of mRNAs regulating >15000 genes (Chou *et al.*, 2018; Kozomara *et al.*, 2019)
snoRNA	>1,500	- 60–300 nt, - involved in modification, maturation and stabilisation of ribosomal RNAs (Jorjani *et al.*, 2016; Bouchard-Bourelle *et al.*, 2019).
snRNA	>1,900	- about 150 nt, - contribute to processing of pre-mRNA in the nucleus (Becker *et al.*, 2019).
piRNA	>90	- 25–33 nt, - repress retrotransposition of repeat elements (Liu *et al.*, 2019).
tRNA	>500	- 73–93 nt, - transfer of amino acids, involved in translation of mRNA into protein (Torres *et al.*, 2019).
Long noncoding RNAs (>200 nt)		
NATs	>5,500	- variable transcript length, - mostly unknown function, but some are involved in gene regulation through transcriptional or post-transcriptional interference (Barman *et al.*, 2019).
eRNA	>2,000	- variable transcript length, - hallmark of active enhancers, - some eRNA interfer with target gene transcription (Ding *et al.*, 2018)
lincRNA	>6,500	- variable transcript length, - some are involved in gene regulation (Ransohoff *et al.*, 2018)
Pseudogene lncRNA	>700	- mostly unknown function, but some may act as miRNA sponges (Kowalczyk *et al.*, 2012b; Ji *et al.*, 2015).

In-depth computational annotation revealed that coding and noncoding transcripts are often clustered in the same genomic loci but are transcribed in opposite orientations. Approximately 20 % of mammalian lncRNA were found to be transcribed in the opposite direction from protein coding genes (i.e. divergent) (Luo *et al.*, 2016) whereas the majority shows convergent transcription generating complementary transcripts (Figure 1.6).

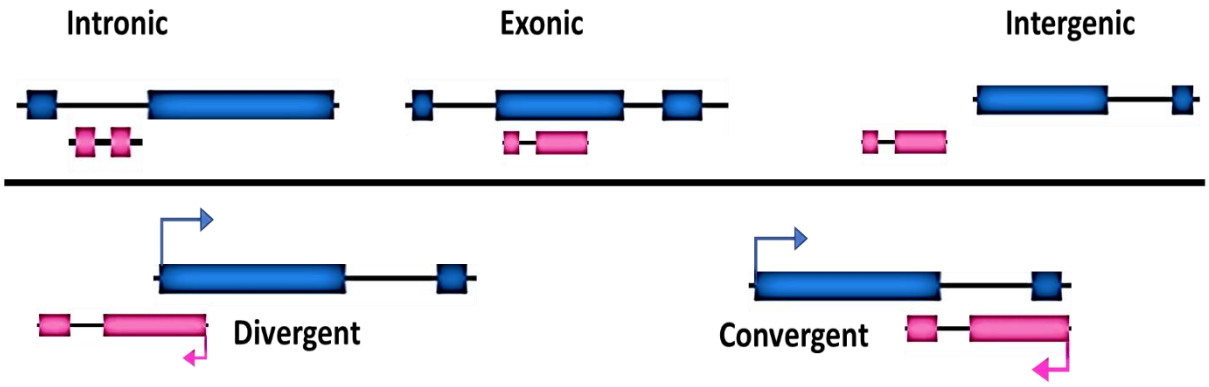

Figure 1. 6: Proposed arrangement of lncRNAs in the human genome. Depending on the intersection with protein-coding genes, there are intergenic and genic lncRNAs which include exonic, intronic and overlapping patterns (upper panel). Another classification of lncRNA is based on the transcription orientation in relation to the protein coding gene (lower panel). The latter classification includes convergent and divergent pattern of transcription.

1.5.1. Natural antisense transcripts (NATs)

Among the large family of non-coding RNAs, NATs are a particularly interesting, well-defined group of transcripts. NATs were first detected in 1982 in prokaryotes and later the scale of antisense transcription became apparent through large scale sequencing (cDNAs and ESTs) and especially from the FANTOM project to sequence all mouse transcripts (Kiyosawa *et al.*, 2003).

In 2004, Chen *et al.,* suggested that approximately 20 % of protein coding genes in humans form duplexes between sense and antisense transcripts (Chen *et al.*, 2004). Thereafter, the advances in nucleic acid sequencing technology and systematic, large-scale cDNA analysis (FANTOM3 project) revealed that sense/antisense co-

expression is widespread. Moreover, in many cases the experimental perturbation of one transcript was shown to alter the expression of the partner transcript (Katayama *et al.*, 2005a; Wight and Werner, 2013).

NATs have been identified in all eukaryotes including human, mouse and yeast. They are defined as capped, mostly polyadenylated RNAs transcribed in the opposite direction to protein coding genes and often partly complementary to sense protein coding transcripts.

The majority of NATs are expressed at low levels and show high tissue specificity and co-expression with their related sense transcripts. The examined NATs either repress or promote the expression of the cognate sense transcripts in a concordant" pattern (expression of sense/antisense transcripts both increased or decreased), or in discordant pattern (expression of sense reduces antisense expression, and vice versa) (Wang *et al.*, 2014; Balbin *et al.*, 2015).

NATs are sub-classified into two major categories according to their origin and mode of action (Lavorgna *et al.*, 2004; Li *et al.*, 2006): cis-NATs are transcribed from the opposite strand of protein coding genes and display perfect (partial) complementarity to their sense RNA strand. The resulting sense/antisense transcripts appear in three different configurations: head-to-head (5' overlap), fully overlapping and tail-to-tail (3' overlap) (Figure 1.7).

Cis-NATs constitute the vast majority of lncRNA antisense transcripts. For instance, Zhoe *et al.,* investigated the role of NATs transcripts during muscle development for two different breeds of pigs. The transcriptome analysis showed that 80 % (i.e. about 1200 out of 1400 transcripts) of the detected NATs were transcribed in *cis* and concordantly co-expressed with their sense transcripts (Zhao *et al.*, 2016).

The second group of NATs known as trans-NATs, are transcribed from a separate genomic locus as their potential target and have only partial complementarity to the sense transcripts (Kiss, 2002). Most of the identified trans-NATs show imperfect base-pairing with the target RNA molecules (Brennecke and Cohen, 2003). In general, trans-acting transcripts are less abundant than *cis* antisense transcripts. It was suggested that trans-NATs could form complex networks targeting different

sense transcripts at the same time due to the lack of perfect complementarity between sense RNA and trans-NATs (Li *et al.*, 2006). However, more recently this hypothesis was disputed, instead these pseudogene-derived transcripts appear to act as competitors (sponges) for microRNAs rather than as antisense lncRNAs.

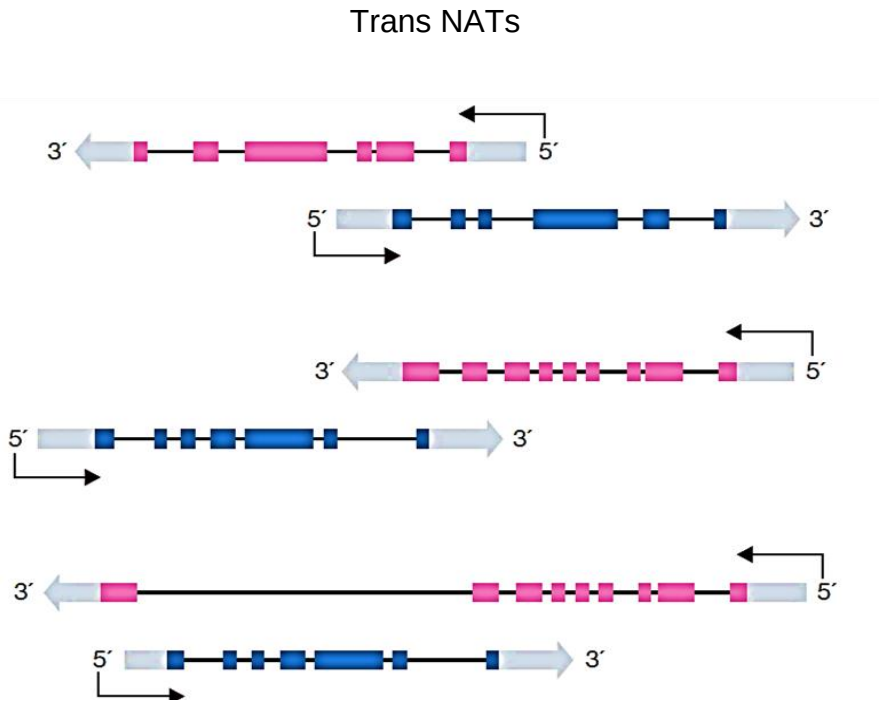

Figure 1. 7: Genomic configurations of Trans NATs. Sense and cis-natural antisense transcripts in head-to-head configuration (top), tail-to-tail (middle) and overlapping (bottom).

1.5.2. NATs mode of function

There are a number of hypothesised mechanisms that explain how NATs can regulate gene expression. It is generally assumed that NATs interfere with the expression of the sense transcripts and consequently induce a phenotypic change. This view has been confirmed by overexpression or knockout experiments of NATs (i.e. loss-of or gain-of function experiments) (Kiyosawa *et al.*, 2003).

Well-studied examples of functional NATs include transcripts from parentally imprinted genes where the antisense RNAs induce the silencing of the sense

transcripts (Airn, Kcnq1ot1 and Tsix) (Brown *et al.*, 1991; Penny *et al.*, 1996; Sleutels *et al.*, 2002). Expression of these NATs leads to chromatin modifications and transcriptional gene silencing of the related sense genes (Jeon and Lee, 2011).

Although the mechanism of action of many NATs remains to be established, three plausible sense/antisense interaction pathways have been suggested as below (Faghihi and Wahlestedt, 2009; Werner, 2013; Wight and Werner, 2013);

1.5.3. Transcription- related modulation (or transcriptional interference)

In convergent transcription, the polymerase complexes on both sense and antisense strands move towards each-other and eventually stall or collide. This mechanism was suggested to account for a large number of discordantly regulated sense-antisense transcript pairs (Katayama *et al.*, 2005a). This hypothesis has been studied in detail in *Escherichia coli* and yeast, *Saccharomyces cerevisiae,* by using promoters that send polymerase complexes on collision course and atomic force microscopy (Prescott and Proudfoot, 2002; Crampton *et al.*, 2006).

In *E. coli* the transcription of oppositely oriented RNA polymerases (RNAP) resulted in collision and stalling of the transcriptional machinery while one or both RNAP remained attached to the DNA template after the collision. In *S. cerevisiae*, the GAL10 and GAL7 genes for example are arranged in convergent orientation and the model has been extensively studied. Transcription of both genes was initiated efficiently, however transcript elongation became limited once the polymerase approached each other, suggesting that the polymerases stall or collide and thus the level of both transcripts is reduced (Prescott and Proudfoot, 2002). It’s worthwhile to mention that transcriptional collision has been engineered in mammalian cell lines, however, this mechanism appears unlikely to be of relevance in higher eukaryotes (Osato *et al.*, 2007).

1.5.4. Double stranded RNA formation (RNA- RNA interactions)

The sense mRNA expression can also be modulated by antisense transcripts as a result of sense–antisense RNA duplex formation. Such duplexes were detected in

cytoplasm and nucleus and are assumed to occur directly after transcription. For example, a number of cellular stress factors such as hydrogen peroxide, serum starvation and reduction in oxygen supply induce nuclear duplex retention particularly for antisense transcripts, which is accompanied by changing levels of the cognate sense transcripts in human HEK293-SW cells (Faghihi *et al.*, 2008b).

Likewise, the duplex between sense mRNA and antisense transcript in the cytoplasm was found to affect mRNA stability by protecting it from degradation. Bolland *et al.,* showed that the β-site amyloid precursor protein-cleaving enzyme 1 (*BACE1*) mRNA was stabilised by the antisense transcript *BACE1-AS*. The latter transcripts mask a miRNA binding site on the sense transcript thus increasing its stability. Additionally, the *HIF1a*-antisense transcript blocks adenylate-uridylate-rich elements (AU-elements) at 3'-UTR end of the sense transcript, suggesting that antisense transcript protects the target mRNA transcript from degradation (Rossignol *et al.*, 2004).

Because dsRNA mimics a viral infection and poses a potential threat to cells, hybridisation between NATs and cognate sense transcripts stimulates enzymes which resolve/edit dsRNA. For example, members of the adenosine deaminase acting on RNAs enzyme family (ADARs) were found to be activated by dsRNA duplex formation. ADARs alter the nucleotide sequence by converting adenosine to inosine and thus 'melt' the dsRNA duplex. Widespread editing from A-to-I can be found in transcripts from repetitive genome sequences (Athanasiadis *et al.*, 2004) or at specific sites in some neurotransmitter receptors (Sapiro *et al.*, 2019).

Other studies found that cytoplasmic dsRNA from endogenous (mitochondrial and repetitive genes) as well as external sources (dsRNA viruses) triggers an innate immune response mediated by protein kinase-R (PKR). PKR recognises its target with two dsRNA binding domains which activates the kinase and triggers translational inhibition and an IFN-mediated innate immune response (Marchal *et al.*, 2014).

1.5.5. NATs regulate chromatin status

Some NATs are thought to work independently of the sense transcripts. A well characterised example is *HOTAIR*, a noncoding RNA originating from the HOXC locus on human chromosome 12. The 5'-UTR of *HOTAIR* acts as scaffold for polycomb repressive complex 2 (PRC2) which in turn enhances histone lysine 27 trimethylation (H3K27me3) over the entire HOX locus and induces transcriptional silencing. In contrast, the 3'end of *HOTAIR* is reported to enhance lysine-specific histone demethylase 1A (*LSD1*) with a positive effect on sense and antisense transcription.

Other cis-antisense transcripts work as platforms for histone/chromatin modifying enzymes which affect the cognate sense genes as well as up-and down-stream neighbouring genes (Bernstein and Allis, 2005). This mode of action has been proposed in different imprinted autosomal loci were genes are expressed monoallelically from either the paternal or maternal chromosome. For example the expression of the lncRNA, *Arin,* plays an important role in inducing transcriptional silencing of *Igf2r* by inducing promoter methylation and histone H3K9 methylation (Andergassen *et al.*, 2019). Whereas in *Tsix/Xist*, the expression of of the noncoding RNA *Tsix* blocks H3K4me3 methylation leading to an accumulation of RNA pol II and impaired *Xist* expression, other mechanisms of transcript silencing have also been suggested (Galupa *et al.*, 2020).

An inverse relationship has been detected between the tumour suppressor gene *p15* and its antisense transcripts, *p15-AS*. The upregulation in *p15-AS* is linked to the silencing of *p15* transcripts. The antisense transcripts induce DNA methylation of the p15 promoter and trigger heterochromatin formation (Yu *et al.*, 2008). A similar mechanism was reported for the alpha-globin gene (*HBA2*) and its antisense transcripts *LUC7* (Tufarelli *et al.*, 2003; Piatek *et al.*, 2016; Zinad *et al.*, 2017).

1.6. Epigenetics and gene expression

Eukaryotic chromatin represents packed genetic material that contains information required for the different biological activities in a cell. Epigenetic marks such as DNA methylation and post translational modification of histone tails represent another reservoir of genetic information (Jaenisch and Bird; Jenuwein and Allis, 2001). Global genomic DNA methylation and histone modifications have been established for many cells and organs in the ENCODE project (Encyclopedia of DNA Elements) (Birney *et al.*, 2007). Both epigenetic marks were found to be highly conserved and to correlate with activating and/or silencing of particular genomic loci (Jenuwein and Allis, 2001). Therefore, the cell-specific chromatin structure influences the expression pattern of both coding and noncoding transcripts and may provide clues to the biological function of the genes.

1.6.1. DNA methylation

DNA methylation is an epigenetic modification where methyl groups (-CH_3) from the methyl donor S-adenosyl-L-methionine (SAM) are transferred to C5 of cytosine in a CpG (cytosine phosphate guanine) context (Bird, 2002). The importance of DNA methylation is to induce long term gene silencing and to provide stable epigenetic information for many cell generations without altering the nucleotide sequence (Cedar and Bergman, 2012; Smallwood and Kelsey, 2012).

DNA methylation is prominently implicated in genomic imprinting, transposon silencing and X-chromosome inactivation (Esteller, 2007; Santos-Reboucas and Pimentel, 2007). In mammals, 60-80 % of CG residues are methylated. In CpG islands associated with promoter regions, 70-90 % of CGs are preserved from methylation. However, methylation of promoters in a non-CG context has been discovered in few cell types such as embryonic stem cells, oocytes and brain cells (Law and Jacobsen, 2010; Tomizawa *et al.*, 2011; Kobayashi *et al.*, 2012).

In mammalian cells, DNA methylation occurs in various genomic regions, most prominently in satellite DNA such as LINEs (long interspersed transposable elements) and parasitic SINES (short interspersed transposable elements) (Yoder *et al.*, 1997). The enzymatic methylation system consists of two main components,

DNA methyltransferases (DNMTs) which catalyse the DNA methylation reaction (writers), and the methyl-CpG binding proteins (MBDs), which are responsible for ‘reading’ the methylated marks (readers) (Mayer *et al.*, 2000).

Furthermore, DNMTs can be classified into de novo methyltransferases (DNMT3A and DNMT3B) which are important for initial DNA methylation in embryogenic tissues (Okano *et al.*, 1998; Okano *et al.*, 1999). On the other hand, DNMT1 is responsible for the methylation of hemi-methylated DNA thus maintaining the epigenetic imprint after cell division (Figure 1.8) (Okano *et al.*, 1999; Hermann *et al.*, 2004). The presence of a methyl group at cytosine inhibits transcription factors from binding to the DNA template and enables the interaction with methyl-CpG binding proteins, both repressing gene expression (Robertson, 2002).

DNA methylation is reversible process. Demethylation opposes the effects of methylation and has been reported mainly during mammalian embryogenesis (Kohli and Zhang, 2013). Other studies propose that demethylation can happen without cell replication in response to environmental stimuli. Hence, two main mechanisms have been identified that induce DNA demethylation (Wu and Zhang, 2010): first, active demethylation involves the release of 5-methylecytosine (5meC) by specific yet uncharacterised enzymes. Second, passive demethylation occurs during embryogenesis or after mutating, blocking or knocking-out DNMT enzymes followed by progressive cellular divisions.

Recent large-scale DNA methylation studies provided a new tool to investigate gene expression patterns (Laird, 2010). Bisulphite sequencing is the quantitative technique used for this purpose and involves treating of genomic DNA with bisulphite compounds to differentiate between the methylated and non-methylated cytosine residues (Lister *et al.*, 2009; Laurent *et al.*, 2010). Many research groups have also illustrated a crosstalk between DNA methylation and histone modification influencing gene expression in different organisms (Du *et al.*, 2015).

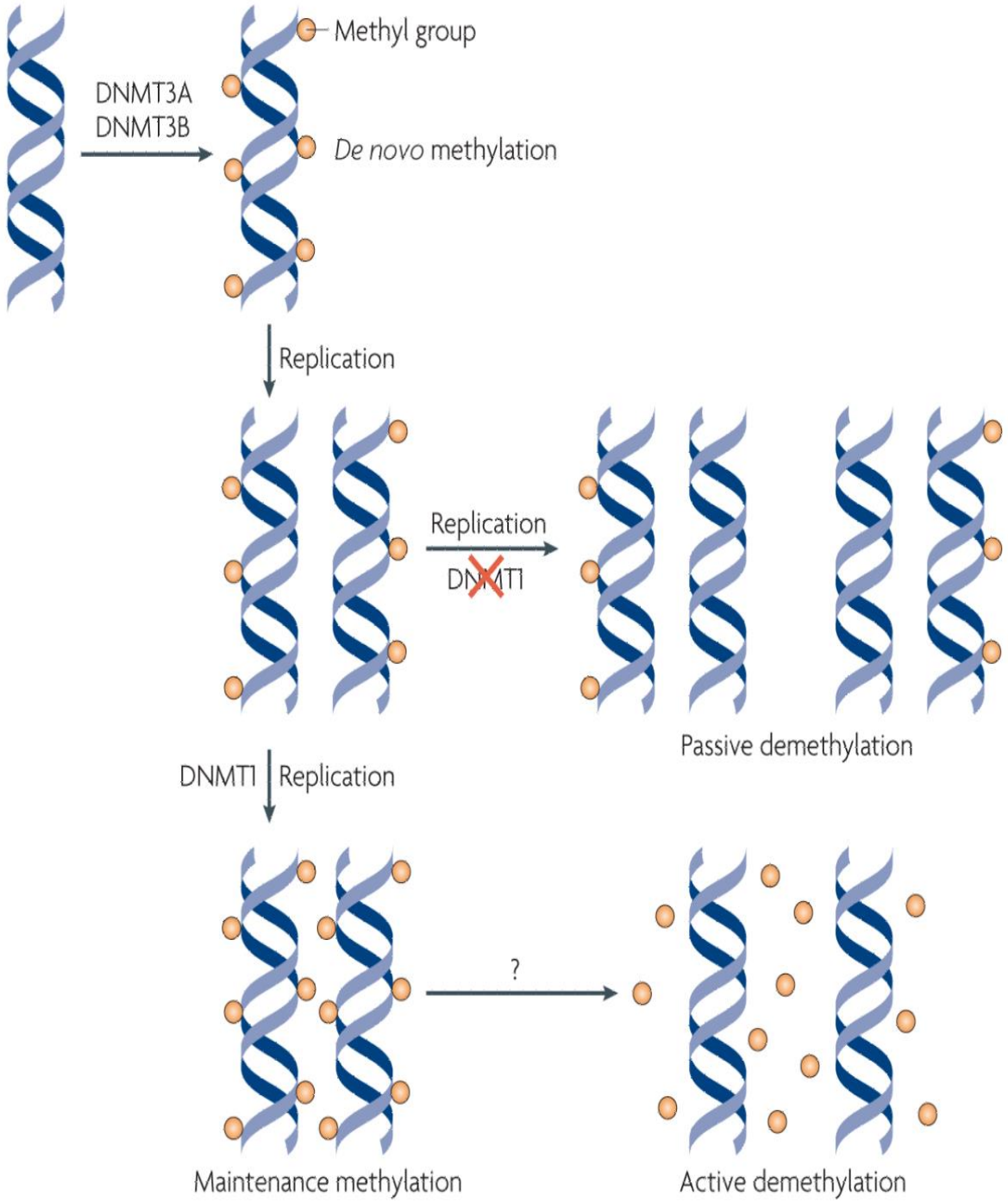

Figure 1. 8: DNA methylation and demethylation. De novo methyltransferases (DNMT3A, DNMT3B) add methyl groups during early development. The methylation pattern is transferred to the daughter cells during replication in the presence of DNMT1. Absence of DNMT1 leads to passive demethylation in contrast to active demethylation that happens under the effect of yet unrecognized enzymes. Figure adopted from (Wu and Zhang, 2010).

1.6.2. Histone modification

In eukaryotes, negatively charged DNA is wound around a positively charged protein complex, forming the so-called nucleosome. Each nucleosome is composed of two copies the histone proteins H2A, H2B, H3 and H4 plus 147 bp of DNA and appears as thread like structure (Luger *et al.*, 1997). The transcriptionally silent and tightly packaged chromatin (i.e. heterochromatin), results from hydrogen bond formation between histone tails with the adjacent nucleosome. These bridges prevent transcription factors from accessing the promoter region in the chromatin. Histone modifications are considered as short-term epigenetic marks which are lost after few cell divisions (Ma *et al.*, 2015). Histones are modified mainly by methylation/acetylation and their influence on the structure of chromatin is well established (Strahl and Allis, 2000). However, other modifications such as phosphorylation, ubiquitination and SUMOylation, facilitate/restrict access to DNA and are associated with active/ silenced genes.

1.6.3. Histone Methylation

Methylation of histone proteins represents a prominent post translational modification by which methyl groups are added to the N-terminus of histone H3 on arginine and lysine residues only. Arginine is found to be either mono- or di-methylated with symmetrical or asymmetrical configuration. The methylation reaction is catalysed by protein arginine methyltransferases (PRMTs I & II). On the other hand lysine methylation can involve a single, two or three methyl groups and all reactions are catalysed by the histone lysine methyltransferase (HKMT) (Zhang and Reinberg, 2001; Andreoli and Del Rio, 2015), as shown in figure 1.9.

In contrast to acetylation, histone methylation does not change histone charge distribution and establishes a base for the binding of regulatory proteins. Hence, histone methylation shows diverse effects on transcription which can be activating or repressive depending on the genomic context and the degree of methylation (Black *et al.*, 2012). Moreover, glutamine, aspartic acid and proline have also been

identified as potential methyl group acceptors (Bannister and Kouzarides, 2011; Tessarz *et al.*, 2014).

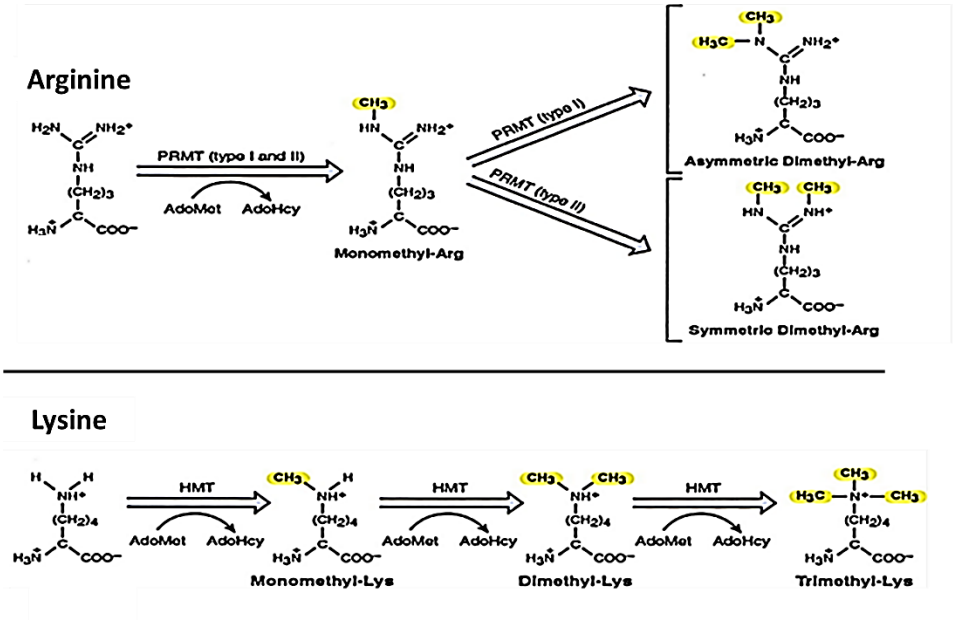

Figure 1. 9: Histone (H3) methylation of lysine and arginine residues. The PRMT enzyme induces arginine methylation to form mono or di methylarginine. Arginine di-methyl configuration can be symmetric or asymmetric. Lysine methylation catalyzed by HMT leads to mono, di and tri-lysine methylation (Zhang and Reinberg, 2001).

1.6.4. Histone Acetylation

The acetylation of lysine residues affects the charge of histones i.e. it reduces the affinity to negatively charged phosphate groups in the DNA and introduces a bulky side chain. Thus, the modification decreases the DNA – histone affinity and loosens the wrapping of DNA around the histone core. As a result, the DNA becomes more accessible to transcription factors.

The acetylation status of lysine residues at the N-terminus of histones is regulated by histone acetyltransferase (HAT) or by histone de-acetylase (HDAC) enzyme activity (Carrozza *et al.*, 2005).

While histone acetylation correlates with actively transcribed loci, deacetylation has the opposite effect and leads to repressed transcription (Figure 1.10) (Zhang and Tang, 2003; Sims *et al.*, 2006).

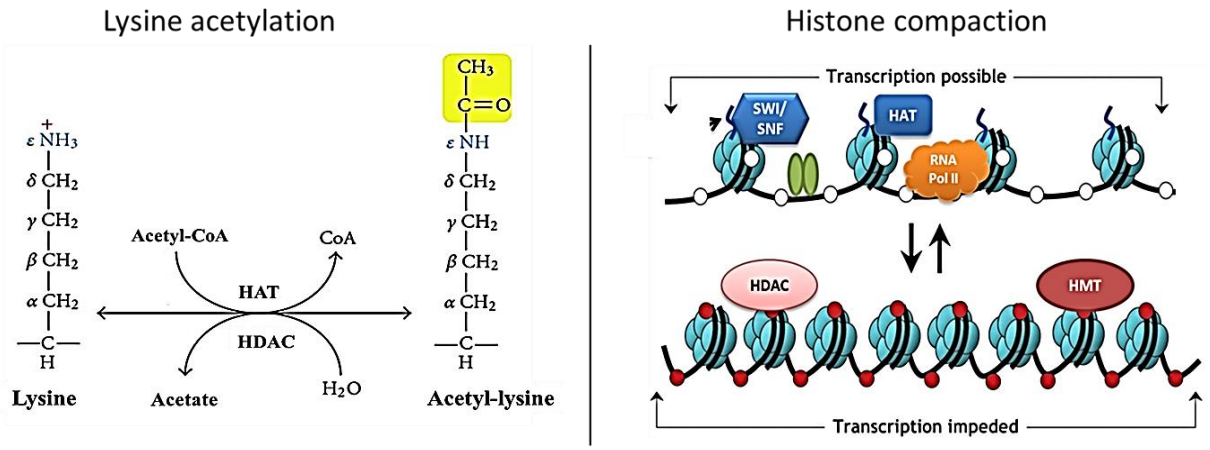

Figure 1. 10: Acetylation of histone lysine residues. Addition of an acetyl group to the histone tail catalysed by histone acetyl transferase (HAT). The removal of acetyl residues is mediated by histone deacetylases (HDAC) (left panel). Histone acetylation makes DNA more accessible to the transcriptional machinery, this is reversed by the action of the HDACs resulting in transcriptionally silent compact chromatin (right panel).

The epigenetic imprint of SLC34A1-sense and-antisense promoters is not established. Though epigenetic regulatory mechanisms involving DNA methylation and histone acetylation are hypothesised to influence the transcriptional activity of the SLC34A1 locus. This hypothesis will be addressed in this thesis using different cellular models.

1.7. Microbiome and phosphate

Microbiota refer to groups of microorganisms such as bacteria, archaea, fungi and viruses that reside inside and/or outside a mammalian body. In human, the microbial communities vary between body organs and this variation depends on the presence or absence of essential growth requirements within the environment. Because of its pivotal role in human health and its interaction with other systematic organs, some recent studies consider the microbiota as an actual organ in the body (Huttenhower *et al.*, 2012).

The gastrointestinal tract (GI) is colonized by approximately 100 trillion prokaryotic cells which belong to about 1000 bacterial species (Clark and Coopersmith, 2007; D'Argenio and Salvatore, 2015). Bacteria are considered as the main component of the microbiological ecosystem in different parts of the GI tract. The composition of the so-called microbiome is particularly well investigated in five different body sites, namely gut, skin, respiratory airways, oral cavity and urogenital tract. The percentage of the different bacterial phyla in an adult human are represented in figure 1.11 (Clark and Coopersmith, 2007; D'Argenio and Salvatore, 2015).

In the GI tract the microbes mainly colonise the mucosal layer of the gut in about equal proportions to the number of host cells (Sender *et al.*, 2016) Moreover, the gut microbiome varies along the GI tract, for example the commensal bacteria in stomach are significantly different from those in colon. This is mainly due to the variations in the physicochemical environment such as intestinal motility, pH level and host secretion of bile, gastric acid and enzymes. In addition, external factors contribute in shaping the final format of gut microbiome such as antibiotic usage, aging, dietary status and general health (Figure 1.12) (Woodmansey, 2007; Gerritsen *et al.*, 2011).

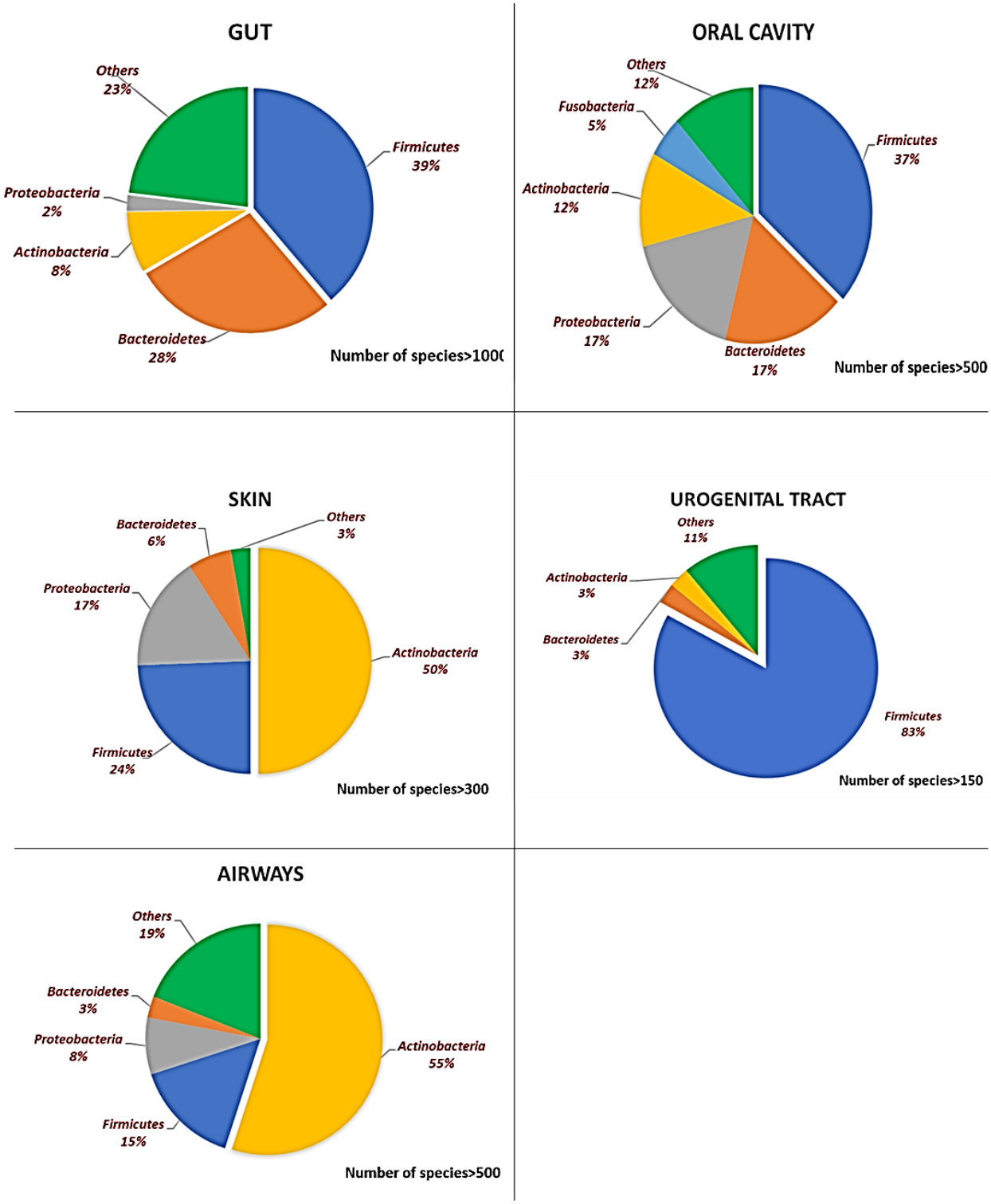

Figure 1. 11: Bacterial phyla diversity across well-investigated human body sites. The microbiome complexity is comparable in airways and oral cavity. Data from (Grice *et al.*, 2009; Dewhirst *et al.*, 2010; Arumugam *et al.*, 2011; González *et al.*, 2014; D'Argenio and Salvatore, 2015).

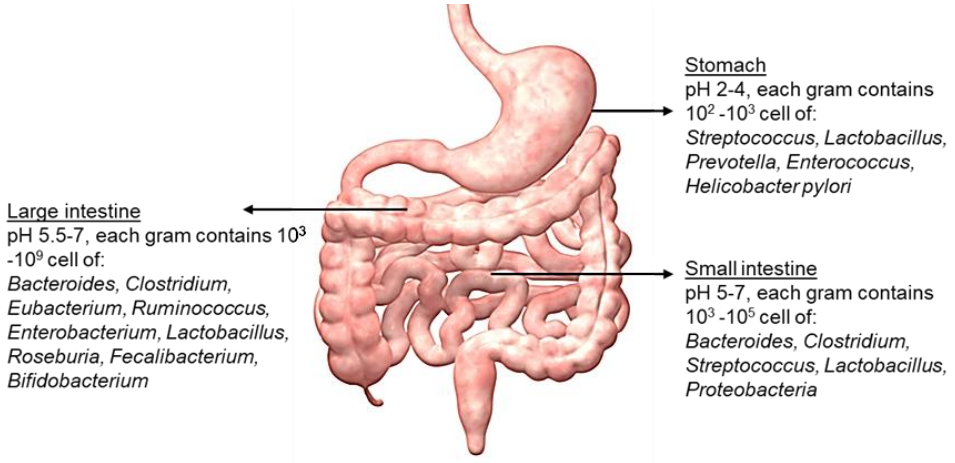

Figure 1. 12: Impact of environment on the most common bacterial species within the human GI tract. The bacterial diversity in the stomach is smaller than in small intestine and colon due to the low pH (Zhang *et al.*, 2015b).

1.7.1. The microbiome impact on health

Under homeostatic conditions in the GI tract, the commensal microbiome is responsible for many basic duties (Mueller and Macpherson, 2006; Hill and Artis, 2010): first, it breaks down and digests macromolecules from nutrients into small molecules and thereby increases the bioavailability of vitamins, carbohydrates and minerals. In addition, certain *E. coli* strains have the ability to synthesise vitamin K_2 and perform redox reactions within the large intestine (Bentley and Meganathan, 1982). Second, other bacterial species such as *Bifidobacterium longum*, *Lactobacillus reuteri* are playing a role in enhancing enteric nerve function and enteric angiogenesis (Kunze *et al.*, 2009; Bercik *et al.*, 2011). Third, some commensal bacteria provide mechanical support to the gut epithelial membrane and enhance barrier integrity by preventing pathogenic bacteria from penetrating the mucosa (Ubeda *et al.*, 2017). Finally, bacteria contribute to the development and adaptation of the host immune system, such as direct interaction with the mesenteric lymph nodes and other gut-associated lymphoid tissue (GALT) (Macfarlane and Cummings, 1999).

All these roles are essential for enteric homeostasis which refers to the balanced status of bacterial communities and their direct interaction with host tissue and dietary factors. An abnormal dietary change could induce the development of a state of microbial imbalance or dysbiosis which eventually could lead to serious pathological conditions such as inflammatory bowel disease and other gastrointestinal (GI) disorders, including gastritis (Bohn *et al.*, 2006; Ding and Schloss, 2014). Despite significant variation of GI microbial load among different individuals, the core components of the microbiome have been identified and show characteristic features in different stages of life (Table 1.4) (Turnbaugh and Gordon, 2009; D'Argenio and Salvatore, 2015).

Table 1. 4: Microbiota in healthy human gut at different stages of life. In general, the most complex bacterial structure is observed during adulthood whereas infants and the elderly tend to have less microbial variety. Factors that essentially affect the composition of the microbiome are listed in the right panel. Table adapted from (Turnbaugh and Gordon, 2009; D'Argenio and Salvatore, 2015).

Age	Dominant bacterial Phyla (from highly to less abundant)	Determining factor(s)
Infant (2-3 years)	*Actinobacteria, Proteobacteria, Firmicutes, Bacteroidetes*	− Vaginal vs caesarian delivery − Gestational age − Infant hospitalization − Breast vs formula fed − Age at solid food introduction − Malnutrition − Antibiotic treatments
Adult	*Firmicutes, Bacteroidetes, Actinobacteria, Proteobacteria*	− Diet − Hormonal cycle − Travel − Therapies − Illness
Elderly (>70 years)	*Firmicutes, Actinobacteria, Bacteroidetes, Proteobacteria*	− Lifestyle changes − Nutritional changes − Inflammatory diseases − Increasing use of medication

1.7.2. Diet and microbiome composition

Many factors play pivotal roles in determining the composition of bacterial species in the GI tract. These factors are of physiological, pathological and dietary nature and each one promotes the growth of particular bacteria (Macfarlane *et al.*, 2009). Recent evidence suggests that a change in gut bacterial composition could promote progression of pathological conditions and disrupt symbiosis (Ramezani and Raj, 2014). The diet is considered as a particularly important factor that affects bacterial colonization in the intestine. The infant gut for example, contains a significantly different bacterial load in breast versus formula milk fed babies (Fallani *et al.*, 2010; Brown *et al.*, 2012).

The effects of diet on the gut microbiome have been intensely studied. Tachon *et al*., reported a remarkable difference in the bacterial microbiome between one group of mice fed a western diet and other group fed a low-fat-chow-diet. Accordingly, an increase in *Bacteroidetes* and *Proteobacteria* was found in the low-fat diet group whereas a decrease of *Firmicutes* was observed with the western diet. Interestingly, *Lactobacillus gasseri* was reported to form 4.3 % of the total bacterial load in the low-fat-chow-group whilst this bacterium could not be detected in the western diet group (Tachon *et al.*, 2014).

Another study involved two groups of healthy volunteers fed a short-term animal-based or a plant rich diet. Bacterial sequencing showed an increase in bile tolerant bacteria such as *Alistips, Bilopila* and *Bacteroides* in the animal-protein diet group as well as a decrease in carbohydrate fermentation. The short intervention indicates that the composition of the GI tract microbiome rapidly adapts to dietary changes (David *et al.*, 2014).

A similar study included 98 healthy volunteers divided into two groups: the first group was given a long- term high fat/low fibre diet while the second group received a short-term low fat/high fibre diet. The dietary intervention resulted in an altered composition of GI tract bacteria which occurred within 24 h (Lee *et al.*, 2006).

Since Pi is essential for many biological structures and processes, it is in consistent demand for both eukaryotes and prokaryotes. This suggests a potential competition between the host and the microbiome for Pi in the gut.

There is growing concern about the high Pi levels in the western diet, generally in processed food which often contain Pi as a preservative. Many reports recorded clinical and subclinical disorders in response to Pi imbalanced diet, such as impaired renal function, hyperphosphatemia and cardiovascular calcifications (Uribarri, 2007; Sullivan *et al.*, 2009). On the other hand, epidemiological studies indicate that Pi-rich processed food may be associated with microbial imbalance in the GI tract (Ohnishi and Razzaque, 2010; Ritz *et al.*, 2012b).

Approximately 50-70 % of dietary phosphate is absorbed in the intestine mainly via SLC34A2 transporter (Knöpfel *et al.*, 2017). This raised the question of how the microbiome competes with intestinal epithelial cells to take up Pi from the diet.

1.7.3. Bacterial genome sequencing approaches

The Human Microbiome Project Consortium has demonstrated that the GI tract alone contains over 3 million bacterial genomes. The characterisation of GI tract bacterial communities by traditional standard microbiological techniques which are based on biochemical and phenotypic characteristics is time consuming and very challenging. Fastidious growth requirements for many well-known bacterial species complicate culture and yet uncultured species are difficult to characterise (Weinstock, 2012).

Various genetic methods have been developed and have contributed to the exponential increase of studies focusing on host- microbiome interactions over the last 25 years. These methods are based on PCR product sequencing and analysis of 16S ribosomal RNA (rRNA). The 16S rRNA genes are well conserved between different species with more than 97 % identity. However, the 1.5 kb sequence contains 9 short hypervariable regions that allows for classification (Olsen *et al.*, 1986). The specific approach starts with amplifying the full sequence of the 16S rRNA using primers to highly conserved regions. The resulting fragments are then cloned and sequenced with Sanger sequencing. The major drawback in applying this technique is limited sequencing throughput. Moreover, the determination of the exact proportions of individual bacterial species in specimens by this method is difficult (Bent *et al.*, 2007).

Nowadays, next generation sequencing (NGS) or high throughput sequencing is the method of choice for microbiome analysis. This method is considered as an advanced version of shotgun sequencing and includes the entire scale of genetic material (both 16S rRNA and whole-genomes) in microbial communities (Angelini *et al.*, 2016). In NGS, millions of genomic fragments are sequenced in parallel in four main steps: library preparation, cluster generation, sequencing and alignment, and data analysis. The analysis and interpretation of the collected data requires advanced bioinformatics expertise (Claesson *et al.*, 2010).

1.8. Aims

Considering the impact of epigenetics and the gut microbiome on general health, this PhD aims to explore these novel physiological regulators in the context of Pi homeostasis. The specific aims are:

- **To study the expression and the epigenetic status of the bidirectionally transcribed SLC34A1 locus in renal epithelial model cell lines.** In particular, compounds to modify epigenetic marks are applied to induce the expression of SLC34A1 loci. These are zebularine, an inhibitor of DNA methyl transferases (DNMTs), trichostatin A which inhibits histone deacetylases (HDACs) (Chapter 3) as well as dexamethasone, which interferes with histone acetyl transferases (Chapter 4).
  This part of the project aims to determine the methylation status of promoter sites for the SLC34A1-sense and-antisense transcripts and to quantify histone acetylation marks. In addition, transcription of the locus is altered via CRISPR-Cas9 knock-in experiments (Chapter 5).

- **To determine the impact of oral Pi supply on gut microbiota.**
  Two groups consisting of four volunteers each are included in a cross-over study. At the end of each intervention stool samples are collected (16 in total). High throughput sequencing is used to determine the microbiome diversity in the samples (Chapter 6). This part of the PhD is a collaboration with the group of Prof Carsten Wagner (University of Zurich, Switzerland), Dr Lindsay Hall (Norwich Medical School, University of East Anglia, Norwich, UK) and Dr Christopher J. Stewart (Translational and Clinical Research Institute, Newcastle University, Newcastle Upon Tyne, UK).

Chapter 2: Material and methods

2.1. Cell lines and tissue culture

Human renal proximal tubular epithelial cell lines (HEK293 and HKC8) were cultured in DMEM-high glucose (HEK293) or DMEM/HAM-F12 medium (HKC8), supplemented with 10 % fetal calf serum (FCS), 2 mM L-glutamine, 1 % non-essential amino acid (NEAA), 100 U/mL penicillin and 100 µg/mL streptomycin. Cell culture media and supplementary reagents were purchased from (Sigma-Aldrich, UK). Both cell lines were incubated at 37 ºC in 5 % CO_2 in humidified incubators. Culturing procedures were performed under aseptic conditions in a laminar flow hood. Cells were passaged every 3 days or when flasks became 80 % confluent. Most of the cell lines used in the thesis were obtained from the Cell Bank (Biosciences Institute, Newcastle University), at which cells are purchased from repositories such as ATCC, authenticated, cryopreserved according to established guidelines, in addition to the screening for mycoplasma contamination tests (Geraghty *et al.*, 2014).

2.1.1. Cell treatment

Zebularine (Zeb, DNMT inhibitor) and dexamethasone (Dex) were obtained from Abcam, UK, while trichostatin A (TSA, HDAC inhibitor) was from Sigma-Aldrich, UK. Stock solutions were dissolved in water unless otherwise stated and aliquoted, each containing sufficient material for one experiment. Several studies were performed in different cell lines with the various compounds and a wide range of concentrations: Zeb 25, 50, 100 and 200 µM; TSA 0.1, 0.2, 0.5, 1 and 2 µM and Dex 0.01, 0.1, 1, 10 µM were used. Furthermore, HEK293 and HKC8 cells were treated with each compound in time-and-dose dependent manner to determine the optimal treatment conditions to promote *SLC34A1*-sense and- antisense expression levels.

2.1.2. Cell viability (XTT assay)

HEK293 and HKC8 viability was measured using the colorimetric 2,3-bis-(2-methoxy-4-nitro-5-sulfophenyl)-2H-tetrazolium-5-carboxanilide (XTT) assay (Roche, Sigma-Aldrich, UK) as previously described (Hahm *et al.*, 2001). Briefly, cells were seeded in 6 replicates for each treatment condition at 4×10^4 cells/well in a 96-well plate and incubated for 24 h followed by drug treatment for 12, 24, 48, 72, 96 and 120 h.

At the day of the experiment, the XTT reagent was mixed with the electron coupling agent at (50:1) and added to each well for 1-2 h. The absorbance was measured using an iMark™ Microplate Absorbance Reader (Bio Rad, USA) at 415 nm wavelength. The data were compared to non-treated cells (control) and cell culture medium alone. The experiments were repeated at least in three independent biological replicates.

2.2. Real time quantitative PCR (RT-qPCR)/two-steps

2.2.1. TRIzol®-based RNA extraction

RNA was extracted form confluent cell monolayers using TRIzol® Reagent (Ambion, UK). 1 mL of Trizol was used per 10 cm^2 of culture and cells were lysed by pipetting up and down several times. Chloroform was added to separate the phases (200 µl/ 1 mL of Trizol). After centrifugation (14,000 rpm, 15 min at 4 ºC) the upper aqueous phase containing the RNA was transferred to an RNase-free tube and precipitated using 100 % isopropanol (500 µl/ 1 mL of Trizol). After centrifugation as above the RNA pellet was washed with 1 mL of 75 % ethanol, air-dried and re-suspended in 20 µl of RNase-free water.

2.2.2. DNase-I treatment

The extracted RNA was treated with DNaseI (2 U/µl) (ThermoFisher, UK) for 30 min at 37 ºC. The resulting RNA was purified through SigmaSpin™ reaction clean-up columns (Sigma-Aldrich, UK). The concentration and the purity (ratio of absorbance at 260/280 nm) of the extracted RNA was determined using Nano drop (Thermo scientific, UK).

2.2.3. RNA gel electrophoresis

RNA integrity was tested by agarose gel electrophoresis. 2 % agarose powder (Bioline, UK) was dissolved in 1x TAE buffer (w/v) (40 mM Tris-acetate and 10 mM EDTA). The mixture was boiled using microwave (SHARP, Japan) on mid-power for 1 min with constant agitation. The nucleic acid dye GelGreen (Biotium, USA) was added to the melted mixture at a 1:10,000 ratio. Melted agarose was poured into an RNase-free casting tray and allowed to solidify for 1 h.

About 500 ng of purified RNA were mixed with equal volumes of Gel Loading Buffer II (Invitrogen, UK). Heat denaturation at 65 ºC for 15 min followed by instant cooling on ice for 5 min was performed prior to electrophoresis. Samples were loaded onto the gel and run at 60 V for 45 min. The RNA was visualised using a Gel Doc XT+ Gel Documentation System (Bio Rad, USA).

2.2.4. Reverse transcription

For single stranded cDNA synthesis, the Omniscript RT-PCR kit (Qiagen, Germany) and random nonamer primers (2.5 µM, Sigma-Aldrich, UK) were used following the manufacturer's protocols. The total volume of the reactions was scaled down to 10 µl containing: 2 µl RNA template (50 ng- 1 µg), 1 µl of Random nonamers, 1 µl 10x RT buffer, 1 µl of dNTP mix (5 mM), 0.5 µl of RNase inhibitor (40 U/µl), 0.5 µl of Omniscript Reverse Transcriptase (4 U/µl) and RNAse free water up to the final volume. The reactions were incubated at 37 ºC for 1 h followed by denaturation for 10 min at 65 ºC. Samples were stored at – 20 ºC.

2.2.5. Reaction assembly

To optimise qPCR conditions for the *SLC34A1*-sense transcript, RNA from day 0 (freshly isolated) and day 10 (sub cultured) human primary renal proximal tubule epithelial cells (PT cells) was used (gift from Dr Colin Brown, Newcastle University, UK). Human testis RNA (HT) was used as a positive control to assess *SLC34A1*-antisense transcripts expression (TaKaRa, USA) (Cabili *et al.*, 2011; Washietl *et al.*, 2014).

The transcriptional profile of genes was determined by quantitative RT-qPCR using LightCycler® 480 System Technology (Roche). All primer pairs were synthesised by IDT (UK) (Table 2.1). The cDNA was diluted (1:3) in RNase free water for the housekeeping gene (*GAPDH*), t to monitor *SLC34A1*-sense/antisense gene expression 1 µl of cDNA per 96 well were used. Master-mixes comprising of LightCycler ® 480 Sybr Green I Master mix, primers and water were made prior to distribution into 96-well plates. Each well contained 5 µl of LightCycler ® 480 Sybr Green I Master mix, 0.5 µl forward primer of 10 µM stock, 0.5 µl reverse primer of 10 µM stock, 3 µl water and 1 µl cDNA, RNA or water. Plates were centrifuged for two 20 second intervals at full speed prior to loading into the LightCycler ® 480. Other samples such as RNase-free water and (1:10) diluted RNA were included and used as negative template control (NTC).

Amplified products were initially examined on 2 % agarose gels followed by sending purified PCR product for custom Sanger sequencing. The temperatures and cycle conditions are listed below:

Step	Temp. (ºC)	Time	Cycle number
Pre-incubation	95	10 min	1
Initial Denaturation	95	1 min	1
Denaturation **Annealing** **Extension**	96 55 72	20 30 10 } sec	45
Melting Curve	95 60 95	15 15 0 } sec	
Cooling	40	30 sec	

Expression levels for each gene were normalised to the internal reference gene *GAPDH*. All samples including target genes (i.e. *SLC34A1*-sense and -antisense), NTC and *GAPDH* were run in triplicate on one plate and each experiment was performed in at least three biological and technical replicates. All data were carefully scrutinised using melting curves and Ct values above 36 were discarded as not significant above background levels.

2.3. Column-based RNA purification and One-step RT-qPCR

Due to an increasing number of samples (i.e. different treatment conditions and knock-in cell lines), the toxic nature of TRIzol® Reagent and concerns with DNA contaminations during RNA extraction, an alternative protocol including a column-based RNA purification kit and one-step RT-qPCR were established for quantitative expression analysis.

Cells were seeded 24 h prior to the treatment in 6 well plates at 0.8x 10^6 cell density. On the following day, the cells were washed with 1x PBS (Sigma-Aldrich, UK). Total RNA was extracted using a Quick-RNA^{tm} Miniprep Plus Kit (Zymo Research, USA). According to the protocol 600 µl of RNA lysis buffer were used per well (5x10^6-10^7 cells) followed by mechanical homogenisation using a syringe with a 25-G needle.

For DNA digestion, 5 U of DNase I mixture (provided in the kit) were placed on RNA containing columns, followed by washing steps performed according to the provided protocol. Total RNA was eluted and quantified using Nano drop (Thermofisher, UK) and the integrity was confirmed by 2 % agarose gel electrophoresis prior to qPCR experiments (2.2.3).

For the RT-qPCR experiments, the Luna Universal One-Step RT-qPCR kit (New England Biolabs, UK) was used. The samples containing 100 ng/µl of purified RNA for *SLC34A1*-sense/antisense transcripts and 25 ng/µl for *GAPDH* were used. Reactions were assembled in 96 well plates and run using a Lightcycler 480 (Roche) qPCR machine with the following cycling conditions:

Step	Temp. (ºC)	Time	Cycle number
Reverse transcription	55	10 min	1
Initial Denaturation	95	1 min	1
Denaturation **Extension**	95 60	10 sec 10 sec	45
Melting Curve	95 60 95	15 15 } sec 0	
Cooling	40	30 sec	

Primers used for the RT-qPCR reactions are listed in table 2.1 and the expression of the tested genes was compared the non-treated samples and the fold change (R) was calculated as ΔΔCt value (Cikos *et al.*, 2007):

ΔCt = Ct gene of interest– Ct reference gene

ΔΔCt = ΔCt (non-treated) – ΔCt (treated)

$R= 2^{(-\Delta\Delta Ct)}$

Table 2. 1: Primer sequences and product length for RT-qPCR of *SLC34A1* sense/antisense and *GAPDH*.

Oligo ID	Sequence (5'-3')	Amplicon (bp)
SLC34A1-F	CAGCCCTCAGGTCCTACACA	163
SLC34A1-R	CTCTGGCTTCTGCTCCTCCT	
SLC34A1-AS-F	TGGGCGACTGGAAGGTCTACA	182
SLC34A1-AS-R	GTCTTCGGCACCACCACAATTA	
GAPDH-F	TGAAGGTCGGAGTCAACGGATTTG	128
GAPDH-R	CATGTAAACCATGTAGTTGAGGTC	

2.4. Nuclear and cytoplasmic RNA purification

For nuclear and cytoplasmic RNA separation from HEK293 cells, the SurePrep™ Nuclear or Cytoplasmic RNA Purification Kit (Fisher BioReagents, UK) was used. The separation steps were performed according to the manufacturer's protocol with few modifications: the cells were initially washed with 1x PBS and lysed with ice-cold lysis buffer (provided by the kit). The cell lysates were centrifuged at 21000xg at 4 ºC for 30 min (Eppendorf™ 5424R Microcentrifuge, Fisher Scientific, UK). Approximately 70 % of the supernatant were collected and later used to isolate the cytoplasmic RNA. The rest of the supernatant was carefully removed and the pellet-containing Eppendorf tubes were placed upside-down at 4 ºC for 30 min prior to purification of nuclear RNA. Cytoplasmic and nuclear RNA was then extracted as described using the Quick-RNA Miniprep Plus Kit. One-step RT-qPCR were performed (section 2.3) and the fold change (R) was calculated as ΔCt value:

$$\Delta Ct = Ct \text{ (gene from nuclear/cytoplasmic RNA)} - Ct \text{ (gene from total RNA)}$$

$$R = 2^{(-\Delta Ct)}$$

2.5. SLC34A1 transporter functional tests/ Western blot

2.5.1. Preparation of whole cell protein extract

Prior the experiment, 1x Tris-buffered saline (TBS) buffer was prepared and filtered using 0.2 µM pore size filters. Culture plates were washed with 500 µl of 1x ice-cold PBS followed by cell lysis. The lysis buffer contained 10 mL TBS (5 mM Tris-Cl pH 8, 15 mM NaCl) with 50 µl of Igepal® CA-630 and cOmplete™ EDTA-free Protease Inhibitor Cocktail (one tablet/ 10 mL extraction buffer) (Sigma-Aldrich, UK). 500 µl of lysis buffer cocktail was added and the plates were kept on ice for 15 min. Mechanical homogenisation with 25-G syringe (5-10 times) was performed and protein lysates were cleared by centrifugation for 2 min at 12,000 rpm.

All the steps were performed on ice and the extracted protein samples were kept at -80 ºC until the day of the experiment.

2.5.2. Determination of protein concentration

The protein concentration was quantified using a DC protein quantification assay (BioRad, USA) with bovine serum albumin (BSA) as a standard. The experiments were performed using 96-well plates and in triplicates according to the provided protocol. Absorbance was measured using a microplate reader, MQX200 uQuant (Biotek spectrophotometer) at a wavelength of 595 nm.

2.5.3. Polyacrylamide gel electrophoresis (SDS-PAGE)

DL-dithiotreitol (DTT) (Fluka, USA) powder was freshly dissolved in 100 µl of distilled water at a final concentration of 1 M. Sodium dodecyl sulphate polyacrylamide gels were prepared from 20 % SDS, Acrylamide stock, Ammonium persulfate, TEMED and Tris HCl (pH 8.8 and 6.8). All reagents were purchased from (Sigma-Aldrich, UK) and gels prepared according to published protocols (He, 2011) . 40 µg of cell extract were loaded per lane in 20 µl total volume including 5 µl of loading buffer. Mouse renal brush border membrane protein extract was used as a positive control in addition to a ready to use molecular weight ladder (Precision Plus Dual Color standard (Bio Rad, USA). Gels were run in SDS-PAGE 1x running buffer (25 mM Tris base, 192 mM Glycine and 1 % of SDS) at a constant current of 120 mA for 2 h.

2.5.4. Protein blotting

Following protein separation on SDS-PAGE, proteins were blotted onto polyvinylidene fluoride (PVDF) membrane (Millipore, Switzerland) by wet transfer (25 mM Tris, 192 mM glycine, 20 % (v/v) methanol, pH 8.3) at 100 volts for 1 h.

Blotting efficiency was examined using Ponceau S staining (2.5.5). Blots were blocked in blocking solutions, 5 % milk powder (Coop, Switzerland) dissolved in TBS for at least 30 min at room temperature with constant agitation, then blots were incubated with the primary antibody overnight at 4 ºC. The dilutions of the antibody are shown in table 2.2.

On the next day, membranes were washed 3 times with TBS for 15 min, followed by a second blocking step as above. Membranes were rinsed briefly with 1x TBS buffer and treated with secondary antibody conjugated with horse radish peroxidase (GE Healthcare, UK) (Table 2.2) for 2 h at room temperature. The blots were washed 3 times with TBS followed by chemiluminescent detection according to the manufacturer's protocol (Supersignal, West Pico, USA). The chemiluminescent signals were detected using a LAS-4000 luminescent image analyser (Fujifilm, USA) at different exposure times (10, 20, 30 and 60 sec).

Table 2. 2: Primary and secondary antibodies used for western blotting.

Antibody	Dilution	Specificity	Manufacturer
Rabbit α-mouse Slc34a	1:2000	N-terminal peptide	Designed and produced at the Institute of Physiology, Zurich University, Zurich, Switzerland (Custer *et al.*, 1994b).
Rabbit α-mouse Slc34a1	1:3000	C-terminal peptide	
Goat or mouse α-rabbit HRP	1:5000		Promega AG, Switzerland
Rabbit α-mouse β-actin	1:5000		Sigma-Aldrich, Switzerland

2.5.5. Ponceau S staining

To confirm the efficiency of protein transfer from the SDS-gel to the PVDF membrane, protein bands on the membrane were visualized with Ponceau stain (0.5 g Ponceau stain, 1 % acetic acid (v/v) and 10 mL distilled water). Blots were stained for 3 min, imaged and rinsed with distilled water twice for 5 min to remove the staining.

2.6. Northern blotting

2.6.1. Probe preparation

Approximately 50 ng of newly prepared cDNA template was used to amplify *SLC34A1*-sense/antisense and *GAPDH* probes with an additional T7 promoter sequence at the 3'end of the reverse primers (Table 2.3). The PCR products were examined on a 1 % agarose gel, purified using a GeneJET PCR Purification Kit (Thermo Scientific, UK) according to the provider's protocol. DNA concentrations and purity were determined using Nanodrop (Thermo Scientific, UK).

Table 2. 3: Primers for the preparation of northern blot probes. Lowercase letters represent the T7 promoter sequence.

Oligo ID	Sequence (5'-3')	Amplicon (bp)
SLC34A1-F	CTTCACCTGGGTCACAG	667
T7–SLC34A1-R	agccactaatacgactcactatagggCTCTGCAGGACATTGATGA	
SLC34A1-AS-F	CACTCGGAGCGCGATG	650
T7–SLC34A1-AS-R	agccactaatacgactcactatagggGTGGAAACTTTCCTGCTG	
GAPDH-F	GTGGATATTGTTGCCATC	466
T7–GAPDH-R	agccactaatacgactcactatagggCAGTGATGGCATGGACTGTG	

Approximately 50 ng of the PCR product with added T7 binding site were used as template for in vitro transcription using the MEGAscript™ T7 Transcription Kit (Invitrogen, UK). For control purposes, the probes were in vitro transcribed in two forms, as unlabelled probe using MEGAscript™ provided nucleotides and as labelled probes with digoxigenin labelled UTP (DIG RNA Labelling Kit, Table 2.4). Both reactions were assembled on ice and incubated at 37 ºC for 2 h. Labelled and unlabelled probes were denatured at 65 ºC for 10 min and chilled on ice for 5 min prior to examination on a 2 % agarose gel.

Table 2. 4: Northern blot probe in vitro transcription using labelled and unlabelled nucleotides.

Unlabelled		Labelled	
Reagent	**Volume (µl)**	**Reagent**	**Volume (µl)**
T7 enzyme mix	1	**T7 enzyme mix**	1
10x buffer	1	**10x buffer**	1
PCR product	50 ng	**PCR product**	50 ng
ATP, GTP, CTP, UTP	1 each	**10x DIG mix**	1
Water	Up to 10 µl	**Water**	Up to 10 µl

2.6.2. Northern blotting- RNA electrophoresis

The RNA separation for northern blotting was similar to routine RNA agarose gel electrophoresis, however no nucleic acid dye was added to the gel. 7.5-10 µg of RNA were mixed with RNA loading buffer, heat-denatured and loaded on 2 % TAE agarose gels. The samples were run at 90 volts for 120 min. Following RNA electrophoresis, the gel was soaked in 20x SSC buffer (3 M NaCl in 0.3 M sodium citrate, pH 7.0, all reagents from Sigma-Aldrich, UK) for 30 min prior to RNA blotting (Masek *et al.*, 2005).

2.6.3. RNA capillary blotting

For blotting, two sponge pads (8 x 11 cm) were soaked in 10x SSC buffer (1.5 M NaCl and 150 mM sodium citrate, pH 7.0), the positively charged nylon membrane (Roche, UK) was cut to gel size, wetted in distilled water and soaked for 5 min in 10x SSC. In a shallow tray filled with 10x SSC, the blotting stack was assembled in the following order: sponge pads, sponge size Cellulose Chromatography Papers (Whatman paper, GE Healthcare Life Sciences, USA), overturned gel (the well openings facing the Whatman paper), positively charged blotting membrane (no bubbles between the gel and the membrane), membrane size Whatman paper stack (10-15 sheets), paper towel stack and a weight on top. The assembled stack was left at room temperature for 6 h with periodical refilling of the transfer buffer (10x SSC).

After blotting, gel slots were marked on the membrane with a pencil. The membrane was washed with 1x SSC buffer and moist RNA blots were cross-linked using a UV crosslinker, setting ‘autocrosslink’, 1200 µJoules (Stratalinker 2400, Stratagene, USA).

2.6.4. Pre-hybridisation and hybridisation

For pre-hybridisation, the cross-linked membrane was placed in a 50 mL Falcon tube (Starlab, UK) and incubated in 5 mL of pre-warmed (55 ºC) hybridisation buffer (10 % of blocking reagent DIG Easy Hyb, Roche, in 0.1 M maleic acid (pH 7.5), 0.15 M NaCl and 0.3 % (v/v) Tween 20). Pre-hybridisation was performed in a HB-1000 hybridizing oven at 55 ºC for 60 min, with continuous tube rotation.

For hybridisation, 10 µL of the DIG-labelled probes were mixed with 10 mL of pre-warmed at 55 ºC hybridisation buffer. This was added to the membrane and incubated at 55 ºC overnight, again with continuous rotation**.** Blots were then washed with 15 mL of 0.5x SSC at room temperature for 15 min. This step was repeated twice with 0.1x SSC at 55 ºC for 15 min.

2.6.5. Detection

For detection, blots were processed according to the DIG Detection system manual with slight modifications. The blots were washed with 1x washing buffer (0.1 M maleic acid, 0.15 M NaCl; pH 7.5; 0.3% (v/v) Tween 20) twice for 15 min at room temperature with continues agitation followed by blocking with 10 mL blocking buffer (10 % of blocking reagent in maleic acid buffer (w/v, 0.1 M maleic acid, 0.15 M NaCl; adjust with NaOH to pH 7.5)) at room temperature for 30 min. The membranes were then incubated with Anti-Digoxigenin antibody (Roche, UK) in blocking buffer (1:10,000) for 30 min at room temperature. In a dark container, blots were briefly washed with 1x washing buffer, followed by addition of 5 mL of detection buffer (0.1 M Tris-HCl, 0.1 M NaCl, pH 9.5) and incubation for 5 min.

The blots were sprinkled with approximately 1 mL of CSPD ready-to-use solution (Roche, UK) and wrapped in cling film. After 5 min incubation at room temperature,

the blots were visualised using a GBOX-Chemi-XRQ gel documentation system (Syngene) with multiple exposure times.

2.7. ^{32}P uptake measurements

The ^{32}P uptake protocol was adopted from published methods (Brown *et al.*, 2008). HEK293 cells were seeded in 24-well plates (Sigma Aldrich, UK), at a density of $5x10^4$ cells in 500 µl of medium per well. The experiments were designed in four replicates for each treatment condition. Once the cells reached 75-80 % confluency, Dex (100 nM/mL) was added. Dex-containing growth medium was replaced after every 48 h.

On the day of the ^{32}P uptake experiment, the number of cells were counted from a representative well for each treatment condition using a Cellometer Auto T4 Bright Field Cell Counter (Nexcelom, UK). Counts were used for uptake normalisation.

For the uptake experiments, the cells were washed gently 3 times with 500 µl of warm phosphate-free Kreb's buffer (140 mM NaCl, 5.4 mM KCl, 1.2 mM, $MgSO_4$, 4 mM glucose, 2 mM $CaCl_2$, 10 mM HEPES/Tris pH 7.4). 1 mL of Kreb's buffer was added per well and the plates were placed on a thermostat-controlled platform at 37 ºC for 30 min. In timed steps, the cells were exposed to 1 mM $NaHPO_4$ containing 1 µC/mL ^{32}P tracer for 5 min followed by three washes with ice cold Kreb's buffer.

Cells were lysed with 250 µl of 0.1 % SDS (v/w). Radioactive Pi was quantified by scintillation counting (Beckman LS5000 liquid scintillation counter, Beckman-Coulter, UK).

2.8. Pyrosequencing

Pyrosequencing is a real-time quantitative approach in which the methylation percentage of target CpGs dinucleotides at promoter regions is quantified. This reaction starts with the bisulphate conversion of unmethylated cytosines to thymines, followed by PCR amplification and quantitative sequencing as described below:

2.8.1. Genomic DNA (gDNA) purification

In order to study the methylation level of the promoter regions, HEK293 and HKC8 cells were seeded in 6 well plates at $0.8x10^6$ cells/well, after 24 h the cells were treated with the appropriate drug. At the harvesting day, the plates were washed gently with 1x PBS. DNA was purified using the Wizard® Genomic DNA Purification Kit (Promega, UK). 600 µl of the lysis buffer were added per well followed by mechanical lysis using a G-25 needle, for 10-15 times. Cell lysates were applied to the columns, followed by centrifugation. The columns were washed 3 times with 1x washing buffer followed by DNA elution with 400µl of nuclease-free water.

2.8.2. Bisulfite modification and Pyrosequencing

The methylation status of the promoters was measured using the Pyromark Q96 ID system (Qiagen). 450-500 ng of gDNA were subjected to sodium bisulfite treatment using the EZ DNA Methylation Gold Kit (Zymo research, USA). Four CpG rich promoter regions (S1, S2, AS1 and AS2) were PCR amplified using forward and biotinylated reverse primers (S=SLC34A1-sense, and AS=SLC34A1-antisense, Table 2.5). PCR products were examined on a 2 % agarose gel and confirmed by Sanger sequencing (GATC Biotech, Germany). Using PCR plates, 25 µl of PCR amplicons were mixed with Binding Buffer (Qiagen, Germany), then Streptavidin Sepharose High Performance beads were added (GE Healthcare, Life Sciences, UK). Beads were washed progressively on the PyroMark vacuum workstation with the following solutions: 70 % ethanol, PyroMark Denaturation Solution, PyroMark Washing buffer (Qiagen, Germany) and high-purity water. Annealing Buffer and the sequencing primers were added to the washed amplicons and mixed. Pyrosequencing plates were then processed using the PyroMark pyrosequencer (Tost and Gut, 2007; Au - Cummings *et al.*, 2013).

As a positive control (100 % methylation), 0.5 µg gDNA from HEK293 and HKC8 cells were treated with 10 U of CpGs methyltransferase (*M.Sss*I) (New England Biolabs, UK) in the presence of 32 mM S-adenosylmethionine (SAM) at 37 ºC for 1 h. The enzyme was heat inactivated at 65 ºC for 20 min followed by purification using SigmaSpin™ reaction clean-up columns (Sigma-Aldrich, UK).

To generate unmethylated DNA (0 % methylation), a whole genome amplification kit was used (Qiagen, Germany) with 100 ng of gDNA for amplification followed by column purification.

Table 2. 5: Pyrosequencing primers. All primers were designed using MethPrimer webtools and synthesised by IDT, UK.

Oligo ID	Orientation	Sequence (5'-3')	bp	No. of CpG
AS1	F	TTTGTAGGAAGGTGTGTTTGTT	173	3
AS1-(bio)	R	CTAAAAAATCTACATCAATACAA TAC		
AS1	SP	TTTGTAGGAAGGTGTGTTTGTT		
AS1	Sequencing entry	C/TGGTTTC/TGTGAGTAC/TGTTT ATTTTTTGC/TGGC/TGAGATGGT C/TGTTAGTAGGTT		
AS2	F	GTATTGTATTGATGTAGATTTTTT AG	461	5
AS2- biotin	R	CCTAAACAACATAATAAAACCTC ATCTC		
AS2	SP	TTGTGAGGTAGGTTGGG		
AS2	Sequencing entry	C/TGGGGTTGTGAC/TGTTATATA AGGC/TGTC/TG		
SLC34A1-S1-	F	AGTGGGAGTAAATTTTTATGGAG GT	339	7
SLC34A1-S1biotin	R	CATCCCAACAAACTAAAATCAAA A		
SLC34A1-S1-	SP	AGTGGGAGTAAATTTTTATGGAG GT		
SLC34A1-S1-	Sequencing entry	C/TGTTTTTTTTAGTGTTTTC/TGC /TGGAGATTC/TGTTTTTTTAGTGT TTTC/TGC/TGGAGGTTC/TGTTTT TTTAG		
SLC34A1-S2-	F	TATAGGATGTTTGGGTTATTTTTT G	148	2
SLC34A1-S2biotin	R	CTATAATCAAATTCTTCCCATCA AC		
SLC34A1-S2-	SP	GTTTTTGTTTGTAGG		
SLC34A1-S2-	Sequencing entry	C/TGGGGGATGTGTTTGGGTC/T GTGGTTG		

2.9. Global histone acetylation (H3Ac27)

2.9.1. Histone extraction

Total histones were extracted from HEK293 and HKC8 cells using the EpiQuik Total Histone Extraction Kit (EpiGentik, USA). The extraction steps were followed according to the provided protocol. Cells were seeded in 6-well plates, treated with the corresponding drugs, washed with 1 mL of pre-lysis buffer and kept on ice for 10 min. Cells were detached from the well by pipetting force and pelleted at 15,000xg for 1 min. Cell pellets were lysed and homogenised with a 25-G needle. The homogenate kept on ice for 30 min and precipitates were separated by centrifugation (15,000xg for 5 min). The pellet was dissolved in 50 µl of DTT- buffer. The concentration of the extracted proteins was determined with Nanodrop (absorbance coefficient 4120). The samples were aliquoted and stored at -80 ºC.

Approximately 10 µg of cell extract samples were run on a 9 % SDS-PAGE gel (as described in 2.5.3). Purified Caf1 protein (Mw: 15.5 kDa) was included as a positive control, kindly donated by Prof. Jeremy Lakey (Biosciences Institute, Newcastle University, UK) in addition to a molecular weight ladder (Precision Plus Dual Color standard (Bio Rad, USA).

2.9.2. Quantification of acetylated histone protein

The level of acetylated histones was determined by sandwich ELISA, EpiQuik Total Histone H3 Acetylation Detection Fast Kit (EpiGentik, USA). Histone protein samples were thawed on ice and about 50-200 ng of purified protein were incubated in wells coated with anti-acetyl histone H3 antibody. The captured histones were detected by the secondary antibody conjugated to horseradish peroxidase. The colour intensity was measured by an iMark™ Microplate Absorbance Reader (Bio-Rad, USA) at 450 nm.

2.10. SLC34A1-sense and -antisense genome editing

The strategy to edit *SLC34A1*-sense/antisense genes by CRISPR-Cas9 is outlined below (Ran *et al.*, 2013b; Goyal *et al.*, 2017):

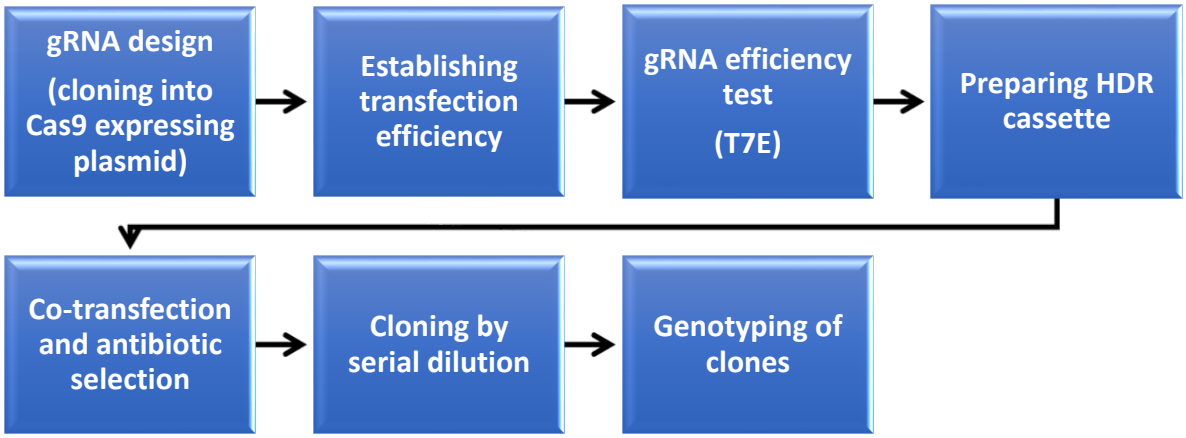

Figure 2. 1: *SLC34A1*-sense/antisense genome editing strategy.

2.10.1. Single guide RNA (sgRNA) preparation

sgRNAs were designed using the online tools. Suggested sgRNA were examined carefully and only those with a CG content between 40 and 80 % and a high on-target probability were considered. Oligonucleotides encoding the sgRNA sequences were ordered from IDT (UK).

sgRNA-top	CACCgNNNNNNNNNNNNNNNNNNN
sgRNA-bottom	AAACNNNNNNNNNNNNNNNNNNc

*N refer to specific gene sequence

Each of the sgRNA oligonucleotides (top and bottom) were designed containing *Bbs*I overhangs to enable vector ligation. The vector pSpCas9 (PX458, Figure 2.2) was

linearised with *Bbs*I at 37 ºC for 1 h (1 µg of plasmid DNA, 2 µl of 10x buffer G, 2 µl of *Bbs*I (Thermofisher, UK) and nuclease free-water to 20 µl). The digested plasmid was run on a 1 % agarose gel and purified from the gel using the GeneJET PCR Purification Kit (Thermo Scientific, UK).

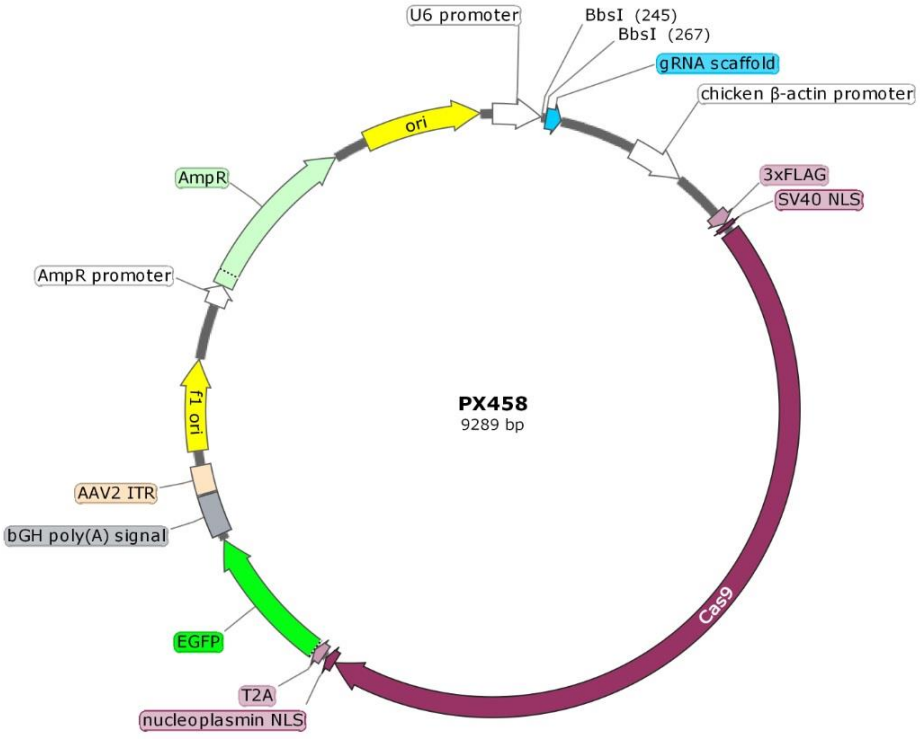

Figure 2. 2: pSpCas9 (PX458) vector map used for SLC34A1sense/antisense gene editing. Annealed oligonucleotides (sgRNA pairs) were cloned into the gRNA scaffold at the *Bbs*I site.

Top and bottom strand oligonucleotides were annealed and phosphorylated using T4 polynucleotide kinase kit (New England Biolabs, UK). 100 µmoles of each oligo were incubated with 0.5 U of T4 PNK kinase in 1x T4 ligation buffer. The reaction was incubated at 37 ºC for 30 min, heated to 95 ºC for 5 min and then cooled to 25 ºC at 5 ºC/ min steps to anneal the phosphorylated oligonucleotides. 3 µl (50 ng) of linearised vector and 1 µl of 1:200 diluted, annealed oligonucleotides were then ligated using Quickligase (Thermofisher, UK) for 50 min. Ligated DNA was used to transform OneShot chemically competent Stbl3 *E. coli* (Thermofisher, UK). 50 µl of transformed cells were plated on Luria broth (LB) agar plates containing carbenicillin (100 µg/ml). Transformed bacteria were incubated at 37 ºC for 24 h. Colonies were screened by colony PCR using the PX458 universal forward primer (U6F, 5'-GAGGGCCTATTTCCCATGATTCC-3') and the reverse sgRNA oligos. The reaction master mix and PCR conditions are as follows:

Table 2. 6: Colony PCR Master Mix and cycling conditions.

<table>
<tr><th colspan="2">Master Mix</th><th colspan="4">PCR conditions</th></tr>
<tr><th>Reagent</th><th>15µl</th><th>Step</th><th>Temp (ºC)</th><th>Time</th><th>Cycles</th></tr>
<tr><td>2x Gotaq master mix (Promega, UK)</td><td>7.5</td><td>Initial Denaturation</td><td>94</td><td>4 min</td><td>1</td></tr>
<tr><td>U6F (10 µM)</td><td>0.5</td><td rowspan="3">Denaturation
Annealing
Extension</td><td rowspan="3">94
55
72</td><td rowspan="3">30sec
10sec
30sec</td><td rowspan="3">25</td></tr>
<tr><td>Reverse gRNA (10 µM)</td><td>0.5</td></tr>
<tr><td rowspan="2">Nuclease-free water</td><td rowspan="2">6.5</td></tr>
<tr><td>Final Extension</td><td>72</td><td>2min</td><td>1</td></tr>
<tr><td colspan="2"></td><td>Hold</td><td colspan="3">4-10 ºC</td></tr>
</table>

2 µl of the reactions were analysed on a 1 % agarose gel, positive colonies were sub-cultured, and plasmids were isolated using the Isolate II Plasmid Mini Kit (Bioline, UK). Sequences were confirmed by DNA Sanger sequencing (GATC Biotech, Germany) using a plasmid specific primer pSp-R (5'-TAGGGGGCGTACTTGGCATATG-3').

2.10.2. gRNA transfection

HEK293 cells were seeded in 24-well plates at 1.3 x10^5 cells in 500 µl complete growth medium. On the next day, the growth medium was replaced with fresh complete growth medium 2 h prior to transfection. Cells were transfected with 500 ng of pSpCas9 (PX458)-gRNA using Lipofectamine 2000 reagent (Lifesciences, UK) following the standard protocol (Ran *et al.*, 2013b). After 24 h, 1 mL of fresh growth medium was added. The transfection efficiency was measured by counting green fluorescent cells expressing GFP using a Nikon fluorescence microscope. Transfected cells were incubated for at least 72 h before testing for Cas9 induced DNA nicks.

2.10.3. sgRNA efficiency test (T7 – endonuclease)

In order to determine the efficiency of the gRNAs, genomic DNA was isolated from the transfected HEK293 cells. For the detection of nicked DNA, the EnGen Mutation Detection kit (New England Biolabs, UK) was used. According to the protocol, primers were designed to amplify a genomic region >1000 bp that spans the gRNA sequence asymmetrically (for example, 400 bp upstream and 600 bases down-stream of the gRNA sequence, Table 2.7).

Table 2. 7: Oligonucleotide sequences used for the T7-endonuclease test. The primers were ordered from IDT, UK.

Oligo ID	Sequence (5'-3')	Oligo ID	Sequence (5'-3')
S-g-1F	GTGAGGGTGTGTGGG CATGAGT	**AS-T7E1234 F**	CTCTAAATTCACCCAC CTCAG
S-g-1R	GAGCAGACGAAG AGGTAGAG	**AS-T7E1234 F+**	CAGCCACACATCACTC CTTCCTG
S-g-2F	CTCTACCTCTTCGTC TGCTC	**AS-TE71234 R**	CATCAGGGTGTCAGG CTGGAG
S-g-2R	CAG CCT TACTGG GGTCACGCT	**AS-TE71234 R+**	CTAGGGACTCCGCAG CTGAG
S-T7E1R	CAGGGGCAGGTGTG CTCAGC	**AS-T7E5678 F**	CTCAAAATCCCGGCTC CACCAG
S-T7E123 F+	CAAGCCTCTGGTTCG GAGC	**AS-T7E5678 F+**	CAAGTGGAGGAGGAG CCAGC
S-T7E123 F++	CTGGGCGTCCTCAGT TCTC	**AS-T7E5678 R**	CATGCGGACAACAGCT GCGTG
S-T7E123 R+	GTCCAGGGAGCAGAC GAAGAG	**AS-T7E5678 R+**	GAAGGTCTACATCAGT GCAGTG
S-T7E123 F	CTGGGCTAGAGCTCA ATAATAC	**AS-T7E1234 F**	CTCTAAATTCACCCAC CTCAG
S-T7E23 R	GTGTAGGACTAGGGA GGGAG	**AS-T7E1234 F+**	CAGCCACACATCACTC CTTCCTG

The PCR reactions were performed using a proofreading polymerase (Q5 Hot Start-High Fidelity, New England Biolabs) to minimise PCR errors. The cycling conditions are given in table 2.8.

Table 2. 8: PCR Master Mix and cycling conditions.

Master Mix		**PCR conditions**			
Reagent	**25µl**	**Step**	**Temp. (ºC)**	**Time**	**Cycle**
Q5 Hot Start-High Fidelity 2X Master Mix	12.5	**Initial Denaturation**	98	30 sec	1
Forward (10µM)	1.25	**Denaturation**	98	5 sec	25
Reverse (10µM)	1.25	**Annealing**	*	10 sec	
Template DNA (ng)	500	**Extension**	72	2 min	
		Final Extension	72	2 min	1
Nuclease-free water	to 25	**Hold**	4-10 ºC		

* annealing temperature was determined according to the IDT oligo analyser tool, however it generally varied between 56-63 ºC.

For hetroduplex formation, approximately 250 ng (5µl) of unpurified PCR product was denatured and annealed (Table 2.9). DNA mismatches formed between Cas9 mutated and wild type alleles were then detected and cleaved by the T7 endonuclease. Following digestion, the reaction was examined on a 2 % agarose gel and the intensity of the bands was determined using a Gel Doc XT+Gel Documentation System (Bio Rad, USA).

Table 2. 9: Thermocycler conditions for heteroduplex formation in the T7 endonuclease assay.

Cycle step	Temp (ºC)	Ramp rate	Time
Initial Denaturation	95	**-------**	5 min
Annealing	95–85 85–25	**-** 2 ºC/sec **-** 0.1 ºC/sec	
Hold	4–10 ºC		

2.10.4. Homology directed repair (HDR)

Once efficient sgRNAs were determined for both SLC34A1-sense and- antisense, the homology repair template was designed with up- and down-stream recombination arms that centre around the predicted CRISPR-Cas9 cleavage site. A transcriptional termination cassette which contains an antibiotic selection marker (puromycin) driven by the CMV promotor and a transcriptional terminator sequence, BGH-PolyA (boving growth hormone polyadenylation), were designed to be integrated into the *SLC34A1* sense and antisense loci (Liu *et al.*, 2017). The knock-in cassette is shown in figure 2.3.

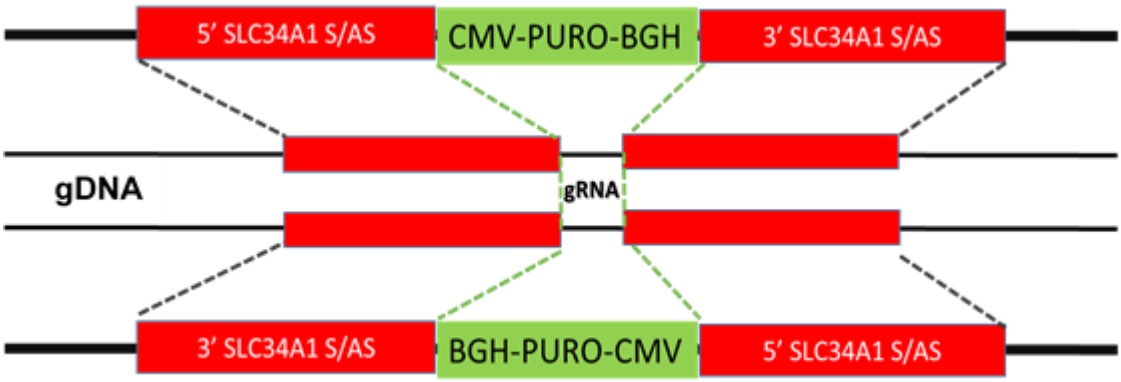

Figure 2. 3: Homology directed repair template for CRISPR-Cas9 knock-in experiments.

2.10.5. Cloning of SLC34A1-sense and- antisense homology repair template

Nested PCR was used to amplify *SLC34A1*-sense/antisense flanking arms from HEK293 genomic DNA, the strategy is explained in figure 2.5. In a first step, forward and reverse primers were designed to amplify approximately 2500 bp of DNA (PCR1). Further PCR primers were designed according to NEBuilder® HiFi DNA Assembly (New England Biolabs, UK) containing a 15-20 nucleotide overlap with the adjacent fragments. Amplicons from PCR1 were used as a template for the nested PCRs to amplify 5' and 3'recombinatation arms (PCR2 and PCR3, respectively).

In parallel, the CMV-PURO-BGH cassette (PCR4) was amplified from the plasmid obtained from Hengmi Cui, Yangzhou University, China (Liu *et al.*, 2017). All PCR fragments were examined on a 1 % agarose gel, purified using the GeneJET PCR Purification Kit (Thermo Scientific, UK) and sequenced (GATC Biotech, Germany). PCR Mix and cycling conditions are given in table 2.8. Oligonucleotides were purchased from IDT, UK, and are listed in table 2.10 below:

Table 2. 10: Primers used to generate the HDR template. Lowercase letters show the overlapping region with adjacent fragments. S and AS refers to *SLC34A1*-sense and-antisense transcripts, respectively.

Oligo ID	Sequence (5'-3')
S-PCR1-F	CACCGCGCCCCATATAACATGTC
S-PCR1-R	CAATGCCCTGGCCTACGGATTC
S-PCR2-F	CAACTCTTCACACCCCTACAAC
S-PCR2-R	caaatgtaacgcgtctcatagGACAACATCCTGGGCACCCAC
S-PCR3-F	gttacattttgctcacgtctcgcTACTACGGAGAGAGGCTGGGGTCCCCTGCTG
S-PCR3-R	cattttgctcacgtctcgctacTACGGAGAGAGGCTGGGGTC
S-PCR4-F	gtgggtgcccaggatgttgTCCTATGAGACGCGTTACATTTG
S-PCR4-R	gaccccagcctctctccgtagTAGCGAGACGTGAGCAAAATG
AS-PCR1-F	GAGTTCCTCCCTCTAGTCCAG
AS-PCR1-R	CTGGGCAACATAGTGAGACCTC
AS-PCR2-F	CAGCACCATCTCCCCTCAAAGAC
AS-PCR2-R	gtaacgcgtctcatagggggGCATCCTCAACAAGAC
AS-PCR3-F	tgttgaggatgccccccTATGAGACGCGTTACATTTG
AS-PCR3-R	gacgcggcgtacattagCGAGACGTGAGCAAAATG
AS-PCR4-F	ctcacgtctcgctaATGTACGCCGCGTCGG
AS-PCR4-R	CTCGCTCTGTGGCTCAGGCT

2.10.6. HDR fragment assembly

PCR fragments were assembled using the NEBuilder® HiFi DNA Assembly Cloning Kit (New England Biolabs UK). The proportion of each fragment was calculated according to NEBuilder Calculator (New England Biolabs, UK, Table 2.11). Assembled reactions were incubated in a thermocycler at 50 ºC overnight. On the next day, 5 µl of the ligated reaction was examined on a 1 % agarose gel together with non-ligated PCR fragments.

The other 5 µl of the ligated construct were used to transform OneShot Stbl3 chemically competent *E. coli* (Thermofisher, UK). Resulting colonies were screened by colony PCR and submitted for sequencing (GATC, Biotech, Germany) using the primers listed in table 2.12.

Table 2. 11: HiFi assembly reaction to generate the HDR cassette. The volume of each fragment was adjusted to achieve equimolar concentrations in the final reaction.

Fragment ID	Amplicon (bp)	Concentration (ng/ µl)	Volume added to assembly reaction (µl)
PCR2	850	50	0.7
PCR3	940	50	0.7
PCR4	1890	50	1.0
pMiniT2.0 vector	2610	50	2.0
NEB Master Mix	-------	-------	5
Nuclease free-water	--------	-------	0.6

Table 2. 12: Sequencing primers for the SLC34A1-sense and- antisense HDR cassette.

Oligo ID	Sequence (5'-3')
F1-Puro	GTCGACAATCAACCTCTG
R1-Puro	AGAAGGCACAGTCCTAGAG
R2-Puro	CAGAATAGAATGACACCTAC
R3-Puro	GAAGGCATAGGCAGAGGTC
F2-Puro	CTCTAGGACTGTGCCTTCT

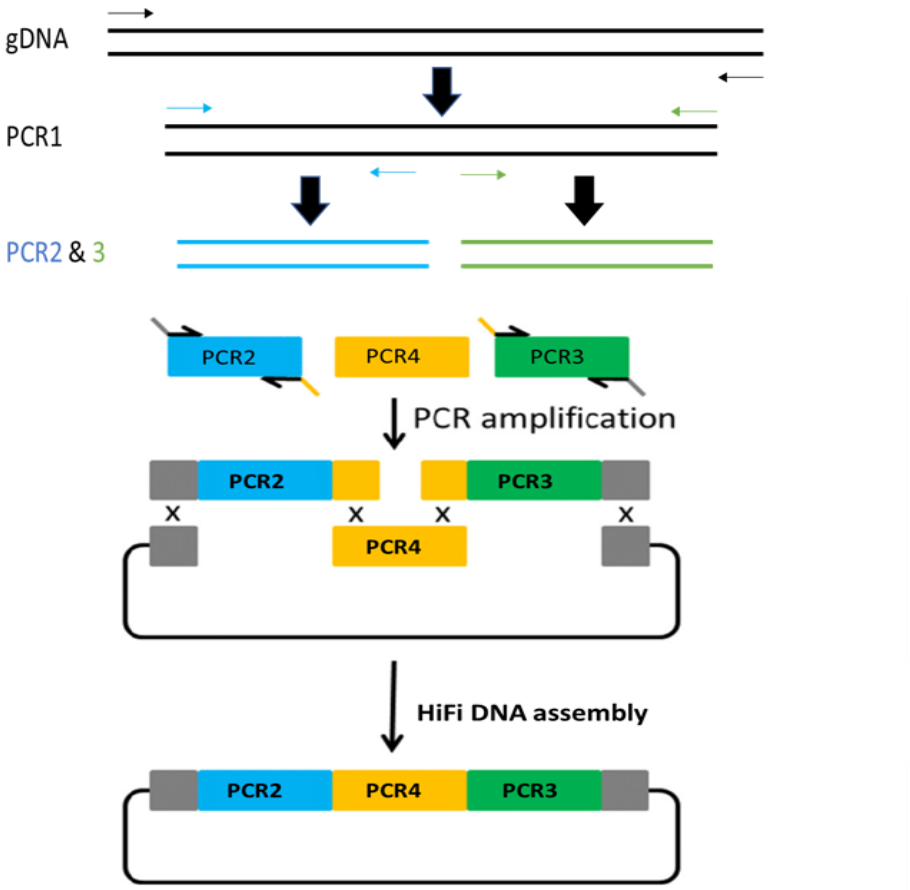

Figure 2. 4: Cloning strategy for SLC34A1-sense/antisense HDR templates. The individual amplicons were assembled using a HiFi assembly cloning kit. PCR1 represent the first PCR products (black), PCR2 (blue) and PCR3 (green) are the 5' and 3' flanking arms. PCR4 (yellow) represents the transcription termination cassette (CMV-PURO-BGH).

2.10.7. Antibiotic killing curve

Prior to the co-transfection of HEK293 cells with the Cas9 plasmid and the HDR constructs, the susceptibility of cells to the selective antibiotic, puromycin, was determined. HEK293 cells were seeded in 24-well plates at a density of $5x10^4$ cells in 500 µl of complete growth medium per well. On the next day, confluent cells were exposed to a range of puromycin concentrations, i.e. 0, 0.1, 0.25, 0.5, 1, 2, 3, 4, 5, 6, 8 and 10 ug/mL. The media containing the antibiotic were replaced every 48 h. The wells were examined daily, and images were taken using the EVOS™ XL Core Imaging System.

The optimal antibiotic concentration was determined as the lowest antibiotic dose that kills all the cells after 7 days of treatment. A similar approach was followed for neomycin and hygromycin which were also used in other experiments.

2.10.8. Co-transfection and serial dilution

HDR plasmids were linearised with *BamH*I enzyme (NEB, UK). The digestion reaction was assembled as in table 2.13. Next, 1 µl of the linearised plasmid was analysed on a 1 % agarose gel and the rest was purified using the GeneJET PCR Purification Kit (Thermo Scientific, UK). Eluted DNA concentrations were quantified with Nanodrop (Thermofisher, UK).

Table 2. 12: HDR cassette linearisation with *BamH*I

Reagent	Volume (µl)
10x CutSmart® Buffer	2
***BamH*I**	1
DNA (1-2ug)	variable
Nuclease-free water	To 20
incubation at 37 ºC for 1 h	

For co-transfection, HEK293 cells were seeded in 24-well plates at $5x10^4$ cells in 500 µl of complete growth medium per well. At 70-80 % confluency, the growth medium was replaced with 500 µl of pre-warmed medium for 2 h prior to co-transfection. HEK293 co-transfection was performed in duplicates for each condition using Lipofectamine 2000 (Thermo Scientific, UK) as follows:

Table 2. 13: HEK293 HDR and sgRNA co-transfection conditions.

Co-transfection condition	pSp-Cas9 (ng)	Linearised HDR cassette (ng)	Note
1	250	None	Plasmid integrity/GFP, Cas9 and gRNA expression
2	250	250	Co-transfection
3	None	250	Transfection efficiency (HDR cassette cytotoxicity)
4	None	None	Negative control

On the following day, the transfection mix was replaced with fresh pre-warmed medium and the transfection efficiency was measured using fluorescence microscopy (Nikon A1R fluorescence microscope, Bio-Imaging Facility, Newcastle University). Transfected cells were incubated for at least 72 h prior to antibiotic selection.

In order to isolate single clones with an integrated HDR cassette in SLC34A1-sense and- antisense orientation, co-transfected cells were serially diluted in a 96-well plate. An initial cell inoculum (4000 cells) was placed in A1 of the 96-well plate and then diluted across the entire plate (Figure 2.5). Complete growth medium supplemented with puromycin (1 µg/mL) was used to grow the cells and was replaced twice a week. At day 10, wells were examined and wells which showed a single cell colony were marked and transferred into a 24-well plate in duplicates. The first well was used for gDNA extraction, the second one was further propagated.

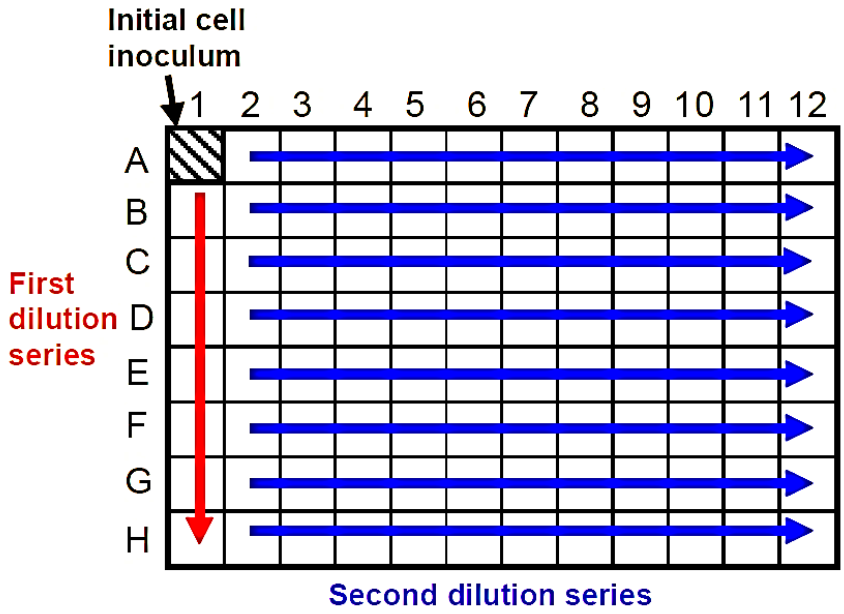

Figure 2. 5: Serial dilution of co-transfected HEK293 cells in 96 well plates.

2.10.9. Genotypic PCR

The gDNA was purified from one of the two wells using the Wizard® Genomic DNA Purification Kit (Promega, UK). For detection of the HDR cassette within SLC34A1-sense and- antisense genomic regions, HDR-targeted genotyping was performed according to Ran *et al* (2007). Primer pairs which anneal approximately 500 bp up- and down-stream of the HDR cassette were designed (Table 2.15).

Table 2. 14: SLC34A1-sense/antisense genotyping PCR primers and amplicon lengths.

Oligo ID	Sequence (5'-3')	Amplicon (Knock-in)	Amplicon (control)
Sense-F	CACCGCGCCCCATATAACATGTC	4112	2222
Sense-R	CAATGCCCTGGCCTACGGATTC		
Antisense-F	CATGGGACTTCCTGCCTCGCTG	4315	2425
Antisense-R	CATCGTGGGCCATGCGGACA		

PCR annealing and extension temperatures for SLC34A1- sense and-antisense primers pairs were optimised (Table 2.16) using the GoTaq® Long PCR 2 x Master Mix. PCR products were separated on a 1 % agarose gel and clones which showed mono- or bi-allelic HDR cassette insertion were confirmed by sequencing (GATC Biotech, Germany).

Table 2. 15: PCR master mix and cycling conditions for *SLC34A1*-sense and-antisense genotyping.

Master Mix			**PCR conditions**				
Reagent	**25 µl**	**Step**	**Temp ºC**		**Time**		**Cycle**
			S	**AS**	**S**	**AS**	
GoTaq® Long PCR 2xMaster Mix	12.5	**Initial Denaturation**	94	94	2 min	2 min	1
Forward (10µM)	1.25	**Denaturation**	94	94	30 sec	30 sec	25
Reverse (10µM)	1.25	**Annealing**	59	59	10 sec	10 sec	
Template DNA	100 ng	**Extension**	65	70	4 min	3 min	
		Final Extension	72	72	10 min	10 min	1
Nuclease-free water	to 25	**Hold**	4-10 ºC				

2.11. Chromatin Immunoprecipitation (ChIP)

To perform ChIP experiments, HEK293 cells were seeded at $1.5x10^6$ cells in T-25 flasks. When cells reached 70-75 % confluency, the growth medium was replaced with medium containing 100 nM/mL Dex. Treated and non-treated cells were maintained 5 days and growth media (±Dex) were replaced every 48 h. ChIP experiments were planned and executed in collaboration with Prof Jelena Mann, Translational and Clinical Research Institute, Newcastle University.

2.11.1. Crosslinking and chromatin sharing

Chromatin was cross-linked by adding 1 % formaldehyde to the cell medium, gentle swirling and incubation for 5 min at room temperature. The crosslinking reaction was terminated by adding 0.125 M glycine for 5-10 min. Cells were washed with 1x PBS and harvested using a cell scrapper in 10 mL of ice-cold PBS. The cells were centrifuged (15,000xg for 5 min), the resulting cell pellets were lysed in SDS lysis buffer and incubated on ice for 20-25 min (1 % SDS, 10 mM EDTA, 50 mM Tris-HCl pH 8.1, 300 µl/ $2-3x10^6$ cells).

The lysed cells were sonicated using a Bioruptor® Pico sonication device (Diagenode sonication, UK), with 10 cycles at high intensity for 30 sec on and 20 sec off. After completion, samples were centrifuged for 10 min at 17,000xg at 4 ºC and the supernatant was collected. Chromatin concentration (2 µl of supernatant in 98 µl of water) was measured using Nanodrop (Thermofisher, UK). The chromatin samples were stored at -80 ºC.

2.11.2. Immunoprecipitation

For the immunoprecipitation reactions, sheared chromatin samples were diluted 1:10 in dilution buffer (0.01 % SDS, 1.1 % Triton, 1.2 mM EDTA, 16.7 mM Tris-HCl pH 8.1 and 167 mM NaCl). 50 µl of Pierce™ Protein A/G Magnetic Beads (Thermo Scientific, UK) were added to each 1 mL of the diluted chromatin samples and incubated at 4 ºC for 15-20 min, with constant rotation to remove material that binds unspecifically to the beads. The mixture was centrifuged using a table top centrifuge at 4500xg, 4 ºC for 5 min and the supernatant was recovered. 5 µg of the selected antibodies (Table 2.17) were added to the cleared supernatant and incubated overnight at 4 ºC.

On the next day, another 50 µl of Protein A/G Magnetic beads were added and the mixture was incubated for 45 min at 4 ºC and 15 min at room temperature. The chromatin bound to the beads was centrifuged as above and the pellet was washed twice with 1 mL of low salt buffer (0.1 % SDS, 1 % Triton, 2 mM EDTA, 20 mM Tris-HCl pH 8.1 and 150 mM NaCl), high salt buffer (0.1 % SDS, 1 % Triton, 2 mM EDTA, 20 mM Tris-HCl pH 8.1 and 500 mM NaCl), LiCl buffer (0.25 M LiCl, 1% NP40, 1 % deoxycholate, 1 mM EDTA and 10 mM Tris-HCl, pH 8.1) TAE buffer (Tris-EDTA) followed by centrifugation in a refrigerated table top centrifuge (5000x g for 1 min). Chromatin was eluted with 250 µl of nuclease free water.

2.11.3. Reverse crosslinking and DNA purification

20 µl of 5 M NaCl were added to 500 µl of immunoprecipitated chromatin. The samples were incubated at 65 ºC for 4 h. Histones were digested with proteinase K (2 µl of 10 mg/mL stock) at 45 ºC for 1 h after adjusting the reaction conditions with 10 µl of 0.5 M EDTA, 2 µl 1M Tris-HCl, pH 6.5. DNA was recovered by phenol/chloroform extraction and ethanol precipitation. Recovered DNA was dissolved in 40 µl of nuclease-free water.

Table 2. 16: Antibodies used for HEK293 Chromatin immunoprecipitations.

Antibody	Source	Cat no.	LOT no.	Amount used/ IP (µg)
H3K27ac	Diagenode	C15410174	A7071-001P	5
H3K4me3	Diagenode	C15410030	002	5
Rabbit IgG	Diagenode	C15410206	RIG001S	4

2.11.4. ChIP-qPCR

Real time PCR was used to quantify the level of histone modification at SLC34A1-sense and- antisense promotor and enhancer regions. Three pairs of primers were designed to anneal approximately 400- 500 nucleotides upstream of the transcriptional start site (TSS) of SLC34A1-sense and (700-800) nucleotides upstream of the first SLC34A1-antisense transcript exon. Additional primers were designed to span an SLC34A1-sense intronic enhancer region (Table 2.17, Figure 4.9).

Table 2. 17: Primers for ChIP-qPCR and product length. Amplicons cover the SLC34A1-sense and -antisense promoters and an SLC34A1-sense internal enhancer (i.e. SLC34A1-B).

Oligo ID	Sequence (5'-3')	Amplicon (bp)
SLC34A1-A-F3	GCCATAGGATGTTTGGGTCA	167
SLC34A1-A-R3	AGCTCTGCATGGGGAATCTA	
SLC34A1-B-F2	GTGTTTGTGCGTGTGAGTCT	193
SLC34A1-B-R2	CCACTATGAGGTCTGCAGGT	
AS-SLC34A1-F3	TATAGGATCGTGTCGCTGCA	193
AS-SLC34A1-R3	ACGCCTGTAATCTCGTCACT	

ChIP-qPCR comprised 5µl Sybr Green I Master mix, 0.5 µl forward and 0.5 µl reverse primers (10 µM), 2 µl of the eluted DNA and 2 µl of water per well. Plates

were centrifuged briefly using a plate centrifuge for 2 × 20 sec intervals at full speed; the temperatures and cyclic conditions are given in table 2.19.

Table 2. 18: ChIP-qPCR cycling conditions.

Step	Temp °C	Time	Cycles
Pre-incubation	95	10 min	1
Initial Denaturation	95	1 min	1
Denaturation **Annealing** **Extension**	96 57 72	20 sec 30 sec 10 sec	45
Melting Curve	95 60 95	15 15 0 } sec	
Cooling	40	30 sec	

2.11.5. ChIP- qPCR data normalization

All ChIP-qPCR data were normalized to the negative control consisting of rabbit anti-IgG precipitated material. The fold change (R) was determined using the formula below (Haring *et al.*, 2007):

$$R = 2^{(Ct\ of\ H3K27Ac/H3K4Me3 - Ct\ of\ IgG)}$$

2.12. Microbiome experiment design

The microbiome part of this thesis represents a significant part of an extended project previously designed by Prof Carsten Wagner, Institute of Physiology, Zurich University. The study aimed to mimic high/low Pi – but a low Pi diet without medical reason is a health risk, hence Pi binders were used to lower dietary Pi load.

Two groups of probands consisting of eight male volunteers each were included in a cross-over study (Figure 2.6): The first group started with a high phosphate diet for 5 days (1000 mg/lunch and dinner meal) followed by a wash-out period of 10 days and a period of phosphate binder intake with normal Pi diet for 5 days. The second proband group followed a similar regime, however they started with the phosphate binder. At the end of the intervention, samples of stool, urine and blood were collected.

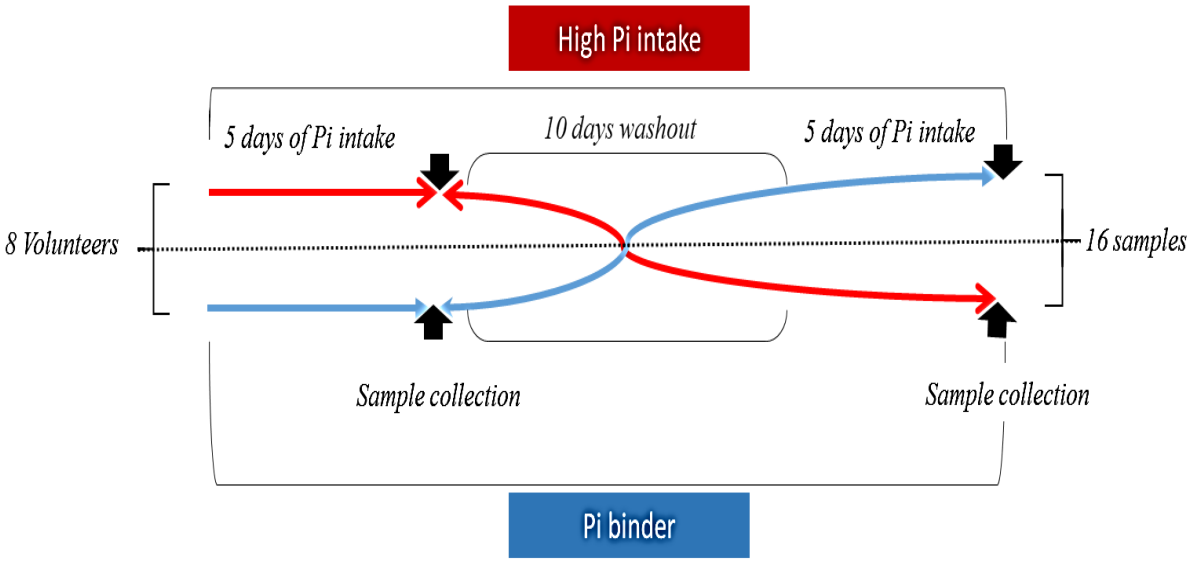

Figure 2. 6: Schematic presentation of the high and low Pi diet regime applied in the human cross-over study.

While other parameters such as urine phosphorus level, kidney function and liver function were measured using the urine and serum samples, the collected stool samples were shipped in to the Institute of Food Research in (Norwich, UK) for downstream analysis.

2.12.1. DNA extraction from stool samples

DNA was extracted from stool samples using the FastDNA™ SPIN Kit for Soil (MP biomedicals, UK). Stool samples were thawed on ice for 1 h prior to the experiment. Approximately 500 mg of each sample was weighted and loaded on Lysing Matrix E tubes containing 987 µl of PBS and 122 µl of MT buffer. Samples were homogonised using a Fast Prep homogeniser (MP Biomedicals, UK) for 40 sec at 6.0 speed setting. Contaminating debris were eliminated by centrifugation at 14,000xg for 15- 30 min.

The supernatant was transferred to a 1.5 mL Eppendorf tube containing 250 µl of protein precipitation solution and mixed immediately by inverting the tubes 4- 6 times. The samples were centrifuged at 14000xg for 5 min and the supernatant was collected in 1.5 mL Eppendorf tubes. 1 mL of binding matrix suspension was added, mixed by inversion for 2 min and the tubes were left for 3 min for the resin to settle. 500 µl of the supernatant were discarded carefully and the remaining matrix was transferred into SPIN™ Filter columns and centrifuged at 14,000xg for 1 min. The filters were washed with 500 µl of SEWS-M solution and air dried for 5 min at room temperature. Genomic DNA was eluted by adding 30 µl of nuclease free water and centrifugation at 14,000xg for 1 min. The collected DNA samples were quantified and stored at -20 ºC.

2.12.2. DNA quantification

The extracted DNA was quantified using a Qubit Fluorometric Quantitation unit (Invitrogen, UK). According to the manufacturer's instruction, a working solution was prepared by diluting the Qubit reagent in dsDNA Qubit buffer (1:200) for both standard and test samples. 190 µl of working solution were used for the standard and 198 µl for the test samples and the volume was brought to 200 µl with the standard and DNA samples, respectively. The tubes were vortexed for 2-3 sec, incubated at room temperature for 2 min and DNA concentrations were recorded from the Qubit® 2.0 fluorometer. DNA extraction was repeated for samples that showed a concentration of less than 30 ng/µl.

2.12.3. DNA sequencing and data analysis

Approximately 500 ng of genomic DNA per sample were custom sequenced at the Sanger Institute, Cambridge, UK using a MiSeq platform (Illumina) following established protocols.

The data were analysed in collaboration with Dr Christopher J. Stewart. The cut-off level of sample readout was set at 95,200 reads to eliminate noise that could result from the DNA extraction procedure. The bacterial communities were visualised using R (R Development Core Team, 2014). Statistical analysis to determine Alpha diversity was done by Kruskal–Wallis testing and determination of the Shannon index (Kruskal and Wallis, 1952; DeJong, 1975). The differences in the microbial composition between samples (Beta diversity, or Bray Curtis) were assessed using Permutational analysis of variance (PERMANOVA). Using the R lm () function simple regression models to compare multiple measures in alpha diversity or for multiple taxonomic genera were created.

2.13. Statistical Analysis

Unpaired student t-testing was used to compare pyrosequencing data. For RT-qPCR data, one-way ANOVA followed by Games-Howell Post-Hoc test or Tukey's test for multiple comparisons was performed using GraphPad Prism version 6.00 (GraphPad Software, USA). Values of $p<0.05$ were considered as significant, unless otherwise mentioned. Data are presented as mean ± standard error of the mean (SEM).

Chapter 3: The impact of DNMT and HDAC inhibitors on *SLC34A1*-sense and *SLC34A1*-antisense expression

3.1. Introduction

Eukaryotic chromatin represents packed genetic material that encodes for proteins with biological activities to coordinate development, metabolism and ensure tissue specificity. As described in Chapter 1, DNA methylation and histone modifications regulate the transcription process (on/off switch). These marks are called epigenetic modifications and are defined as regulators of gene expression independent of specific genomic sequences. Aging as well as nutritional and environmental factors affect the epigenetic status (Heerboth *et al.*, 2014). For example, natural and synthetic compounds can induce alterations in epigenetic marks with a regulatory effect on specific genes or genome wide expression (Ma *et al.*, 2014).

Aberrant DNA methylation interferes with the expression of coding and noncoding genes and may result in pathological conditions and promote tumorigenesis. Hypermethylated DNA is transcriptionally inactive, but compounds that reduce global DNA methylation can activate gene expression. Inhibitors of DNA methylation act either by forming a covalent bond with the DNMT enzymes (DNMT1, DNMT2, DNMT3a, DNMT3b, and DNMTL) and/or by substrate competition as cytidine analogues (Zhou *et al.*, 2002).

Zebularine (Zeb) is a potent second-generation DNMT inhibitor, a member of a drug family which also includes 5-azacytidine and decitabine, and acts as a cytidine analogue (Figure 3.1). In comparison to 5-azacytidine and decitabine, Zeb is characterised by low cytotoxicity and a long half-life at different environmental pH (i.e. the half-life of Zeb at pH 1.0 is 44 h and at pH 7.0 is 508 h) (Cheng *et al.*, 2003).

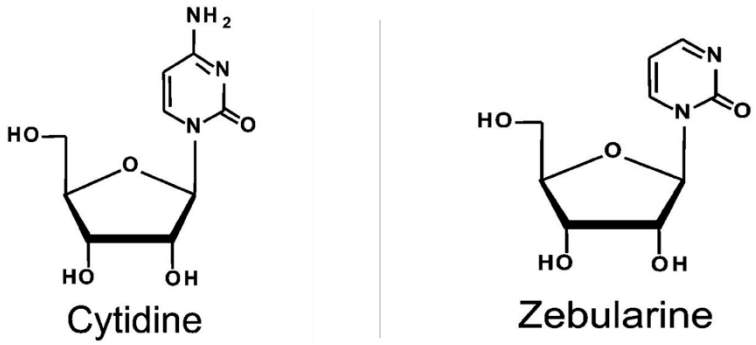

Figure 3. 1 : Chemical structure of cytidine and its analogue Zebularine. The structure of Zebularine is almost identical to cytidine with only the amino acid group at position 4 lacking (Yoo *et al.*, 2004).

Histone de-acetylase (HDAC) inhibitors are another group of powerful epigenetic regulators of gene expression. For example, trichostatin A (TSA), an irreversible inhibitor of HDAC
type I and II enzymes, has diverse effects on both coding and noncoding RNA expression and has been applied in various cells models (Serman *et al.*, 2006; So *et al.*, 2007; Yang *et al.*, 2013).

In the present study, we hypothesised that the two drugs Zeb (DNA methylation inhibitor) and TSA (histone deacetylation inhibitor) could potentially induce transcription of the bi-directional SLC34A1 locus, thus providing clues for the biological function of the antisense transcript.

3.2. Aims:

This chapter aimed to establish and characterise a cellular system that enables research into the expression of endogenous sense and antisense RNA and their interaction at transcriptional level. The specific goals are:

- Identify one or more cell lines that express *SLC34A1*-sense/antisense transcripts in response to DNMT and HDAC inhibitors. Moreover, the expression levels of both transcripts will be quantified.
- Determine the epigenetic imprints that may be responsible for the transcriptional changes.

3.3. Results

3.3.1. Optimisation conditions

Total RNA was purified from human-derived kidney cell lines including HEK293, HKC8 and HK2 in addition to primary human renal epithelial cells at the time they were taken into culture (PT0) and after 10 days (PT10) as positive controls. TRIzol® was used for RNA extraction followed by DNase-I digestion. RNA integrity was usually examined by 2 % agarose gel electrophoresis (Figure 3.2). The experiment was repeated routinely following RNA extraction for each treatment condition.

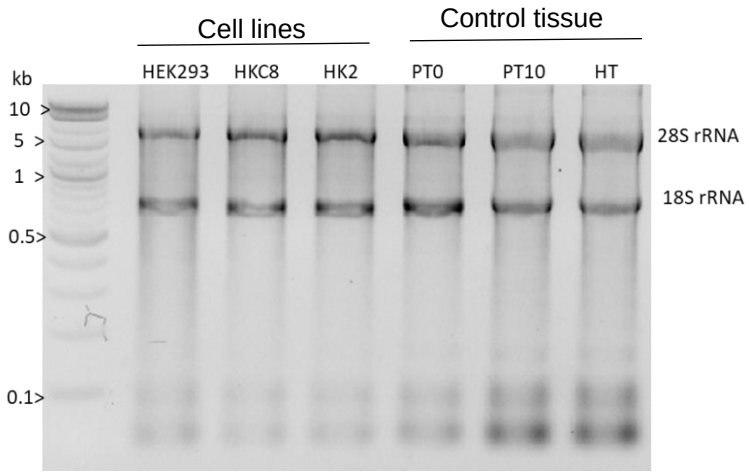

Figure 3. 2: RNA integrity test. About 0.5-1µg of purified RNA was examined using 2 % agarose gel electrophoresis prior to cDNA synthesis and RT-qPCR.

To establish a robust PCR-based quantification strategy, a total of eleven primer pairs for each *SLC34A1*-sense and *SLC34A1*-antisense transcripts were designed and tested by RT-PCR (Appendix A and B). As positive controls, proximal tubular cells and human testis RNA (HT) were used, shown in figure 3.3.B. The sense primer pairs 4, 5, 10 and 11 and the antisense primer pairs 2 and 9 showed specific amplicons of the correct size. The assays including primers 5 and 9 for the sense and antisense, respectively, were selected for RT-qPCR after sequence confirmation. Since RT-qPCR is very sensitive and secondary primer products could form, different annealing temperatures were tested. Gradient PCR examination showed that 63 ºC were considered as the optimal temperature for *SLC34A1*-sense/antisense as well as *GAPDH* amplification as illustrated in figure 3.3.C.

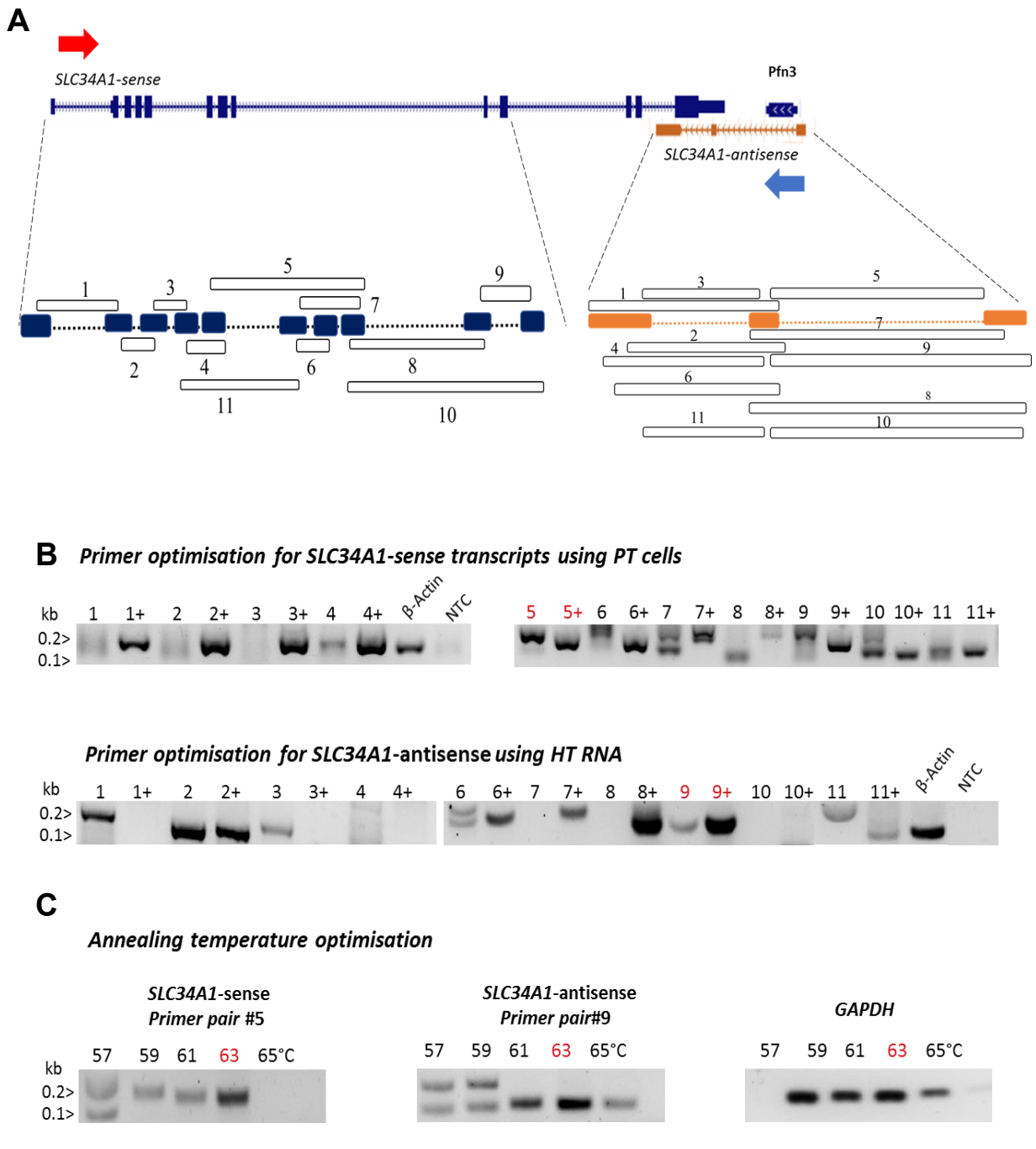

Figure 3. 3: Optimisation experiments for RT-qPCR. A) Diagram of SLC34A1 locus showing primer pairs that target SLC34A1-sens/*antisense* transcripts. B) RT-PCR for eleven different *SLC34A1*-sense/antisense primer pairs using PT and HT RNA, respectively. The lanes labelled (+) refer to control reactions using plasmid DNA as a template. Negative template control (NTC, no DNA) were included. C) Different annealing temperatures were tested for the chosen *SLC34A1*-sense/antisense and housekeeping (*GAPDH*) genes. Red highlighted pairs/conditions were chosen for further experiments. The red highlighted numbers indicate to the optimally working primer pairs and annealing temperature.

3.3.2. Screening of cell lines

The next step was to establish the expression status for *SLC34A1*-sense and-antisense transcripts in the human renal cell lines HKC8, HK2 and HEK293. Human primary renal proximal cells (PT0 and PT10) and human testis RNA (HT) were included as controls in RT-qPCR experiments.

As presented in figure 3.4.A, *SLC34A1*-sense expression was found at various levels in HKC8, HK2, PT0, PT10 and HT, but not in HEK293 cells. Interestingly, HKC8 cells were found to express *SLC34A1*-sense transcripts at higher levels than HK2 cells (ΔCt 18.56 ±1.19 versus 21.39 ±0.46). This suggested that HKC8 may be used to study the sense transcript expression in further investigations during the thesis.

In line with observations in the Brown lab, a gradual reduction in transporter mRNA levels was observed between PT0 and PT10 cells (ΔCt 12.40 ±0.12 and 20.70 ±0.52, respectively) which points to altered primary cell characteristics with continued culture time (Kaur and Dufour, 2012).

On the other hand, none of the tested cells expressed the *SLC34A1*-antisense transcript. Only the positive control, HT, showed a detectable signal (ΔCt average 18.5 ±49) as demonstrated in figure 3.4.B.

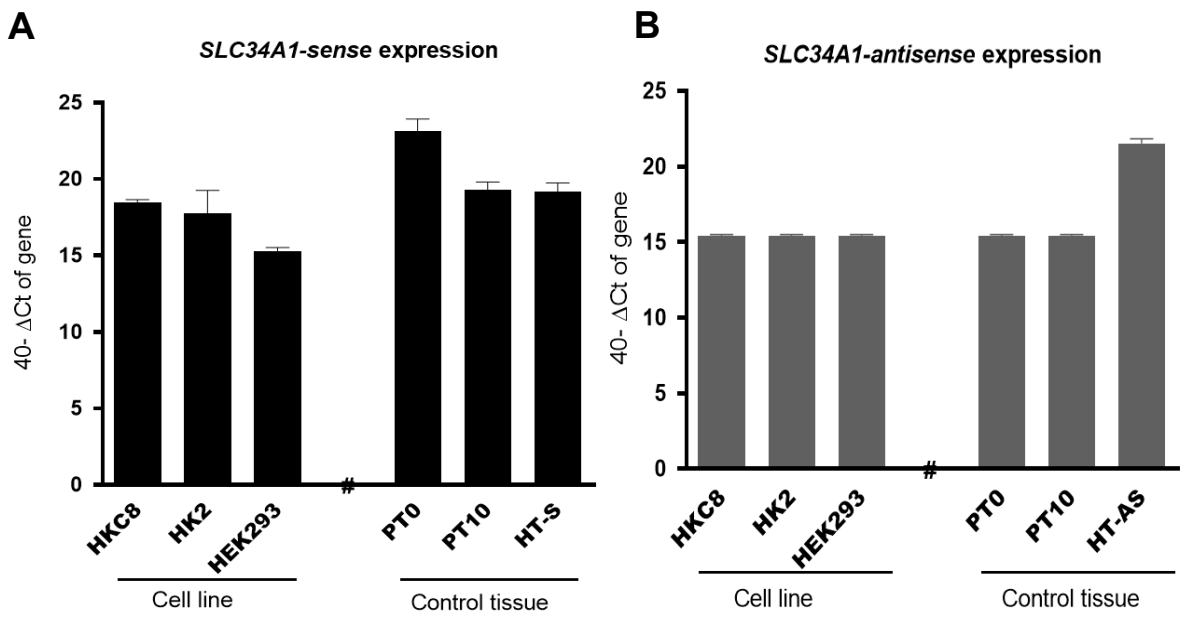

Figure 3. 4: *SLC34A1*-sense/antisense gene expression using RT-qPCR. A) *SLC34A1*-sense expression in PT0, PT10, HKC8, HK2, HEK293 cells and HT. B) *SLC34A1*-antisense gene expression. Data presented are from three independent experiments each done in triplicate. The data were normalised to *GAPDH*, and gene expression calculated as ΔCt. For clarity reason the difference shown as (40- ΔCt).

The antisense transcript expression was previously detected in HEK293 cells (Piatek *et al.*, 2016), however, these findings were later suspected to be a PCR artefact. However, NATs expression could also be variable and inconsistent with different cell passages. Hence, HEK293 and HKC8 cells were therefore used for further experiments.

3.3.3. The effect of Zeb and TSA on cell viability

The effect of Zeb and TSA on HEK293 and HKC8 cells was determined using the XTT assay (Berridge *et al.*, 2005). The assay is based on the reduction of the XTT (2,3-bis-(2-methoxy-4-nitro-5-sulfophenyl)-2H-tetrazolium-5-carboxanilide) into orange coloured formazan salts in the presence of mitochondrial dehydrogenases (Figure 3.5). The accumulation of formazan salts changes the colour of the growth medium to dark-brown which is subsequently quantified by spectrophotometry. The

absorbance values were corrected by subtracting the background (growth medium alone) and normalised to the negative control (non-treated cells).

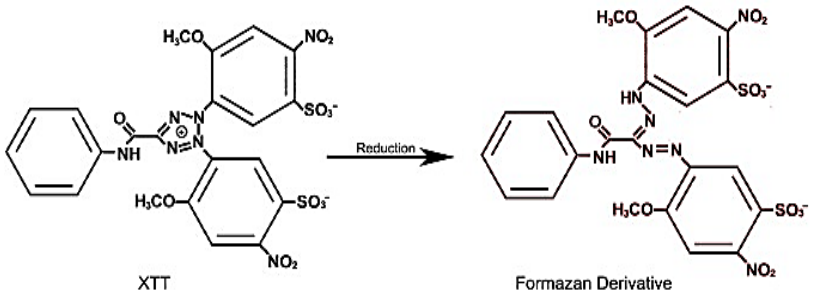

Figure 3. 5: Mechanism of action for the XTT assay. XTT is reduced to formazan in the presence of mitochondrial dehydrogenases, figure adapted from (Berridge *et al.*, 2005).

HEK293 and HKC8 cells were seeded in 96-well plates and each treatment condition was tested in 6-wells. Zeb was used at 25, 50, 100 and 200 µM concentrations and viability was assessed after 12, 24, 48, 72 and 96 h of treatment.

HEK293 cells showed reduced viability in a time-depended manner when treated with 25, 50, 100 and 200 µM Zeb for 96 h to 62.6, 56.6, 54.3 and 37.8 %, respectively. In contrast, HKC8 showed decreased viability only with the two highest concentrations tested (100 and 200 µM, 30.2 and 13.04 % remaining of viability, respectively). The effect was seen across all time-points (Figure 3.6.A).

The histone deacetylase inhibitor TSA was used at various concentrations, i.e. 0.25, 0.5, 1 and 2 µM. In HKC8, TSA treatment with 1 and 2 µM of the drug was found to dramatically reduce metabolic activity in a time-and -dose dependent manner. At concentrations higher than 1 µM the drug gradually killed the cells within about five days. Conversely, HEK293 were more resistant to TSA, as demonstrated in (Figure 3.6.B).

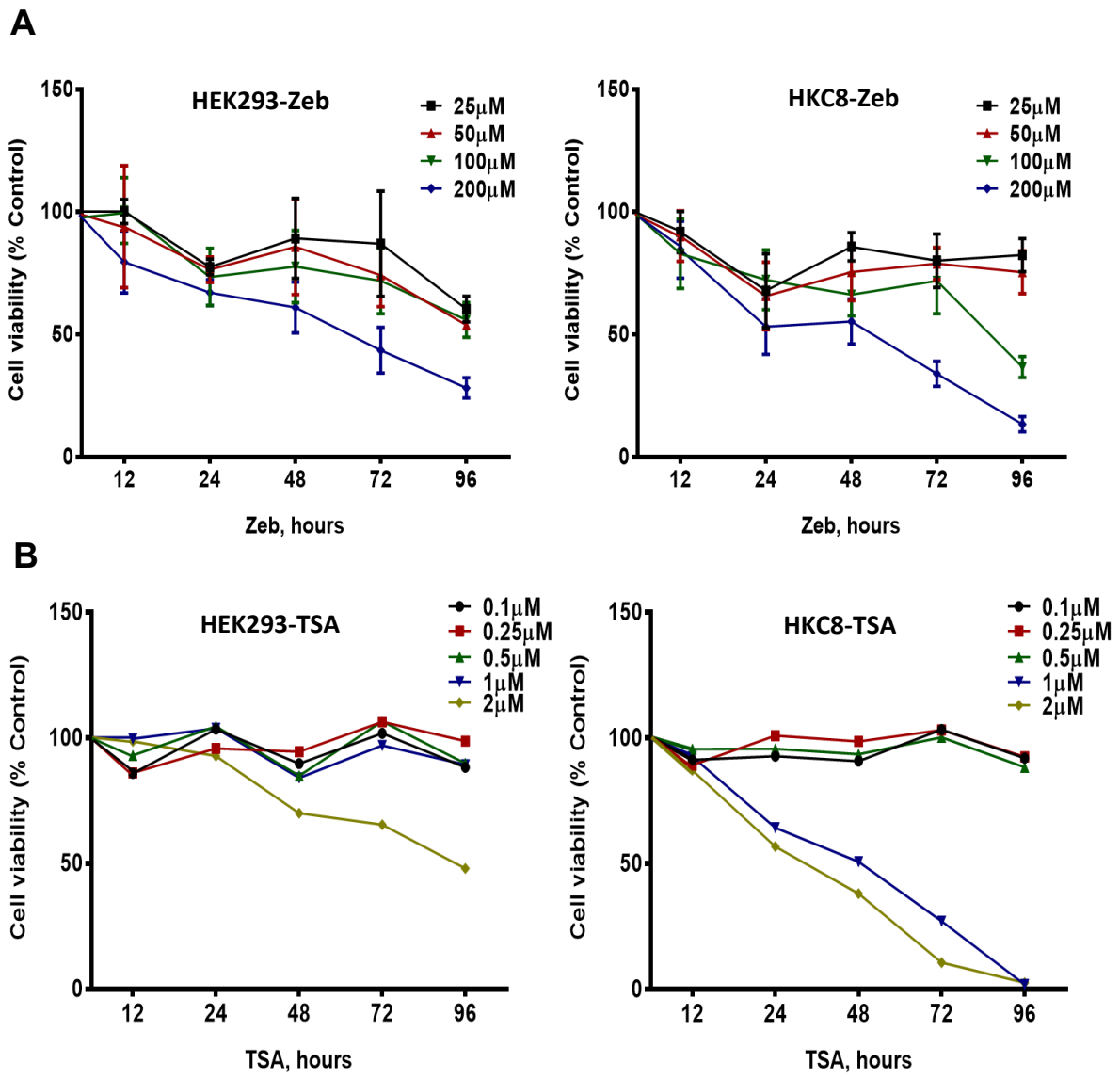

Figure 3. 6: HEK293 (left panel) and HKC8 (right panel) cell viability in response to Zeb and TSA treatment. A) Zeb induced reduction in viability in HEK293 and HKC8 cells. B) TSA treatment reduced cell viability in HKC8, and to lesser extend in HEK293 cells. Measurements were corrected for the absorbance of the culture medium and then normalised to the control sample (non-treated condition).

3.3.4. Zebularine induces SLC34A1-sense upregulation

The effect of DNMT inhibitors on the transcription of *SLC34A1*-sense and- antisense RNAs has not been investigated and may reveal mechanistic insights into the regulatory impact of NATs in somatic cells. Previous work showed that continuous

treatment of the human bladder transitional carcinoma-derived cell line T24 with low concentrations of Zeb resulted in reduced DNMT activity and global demethylation. As a consequence, increased expression of various genes was driven by poorly methylated CpG-rich promoters (Cheng *et al.*, 2004). Comparable observations were made with human breast cancer cell lines (MDA-MB-231 and MCF-7) where Zeb induced the expression of *p21* and decreased cyclin-D transcription in time-depended manner. These results suggested that Zeb could be used as a potent demethylating agent (Baubec *et al.*, 2009; Billam *et al.*, 2010). Hence, we hypothesised that continuous exposure to Zeb could also impact on transcription levels of the SLC34A1 locus.

Based on the results of the XTT assay, HKC8 and HEK293 cells were treated with Zeb at different concentrations (i.e. 25, 50, 100 and 200 µM) for 72 h followed by RNA extraction and RT-qPCR. The data were normalised to *GAPDH* and expression changes refer to non-treated cells.

In general, Zeb induced upregulation of *SLC34A1*-sense in a dose-dependent manner in HKC8 and HEK293 cells after 72 h, however no effect on the *SLC34A1*-antisense transcript was detected. HKC8 cells showed significant upregulation of *SLC34A1*-sense transcripts at 50 µM (2.99 ±0.84-fold, $p<0.05$), whereas with 100 and 200 µM *SLC34A1*-sense increased 1.06 ±0.55 and 1.74 ±0.37-fold, respectively.

In contrast, HEK293 cells exposed to 50 µM Zeb for 72 h only showed a slight increase of *SLC34A1*-sense expression (1.40 ±0.67-fold) with minimal effects of other doses of Zeb (Figures 3.7.A and B). The observation that 100 and 200 µM of the drug reduced the expression of the *SLC34A1*-sense transcript as compared to the 50 µM dose is probably due to toxicity of the drug at higher doses and a concomitant decrease in RNA quality (Figure 3.7).

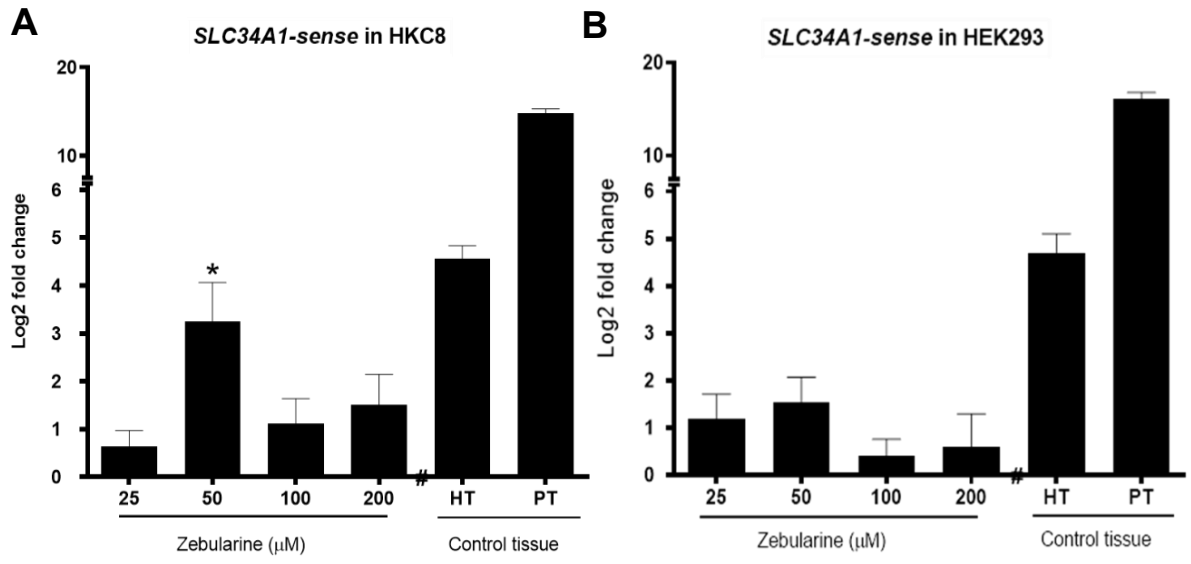

Figure 3. 7: Zebularine upregulates *SLC34A1*-sense expression in HKC8 and HEK293 cells in a dose-independent manner. A) HKC8 and B) HEK293 cells were treated with 25, 50, 100 and 200 µM of Zeb for 72 h. The experiments were performed in three independent replicates. Experimental controls from human proximal tubular cells and human testis (PT and HT) were routinely included in RT-qPCR experiments. The data were normalised to *GAPDH* and the fold change ($2^{-\Delta\Delta Ct}$) were calculated in comparison to the non-treated cells. To compare between treatment conditions, statistical differences were determined by One-Way ANOVA and Games-Howell Post-Hoc test (* P<0.05).

3.3.5. Temporal effect of zebularine on SLC34A1-sense and- antisense transcripts

Since both *SLC34A1*-sense and *SLC34A1*-antisense transcripts derive from the same bidirectional genomic locus, it is conceivable that potential epigenetic modifications would impact on the expression levels of both transcripts in a time-dependent manner. Therefore, a time-course investigation was performed to further characterise the effect of Zeb on the potentially co-regulated locus. HEK293 and HKC8 cells were treated with 50 µM Zeb for 12, 24, 48 and 72 h followed by RNA extraction and RT-qPCR.

In HEK293 cells, neither sense nor antisense expression was detected at any tested time-points, except the slight upregulation of *SLC34A1*-sense in response to 50 µM after 72 h (as described in 3.3.4).

In contrast, time-dependent expression was observed for both SLC34A1-sense and SLC34A1-antisense transcripts in HKC8 cells (Figure 3.8). Zeb exposure induced a gradual increase in sense transcripts levels of 0.92 ±0.61-fold after 12 h, 1.85 ±0.31 after 24 h, 2.90 ±0.31 after 48 h and 2.66 ± 0.60 after 72 h. Changes were statistically significant at 48 and 72 h (at $P<0.05$). Meanwhile, expression of the antisense transcript coincided with an increase of the sense transcript. SLC34A1-antisense transcripts were only transiently detected after 24 h of drug treatment (i.e. 0.90 ±0.51-fold).

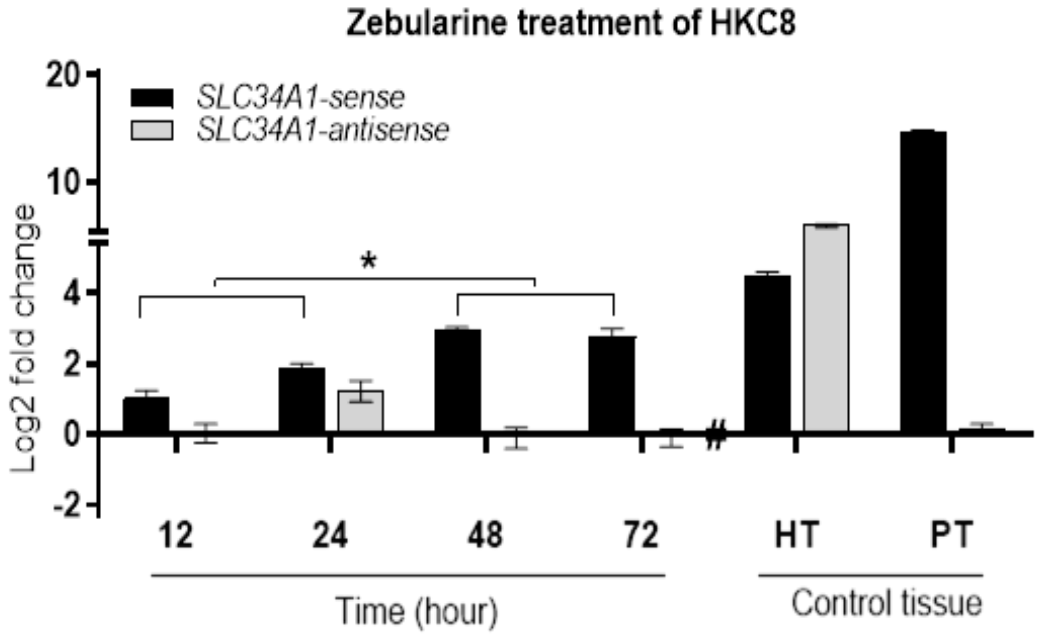

Figure 3. 8: Temporal expression of *SLC34A1*-sense and- antisense transcripts after treatment with zebularine. *HKC8 cells were treated with 50 µM of Zeb and RNA was extracted at different time points (12, 24, 48 and 72 h) followed by RT-qPCR. The experiments were performed in three independent replicates. Experimental controls from human proximal tubular cells and human testis (PT and HT) were routinely included in RT-qPCR experiments. The data were normalised to GAPDH and the fold change (2-ΔΔCt) were calculated in comparison to the untreated cells. To compare between treatment conditions, statistical differences were determined by One-Way ANOVA and Games-Howell Post-Hoc test (* p<0.05).*

3.3.6. Effect of TSA on SLC34A1-sense and- antisense expression

Previous experiments with HKC8 and HEK293 cells treated with TSA at different concentrations (0.1, 0.2, 0.5, 1 and 2 µM) confirmed the effect of the drug on cell viability. It was therefore conceivable that TSA may induce *SLC34A1*-sense and *SLC34A1*-antisense expression. According to TSA toxicity testing (Figure 3.6.B), HKC8 cells were treated for 24 h and HEK293 for 48 h with the indicated concentrations of TSA followed by total RNA extraction and RT-qPCR. The RT-qPCR data showed that TSA affected neither *SLC34A1*-sense nor the antisense expression in the tested cell lines (all values were within 10% of the untreated controls), hence global acetylation and H3 acetylation was assessed. HEK293 and HKC8 cells were treated with TSA at 0.1, 0.2, 0.5, 1 and 2 µM for 24 h followed by purification of histone fractions and SDS-PAGE separation. Furthermore, the level of H3 acetylation were quantified using EpiQuik Total Histone H3 Acetylation Detection Fast Kit. The absorbance ratios were first normalised to blank and the acetylation percentage were calculated based on the non-treated conditions (as discussed in section 2.9).

The result showed that high doses of TSA (i.e. 1 and 2 µM) increased acetylated H3 in both HEK293 and HKC8 cells, however, with a more pronounced effect in HEK293 cells. For instance, 0.5, 1 and 2 µM TSA in HKC8 caused a 20-30 % increase in H3 acetylation (127.9, 121.14 and 126.49 %, respectively). On the other hand, in HEK293 cells the amount of acetylated H3 increased significantly at 1 and 2 µM TSA to 202.13 and 191.98 %, respectively (Figures 3.9.A and B).

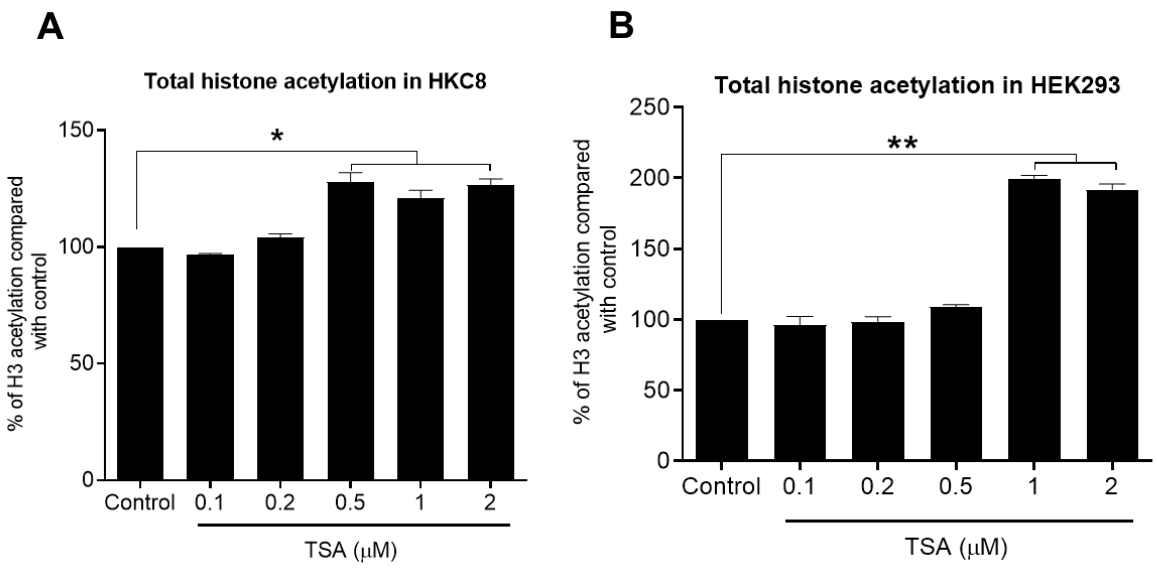

Figure 3. 9: Global histone H3 acetylation. A) HKC8 and B) HEK293 cells show a dose-dependent response to TSA. The data were normalised to control cells (non-treated) and treatment conditions were compared by One-Way ANOVA test using Tukey's test (* $p < 0.05$, ** $p < 0.01$).

3.3.7. The effect of Zeb and TSA in combination on SLC34A1 locus

Previous work by Olaharski *et al.,* have shown that both Zeb and TSA target different epigenetic marks and could have synergistic effects when used in combination (Olaharski *et al.*, 2006). This assumption has also been approved in human breast adenocarcinoma cells when the combination between Zeb and TSA induced upregulation in tumor necrosis factor-related apoptosis inducing ligand (TRAIL) transmembrane protein family (Kong *et al.*, 2019). Hence, Zeb and TSA were applied together to further characterise the effect of histone deacetylation and promoter demethylation on transcriptional activity of the SLC34A1 locus. The dose response of both compounds was tested in HKC8 and HEK293 cells with working concentrations of 50 µM Zeb and 1 µM TSA. The combination experiments were performed in three forms as suggested by (Herman *et al.*, 1995; Herman *et al.*, 1996) and illustrated in figure 3.10: (i) Zeb at 50 µM for 72 h followed by TSA at 1 µM for 24 h, (ii) 1 µM TSA for 24 h followed by Zeb at 50 µM for 72 h and (iii) both Zeb and TSA for 24 h at 50 µM and 1 µM, respectively.

RT-qPCR showed that none of the drug regimens had an impact on *SLC34A1*-sense and- antisense expression (all values were within 5% of the untreated controls). These findings were somehow unexpected since Zeb alone upregulated the expression of *SLC34A1*-sense and- antisense in a time-dependent manner. A possible explanation for the contradictory finding is that TSA combined with 5-mC inhibitors may have antagonistic rather than synergistic activity (Yang *et al.*, 2013). To further investigate the effect of Zeb on *SLC34A1*-sense/antisense expression, methylation of both sense- and antisense promoter regions was assessed by pyrosequencing.

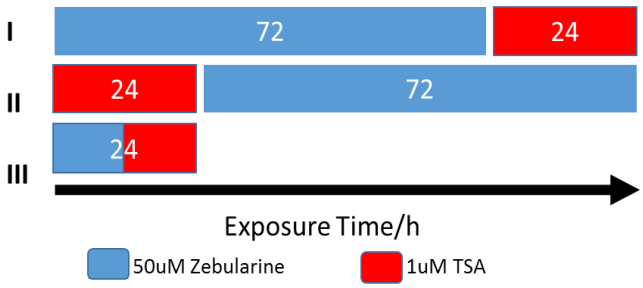

Figure 3. 10: Chart of combined Zeb and TSA incubation. The treatment included three conditions; the blue bars refer to 50 µM Zeb and the red to 1µM TSA.

3.3.8. Pyrosequencing Optimisation experiments

The reason of using this technique is to estimate and quantify the methylation percentage of target promoter in response to treatment with epigenetic compounds (see Section 2.8). However, defining the CpG rich promoter regions and the design of pyrosequencing primers is challenging because bisulfite treatment alters the DNA sequence depending on the methylation status of cytosines. The UCSC (http://genome.ucsc.edu/) and Methprimer (http://www.urogene.org/cgi-bin/methprimer/methprimer.cgi) genome browsers were used for these purposes (Kent *et al.*, 2002; Li and Dahiya, 2002). The identified CpG islands and the primers to amplify the particular regions after sodium bisulfite treatment are shown in figure 3.11.

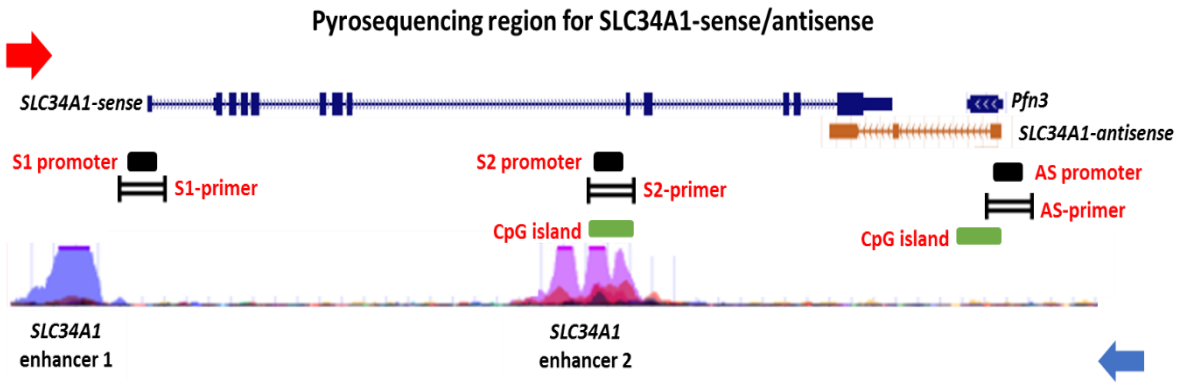

Figure 3. 11 : SLC34A1-sense and antisense regions identified for pyrosequencing. S1 and S2 refer to the sense regions with nine CpG sites whereas a region with six CpGs sites was examined in the antisense promoter region (AS). The pyrosequencing entry sequences are shown with the CpGs of interest in red.

Using bisulfite converted DNA as a template for end-point PCR proved difficult. To overcome this challenge, various polymerases were tested in addition to adjusting the annealing temperature and reducing the extension temperature to 60 °C for 5 sec (Figures 3.12.A and B) (Su *et al.*, 1996; López-Barragán *et al.*, 2011). All PCR products were examined on agarose gels (Figure 3.12.C), purified, sequenced and

confirmed against bisulfite converted DNA sequences before moving to the actual pyrosequencing experiments.

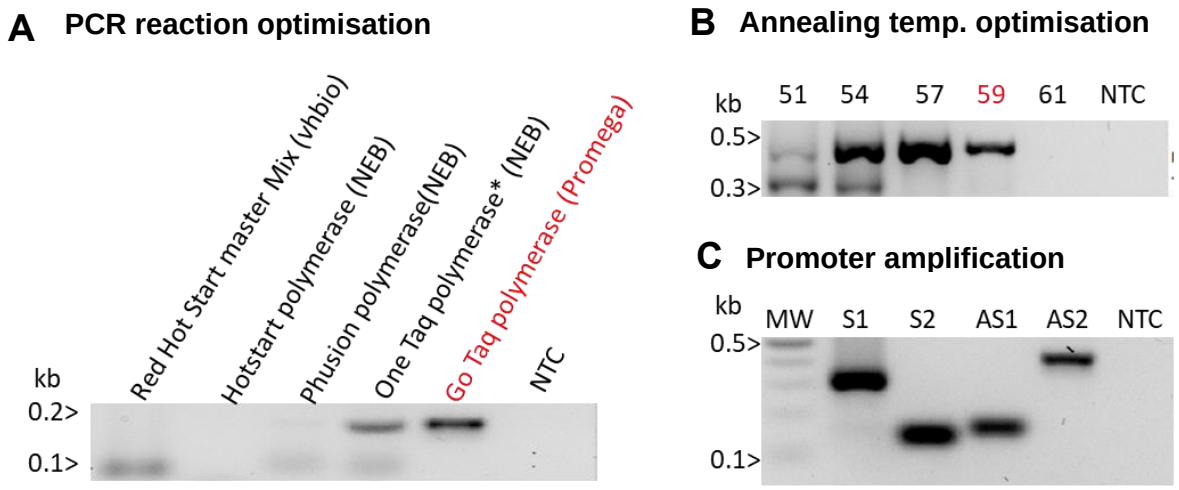

Figure 3. 12: PCR- optimisation for pyrosequencing experiments. A) Different polymerases used in end-point PCR for amplifying the target region using bisulfite modified DNA. B) Followed by gradient annealing temperature optimisation using Go Taq polymerase. C) Similar steps were applied to the other regions (S1, S2 and AS) and examined on 2 % agarose gel electrophoresis. The lengths of the amplified region as follow S1=339, S2= 148 and AS1=173bp.

3.3.9. Analysis of methylation status of selected promoters

For SLC34A1-sense, two regions were identified with typical promoter features, S1 (chr5: 176823406-176823435) and S2 (chr5:176811239-176811258) with nine CpG sites overall. For SLC34A1-antisense, one CpG island was amplified in two fragments; however, due to problems with PCR amplification, only one region was investigated with six CpG sites (AS, chr5:176827416-176827447) as demonstrated in figure 3.11.

To generate fully methylated DNA (100 % methylation) as reference sample, gDNA from non-treated HKC8 and HEK293 cells was incubated with CpG

methyletransferase (*M.Sss*I) to obtain the 100 % methylation control. In addition, whole genome amplification (WGA) was used to generate unmethylated DNA (0 % methylation). Samples were treated with *M.Sss*I followed by PCR amplification of the fragments S1, S2 and AS. The methylation of the different fragments was quantified by pyrosequencing (Table 3.1).

Table 3. 1: Average values of DNA bisulfite conversion controls (0 and 100%) in S1, S2 and AS promoter fragments.

Promoter region	% of CpG methylation in HEK293		% of CpG methylation in HKC8	
	0	**100**	**0**	**100**
AS1	1.5	89.7	1.8	98.8
S1	4.4	93.8	4	93.8
S2	2.3	97.8	1	99.1

Based on the expression changes established by RT-qPCR, the methylation status was measured after treatment with Zeb (50 µM) for 24 and 72 h in HKC8 cells and for 72 h in HEK293 cells, respectively. The methylation status of DNA from treated cells was compared with non-treated controls. All experiments were repeated in three independent biological replicates.

In HKC8, an inverse relationship between the sense and the antisense CpG marks was found after 24 h drug treatment when the antisense promoter showed significant hypomethylation ($p<0.01$) while sense promoter methylation remained unchanged (Figure 3.14.A). Whereas after 72 h of Zeb treatment, the cells showed hypomethylation in all promoter-related CpG islands, S1, S2 and AS ($p<0.05$, $p<0.01$ and $p<0.01$, respectively). Interestingly, this finding correlated with a detectable increase in *SLC34A1*-sense mRNA levels as shown in figure 3.7.A. Although hypomethylation of SLC34A1-antisense promoter was observed, no *SLC34A1*-antisense transcripts could be detected.

On the other hand, HEK293 cells showed significant hypomethylation of the S1 promoter region at $p<0.05$, but not S2 or AS (Figure 3.14.B). This finding indicates that the S1 promoter is poorly methylated and likely plays a role in *SLC34A1*-sense expression, moreover, S1 is located closely to the transcription start site (TSS).

A CpG methylation in HKC8:

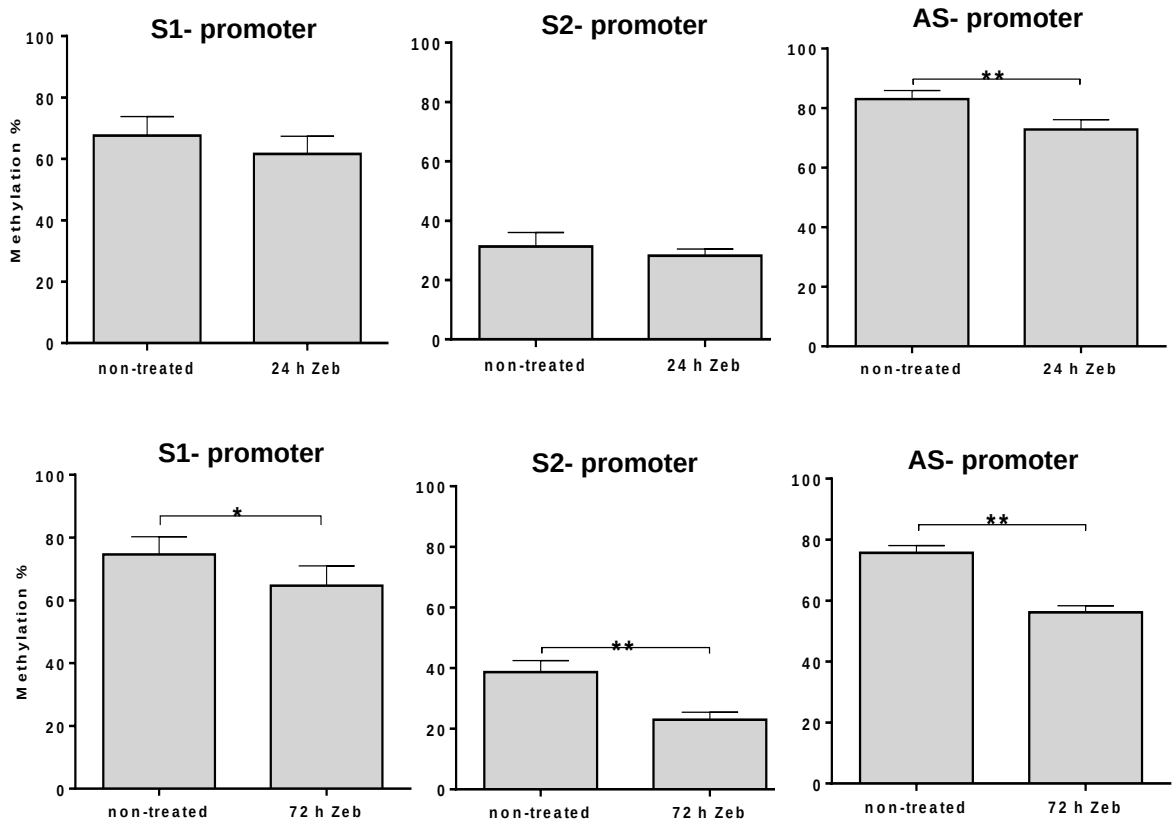

B CpG methylation in HEK293:

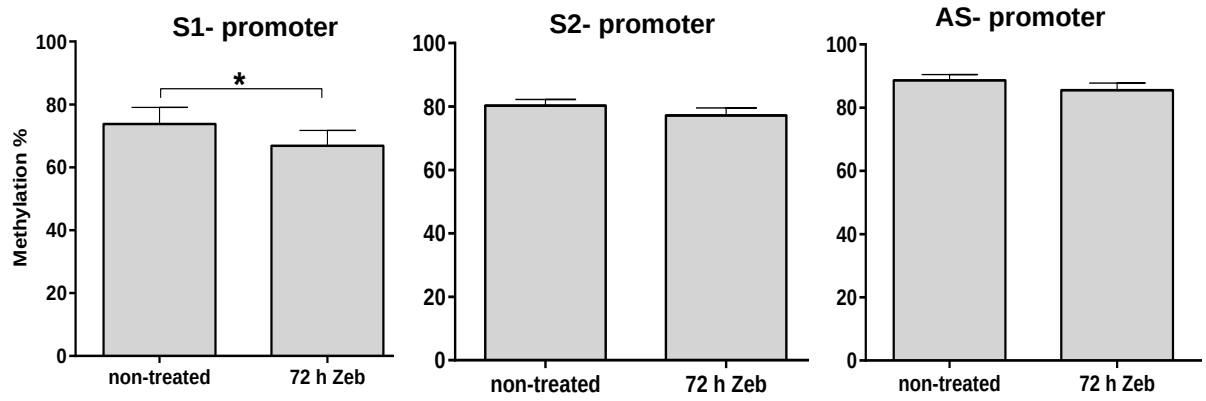

Figure 3. 13: DNA methylation analysis of SLC34A1-sense (S1, S2) and SLC34A1-antisense (AS) promoters. A) HKC8 cells treated for 24 and 72 h with 50 µM zebularine. B) HEK293 cells treated for 72 h with 50 µM zebularine. Statistical analysis for comparing the treated cells with the control was performed by unpaired students t-test, (*= $p<0.05$ and **= $p<0.01$).

3.4. Discussion

Most of renal proximal epithelial-derived cell lines have their SLC34A1 locus silenced, with the exception of expression of *SLC34A1*-sense in OK (opossum kidney) cells and the *SLC34A1-antisense* transcripts in HEK293 cells, respectively. In order to establish a system where the interplay between sense and antisense transcripts could be studied, the expression of both transcripts was assessed in various established cell lines including HEK293 cells, HKC8 and HK2 at the beginning of this thesis. These cell lines have been used previously in the lab to assess the expression of exogenous SLC34A1 wild-type and mutant transporters. The proteins were found to be sorted to the apical membrane as expected in renal epithelial cells(Fearn *et al.*, 2018). However, RT-qPCR data showed that none of the above-mentioned cell lines expressed neither the sense nor the antisense transcript at significant levels (i.e. both transcripts were below detection limits). This finding attributed to two possibilities: either the cells are de-differentiated, or the expression of these transporter has been down regulated as suggested by (Lorenz-Depiereux *et al.*, 2006).

The cell screening results agree with Wu *et al.,* who assessed *SLC34A1*-sense transporter expression in kidney-derived cells (Wu *et al.*, 2013). The researchers concluded that the transporter loci are mostly silenced in immortalised cell lines due to the deleterious effect of excess Pi inside the cells. Thus, epigenetic compounds (such as Zeb and TSA) may re-activate the SLC34A1 locus and enabling research into the interplay of sense and antisense transcript expression.

3.4.1. The effect of Zeb and TSA on cell viability

The XTT assay showed that Zeb reduced HEK293 and HKC8 viability in a dose-dependent manner. This pattern of response was also observed by Nakamura *et al.,* who found that Zeb at relatively high doses (i.e. higher than 100 µM) could induces cell apoptosis in various human epithelial cells (Nakamura *et al.*, 2015). In contrast, others reported that Zeb preferentially reduces the growth rate of cancerous cell

lines, but not primary cells. This effect was linked to the hypomethylation of the *p16* locus (multiple tumor suppressor 1 locus) (Yoo *et al.*, 2008; Andersen *et al.*, 2010).

TSA reduced HEK293 and HKC8 cells viability in a dose-and-time dependent manner. This result was expected as the majority of HDAC inhibitors were reported to induce cell death of transformed- but not in primary cells (Ruefli *et al.*, 2001; Ungerstedt *et al.*, 2005a; Ungerstedt *et al.*, 2005b).

3.4.2. The effect of Zeb and TSA on SLC34A1 locus expression

Zeb appeared to gradually upregulate the sense transcript in HKC8 cells, reaching the peak after 48-72 h, as shown in figure 3.8. Meanwhile, the antisense transcript was only co-expressed after 24 h, suggesting that the antisense RNA could play a transcriptional regulatory role in repressing the sense transcript (Shen *et al.*, 2018). Another possible interpretation for the observed antisense expression pattern could be that the sense transcript is dominantly expressed and overcomes the lower expressed antisense transcript according to the genetic “switch off’’ theory between sense and antisense-related transcripts (Xu *et al.*, 2011).

Zeb promotes demethylation and consequently the transcription process within SLC34A1 locus. Collectively, these observations agree with Horillo *et al.,* who reported that mouse embryonic stem cells (mESCs) treated with Zeb had a significantly altered expression profile including 266 genes i.e.119 genes up-regulated and 147 genes were down-regulated (Horrillo *et al.*, 2013).

TSA on the other hand is known to inhibit HDAC enzymes (I and II) with an impact on the expression of various coding and noncoding genes as well as global histone H3 acetylation. In this thesis, no detectable impact of TSA on the transcription of the SLC34A1 locus was detected. Nevertheless, the elevation in H3 acetylation confirmed that TSA induced global changes of H3 acetylation in dose-dependent manner as reported earlier. The differences in global acetylation levels in response to TSA between HEK293 and HKC8 cells could be due to variability of intrinsic HDAC activity between the two cell lines (Chang *et al.*, 2012).

Cell viability, RT-qPCR and H3 acetylation results suggest that the SLC34A1 locus is either highly acetylated or type I and II HDAC family members have no impact on the tested locus (Sanchez *et al.*, 2018).

3.5. Conclusions

To understand the dynamic interactions between *SLC34A1*-sense and *SLC34A1*-antisense transcripts, it was essential to establish one or several cell lines where the expression of the transcripts could be influenced experimentally. HKC8 were chosen as cells that expressed *SLC34A1*-sense and HEK293 for the antisense transcript expression. Furthermore, to identify an inducible system with epigenetic drugs, Zeb and TSA were used at different concentrations and time-points. Cell viability assays showed that these compounds were absorbed and induced changes in chromatin marks.

Under specific treatment conditions with Zeb (50 µM for 24 h) both *SLC34A1*-sense and *SLC34A1*-antisense transcripts were slightly upregulated. This concurs with reduced methylation levels of the sense and antisense promoters in HKC8 cells.

The gathered data from this chapter suggested that both *SLC34A1*-sense and *SLC34A1*-antisense transcripts may interact in a concordant manner and the mode of response appears to be cell-context dependent. Therefore, an alternative epigenetic modifying compound with a dual effect on DNMTs and HDACs may induce a stronger stimulatory effect.

Chapter 4: Dexamethasone-induced expression of *SLC34A1*-sense and *SLC34A1*-antisense transcripts

4.1. Introduction

In the previous chapter, the impact of DNMT and HDAC inhibitors on the *SLC34A1* locus were investigated in HEK293 and HKC8 cells. Zeb was shown to induce *SLC34A1*-sense/antisense gene expression. The increase was accompanied with a reduction in SLC34A1-sense/antisense promoter methylation. On the other hand, no effect of TSA on sense/antisense expression were recorded, however, TSA significantly increased the levels of total H3 acetylation. Hence, we hypothesised that an alternative epigenetic reagent with dual impact on DNA methylation and histone acetylation (DNMT inhibitor and stimulatory effect on histone acetyl transferases, HAT) could potentially influence transcription of the SLC34A1 locus.

Dexamethasone (Dex) is a synthetic glucocorticoid which is prescribed to treat various conditions, such as skin diseases, asthma and rheumatoid fever. Dex mechanism of action is well documented- what is maybe not fully understood is the number of receptors Dex binds to and eventually which genes are affected in different contexts.
Generally, Dex predominantly binds to glucocorticoid receptors (GR) which are distributed in the cytosol. Upon stimulation, GR enter the nucleus and bind to specific DNA sequences known as glucocorticoid response elements (GREs). This leads to altered transcription of responsive genes (Newton, 2000). Furthermore, Dex binds to other receptors such as the pregnane X receptors (PXR) on the nuclear membrane and, consequently affects different genes as compared to GRs (Pascussi *et al.*, 2000).

Epigenetic investigations reported that Dex could modulate the level of DNA methylation levels. For example, it has been found that Dex induces DNA demethylation of CpG-dinucleotides in the enhancer region of the rat liver-specific tyrosine aminotransferase (Tat) gene (Thomassin *et al.*, 2001). Likewise, neuronal

stem cells (NSCs) treated with Dex showed decreased DNMT1 expression and significantly reduced global DNA methylation (Bose *et al.*, 2015).
Other epigenetic research showed that Dex treatment stimulates HAT, which consequently reduces the overall chromatin compaction. For instance, L6 myotube cells treated with Dex exhibited enhanced HAT activity mediated by CREB-binding protein (CBP) and other transcription associated cofactors (Figure 4.1), which act as intrinsic modulators of HAT activity (Yang *et al.*, 2007).

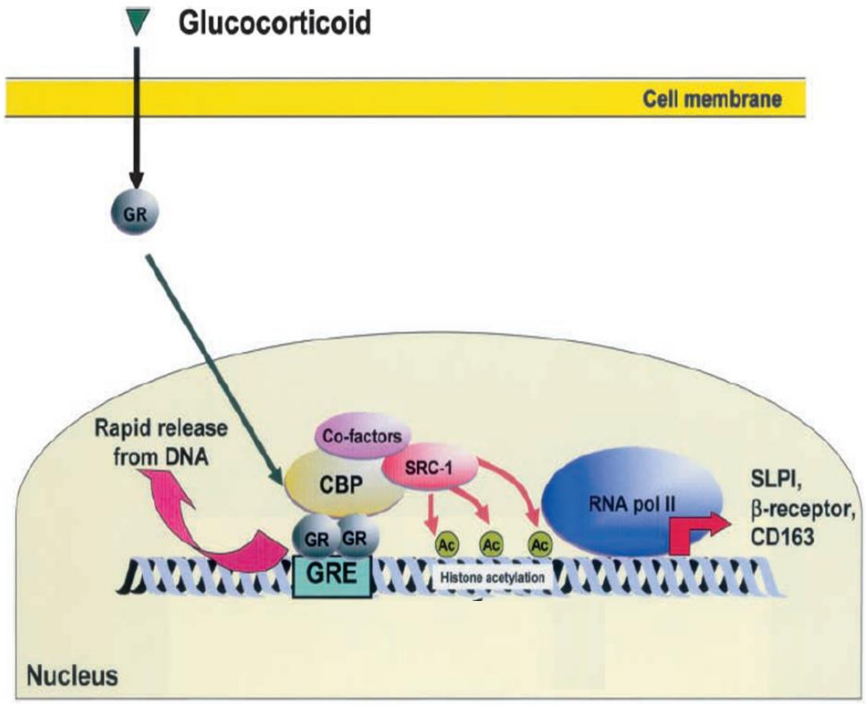

Figure 4. 1: The role of dexamethasone in the activation of histone acetyl transferases (HATs). DEX bound GR molecules activate GREs in the genome. CBP and other co-factors are involved in recruiting HATs to increase histone acetylation. Consequently, chromatin adopts a more open conformation and RNA pol II can bind. Figure adopted from (Adcock *et al.*, 2004).

4.2. Aims

This chapter aims to:

1- Investigate the effect of the epigenetic modifier dexamethasone on the transcriptional activity of the SLC34A1 locus. For this purpose, HEK293 and HKC8 cells were treated with the drug followed by cytotoxicity testing and the quantification of *SLC34A1*-sense and *SLC34A1*-antisense transcripts by RT-qPCR.

2- Characterise the epigenetic status of the SLC34A1 locus after dexamethasone treatment. This will be achieved by measuring the methylation status of CpG-dinucleotides within SLC34A1-sense/antisense promoters using pyrosequencing. Moreover, the enrichment of H3K27Ac and H3K4me at SLC34A1-sense/antisense promoter regions will be determined by chromatin immunoprecipitation (ChIP). The functional consequences of the induced transcription will be tested using northern blotting and ^{32}Pi tracer uptake measurements.

4.3. Results

4.3.1. Dexamethasone and cell viability

To measure cell viability in the presence of Dex, the XTT assay was used. HEK293 and HKC8 cells were seeded in 96-well plates at a density of $4x10^4$ cells per well and each treatment condition was performed in 6-wells. Dex concentrations of 10 nM, 100 nM 1 µM and 10 µM were used and cell viability was assessed after 24, 48, 72, 96 and 120 h.

Dex did not significantly impact on the viability of neither HEK293 nor HKC8 cells and across all incubation times and drug concentrations (Figure 4.2). Under some conditions cell viability appeared to increase in response to the treatment however, this is likely a reflection of cell proliferation.

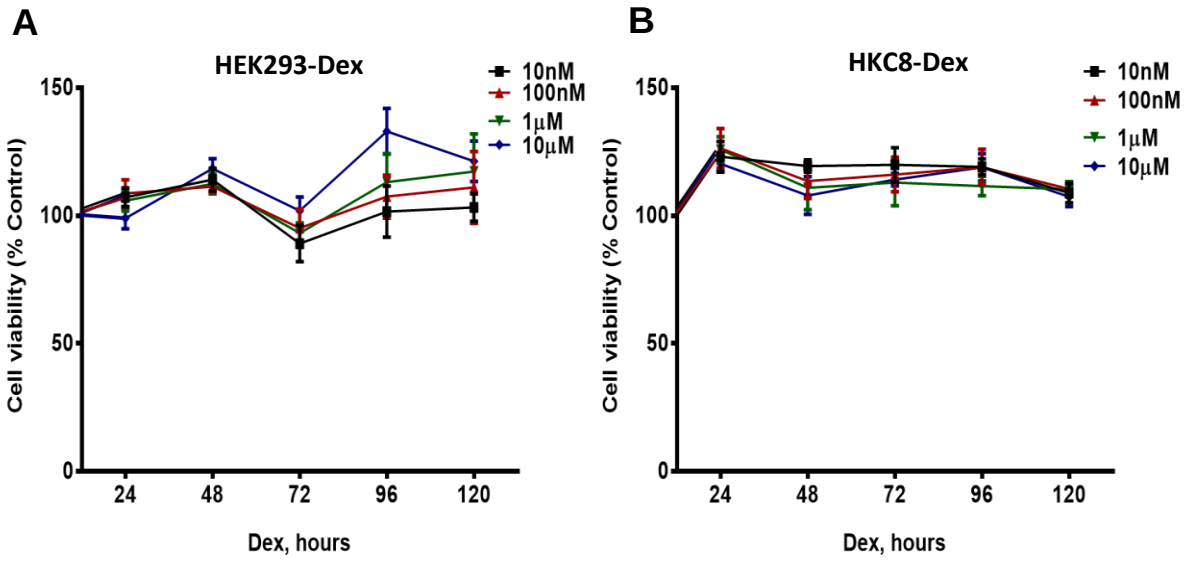

Figure 4. 2: The effect of Dexamethasone treatment on cell viability. A) HEK293 cells and B) HKC8 cells. Cells were treated with 10 nM, 100 nM, 1 µM and 10 µM Dex for 24, 48, 72, 96 and 120 h. Experiments were repeated in three independent biological replicates. Measurements were corrected for the absorbance of the culture medium and then normalised to the control sample (non-treated condition).

4.3.2. Dexamethasone induces SLC34A1-sense expression in HEK293 cells with no effect in HKC8 cells.

To determine the influence of Dex on transcripts from the SLC34A1 locus, it was essential to specify treatment conditions that induce maximal expression with respect to dose- and -time. To test dose dependence HEK293 and HKC8 cells were treated with increasing concentrations of Dex (10 nM, 100 nM, 1 and 10 µM for 24 h followed by total RNA purification and RT-qPCR.

RT-qPCR results showed that Dex induced *SLC34A1*-sense expression in HEK293 cells but not in HKC8 cells (Figure 4.3). For instance, in HEK293 cells Dex at 10 and 100 nM) upregulated *SLC34A1*-sense transcript levels significantly (3.35 ±1.01 and 5.43 ±0.62-fold; $p<0.05$, respectively). In contrast, the two higher doses (i.e. 1 and 10 µM) slightly induced the sense expression with no statistical significance between the groups (0.6 ±1.05 and 0.23 ±1.5-fold, respectively).

On the other hand, Dex did not alter *SLC34A1*-sense expression in HKC8 cells. The maximal expression levels for the sense transcript were found with 100 nM and 10 µM Dex (1.38 ±0.73 and 1.54 ±0.97-fold increase, respectively). Since HEK293 responded to Dex whereas HKC8 cells did not, the activity of the drug is clearly cell type specific. Neither of the cell lines expressed the *SLC34A1*-antisense transcripts after only 24 h exposure to the drug. Next, the time dependence of Dex treatment in HEK293 cells was investigated.

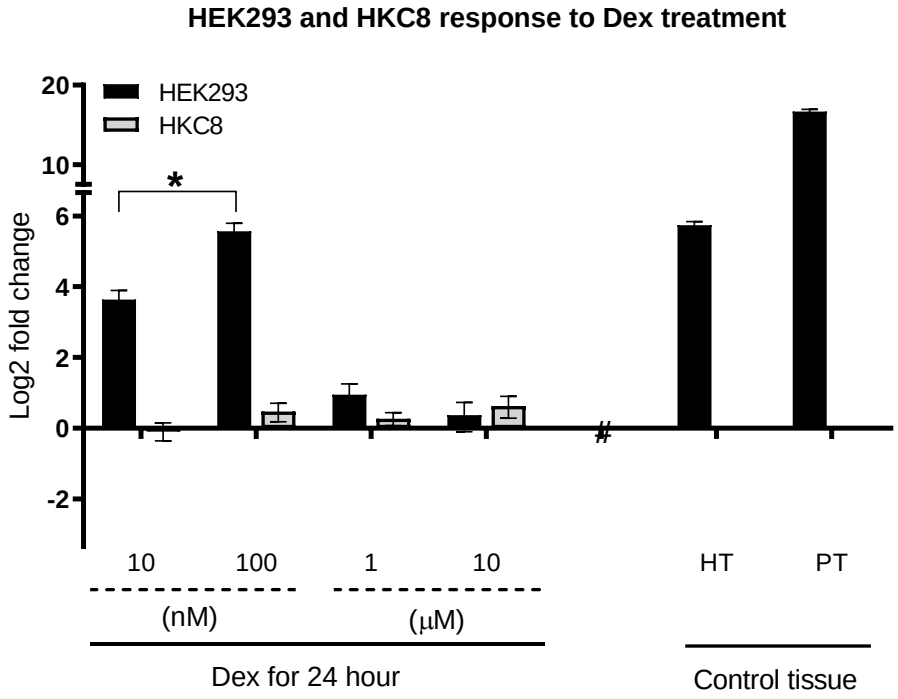

Figure 4. 3: The effect of dexamethasone treatment on *SLC34A1*-sense expression in HEK293 and HKC8 cells. Dex was applied to both cell lines (10, 100 nM and 1, 10 μM for 24 h). The experiments were performed in three independent replicates. Experimental controls from human proximal tubular cells and human testis (PT and HT) were routinely included in RT-qPCR experiments. The data were normalised to *GAPDH* and the fold change ($2^{-\Delta\Delta Ct}$) were calculated in comparison to the non-treated cells. To compare between treatment conditions, statistical differences were measured by One-Way ANOVA using the Games-Howell test to detect significant changes (* $p<0.05$).

4.3.3. Time dependence of dexamethasone treatment on SLC34A1-sense expression

Based on the response of HEK293 cells to 100 nM Dex on *SLC34A1*-sense transcription and following a discussion with Dr. Takishi Hori (Cluster for Science and Technology Hub, RIKEN, Japan), a new treatment regime was applied to HEK293 cells: 100 nM Dex for 1, 3, 5 and 15 days. Moreover, the culture medium was replaced every 48 h with fresh medium containing Dex. RNA was purified and RT-qPCR was performed at the relevant time points.

The expression of *SLC34A1*-sense transcripts was upregulated after 1 and 3 days, 2.46 ±0.55 and 4.57 ±1.69 fold, respectively. Most significantly, however, at day 5

levels increased to 10.78 ±1.34-fold (p<0.001) over control (non-treated), as presented in figure 4.4. After the strong upregulation, *SLC34A1*-sense transcript levels subsequently diminished to 3.14 ±0.73-fold after 15 days. Meanwhile, the *SLC34A1*-antisense transcripts were only detected at day 5 when the transcript was upregulated significantly by 2.50 ±1.16-fold (p<0.001).

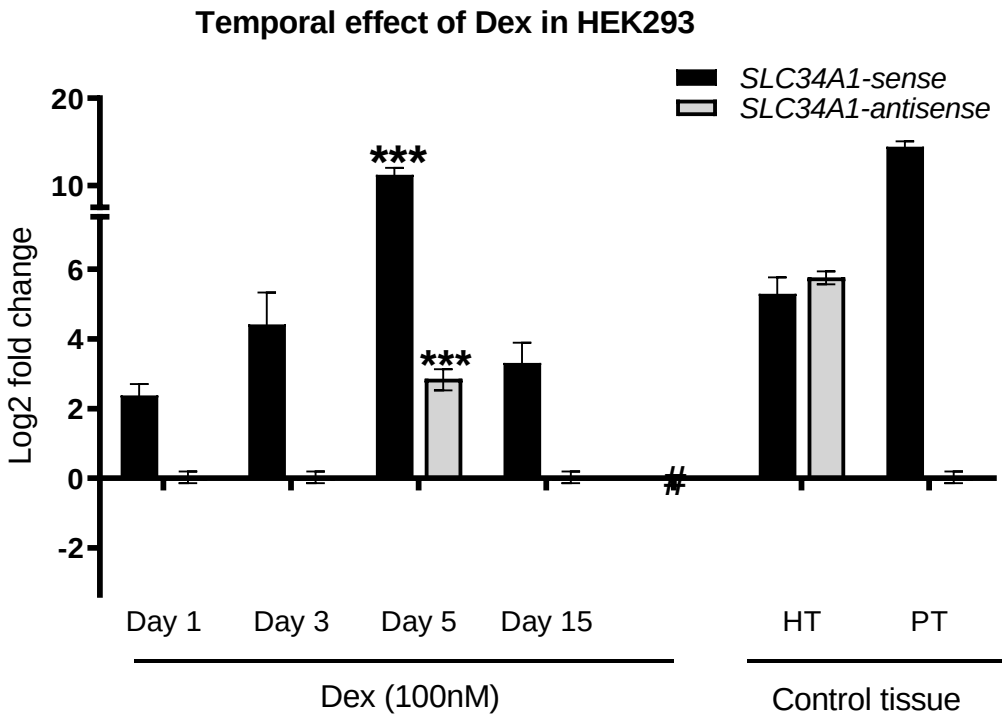

Figure 4. 4: Time dependence of dexamethasone effects on *SLC34A1*-sense/antisense expression in HEK293 cells. The cells were treated with 100 nM Dex for 1, 3, 5 and 15 days. The experiments were performed in three or more independent biological replicates. Experimental control tissue from human kidney and testis (PT and HT) were routinely included. Expression levels were normalised to *GAPDH* and the fold change ($2^{-\Delta\Delta Ct}$) was calculated in comparisons to non-treated cells. To compare between treatment conditions, statistical differences were established by One-Way ANOVA and Games-Howell test (***, p<0.001).

4.3.4. Nuclear and cytoplasmic localisation of the induced SLC34A1-sense/antisense transcripts

The majority of mRNAs are exported from the nucleus to the cytoplasm for protein synthesis, on the other hand an increasing number of noncoding transcripts such as *XIST, Malat1* or *Neat1* function within the nucleus (Bahar Halpern *et al.*, 2015). Moreover, incompletely spliced mRNAs also remain within the nucleus. Evidence also suggest that NATs can act in the nucleus and the cytoplasm, for example to enhance the stability of their target sense transcripts (*BACE1-AS*, *HOTAIR* or *BRK*) (Kang *et al.*, 2014; Noh *et al.*, 2018). Therefore, it was essential to establish the nuclear/cytoplasm distribution of both *SLC34A1*-sense/antisense transcripts following before and after Dex inducement.

Cytoplasmic and nuclear RNA were separated as described in section 2.4. The purified samples were quantified and the integrity was examined on an agarose gel. The expression levels *SLC34A1*-sense/antisense and *GAPDH* transcripts were determined from the nuclear and cytoplasmic RNA samples using RT-qPCR. To validate the nuclear/cytoplasmic RNA separation the predominantly nuclear transcript *XIST* was included in the analysis.

The data in (Figure 4.5) demonstrates the transcripts expression level in nuclear and cytoplasmic RNA samples at pre- and post-Dex inducement levels. Without Dex treatment, *SLC34A1*-sense and -antisense transcripts were detected in HEK293 cells both nuclear and cytoplasmic RNA samples, but at very low levels. For instance, *SLC34A1*-sense and *GAPDH* transcripts were found (1.41 ±0.35 and 1.30 ±0.53-fold) more abundant in the cytoplasm than the nucleus. Conversely, *SLC34A1*-antisense and *XIST* were enriched in the nucleus (at 0.64 ±0.19 and 1.98 ±0.36-fold, respectively).

A similar pattern of transcript distribution was noticed with HEK293 cells stimulated with Dex. Although, the expression level of *SLC34A1*-sense and the antisense transcripts was increased significantly following dexamethasone treatment. *SLC34A1*-sense (3.99 ±0.51-fold) and *GAPDH* (1.96 ± 0.53-fold) were enriched in the cytoplasm whereas *SLC34A1*-antisense transcript (1.23 ±0.46-fold) as well as

XIST (1.54 ±0.27 folds) were detected predominantly in the nucleus, as summarised in the figure.

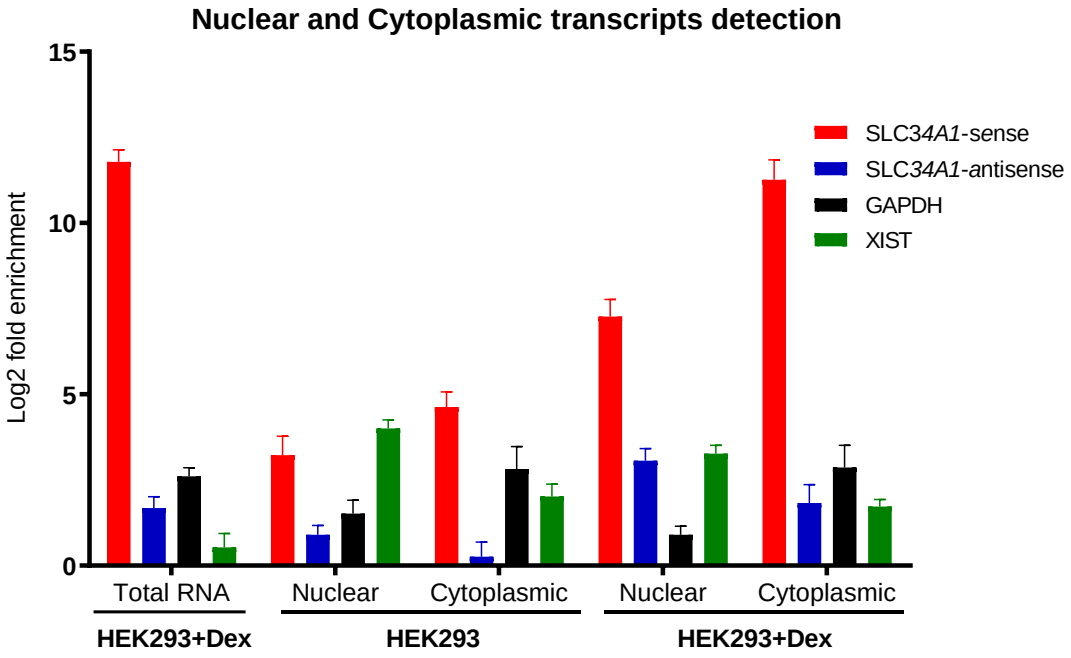

Figure 4. 5: RT-qPCR experiments determining the nuclear and cytoplasmic localisation of *SLC34A1*- sense/antisense, *GAPDH* and *XIST* transcripts in Dexamethasone treated and untreated HEK293 cells. Total RNA samples from HEK293 and HEK293 cells induced with dexamethasone were routinely included. The fold change was calculated as ($2^{-\Delta CT}$). The results are representative of two independent repeats, each performed in three technical triplicates.

4.3.5. Dexamethasone reduces SLC34A1-sense promoter methylation

To determine the impact of dexamethasone treatment on DNA methylation of *SLC34A1*-sense/antisense promoters, HEK293 cells were treated with 100 nM Dex for 1 day, 5 and 15 days followed by genomic DNA (gDNA) purification. The unmethylated cytosine residues in a CpG-context were chemically converted into uracil using sodium bisulfite. SLC34A1-sense and the antisense promoter regions were amplified using biotinylated primers and the PCR products were examined by agarose gel electrophoresis (Figure 4.6.A). The amplicons were confirmed by

Sanger sequencing. The promoter sequences for SLC34A1-sense/antisense are presented in figure 3.11.

For control purposes, gDNA from HEK293 cells was incubated with a CpG methyletransferase (*M.Sss*I) to produce the 100 % methylation sample. In addition, whole genome amplification (WGA) was used to generate unmethylated DNA. Both controls were modified with bisulfite and fragments of SLC34A1-sense /antisense promoters were PCR amplified (Figures 4.6.B). The methylation status for the selected CpG-dinucleotides in the entry sequences was quantified by pyrosequencing.

A

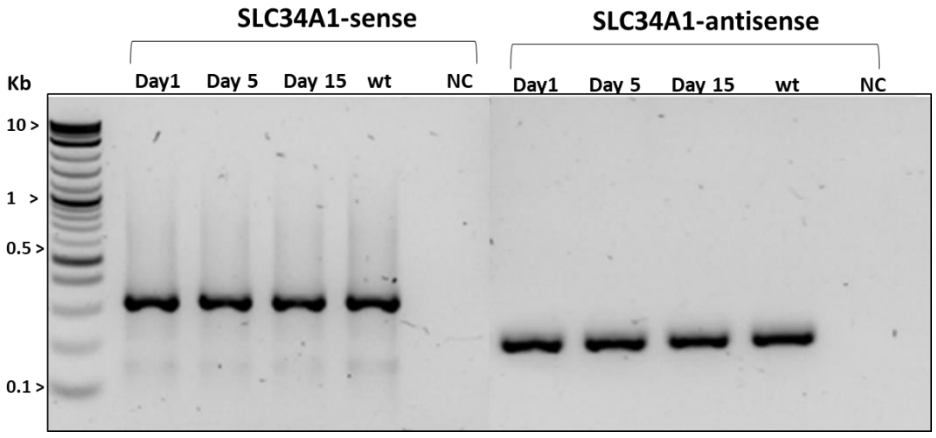

B

Promoter region	% of CpG methylation in HEK293	
	0	**100**
AS	8.1	93.5
S1	4.1	95.7
S2	6.3	91.8

Figure 4. 6: Optimisation experiments for pyrosequencing. A) PCR amplicons from *SLC34A1*-sense and *SLC34A1*-antisense promoters examined on a 2 % agarose gel. B) SLC34A1-sense and SLC34A1-antisense promoter fragments from gDNA treated with *M.SssI* (100 % methylation) and PCR amplified gDNA (0 % methylation). Data in the table is the average values of the target CpGs sites methylation.

The average percentage of CpG-site methylation for SLC34A1-sense/antisense promoters are presented in figure 4.7. In the SLC34A1-sense region, the methylation level decreased significantly from 60.52 ±2.69 % to 50.60 ±1.45 after 1 day and to 49.16 ±1.14 % after 5 days of Dex treatment. However, after prolonged Dex treatment (15 days) the promoter became re-methylated (57.01 ±0.56 % as compared to 60.52 ±2.69% in non-treated cells). Whereas for the antisense promoter, no significant changes were noticed in HEK293 cells in response to Dex. Methylation after 1, 5 and 15 days was 91.17 ±9.65 %, 92.96 ±9.0 % and 89.69 ±12.2 %, respectively, compared with 92.27 ±8.9 % in untreated HEK293 cells.

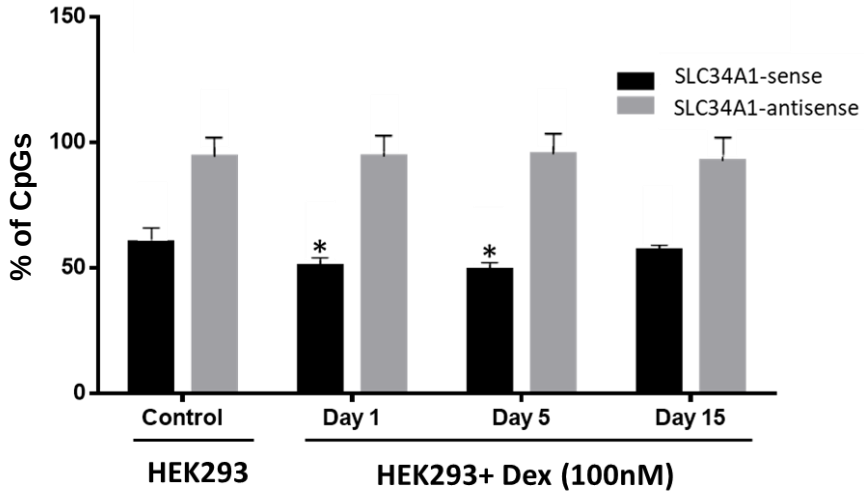

Figure 4. 7: Effect of dexamethasone on DNA methylation of SLC34A1-sense and the antisense promoters. HEK293 cells were exposed to 100 nM Dex for 1, 5 and 15 days. The experiments were repeated in two biological and two technical replicates. Statistical analysis for comparing the treated cells with the control were performed by unpaired students t-test, (*= $p<0.05$).

4.3.6. Dexamethasone induce global histone H3 acetylation

In order to determine the epigenetic role of Dex on histone H3 acetylation, HEK293 cells were treated with the 100 nM of the drug for 1, 5, and 15 days. Following purification and examination of total histone fractions on SDS-PAGE, histone quantification was performed in three biological replicates.

The results in Figure 4.8 illustrate that Dex induced a time dependent change in acetylated H3. No significant change was found after 1 day (129.5 ±16.5 %), however, H3 acetylation significantly increased after 5 days (435.3 ±78.7 %, p<0.001). After 15 days acetylation decreased to 320.3 ±72.0 % but was still significantly higher than in untreated HEK293 cells.

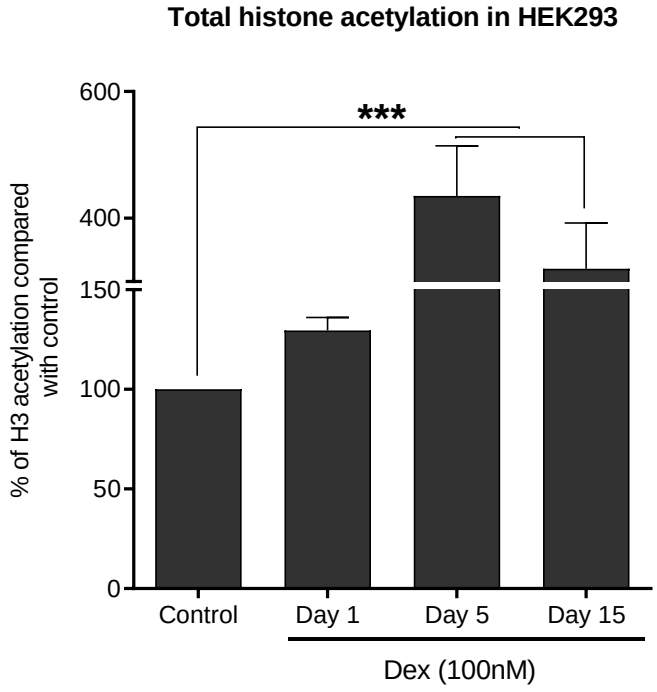

Figure 4. 8: Histone H3 acetylation levels in HEK293 cells in response to dexamethasone treatment. Cells were treated with 100 nM Dex for 1, 5 and 15 days followed by ELISA for H3 acetylation. Each treatment condition was tested in 6 replicates in total (3 biological and two technical). Data were normalised to the untreated control samples. Treated cells were compared to the control using an unpaired students t-test, (***= p<0.001).

4.3.7. Chromatin immunoprecipitation (ChIP)

Global acetylation of histone H3 was significantly increased in response to Dex treatment. It was therefore of interest to investigate the effect of dexamethasone on specific histone marks at the SLC34A1-sense/antisense locus by chromatin immunoprecipitation (ChIP).

Two histone H3 modifications were considered, histone 3 lysine 27 acetylation (H3K27Ac) and histone 3 lysine 4 tri-methylation (H3K4me3). The impact of both marks on gene transcription has been well-characterised by encyclopedia of DNA elements (ENCODE) and epigenomics mapping consortium (Roadmap projects) (Romanoski *et al.*, 2015). Specifically, H3K27Ac is linked with active promoters and enhancers whereas H3K4me3 marks active promoters only (Ernst *et al.*, 2011).

Target regions for SLC34A1-sense/antisense promoter amplification were chosen using online promoter prediction software such as EPD (https://epd.epfl.ch//index.php) and DTU Bioinformatics (http://www.cbs.dtu.dk/index.php) in addition to extensive discussions with our collaborator Prof Jelena Mann, Newcastle University. DNA fragments of 400-500 bp upstream of the SLC34A1-sense TSS and 700-800 bp upstream of the first exon of SLC34A1-antisense were chosen as target for designing PCR primers (Figure 4.9.A) and three primers pairs were designed (table 2.17, material and methods). End-point PCR was performed using cross-linked DNA chromatin as a template. Only primer pairs that gave a single fragment of the exact size were used (Figure 4.9.B). To optimise ChIP-qPCR, selected primer pairs were tested in qPCR reactions with serially diluted chromatin template (Figure 4.9.C).

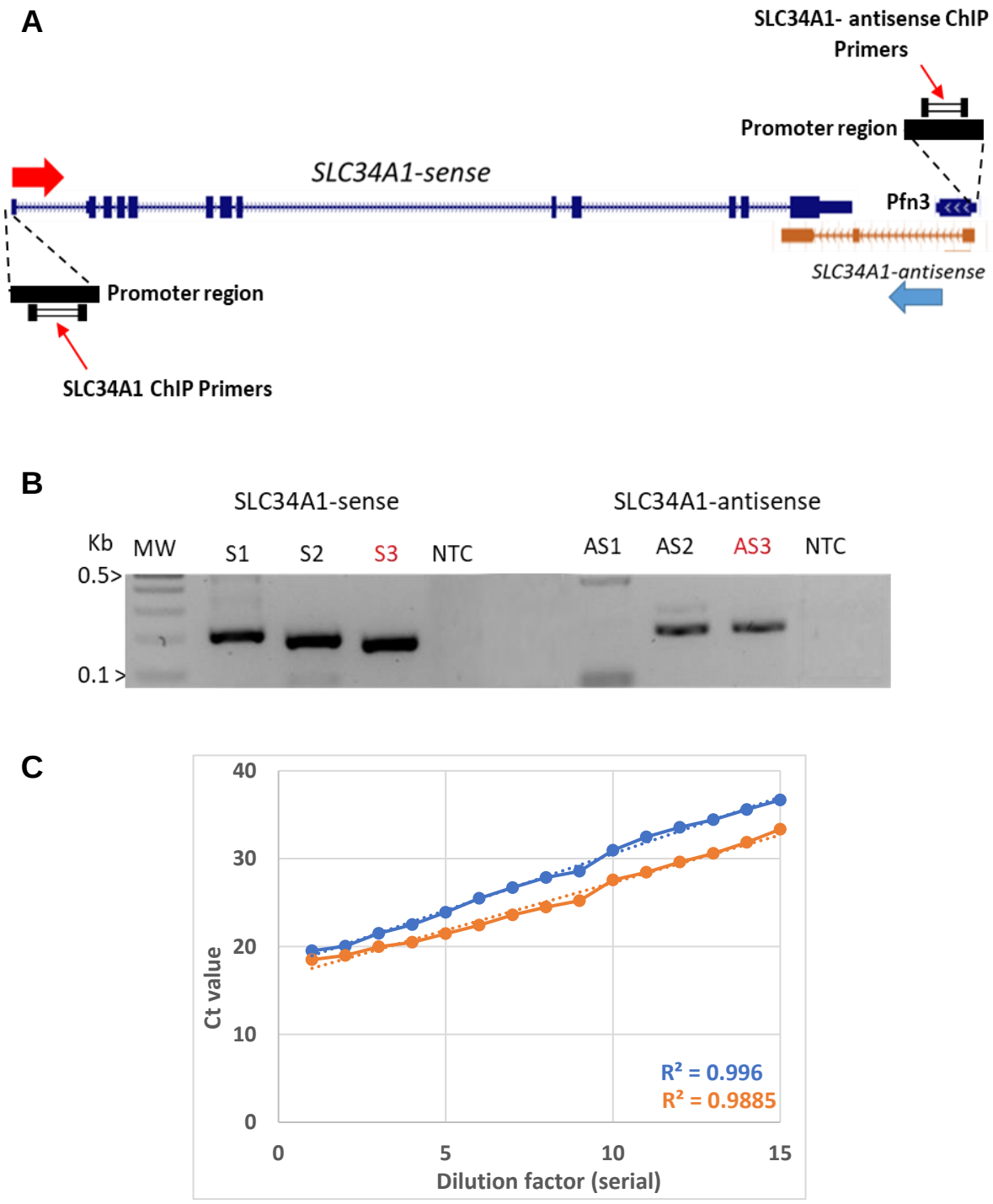

Figure 4. 9: ChIP-qPCR primer validation. A) Edited screenshot from the UCSC genome browser showing the SLC34A1-sense and the antisense target promoter regions. Both promoter regions and the primers are indicated. B) End-point PCR to amplify SLC34A1-sense (S) and the antisense promoters (AS) using three different primer-pairs. The primer pairs highlighted in red were chosen for further applications (S3=166 and AS3= 192bp), AS1 shown not specific banding. C) Amplification efficiency of ChIP-qPCR primers using serially diluted cross-linked chromatin as a template.

4.3.8. Enrichment in H3K27Ac at SLC34A1-sense but not the antisense promoter in response to dexamethasone treatment

HEK293 cells were treated with 100 nM Dex for 1, 3 and 5 days followed by chromatin cross linking with formaldehyde, gDNA sharing, quantification, reverse cross-linking and immunoprecipitation (all these steps were discussed in chapter 2.7). ChIP-qPCR data were normalised to the internal negative control (IgG) and the fold enrichment was compared to the untreated control cells (HEK293). Experiments were repeated twice, and each sample was tested in two technical replicates.

The results are presented in figure 4.10.A and show a significant increase in H3K27Ac levels bound to the DNA target in response to Dex treatment ($p<0.01$). Strongest stimulation was observed after 5 days, with a 4.24 ±0.50-fold increase compared to 1.84 ±0.12-fold enrichment in untreated cells. No significant effects on H3K27 acetylation were found on day 1 and 3 (1.94 ±0.04 and 1.34 ±0.15-fold over control, respectively). In addition, dexamethasone was found to substantially decrease H3K4me3 levels ($p<0.05$) in the sense region after 1 and 3 days (1.34 ±0.11 and 0.92 ±0.14-fold over control, respectively) compared to non-treated cells (1.71 ±0.1-fold enrichment). The differences in H3K4me3 enrichment disappeared after 5 days of dexamethasone treatment (1.49 ±0.12-fold change).

ChIP-qPCR data presented in figure 4.10.B demonstrates the effect of Dex on H3K27Ac and H3K4me3 epitopes in the SLC34A1-antisense promoter region. In general, Dex treatment reduced the levels for the selected epitopes as H3K27Ac steadily and significantly decreased following Dex exposure: The levels compared to control dropped from 4.93 ±0.70 in untreated cells to 2.0 ±0.214 at day 1 ($p<0.05$) then to 1.35 ±0.04 and 1.12 ±0.02-fold change at day 3 and 5, respectively ($p<0.01$). Similarly, H3K4me4 decreased significantly from 2.91 ±0.19-fold change in control cells to 1.71 ±0.04 at day 1 ($p<0.05$), after 3- and 5-days enrichment fell further to 1.12 ±0.05 and 0.94 ±0.06, respectively ($p<0.01$).

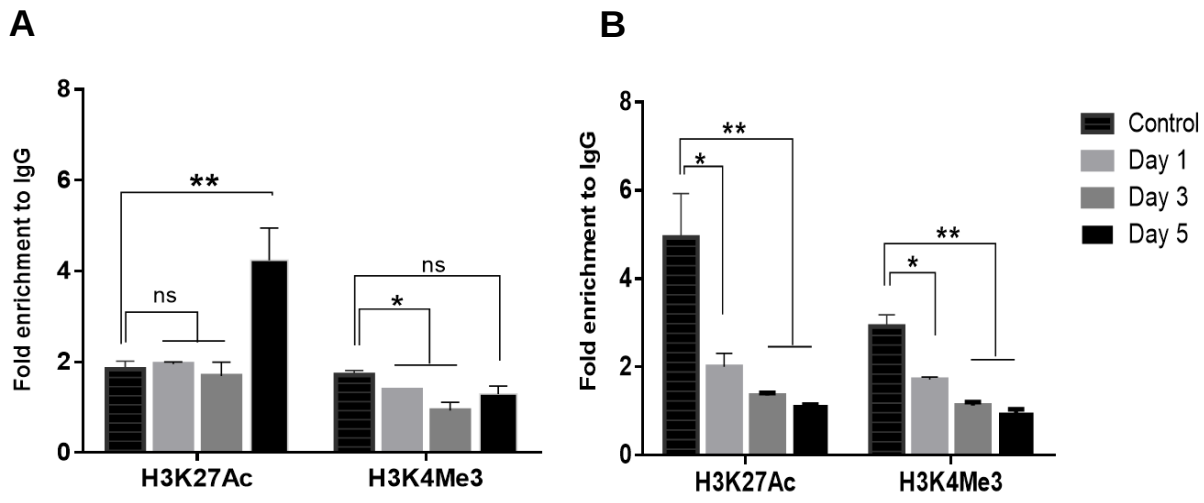

Figure 4. 10: Chromatin immunoprecipitation from HEK293 cells treated with 100 nM Dex for 1, 3 and 5 days. Two histone epitopes were examined, H3K27Ac and H3K4me3. A) ChIP followed by qPCR amplification of the SLC34A1-sense promoter and B) of the SLC34A1-antisense promoter. The experiment was performed in two biological and two technical replicates. The data were normalised to the IgG control samples (fold enrichment) and compared to the untreated control HEK293 cells. Statistical analysis for comparing the treated cells with the control were performed by One-Way ANOVA using the Games-Howell test to detect significant changes (*p<0.05, **= p<0.01).

4.3.9. Functional analysis of the induced SLC34A1-sense transcript

In addition to the epigenetic impact dexamethasone could influence other steps during gene expression. Accordingly, a study by Pufall *et al.,* noticed a decrease of MBNL1, a sequence-specific RNA binding factor, in B-cell acute lymphoblastic leukemia (B-ALL) cells following Dex treatment. Since MBNL1 affects mRNA splicing, the researchers suggested a potential impact of Dex on the mRNA splicing machinery(Pufall *et al.*, 2019). A relationship between corticosteroids and mRNA splicing has also been suggested by (Akker *et al.*, 2004). Hence, the significant stimulatory effect of Dex on *SLC34A1*-sense/antisense expression raised two questions: first, are there obvious splicing differences between the transcripts produced in induced HEK293 and those from control tissue (i.e. renal tubular cells or human testis)? Second, to what extent is the Dex-induced *SLC34A1*-sense transcript

functional? The first question was tackled using northern blotting, the second with functional uptake measurements using radioactive ^{32}Pi.

4.3.10. Northern blotting; preparation of SLC34A1-sense/antisense and GAPDH hybridisation probes

Northern blotting is a routine technique and was applied in this study in order to compare the molecular size and abundance of *SLC34A1*-sense/antisense transcripts, as mentioned by (He and Green, 2013). The RNA was extracted from HEK293 cells incubated with Dex, RNA from proximal tubular cell and human testis were included as controls. Importantly, the sensitivity of northern blotting is considerably lower than RT-qPCR and the generally low expression of the antisense transcript may be below the detection limit. Hence, special attention was given to designing, producing and evaluating probes for *SLC34A1*-sense/antisense and *GAPDH* transcripts.

Because of the effect of Dex on splicing and the database entry of two isoforms for *SLC34A1*-encoded transporters (described in Section 1.4.1), the *SLC34A1*-sense probe was designed to recognise both splice forms (Figure 4.11.A). End-point PCR was performed to amplify the template sequence from cDNA resulting in DNA fragments of 1440, 685 and 466 bp for *SLC34A1*-sense, the antisense and *GAPDH*, respectively.

The PCR products were examined by agarose gel electrophoresis (Figure 4.11.B). Thereafter, PCR reactions were purified, quantified and the sequence for each amplicon was confirmed by Sanger sequencing.

In vitro transcription reactions were performed using Digoxigenin (DIG) labelled nucleotides, reactions with unlabelled nucleotides were included for control purposes. The labelled cRNA probes were heat-denaturated and verified on agarose gels. The gel presented in figure 4.11.C illustrates that both DIG-labelled and unlabelled probes were successfully transcribed. Noticeably, the DIG-labelled probes appear larger than the unlabelled controls due to the differences in molecular weight of the DIG-nucleotides.

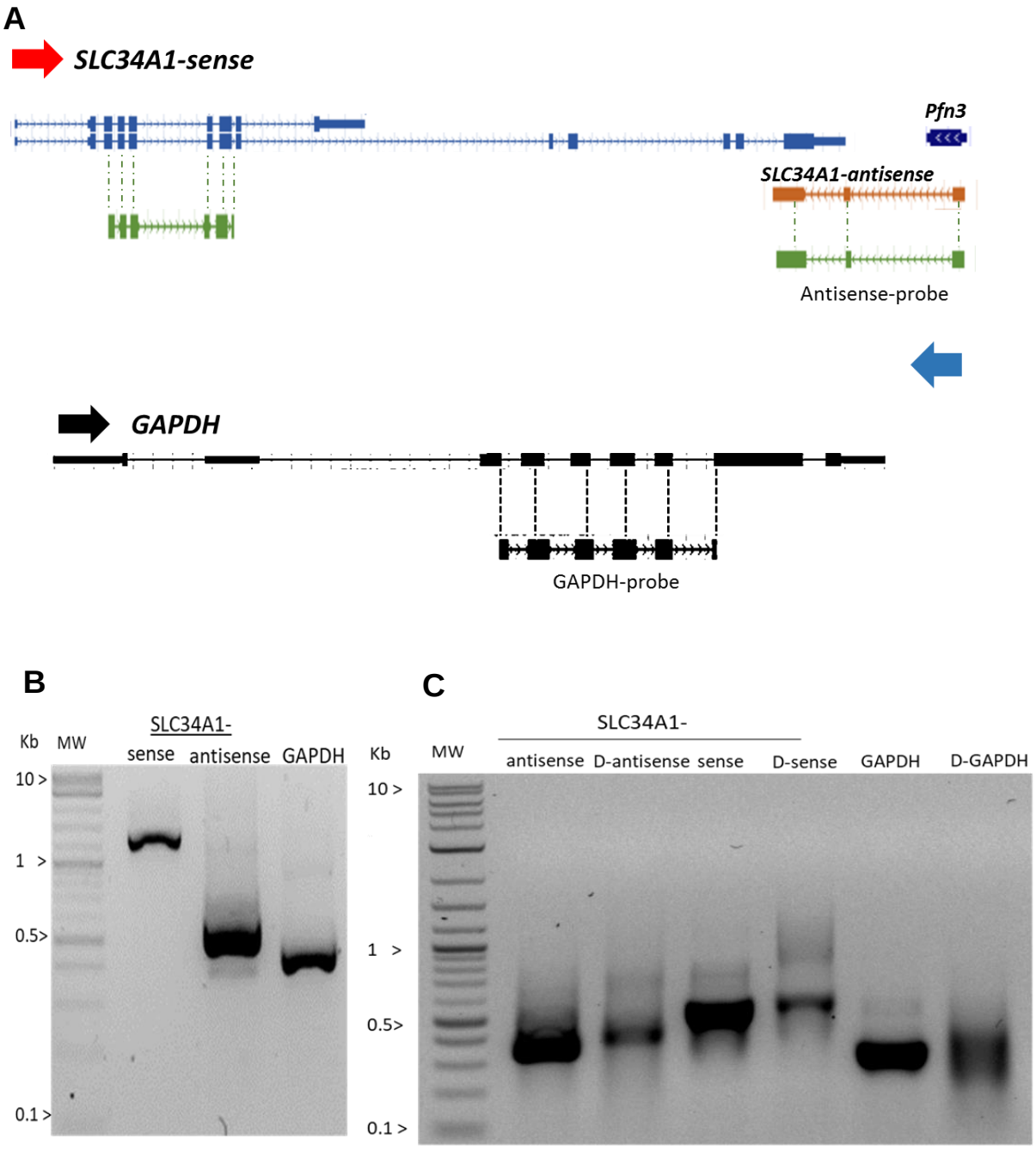

Figure 4. 11: Hybridisation probes for northern blots. A) Diagram showing the exons amplified from SLC34A1-sense, antisense and GAPDH transcripts. B) Probe regions amplified by end-point PCR and the products were visualised by agarose gel electrophoresis (SLC34A1-sense=1400, -antisense= 685 and GAPDH= 446bp). C) *In vitro* transcription reaction with DIG-labelled and unlabelled nucleotides. D-antisense=DIG labelled antisense probe, D-sense= DIG- labelled SLC34A1-sense and DG=DIG-GAPDH).

Dot-blots were performed in order to validate the probes and test their sensitivity. A 1 µl of DIG-SLC34A1, DIG-antisense and DIG-GAPDH were serially diluted (1:10) and spotted onto a positively charged nylon membrane (Figure 4.12.A).

Post hybridisation steps (i.e. blocking, washing, anti-Digoxigenin antibody treatment and detection) were performed as explained in 2.6. The blots showed that all three probes were detected up to a 10^{-6} dilution. This implies that the in vitro transcription reactions were efficient, and the probes contained a significant number of DIG labelled U's. Additionally, the intensity of the dots was measured using Image J and graphically displayed (Figure 4.12.B) (Rueden *et al.*, 2017).

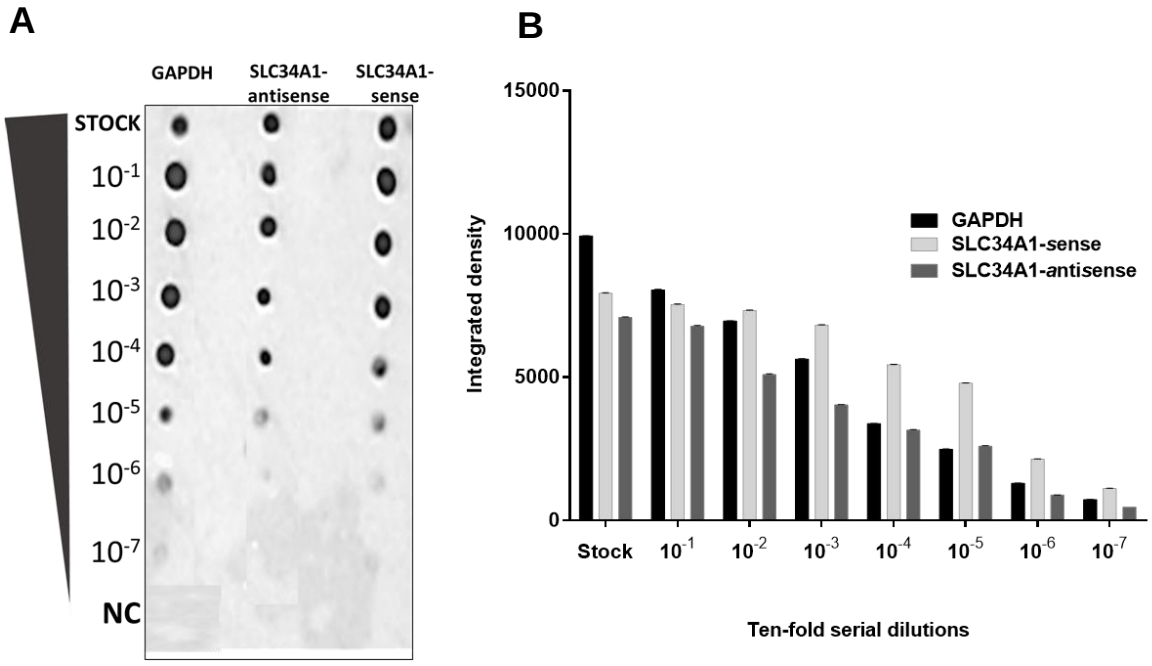

Figure 4. 12: Efficiency of in vitro transcribed probes. A) Serial dilution of DIG labelled *SLC34A1*-sense, antisense and *GAPDH* probes. B) The intensity of dots quantified using Image J software.

4.3.11. Northern blotting: Detection of SLC34A1-sense/antisense and GAPDH transcripts

HEK293 cells were treated with 100 nM Dex for 5 days and the culture medium was replaced every 48 h. Total RNA was purified, quantified, and examined by agarose gel electrophoresis.

A TAE agarose gel was prepared for RNA separation with no nucleic acid stain added (Rio *et al.*, 2010). 7.5-10 µg of total RNA were heat-denatured and separated. RNA was immobilised on positively charged nylon membranes by capillary blotting, followed by hybridisation and detection steps. For reference purposes, RNA from primary renal cells in addition to human testis RNA (PT and HT) samples were run alongside the test samples.

The blots (Figure 4.13) illustrated that *GAPDH* transcripts were detected at comparable size and density among all samples tested. Furthermore, Dex treated HEK293 cells showed two bands on *SLC34A1*-sense blot in addition a much fainter band was detected in the non-treated HEK293 cells. The two detected bands on the sense membrane matches with those on the positive control sample (RNA from PT cells) suggesting the two isoform of the transporter being detected. In contrast, no *SLC34A1*-antisense transcripts were detected in neither induced nor un-induced HEK293 cells, whereas the human testis RNA gave a faint signal (positive control).

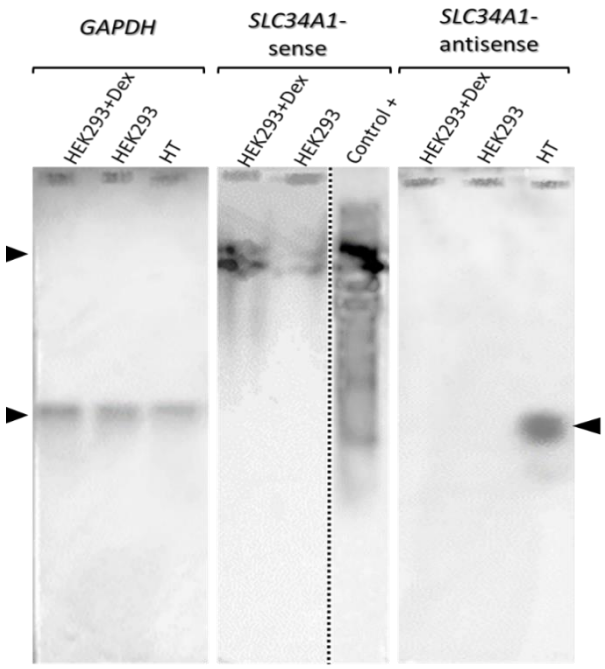

Figure 4. 13: Northern blot of Dex induced HEK293 cells. The expression of *SLC34A1*-sense/antisense transcripts was induced in HEK293 cells using Dex. Black arrows refer to the bands detected in the control (primary renal cells, PT and human testis RNA, HT) and experimental samples. The control lane on the *SLC34A1*-sense blot was only exposed 3 sec as compared to the other two lanes (exposed for 3 min), indicated by the dotted line.

4.3.12. SLC34A1-sense transporter efficiency

The function of the *SLC34A1*-sense encoded transporter in Dex-treated HEK293 cells was assessed by measuring the influx of radio labelled ^{32}Pi, as previously described by others (Biber *et al.*, 1990; Rajagopal *et al.*, 2014). HEK293 cells were seeded in 24-well plates (5x10^4 cells per well) followed by Dex treatment (100 nM for 5 days). Cells were washed with phosphate-free Krebs buffer followed by incubation in Na^+ containing uptake solution in the presence of 1 mM phosphate (carrier) and 1µCi/mL ^{32}Pi tracer and a series of washing steps. Thereafter, the uptake of radioactive substrate was assessed by scintillation counting. The counts were correlated to the total number of viable cells per well. ^{32}Pi uptake was compared between induced and non-induced HEK293 cells. Each condition was measured in two wells in one experiment, repeated in three independent biological replicates.

The data presented in figure 4.14 indicates that the Dex induced *SLC34A1*-sense transcripts lead to significantly increased ^{32}Pi uptake by more than twofold (224 ±81.58 %, p<0.01).

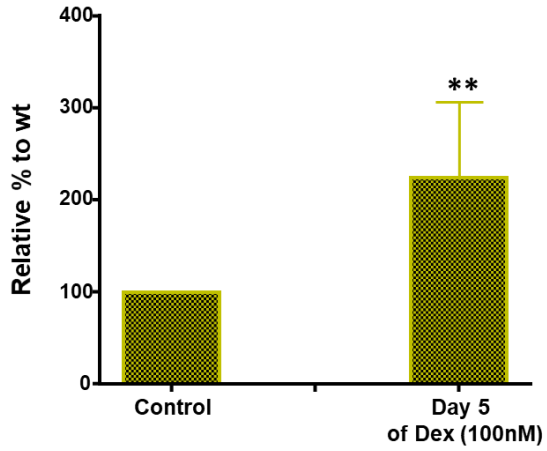

Figure 4. 14: Dex induced *SLC34A1*-sense transport in HEK293 cells. Uptake of radioactive ^{32}Pi was measured for 5 minutes. The experiment was performed in three biological replicates with two technical repeats per condition. Data were normalised to the cell count per well and treated cells were compared to untreated cells. Statistical analysis was performed by unpaired students t-test, (**= p<0.01).

4.4. Discussion

The data presented in this chapter established that dexamethasone induces significant expression of *SLC34A1*-sense/antisense transcripts in HEK293, but not in HKC8 cells. The expression pattern for the sense and the antisense transcripts were in concordance, suggesting that the antisense transcripts could play an important regulatory role. We investigated the epigenetic mechanism by which dexamethasone induced changes to SLC34A1 locus. Dexamethasone was found to decrease methylation levels of CpG-dinucleotides combined with an increase of H3K27Ac marks in the *SLC34A1*-sense promoter region. In addition, northern blotting confirmed the length of the induced sense transcript and the physiological function of the induced *SLC34A1*-sense/antisense transcripts was examined.

4.4.1. Dexamethasone and cell viability

No reduction in viability of HEK293 and HKC8 cells was noticed across all the treatment conditions. Similar effects of Dex on cell viability were observed by others (Petersen *et al.*, 2008), who reported that human lens epithelial cells (HLEC) treated with 100 nM Dex for 24 h caused a moderate increase in cell proliferation. Following the exposure to corticosteroids, an increase in growth factors was measured and thus cell growth rate was affected. Another study found that Dex treatment at low concentrations (10 nM and 10 µM) did not affect proliferation of bovine endothelial cell lines; however, at increased concentrations (1 and 10 mM) cell viability was significantly reduced (Chen *et al.*, 2006). Moreover, other groups tested the sensitivity of a chondrocyte cell line (ATDC5) in response to Dex (1, 10 and 100 µM from 24 to 48 h). They reported that cell viability was reduced significantly at the highest drug dose administered for 48h caused by induction of the autophagy pathway (Zhao *et al.*, 2014; Forst *et al.*, 2017). Based on published evidence the majority of the tested cell lines were unchallenged by low doses of dexamethasone. These reports suggest that the applied concentrations here have not reached the cytotoxic thresholds in HEK293 and HKC8 cells.

4.4.2. Effect of dexamethasone on the SLC34A1 locus in HEK293 and HKC8 cells

HEK293 and HKC8 cells were exposed to low concentrations of dexamethasone for 24 h. RT-qPCR results showed that Dex induced the expression of *SLC34A1*-sense in HEK293, but not in HKC8 cells, suggesting that Dex regulates transcription in a cell/tissue dependent manner. This observation could be explained by a variation in occupancy levels of glucocorticoid receptors (GR) following the treatment (So *et al.*, 2007; Murani *et al.*, 2019). Research by So *et al.,* supported this hypothesis as they found that nearly 90 % of the surveyed genes showed significant responsiveness to dexamethasone treatment in A549 cells, compared to only 1.9 % in U2OS cells. The abundance of GR is significantly higher in A549 cells as compared to U2OS (So *et al.*, 2007). Therefore, in order to explain the difference between the HEK293 and HKC8 response to dexamethasone treatment, the level of GR expression in these cell lines could be measured.

4.4.3. Pattern of SLC34A1-sense/antisense transcript expression

The initial experiments with HEK293 cells indicated significant expression of the *SLC34A1*-sense transcript following Dex treatment. We hypothesised that the antisense transcripts might become detectable with optimised treatment conditions (as demonstrated in Chapter 3) despite the epigenetic status of the SLC34A1 locus which predicts the expression of the sense- but not the antisense transcript.

The *SLC34A1*-sense transcript was upregulated after 24 h Dex treatment, accompanied by a reduction in DNA methylation around the SLC34A1 promoter, but not in the antisense promoter (Figure 4.7). Neither global histone H3 acetylation nor promoter H3K27Ac/H3K4me3 marks were significantly affected at this time-point (Figure 4.8 and 4.10).
Interestingly, the expression of *SLC34A1*-sense and the antisense transcripts were concordantly increased after 5 days (10.78 ±1.34 and 2.50 ±1.16-fold). The concordant pattern of sense/antisense transcript co-expression has also been reported in other bi-directionally transcribed genes such as *C/EPB-delta*, *CDC23*/*Kif20a*, *Gnbp3g*, *CtpW85*, *HIF1α* and *SOX4* (Yelin *et al.*, 2003; Katayama *et al.*,

2005a; Katayama *et al.*, 2005b). These observations confirm the biological role of the antisense transcripts particularly for stabilising the cognate mRNA.
Other groups studied the effect of Dex treatment on the *SLC34A1*-sense transporter activity. For example, Webster S.K. *et al.,* found that dexamethasone inhibited Pi reabsorption in renal proximal tubules in phosphate-deprived rats without an effect on the fractional excretion of phosphate (Webster *et al.*, 1986). Accordingly, *Levi et al.,* measured that the abundance of SLC34A1 transporter in rat renal brush border membranes was decreased 2.5-fold as compared to the control group following dexamethasone administration (Levi *et al.*, 1995). Conversely, Pfister *et al.,* found that exposure to 1 µM Dex for 20 h increased *SLC34A1 transcripts* expression 2-fold in *SLC34A1*-sense transfected OK cells, with no detectable effect on the intrinsic SLC34A1 transporter (Pfister *et al.*, 1997).
Although the results in this thesis do not fully support previous findings, several factors need to be considered such as the route of Dex administration, *in vitro vs. in vivo* biological conditions, exposure time and the dose (Nakamura *et al.*, 1996). Moreover, there is a variation between tissue/cellular responses to Dex as discussed above for HEK293 *vs*. HKC8 cells.

4.4.4. Dex induces epigenetic modifications at the SLC34A1 locus

Bisulfite treatment and pyrosequencing revealed that Dex modifies the methylation of CpG dinucleotides in the SLC34A1 promoter, however no significant effect on the *SLC34A1*-antisense promoter were seen (Figure 4.7). Importantly, the methylation pattern concurs with the expression levels of the two transcripts. These findings are in line with the observation that Dex acts as a DNMT inhibitor predominantly in lowly methylated regions as compared to hypermethylated sites (Matsuda *et al.*, 2015; Zannas *et al.*, 2015). Accordingly, sense and antisense promoters have differential methylation levels in untreated HEK293 cells (57.01 ±0.56 *vs.* 92.27 ±8.9 %). Hence, it may be informative to include highly and poorly methylated CpG-sites for control purposes.

The ChIP experiments (Figure 4.10) confirmed Dex as an epigenetic modifying reagent. Dex affected mainly H3K27Ac, less to H3K4me3 marks after 5 days of treatment. Despite the mechanism by which Dex affects epigenetic marks not being

fully established (Pasini *et al.*, 2010; Xiao *et al.*, 2018), DNA hypomethylation and a prominent enrichment of H3K27 acetylation are likely to cause the upregulation of SLC34A1 expression.

With respect to ChIP-qPCR for the antisense region, Dex induction was minor and could be due to a stabilizing effect of the sense transcription on the spurious antisense transcription. Although HEK293 cells expressed the antisense transcript following treatment, an opposite enrichment pattern was seen for H3K27Ac and H3K4me3 marks. These results point to one of the following scenarios: first, transcription start site and promoter predictions are difficult for lncRNAs, hence the selected *SLC34A1*-antisense region may not include the biologically relevant promoter and/or enhancer sequences (Kashi *et al.*, 2016). Second, the transcription start site could be correct, however, the transcription process of the antisense transcripts could be controlled by more than one promoter region with the main promoter site not covered in this current study (Pennacchio *et al.*, 2013). In fact, the observed upregulation of the *SLC34A1*-antisense transcript favours this assumption.

Third, Quinn J *et al.,* discussed the relationship between the level of expression and the epigenetic status for selected groups of coding and noncoding transcripts. They discovered that in spite of H3K27Ac/H3K4me3 enrichment around the TSS of certain lncRNA classes, most of the transcripts are not actively transcribed. Such phenomenon was linked to the accumulation of other chromatin remodelling complexes (Swr1, Isw2, Rsc and Ino80) particularly around promoters/enhancers enriched with H3K27Ac/H3K4me3 modifications. These complexes were found to interfere with lncRNA transcription thus significantly reducing their expression (Figure 4.15) (Quinn and Chang, 2015). Fourth, stabilisation between the spurious antisense transcript by the cognate sense transcript, and vice versa. This kind of interaction has been previously reported between beta secretase and *HIF1a* or at a large scale by (Katayama *et al.*, 2005a).

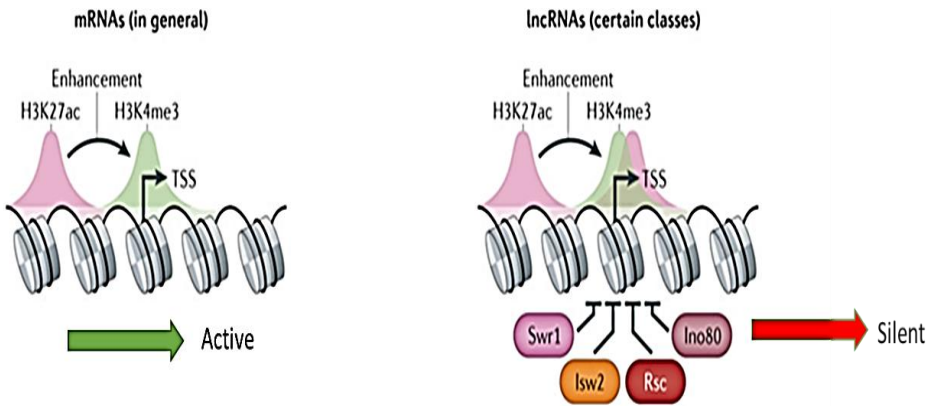

Figure 4. 15: The effect of H3K27Ac and H3K4me3 enrichment on transcription. In certain classes of lncRNAs, enrichment with these marks results in recruiting chromatin remodeling complexes (Swr1, Isw2, Rsc and Ino80), which subsequently repress the transcription machinery. Figure from (Quinn and Chang, 2015).

4.5. Conclusions

With dexamethasone and HEK293 cells, we have successfully established a model for inducing the expression of *SLC34A1*-sense/antisense transcripts. Dexamethasone stimulated the expression of the *SLC34A1*-related transcripts in a cell- specific context and in dose-and-time dependent manner. The mode of interaction between *SLC34A1*-sense/antisense transcripts was found to be “concordantly upregulated”. Moreover, pyrosequencing and ChIP-qPCR data revealed a significant reduction in CpG-dinucleotide methylation and an increase in H3K24 acetylation at the SLC34A1-sense promoter, but not the SLC34A1-antisense promoter. Therefore, as a next step the interplay between sense and antisense transcripts were further investigated. Genome editing (CRISPR-Cas9) was applied to distinguish the mode of interaction between the two transcripts by interfering with *SLC34A1*-sense/antisense expression.

Chapter 5: Genomic manipulation of *SLC34A1*-sense and *SLC34A1*-antisense transcript expression in HEK293 cells

5.1. Introduction

The effects of epigenetic compounds on the SLC34A1 locus suggest that *SLC34A1*-sense/antisense transcripts are positively correlated as under certain conditions, *SLC34A1*-sense and antisense transcripts were co-expressed. To investigate this observation further, the level of *SLC34A1*-sense and/or antisense transcripts were assessed after experimentally interfering with the expression of *SLC34A1*-related transcripts, i.e. monitoring *SLC34A1*-sense expression with the *SLC34A1*-antisense transcript silent and vice versa. Hence, the CRISPR/Cas9 gene editing technique was applied to modulate target transcripts expression.

5.1.1. The CRISPR/Cas9 system

CRISPR stands for Clustered Regulatory Interspaced Short Palindromic Repeats. Since its breakthrough in 2012 (Jinek *et al.*, 2012) CRISPR has become the most extensively used technique to modulate gene expression. CRIPSR elements were first discovered coincidentally by researchers in Japan (Ishino *et al.*, 1987) whilst characterising the protein which is responsible for isozyme conversion of alkaline phosphatase (AP) in the periplasm of *E coli.* A series of 21-40 short palindromic repeats downstream of the translation termination codon of isozyme alkaline phosphatase (iap) were discovered. Later, identical conserved sequences were also identified in the *Salmonella enterica* and *S. typhimurium* genomes. The biological importance of these repeats, however, remained obscure (Newbury *et al.*, 1987).

Mojica *et al*., detected a region of non-protein coding repetitive motifs in archaea such as *Haloferax mediterrane.* The sequence repeats were found identical to the previously identified structures in bacteria and initially termed tandem repeats (TREPs) (Mojica *et al.*, 1993). Similarly, TREPs were identified in *Haloferax volcanii* and it was suggested that these repeats were involved in replicon partitioning (Mojica *et al.*, 1995).

With the improvements in automated DNA sequencing, TREPs were further detected in other microbial species such as *Haemophilus influenza* (Fleischmann *et al.*, 1995)*, Methanocaldococcus jannaschii* (Bult *et al.*, 1996)*, Saccharomyces cerevisiae* (Goffeau *et al.*, 1996) and *Mycobacterium tuberculosis* (Groenen *et al.*, 1993). No evidence for such repeat motifs was found in human and viral genomes (Karimi *et al.*, 2018).

The term 'CRISPR' was first introduced by Jansen (Jansen *et al.*, 2002) and adapted by others describing the following characteristics: (i) CRISPR consists of short palindromic repeats of 21-60 bp, uniquely localised in intergenic regions. (ii) The motifs are highly conserved within species. (iii) Additional, not conserved sequences are interspaced between the palindromic repeat sequences known as spacers.

In 2005, three independent studies discovered that the spacer fragments matched foreign genetic elements found in bacteriophages and plasmids (Bolotin *et al.*, 2005; Mojica *et al.*, 2005; Pourcel *et al.*, 2005). With this in mind, others successfully established the tight association between CRISPR elements and a DNA repair-associated protein family known as Cas (Makarova *et al.*, 2006). The hypothesis was put forward that CRISPR elements, including the inherited genetic information within the spacer fragments, and the Cas protein represent an adaptive immune system for prokaryotes, which can be considered an analogue to RNA interference (RNAi) in eukaryotes (Figure 5.1) (Morange, 2015b; Morange, 2015a).

To prove this hypothesis, a specific sequence from a bacteriophage was inserted within CRISPR loci of *Streptococcus thermophiles* followed by infection of the bacteria with the phage. The modified *Streptococcus thermophiles* strains became resistant to the phage but resistance was lost when the corresponding sequence was subsequently removed from the phage (Barrangou *et al.*, 2007). Sapranauskas *et al.,* illustrated that the CRISPR/Cas system also protected *E coli* from plasmid transformation and phage infection and that the Cas9 protein played an essential role in degradation of the phage DNA (Sapranauskas *et al.*, 2011).

5.1.2. Mechanism of CRISPR/Cas9

The CRISPR/Cas9 system reconstituted from *Streptococcus pyogenes* shows sequence-specific targeting in human and mice cells (Mali *et al.*, 2013). The system includes the helicase Cas9, a palindromic repeat sequence called *trans* activating CRISPR RNA (tracrRNA) and the *spacer* transcript, also known as CRISPR RNA (crRNA). In most currently used systems, the tracrRNA and the crRNA are combined to form a single guide RNA (sgRNA). The sgRNA molecule also offers a platform for Cas9-binding thus playing an essential role in ribonucleoprotein complex formation (Deltcheva *et al.*, 2011). The sgRNA hybridises to the target DNA sequence and Cas9 is recruited which then cuts the DNA approximately three nucleotides upstream of the protospacer adjust motif (PAM). Cas9 is composed of two main domains, the histidine-asparagine-histidine (HNH) domain and a RuvC domain. While the HNH domain induces DNA cleavage of the complementary strand to the sgRNA, the opposite DNA strand is cleaved by the RuvC domain (Cho *et al.*, 2013).

As a consequence of the double-strand break (DSB), the affected cells repair the DNA break either by non-homologues end joining (NHEJ) or homology-directed repair (HDR) pathways. The NHEJ-mediated repair mechanism occurs naturally throughout cell cycle. Here, the two ends of the nicked DNA strands are ligated regardless of sequence complementarity (with the other allele). Consequently, frameshift or point-mutations will frequently take place (Xiao *et al.*, 2019).

Alternatively, the HDR pathway can be triggered, providing a very precise DNA repair mechanism. Here, the CRISPR/Cas9 reaction is complemented with a DNA template that has sequence homology at the DSB region. By utilising this strategy, various engineered templates such as antibiotic selection markers, GFP constructs or transcription terminator signals can be introduced as a part of a repair template (Ran *et al.*, 2013b).

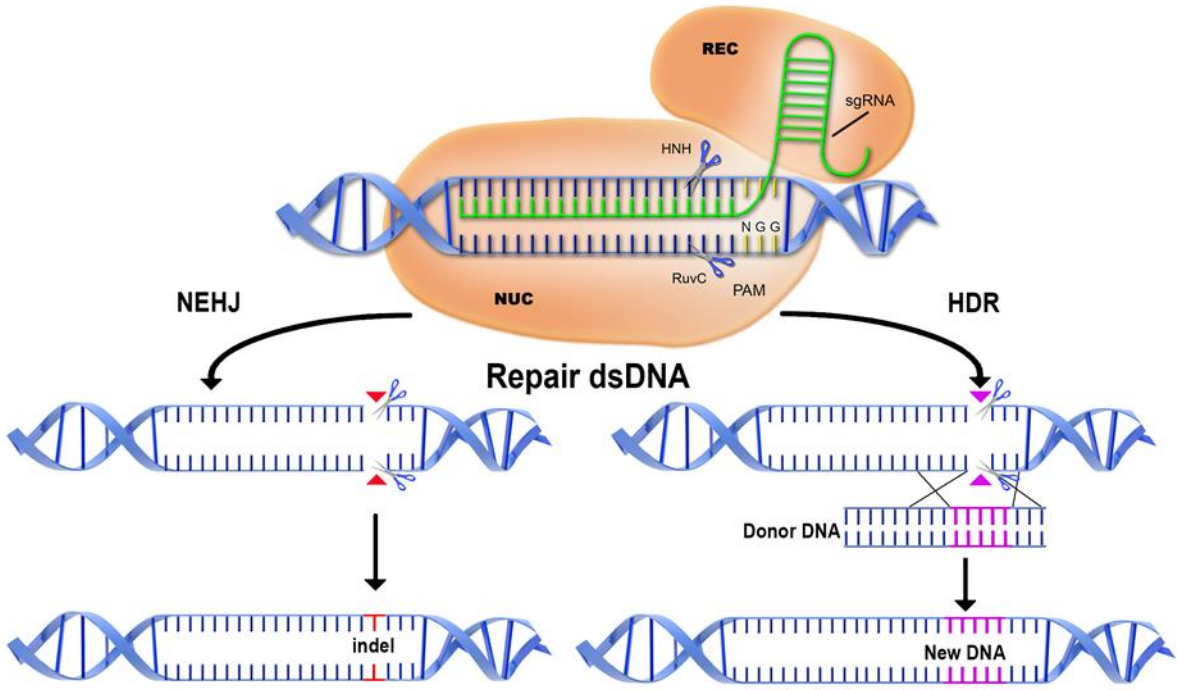

Figure 5.1: Schematic representation of the CRISPR-Cas9 complex. The sgRNA positions Cas9 to the specific locus in the genome where the nuclease inserts double strand breaks. DNA breaks are then repaired either by non-homologues end joining (NHEJ) or homology-directed repair (HDR) pathways. This figure is taken from (Cribbs and Perera, 2017).

5.2. Aims

Using the CRISPR/Cas9 gene editing tool, this work aimed to:

1- Generate *SLC34A1*-sense and *SLC34A1*-antisense knockout cell lines. This will be achieved by integrating an HDR template containing a transcription terminator motif within the SLC34A1 genes in both sense- and- antisense direction.
2- Study the mode of interaction between the sense and antisense transcripts in *SLC34A1*-sense and *SLC34A1*-antisense KO cells by measuring the transcript levels.
3- Investigate the consequences of dexamethasone treatment on *SLC34A1*-sense and -the antisense transcript expression in *SLC34A1*-sense and *SLC34A1*-antisense KO cells.
4- Determine the functional consequences of the gene knock out on Pi transport in KO cell lines.

5.3. Results

5.3.1. sgRNA, selection and cloning

DNA sequences from the first three exons/two introns of SLC34A1-sense, and the first exon/intron of SLC34A1-antisense were submitted to three sgRNA designing websites CHOPCHOP (https://chopchop.cbu.uib.no/), BENCHLING (https://www.benchling.com/) and Zhang lab (https://zlab.bio/guide-design-resources). The resulting sgRNAs were assessed according to the following criteria: CG content 40-80 %, high on-target efficiency, PAM region less than five nucleotides upstream of the sgRNA sequence and finally, sgRNA start with a G nucleotide at 5' terminus. An additional G nucleotide was otherwise added to reduce the likelihood of off-targets effects (Savić and Schwank, 2016). As a result, eight sgRNAs for each SLC34A1-sense and -antisense transcript were chosen as demonstrated in figure 5.2.

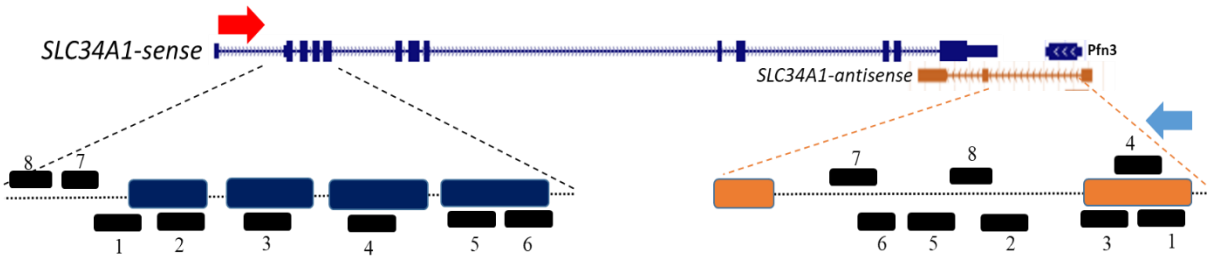

sgRNA	Sequence	PAMs	Strand
S-sgRNA1	GTGCCCAGGATGTTGTCCTA	CGG	+
S-sgRNA2	GGATGTTGTCCTACGGAGAG	AGG	+
S-sgRNA3	TGCCCAGGATGTTGTCCTAG	GGG	+
S-sgRNA4	CAGTGGTTCATGGCGCTCCG	AGG	+
S-sgRNA5	CGCCAGCCTGGCGCAGCTTG	TGG	-
S-sgRNA6	GTTGCCCACATCCCGGATGG	GGG	+
S-sgRNA7	AGCCCCAGGGCCCCAAAGTG	AGG	-
S-sgRNA8	CGGAGCGCCATGAACCACTG	GGG	-

sgRNA	Sequence	PAMs	Strand
AS-sgRNA1	GAGTCCCTGGACTAGAGGGG	AGG	-
AS-sgRNA2	GGCCTGCAGAGTGAGACTCC	CGG	+
AS-sgRNA3	GCCGACGCGGCGTACATGGG	GGG	-
AS-sgRNA4	GTCGCGGATGACGCAGCAGG	CGG	+
AS-sgRNA5	CGGGGGGCCTTTTCGAAGGC	TGG	+
AS-sgRNA6	GTTGCCCACATCCCGGATGG	TGG	+
AS-sgRNA7	GTCGTGCACCGTCTTGTTGG	AGG	+
AS-sgRNA8	GGCGCCTAGCCGGCCAGCCG	AGG	+

Figure 5.2: Summary of the suggested sgRNAs for *SLC34A1*- sense/antisense transcripts. Genomic location (upper panel) and sequence (lower panel) are given.

The selected sgRNAs were cloned into the pSp.Cas9 (PX458) plasmid at the *Bbs*I restriction site (section 2.10.1, figure 2.3). Ligated constructs were transformed into chemically competent *E. coli* (Stbl3). Colony PCRs were performed using the primers U6F (plasmid universal forward) and sgRNA-R (reverse sequence of target gRNA). PCR products were examined by agarose gel electrophoresis (Figure 5.3). Positive clones were confirmed by Sanger sequencing.

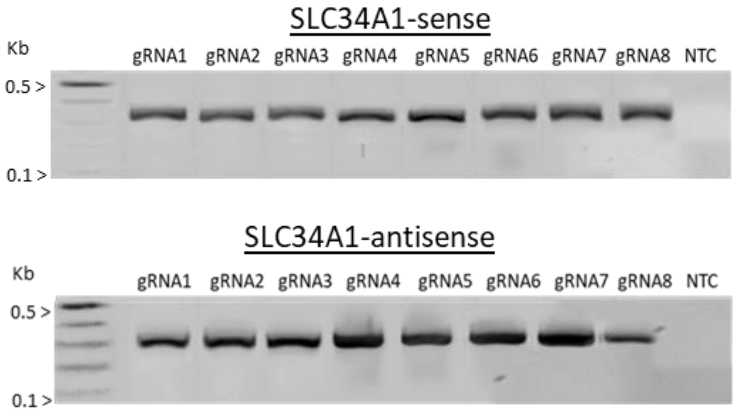

Figure 5.3: Cloning of gRNAs. Colony PCR to screen for constructs containing sgRNAs targeting SLC34A1-sense (upper panel) and SLC34A1-antisense (lower panel). PCR tests were performed for at least 3 randomly picked colonies. The products were examined by 2 % agarose gel electrophoresis including control (NTC, no DNA). The positive plasmids were confirmed by Sanger sequencing using the UR-pSp primer (universal reverse primer).

5.3.2. Optimisation of transfection efficiency

Since the pSp.Cas9 plasmid contains a GFP cassette (as presented in Figure 2.2), the transfection efficiency in HEK293 cells was monitored by measuring the number of green fluorescent cells after plasmid transfection. HE293 cells were seeded in 24-well plates and transfected with different amounts of pSp.Cas9 plasmid (0.5, 1 and 2 µg) without insert. At 72 h post transfection, cells were monitored using widefield fluorescence microscopy. The transfection efficiency was estimated by calculating the number of green fluorescent cells per frame in a total of six frames/well. Approximately 60 % of the cells were transfected with 0.5 µg of plasmid followed by 45 % and 13% for 1 and 2 µg, respectively (Figures 5.4.A and B).

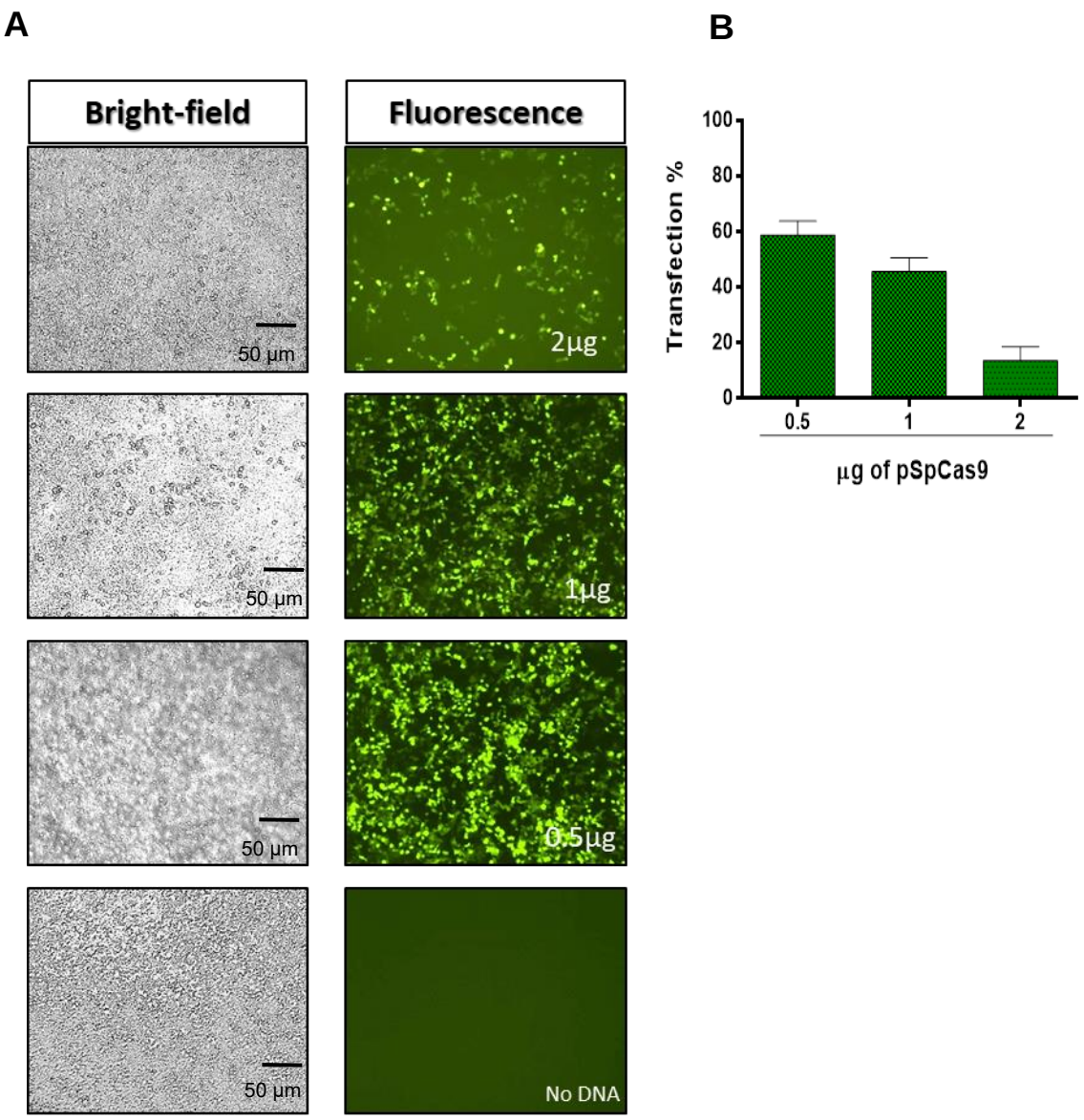

Figure 5.4: HEK293 transfection efficiency for pSp.Cas9. A) HEK293 cells were transfected with three different concentrations of pSp.Cas9 plasmid (0.5, 1 and 2 µg) followed by incubation for 72 h. B) Quantification of transfected cells using image analysis software (Zeiss, Germany).

5.3.3. T7-endonuclease I assay

To assess the level of DNA strand breaks following sgRNA-pSp.Cas9 transfection, the T7 endonuclease I (T7EI) assay was applied. The scope of using T7EI is to

detect DNA heteroduplex formation following sgRNA/Cas9 application that are formed between modified and unmodified sequences.

As recommended (Guschin *et al.*, 2010), a fragment of approximately 2000 bp over the sgRNA target site was amplified using high-fidelity PCR. In addition, a no DNA template, a no T7 enzyme (negative control) and a kit-provided control sample (positive control) were included. The resulting PCR products were treated with T7EI followed by examination on agarose gel. Homoduplexed DNA appears as a single band whereas heteroduplexed DNA will be cleaved by T7EI resulting in two shorter fragments (Kc *et al.*, 2016). Band intensities were quantified using the BioRad gel documentation system software (Laboratories, 2014).

Band intensities predicted that 6 out of 8 sense and 7 out of 8 antisense sgRNAs induce significant DNA nicking manifested by heteroduplex formation and T7EI fragmentation. Moreover, by comparing band intensities reflecting homoduplex and heteroduplex DNA, respectively, the efficiency of the sgRNA-mediated targeting can be estimated. The sgRNA-3 (for *SLC34A1*-sense) with 33 to 67 % and sgRNA-2 (for *SLC34A1*-antisense) with 27 to 73 % were considered as the most efficient and used for downstream CRISPR/Cas9 application (Figure 5.5.A and B).

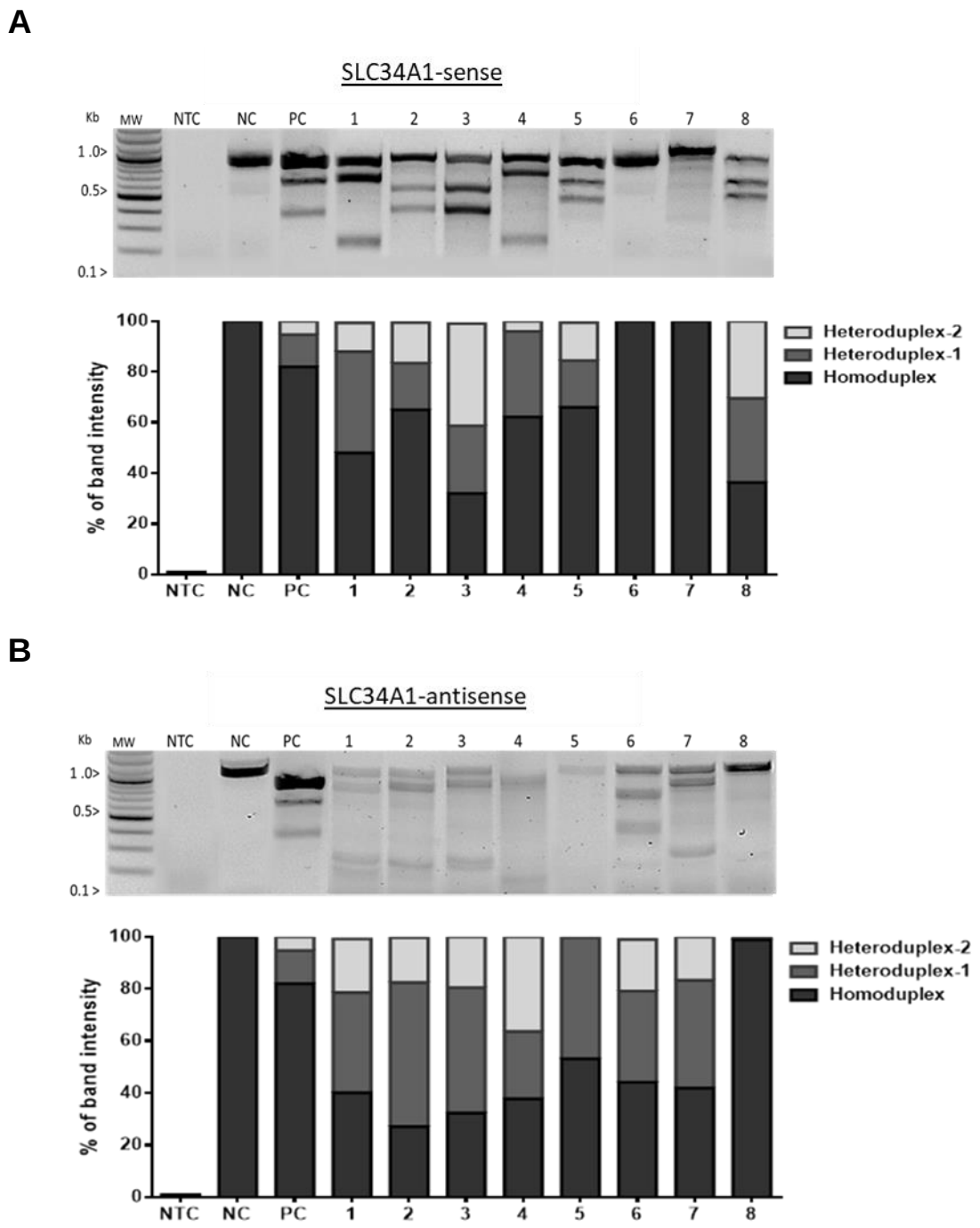

Figure 5.5: sgRNA efficiency to target SLC34A1-sense and -antisense transcripts. HEK293 were transfected with pSp.Cas9 plasmid containing the corresponding sgRNAs. PCR amplification of the target region was performed and the resulted amplicons were treated with T7EI. A) Reactions for SLC34A1-sense and B) SLC34A1-antisense. Bands were examined on 2 % agarose gel electrophoresis (upper panels, including positive control (PC, kit provided) and negative controls (NTC, no DNA and NC, no endonucleases). Band intensities were quantified using the BioRad gel documentation software (lower panels). sgRNA3 (SLC34A1-sense) and sgRNA2 (SLC34A1-antisense) are most efficient and were used for further experiments.

5.3.4. Construction of homology directed repair templates (HDR)

The silencing of *SLC34A1*-sense/antisense transcripts with the aid of CRISPR/Cas9 and HDR followed a strategy described previously (Zheng *et al.*, 2014; Eid *et al.*, 2018). Here, transcription of two protein coding genes and two non-coding transcripts was efficiently terminated by introducing a potent early polyadenylation signal (bovine growth hormone signal polyA signal). The repair template also contained a CMV promoter driven antibiotic selection marker (puromycin) (Liu *et al.*, 2017). Accordingly, similar constructs were designed to silence the *SLC34A1*-sense and -antisense transcripts as shown in figure 2.4.

SLC34A1-sense and -antisense arms of the HDR constructs were PCR amplified from gDNA. Moreover, the core of the template (CMV-puromycin-polyA) were amplified from a plasmid that contained the HDR template, originally designed to silence *HOTAIR*, kindly obtained from the Cui lab (Liu *et al*, 2017). All PCR amplicons were examined on agarose gel followed by Sanger sequencing. The amplicons in addition to *EcoR*I linearised pMini T2.0 vector were joined using the HiFi DNA assembly technique (Figure 5.6) as recommended (Thomas *et al.*, 2015). The constructs were then transformed into chemically competent cells *E. coli* followed by sequence confirmation (Sanger sequencing). The constructs were co-transfected with pSp.Cas9 plasmid into HEK293 cells.

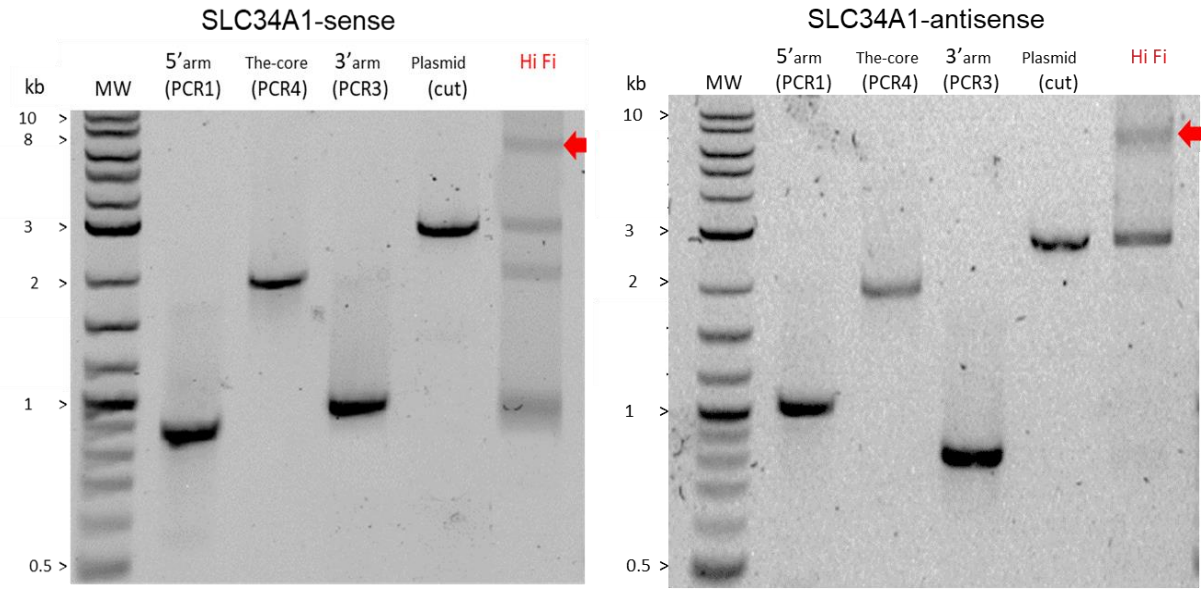

Figure 5.6: Hi Fi Gibson assembly of HDR cassettes for SLC34A1-sense (left panel) and SLC34A1 -antisense (right panel). Each cassette consists of a gene specific 5' arm (PCR1), the core (CMV, puromycin resistance, polyA signal, PCR4), gene specific 3' arm (PCR3) and linearised pMiniT2.0 vector. The molecular size (in bp) for each amplicon is as follows: SLC34A1-PCR1, 850; SLC34A1-PCR3, 940; Antisense-PCR1, 1045; Antisense-PCR3, 810; PCR4, 1890 and linearised pMini T2.0 plasmid, 2610bp. Assembled fragments are marked in red arrow.

5.3.5. Puromycin sensitivity test

The susceptibility of HEK293 cells to puromycin was determined as described in section (2.10.7). HEK293 cells were treated with 0.1, 0.25, 0.5, 1, 2, 3, 4, 5, 6, 8 and 10 µg/mL of the drug for 7 days. The culture medium was replaced every 48 h. The condition of the cells was examined under a bright-field microscope daily. The optimal puromycin concentration which killed all the cells at day 7 was determined to be 1 µg/mL. Thus, this concentration was used for antibiotic selection.

5.3.6. HDR and pSp.Cas9 co-transfection

The vector containing the SLC34A1-sense and -the antisense HDR cassette were linearised with the *BamH*I restriction enzyme followed by agarose gel electrophoresis and band purification prior to the co-transfection step (Figure 5.7.A).

Equal amounts of pSp.Cas9 and purified HDR-template were co-transfected into 70 % confluent HEK293 cells (250 ng of pSp.Cas9 and 250 ng of repair template). The transfection efficiency was examined using florescence microscopy (as previously described in 5.3.2). The estimated number of green fluorescent cells in the co-transfected cells was markedly reduced to less than 5 % as compared to the pSp.Cas9 control (Figure 5.7.B).

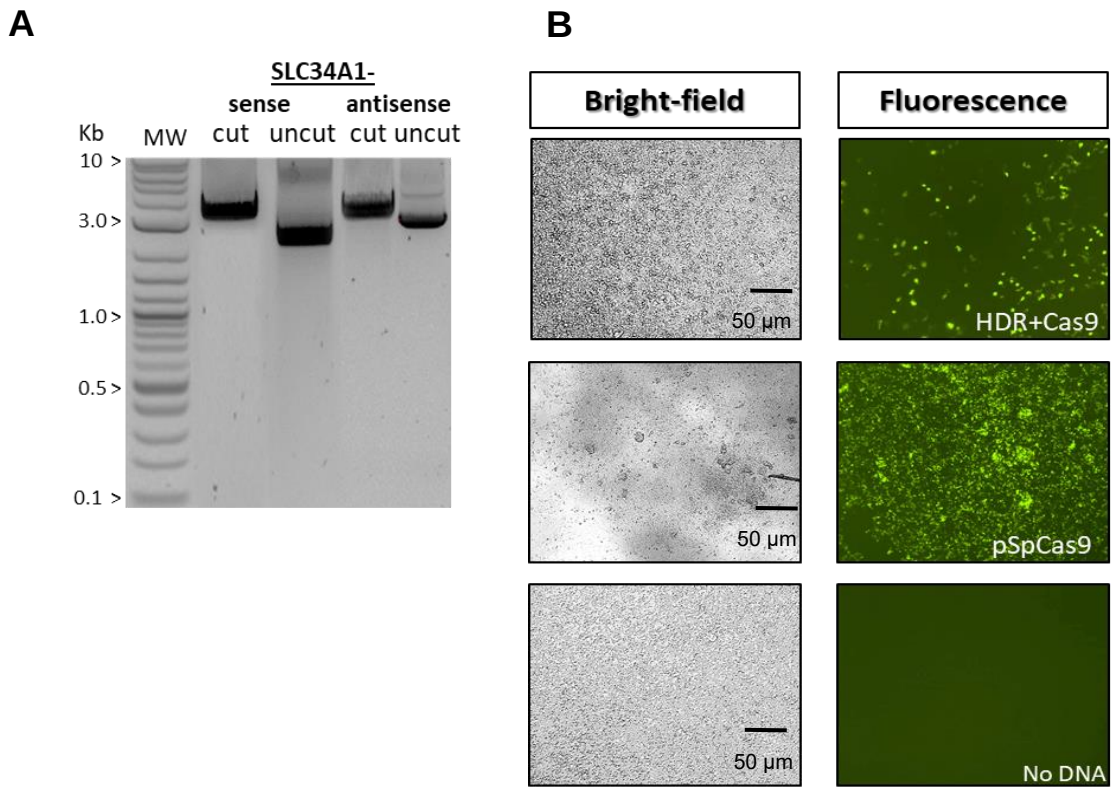

Figure 5.7: Co-transfection of HEK293 cells. A) pMini T2.0 plasmid which contains the *SLC34A1*-sense and -antisense HDR linearised with *BamH*I B) HEK293 cells co-transfected with pSp.Cas9 and the HDR template. pSp.Cas9 was included as transfection control in addition to a reaction without DNA.

5.3.7. Genotypic analysis

In order to isolate cell clones with modified SLC43A1-sense or SLC34A1-antisense alleles, co-transfected cells were cloned by serial dilution in 96-well plates. The growth medium was supplemented with the selective antibiotic puromycin. Only wells that grew from a single colony were subsequently further cultured in duplicates in 24-well plates. Following 7 days, gDNA was purified from the first well whereas cells in the second wells were sub-cultured at a larger scale. Long range PCR reactions were performed to amplify gDNA around the HDR template insertion site. PCR primers were designed to anneal approximately 1000 bp up- and down-stream of the flanking arms. PCR products were examined on a 1 % agarose gel. The length of fragments from edited cells was 4112 bp for *SLC34A1*-sense and 4315 bp for *SLC34A1*-antisense. HDR insertion sites and PCR primers for genotyping are demonstrated in figure 5.8.A.

PCR screening identified 2 out of 68 cell clones with bi-allelic HDR-insertion into the SLC34A1-sense locus (SB1 and SB17). Moreover, another three clones (SM11, SM16 and SM17) showed two bands of 4112 bp and 2222 bp, respectively, suggesting mono-allelic HDR-insertion (Figure 5.8.B).

A similar screening strategy was followed for SLC34A1-antisense edited cells. The PCR amplification demonstrated that only one clonal line of 66 tested showed a bi-allelically modified locus (ASB5). Additionally, two clones (ASM50 and ASM60) with mono-allelically inserted constructs were identified (Figure 5.8.C, the letters B stand for ‘bi-allelic’ and M for ‘mono-allelic’).

In order to generate stable knock-in cell lines, the positive cell clones (SB1, SM11, ASB5 and ASB50) were treated with puromycin for more than 4 weeks (Lo *et al.*, 2017). PCR-amplified fragments from SB1 and ASB5 were submitted for Sanger sequencing. Alignment confirmed the precise integration of the HDR-templates including the polyA motif within the SLC34A1-sense and -antisense loci.

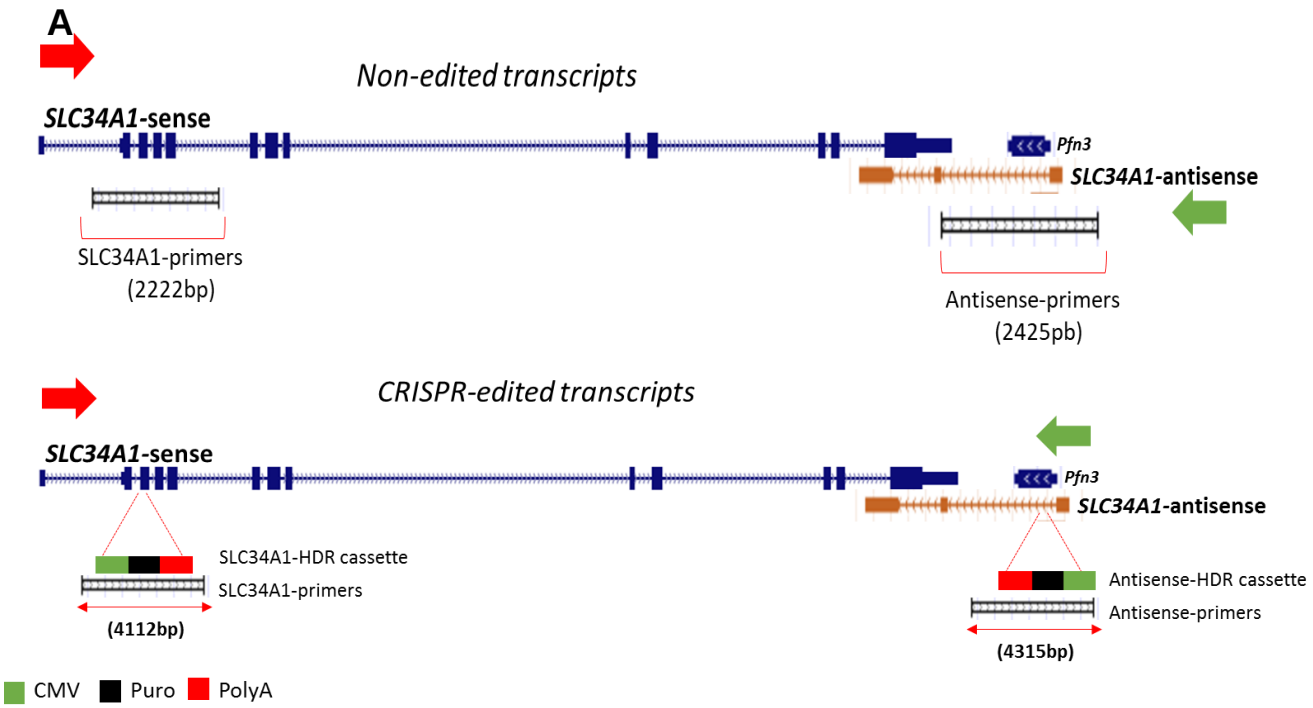

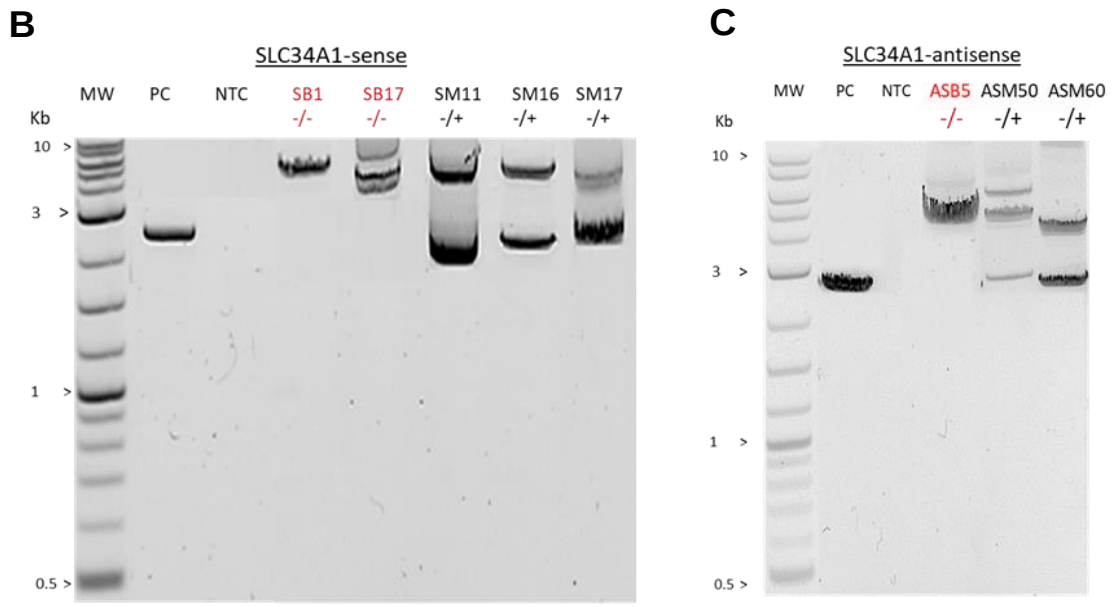

Figure 5.8: Genotypic PCR analysis. A) Diagram showing genotypic PCR primers. For SLC34A1-sense, the expected amplicon is 2222 bp, 4112 bp if the HDR cassette is integrated. Similarly, the SLC43A1-antisense derived amplicon is 2425 bp and 4315 bp with HDR cassette. B) Agarose gel of PCR products including positive (PC, unedited HEK293 cells) and negative controls (NTC, no DNA). SB1 and SB17 show bi-allelic integration (-/-, red), three clonal cells show mono-allelic integration (-/+). C) *SLC34A1*-antisense clone ASB5 with bi-allelic insertion (-/-, red), ASM50 and ASM60 with mono-allelic insertion (-/+).

5.3.8. RT-qPCR analysis of CRISPR/cas9 edited cells

After identifying cell lines with mono- and bi-allelically integrated transgenes, *SLC34A1*-sense and -antisense transcript expression were quantified, including dexamethasone inducement. To achieve this, multiple qPCR primer pairs were designed aiming to determine expression levels of transcripts before and after HDR template insertion (Figure 5.9.A).

SB1, SM11 and ASB5, ASM50 cell lines were seeded in 6-well plates in duplicates to include samples with and without dexamethasone, respectively. Total RNA was purified, integrity examined using agarose gel electrophoresis and expression of transcripts was measured by RT-qPCR.

For *SLC34A1-sense*, transcripts from three genomic regions were quantified by RT-qPCR as shown in figure 5.9.A. *SLC34A1*-specific primers (S1/S8/S9) were validated with RNA extracted from proximal renal tubular cells and Dex treated HEK293 cells (Figure 5.9.B).

In *SLC34A1*-sense edited cells (SM11 and SB1), *SLC34A1*-sense transcripts were unexpectedly upregulated from 5-to 7-fold. This effect was only observed with primers downstream of the transgene (SLC34A1-S8 and SLC34A1-S9), but not with SLC34A1-S1 where no transcripts were detected. These data suggested that transcription was initiated by the HDR-construct with incomplete termination by the polyA signal (Figure 5.9.C and D).

Interestingly, in *SLC34A1*-antisense edited cells (ASM50 and ASB5), full length *SLC34A1*-sense isoforms were detected, and the expression level was increased by more than 4-fold. RT-qPCR measurements recorded comparable levels of *SLC34A1-sense* transcripts quantified with all three primer pairs (SLC34A1 -S1/S8/S9, Figure 5.9.E and F).

On the other hand, although dexamethasone was shown to induce *SLC34A1*-sense and -antisense expression in unmodified HEK293 cells, neither SB1, SM11 nor AB5 and ASM50 clones showed a significant change in *SLC34A1*-sense expression following dexamethasone treatment.

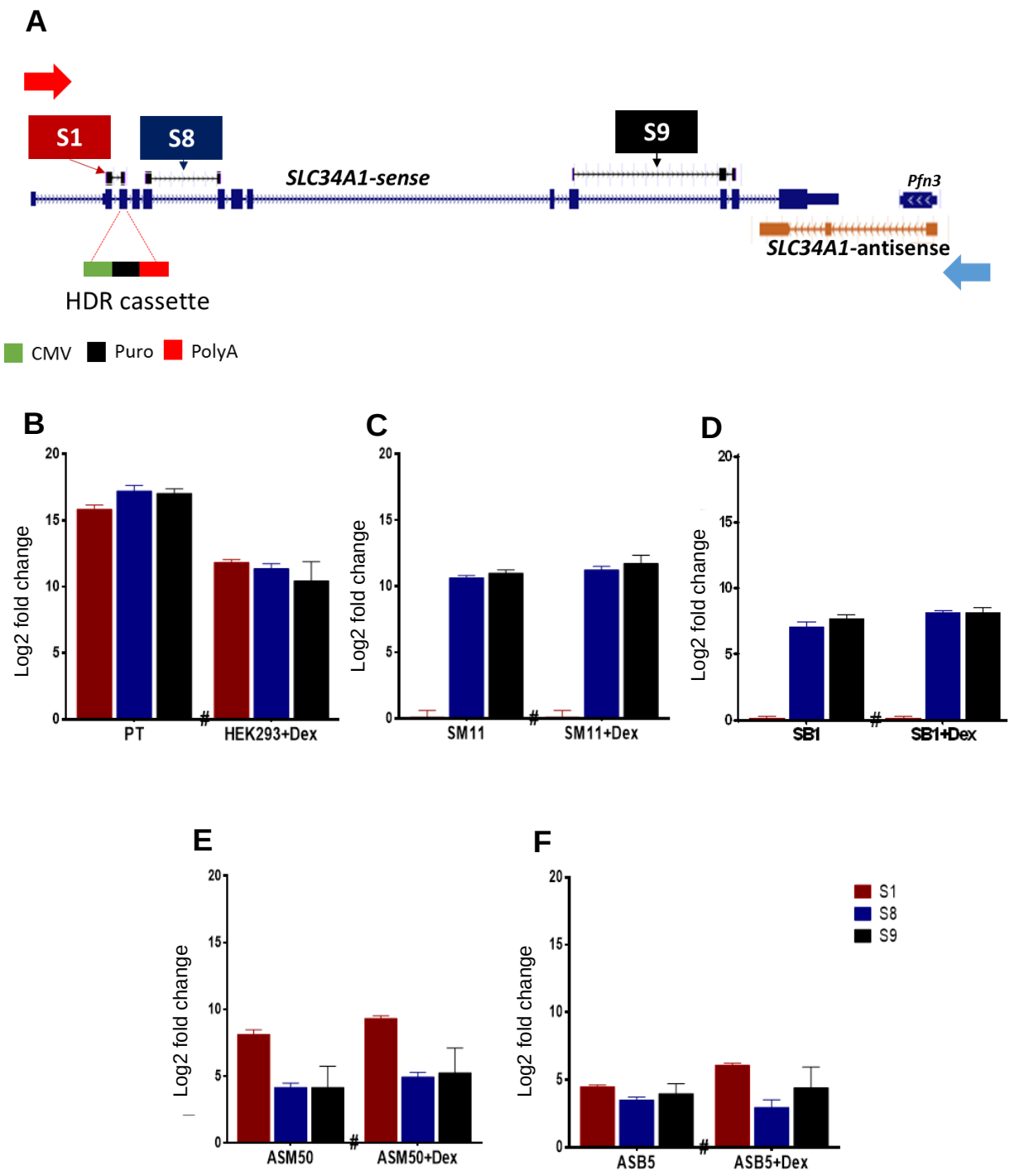

Figure 5.9: *SLC34A1*-sense expression in CRISPR/Cas9 modified cell lines. A) Diagram showing RT-qPCR primer annealing sites. Three pairs to detect *SLC34A1*-sense (S1/S8/S9) were designed. B) Primary renal cells and Dex induced HEK293 cells were used as positive controls. C-F) The *SLC34A1*-sense transcript was quantified in clones SM11 (C), SB1 (D), ASM50 (E) and ASB5 (F). The data are represented as the mean of three independent biological and three technical replicates. The expression levels were normalised to *GAPDH* and the fold change ($2^{-\Delta\Delta CT}$) was calculated in comparison to the non-treated HEK293 cells.

On the other hand, the expression pattern of the *SLC34A1*-antisense transcript was also determined using two pairs of primers, SLC34A1-AS7 and SLC34A1-AS15 (Figure 5.10.A). The primers were validated using human testis RNA and Dex-induced HEK293 cells (Figure 5.10.B).

In ASM50 and ASB5 cell clones, no transcripts were detected with SLC34A1-AS7 which bind downstream of the transgene insertion site. However with SLC34A1-AS15, enhanced expression by more than 3-fold was measured (Figure 5.10.C and D). Unexpectedly, in SM11 and SB1 cells, the entire *SLC34A1*-antisense transcript was detected, i.e. 2.18 ±1.78 and 1.69 ±0.31 fold over background, respectively (Figure 5.10.E and F). Dexamethasone had no impact on most of the cell clones; only in SB1 cells Dex lead to an increase in the antisense transcription by 3.56 ±1.3-fold (Figure 5.10.F).

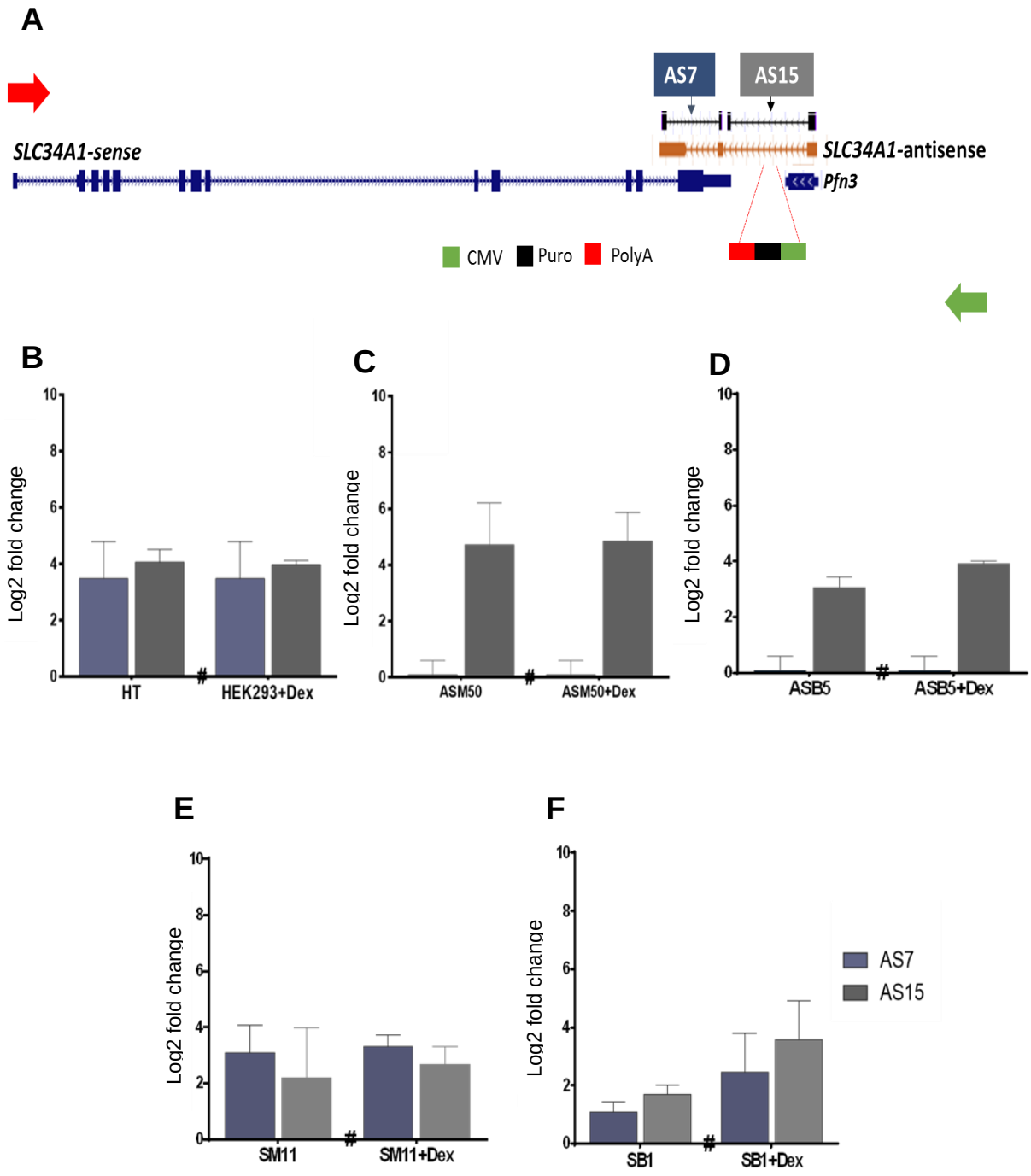

Figure 5.10: SLC34A1-antisense expression in CRISPR/Cas9 modified cell lines.
A) Diagram showing RT-qPCR primer annealing sites. Two pairs to detect SLC34A1-antisense (AS7/AS15). B) Human testis RNA, HT and Dex induced HEK293 cells were used as positive controls. C-E) The expression levels of SLC34A1-antisense in ASM50 (C), ASB5 (D), SM11 (E) and SB1 cells (F). Data are the mean from three independent biological and three technical replicates. Expression levels are normalised to *GAPDH* and the fold change ($2^{-\Delta\Delta CT}$) was calculated in comparison to the non-treated HEK293 cells.

5.3.9. Detection of functional SLC34A1-sense transporter in CRISPR/Cas9-modified cells

Western blots were performed to examine the expression of SLC34A1 protein in mono-allelic (SM11, ASM50) and bi-allelic (SB1, ASB5) cell clones as well as with HEK293 cells, before- and after- Dex inducements. Two primary antibodies were used, both raised in rabbits (AB17 and AB15), against peptides at the N and C-terminus of transporter. Protein lysate from mice renal BBM were included as a positive control. Cell lysates were separated on a 9 % SDS-PAGE gel followed by transfer to PVDF membranes.

As demonstrated in figure 5.11.A and B, the positive control samples (mice renal BBM protein) showed two prominent bands of about 80 kD and 45 kD. In addition, AB15 showed some signal slightly below 100 kD. Bands of similar size were only detected in ASB5 cells treated with Dex. No evidence of the transporter was detected in other samples. The PVDF membranes were stripped and re-probed for β-actin to demonstrate equal amounts of protein were loaded (Figure 12.A and B, bottom panel).

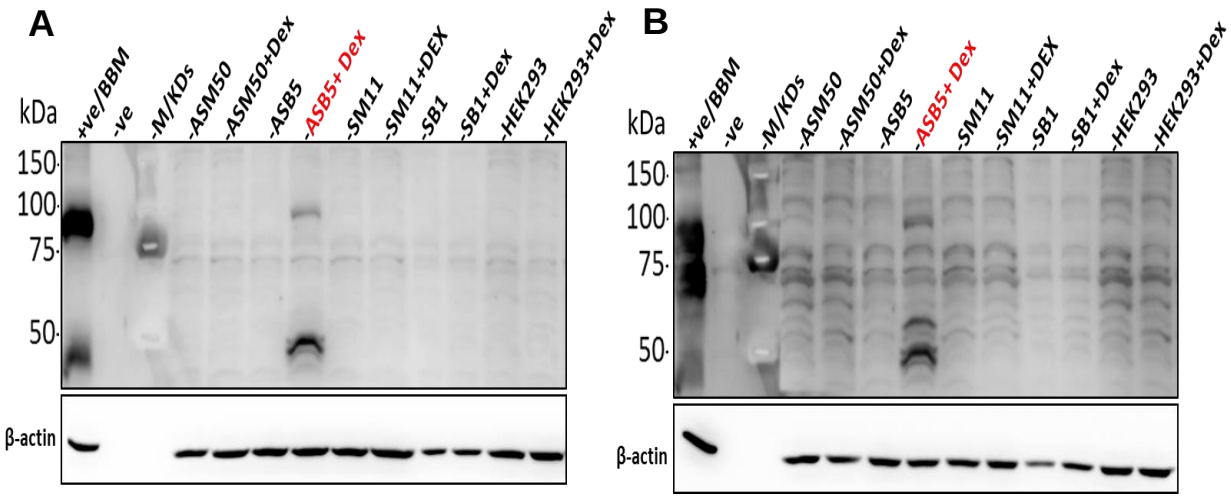

Figure 5.11: Western blot analysis of CRISPR/Cas9-edited HEK293 cells. Two different antibodies were used for the detection of the SLC34A1 transporter, recognising the N and C-terminus of the transporter (AB15 and AB17). Cell lysates were separated on SDS-PAGE gels and transferred to PVDF membranes. Membranes were probed with antibodies AB17 (A) and AB15 (B). The same membranes were stripped and re-probed for β-actin. The red highlighted lanes represent the ASB5+Dex samples which show bands comparable to the control (mice renal BBM protein). For ease identification, cell clones named used as follow; SLC34A1-sense (S), SLC34A1-antisense (AS), mono-allelic (M) and bi-allelic (B).

5.4. Discussion

The mode of interaction between a protein coding and non-coding transcript sharing a bidirectionally transcribed locus has been investigated in a number of studies. In general, either a concordant or a discordant mode of regulation can be established (Wood *et al.*, 2013). Our previous experiments using HEK293 cells and Dex suggested a concordant pattern of interaction between *SLC34A1*-sense and -antisense transcripts. Therefore, we sought to strengthen this assumption by interfering with *SLC34A1*-sense and *SLC34A1*-antisense transcription using the CRISPR/Cas9 genome-editing tool.

5.4.1. CRISPR/Cas9 strategy

The CRISPR/Cas9 system represents a powerful approach to modulate protein coding and non-coding gene expression. Nevertheless, several limiting factors were found to challenge the efficiency of the technique. For example, the complexity of the target locus with multiple transcripts from overlapping genes may complicate interference with one specific gene. Moreover, some type of the cells are better suited than others such as primary cells or polyploid cell lines. Then, the transcriptional activity of the selected genes, active or silent, may influence the outcome of the experiment (Goyal *et al.*, 2016). The work here was fortunately not affected by these pitfalls, nevertheless, established protocols were very carefully followed and critical steps such as gRNA selection and transfection efficiency were optimized (Ran *et al.*, 2013a; Goyal *et al.*, 2017).

Interfering with transcription to knock out a transcript is more challenging than eliminating a functional protein –which often requires a simple frame shift shortly after the translation start site. Therefore, a strategy to delete short- or long-DNA fragments from promoter regions have been used to modify both coding and noncoding transcript expression. From a technical point of view, a deletion approach could be performed by co-transfection of multiple sgRNA's. However, this approach has limitations such as sgRNA's off-target effects that could lead to phenotypic and functional changes. Moreover, ncRNA transcripts were often found not to be silenced, possibly driven by alternative promoters (Chiruvella *et al.*, 2013; Han *et al.*, 2014). Alternatively, HDR genomic integrations represent a powerful tool particularly for modifying coding and non-coding transcript expression (Liang *et al.*, 1998; Perez *et al.*, 2008; Santiago *et al.*, 2008).

The strategy of inserting transcription termination signals was adopted to suppress the expression of specific genes (Calvo and Manley, 2003; Goyal *et al.*, 2017). The efficiency of this approach have been examined with both protein coding and non-coding transcripts such as protein phosphatase 1 regulatory subunit 12c (*PPP1R12C*), nop2/sun RNA methyltransferase 2 (*NSUN2*) and antisense of *IGF2R* non-protein coding RNA (*Airn*) transcripts (Batt *et al.*, 1994; Latos *et al.*, 2012; Liu *et al.*, 2017).

Because of the heterogeneous nature of noncoding RNA transcripts, some challenges have be taken into account when silencing such transcripts. For example, Gutschner *et al.* aimed to knock out *MALAT1* in A549 cells using either a polyA signal or a simian virus 40 (SV40) termination sequence. Despite the noticeable reduction in *MALAT1* expression with the SV40 motif, a strong reduction of more than 1000-fold was only achieved with the polyA termination cassette. Considering these findings a protocol including a polyA termination sequence was planned to silence the SLC34A1-sense/antisense transcripts (Gutschner *et al.*, 2011).

A complicating factor was that the endogenous promoter for both *SLC34A1*-sense and -antisense transcripts is relatively inactive in HEK293 cells. As a result, an antibiotic resistance encoding transgene that would solely depend on the intrinsic promoter for expression may not be expressed at a level sufficient to protect the transfected cells. Therefore to avoid compromising cell viability following antibiotic

treatment, the expression of the inserted template was driven by a CMV promoter (Supharattanasitthi *et al.*, 2019).

5.4.2. SLC34A1-sense and SLC34A1-antisense expression profiling

Surprisingly, the expression profiles for *SLC34A1*-sense and *SLC34A1*-antisense were found to be up- rather than down-regulated in response to the inserted transgenes. Initial experiments showed no evidence of transcriptional termination in cell lines with both mono- and bi-allelic integration. Therefore, extensive expression analysis was performed using multiple primer combinations up- and downstream of the HDR-integration site (Figure 5.9.A and 5.10.A).

Importantly, in *SLC34A1*-sense modified cells (SB1 and SM11), full-length *SLC34A1*-antisense transcripts were detected using SLC34A1-AS7 and AS15 primer pairs. Conversely in the antisense modified cells (ASM50 and ASB5), the expression of the *SLC34A1*-sense transcript was increased as recorded by SLC34A1-S1/S8/S9 primer pairs. This observation corroborates previous findings that the expression of the two complementary transcripts is positively correlated. This suggests that the *SLC34A1*-antisense transcript could play a significant role in stabilizing the *SLC34A1*-sense transcript, and vice versa. The scenario of transcript stabilsation has been reported for several coding/noncoding transcript pairs. For example, the *HIF1a* gene is bi-directionally transcribed and the antisense transcript stimulates the expression of the sense encoded hypoxia inducible factor 1 subunit alpha (*HIF1a*) by masking an RNA degradation motif. A resemble mode of action has been proposed for antisense transcripts regulating angiopoietin 1 (*ANG-1*), angiopoietin 2 (*ANG-2*), transforming growth factor alpha (*TGF-α*) and vascular endothelial growth factor (*VEGF*) genes (Xie *et al.*, 2019). Similarly, the *BACE1-AS* transcript blocks a miRNA sites in the *BACE* transcript, this mode of action was also found in patients with Alzheimer disease (Faghihi *et al.*, 2008a).

As a result of genomic editing, truncated *SLC34A1*-sense and -antisense transcripts were detected downstream of the transgene cassette, with no transcripts detected upstream of the insertion, using primers SLC34A1-S1 and SLC34A1-AS7, respectively. A likely interpretation for this scenario predicts that the strong CMV-

promoter activates transcription to provide antibiotic resistance but also produces a read-through transcript across the polyA signal leading to truncated *SLC34A1*-sense and -antisense transcripts. Furthermore, the stabilisation of the two complementary transcripts may have favoured the read-through.

Although a read-through as a consequence of genome editing appears to be a rare event, others used repeats of polyadenylation signals to mitigate a potential read-through scenario, particularly following strong endogenous or exogenous promoters (Batt *et al.*, 1994; Latos *et al.*, 2012; Lv *et al.*, 2016; Liu *et al.*, 2017; Wang *et al.*, 2018). Alternatively, a human β-globin termination motif could have been used to terminate transcription or multiple polyadenylation sites (Ashe *et al.*, 1997).

5.4.3. SLC34A1-sense transporter detection

The presence of the SLC34A1 transporter was relatively difficult to detect by western blot experiments. Despite considerable efforts, correct bands could only be detected in genetically modified cells (ASB5) stimulated with Dex. Neither in wild type nor most Dex treated cell lines (SB1, SM11, ASB5 and ASM50), SLC34A1 related protein was detected. This may be due to a dosage effect, both with expression and detection. For instance, a certain level of transcripts needs to be reached to result in a detectable export/translation/membrane delivery of the protein. Similarly, the antibody detection is not linear, as the minimum differences in protein concentration may have a much more pronounced signal difference in western signal. Moreover, our western blot results suggested that although Dex had a positive impact on *SLC34A1*-sense transcription, the translation mechanism could be affected. Similar observations have been reported by others, specifically that Dex treatment after extended exposure can negatively impact on protein synthesis and stability (Crisafulli *et al.*, 2018).

Another possible interpretation is that the 3’ overlap between *SLC34A1*-sense and -antisense transcripts leads to sense/antisense double-strand RNA formation which could significantly modulate processing, transport, modification and translation of *SLC34A1* mRNA (Djebali *et al.*, 2012a; Sinturel *et al.*, 2015).

Although RT-qPCR showed *SLC34A1*-sense upregulation in different modified cell lines (including ASM50), a frameshift or mutation within the transporter following CRISPR intervention may have caused a reduction of detectable protein on western blots (Bass *et al.*, 2017).

5.5. Conclusions

Despite the fact that the read-though scenario was totally unexpected, the collected expression data from CRISPR/Cas9 modified cell lines corroborates the positive relationship between *SLC34A1*-sense and -the antisense expression.

To better understand the role of the *SLC34A1*-antisense transcript (particularly in SLC34A1-antisense edited cells, SM11 and SB1), in-depth epigenetic analysis (i.e. DNA methylation and histone epitope analysis) at the SLC34A1 locus should be performed.

Chapter 6: Pi homeostasis and the human gut microbiome

6.1. Introduction

Gut microbiota coevolve with host organs in performing various functions such as food digestion, vitamin biosynthesis, enhance mineral bioavailability, protection against other pathogens and immune system development (Backhed *et al.*, 2005). Some researchers refer to the gut microbiome as an additional body organ without distinct structure (Shanahan, 2002).

Based on phylogenetic classifications the most dominant bacteria in the human gut can be divided into *Bacteroidetes, Firmicutes, Actinobacteria, Proteobacteria* and *Cerrucomicrobia* (Tang *et al.*, 2017). Under healthy circumstances, an individual's enterotype, the blueprint copy of phyla, taxa and species, is unique for each person. Dysbiosis (imbalanced microbiome communities) is diagnosed mainly in response to dietary change, environmental factors and prolonged antibiotic treatment (Gorvitovskaia *et al.*, 2016; Tamburini *et al.*, 2016).

The diet is considered as one of the essential factors that modulate the composition of an individual's enterotype. In this context, many studies have evaluated the relationship between certain nutritional components and the gut microbiome. For example, the level of bile-tolerant bacterial species was increased after shifting to an animal-based diet rich in carbohydrates and protein (David *et al.*, 2014). Similarly, food supplemented with an excess of minerals such as iron (Dostal *et al.*, 2015), zinc (Zhang *et al.*, 2015a), calcium (Whisner *et al.*, 2016), magnesium, selenium or silver (Kortman *et al.*, 2014; Asemi *et al.*, 2017; Skrypnik and Suliburska, 2018), significantly alter human gut bacterial composition, as compared to control individuals.

With respect to the production of processed food, many phosphorus-based compounds such as phosphoric acid, sodium phosphate, potassium phosphate, calcium phosphate, magnesium phosphate and sodium aluminum phosphate are added for different purposes, as preservatives, acidifying agent, to prevent powdered food from clumping and to enhance flavour.

Although Pi levels in plasma are tightly controlled by hormonal and non-hormonal mechanisms, both high and low Pi diet have deleterious health consequences. Free Pi is absorbed by the GI tract predominantly via the paracellular pathway along its concentration gradient. This leads to postprandial Pi spikes in plasma (Uribarri, 2007) and there is growing concern that Pi in food additives could increase the risk of hyperphosphatemia and cause renal and cardiovascular complications (Gutiérrez, 2013). On the other hand, prolonged consumption of a low Pi diet is linked to hypophosphatemia associated with skeletal complications such as osteomalacia and rickets (Sahay and Sahay, 2012).

Comprehensive surveys revealed that the daily Pi intake with a western diet is increasing and has surpassed the recommended maximal daily consumption of 700 mg/day (Chang and Anderson, 2017). For example, according to the National Health and Nutrition Examination Survey in the United States, the average dietary Pi intake has risen from 800 to more than 1200 mg/day between 1994 and 1998. While the Pi load continues to increase, the deleterious consequences have become apparent already in a follow-up study in 2006, which reported that most of the volunteers participating in the survey developed cardiovascular complications and had a higher mortality rate, potentially linked to high Pi intake (Chang *et al.*, 2014). As a consequence, new regulations were issued by European authorities restricting the amount of Pi added to soft drinks to a maximum of 700 mg/L (Ritz *et al.*, 2012a). Excessive intake of dietary Pi is now considered as a major health concern (Sherman and Mehta, 2009).

Prophylactic measures are required to mitigate the high Pi load, especially in patients with renal complications and hyperphosphatemia (Chan *et al.*, 2017). These recommendations include the prescription of phosphate-binders such as calcium, aluminium as well as ferric and lanthanum- based drugs. These chemicals exhibit high affinity to and complex free, anionic Pi. The Pi binders reduce the level of free Pi, hence reduce its bioavailability and absorption across the intestinal epithelium. The complexed Pi is eventually eliminated with the faeces. Although the levels of blood Pi only decrease by about 30 % in response to Pi binders (Chan *et al.*, 2017), the consequences of using these drugs on the gut microbiome could be significant and merits to be investigated further.

6.2. Aims

In this chapter of the thesis the aims are:

1. Isolate and sequence DNA from stool samples and eventually determine the gut microbiota composition following a high (1000 mg Pi in lunch and dinner) and a low Pi diet induced by taking the Pi binder Sevelamer.
2. Determine and examine the abundance of bacterial phyla, taxa and species in response to the high/low Pi diet.

6.3. Experimental design

The experiment was originally designed by Prof Carsten Wagner, Institute of Physiology, Zurich University. The study aimed to mimic high/low Pi intake– but a low Pi diet without medical reason is a health risk and hence an unethical intervention. The study was designed as a cross-over study with two groups of 4 probands. The first group was given a premade diet with fixed high phosphate content (HP) of 1000 mg per meal for 5 days. Other parameters such as salt content, calories, carbohydrates, fat, and protein were kept constant. The probands received these diets for lunch and dinner, moreover, recommendations were given for breakfast meals. The second group received the phosphate binder Sevelamer with the meals to simulate a low phosphate diet for 5 days (LP) followed by a washout period of 10 days. After the washout period, the two proband groups were crossed-over, i.e. the HP group was given Sevelamer for 5 days, and the LP group received HP for another 5 days but without the phosphate binder. Urine, stool and blood samples were routinely collected (see also Figure 2.6).

The study included only male, healthy volunteers, aged between 20-45 years. All participants were pre-screened, some were given vitD3 supplements to bring their vitD3 levels into the normal range. Exclusion criteria were: kidney disease, diabetes mellitus, hypertension, hypotension, regular medication, vegetarian/vegan diet, history of kidney stones, allergy to sulphonamides or penicillin, known hypersensitivity or allergy to the class of drugs used in this study, glaucoma, hyper- or hypo-parathyroidism, hypo- or hyperaldosteronism, use of drugs by the probands and participation in any other study.

6.4. Results

6.4.1. Blood and urine Pi measurements

Pi levels were determined from the collected blood and urine samples. The initial results showed an overall reduction in urine Pi levels in response to Sevelamer treatment from 390 to 195 mg/24 h in bander probands, with no effect on serum Pi, as compared to HP members (Figure 6.1.A and B).

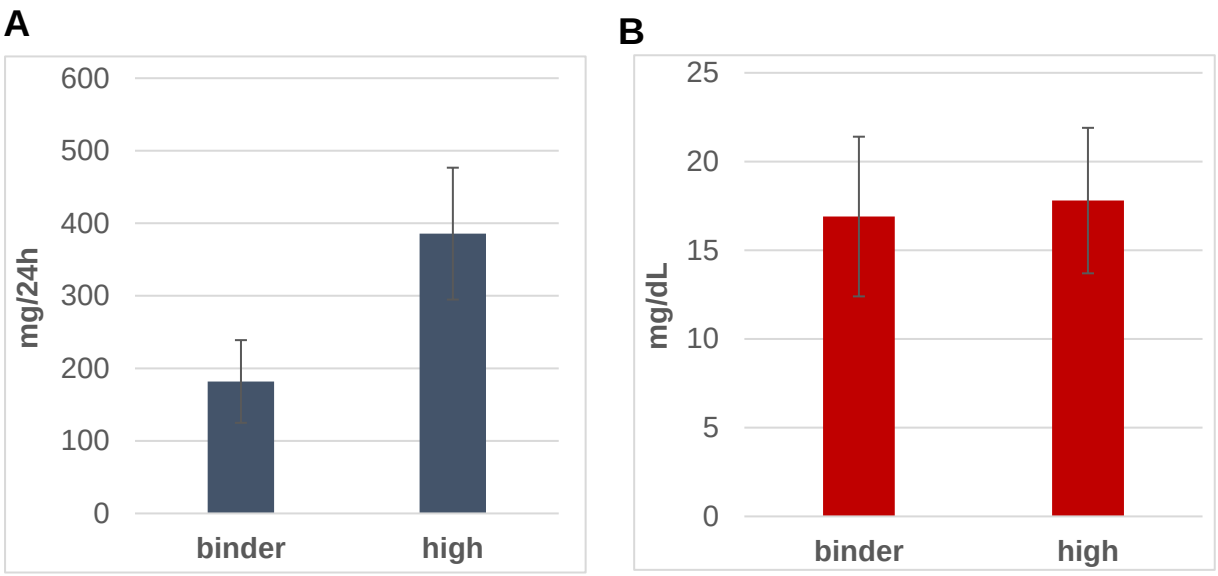

Figure 6.1: The level of Pi in (A) urine and (B) serum following high Pi diet and Sevelamer treatment.

6.4.2. DNA quantification from the stool samples

By the end of the treatment regimen, a total of 16 stool samples were collected. For referencing, the probands 1, 6, 7 and 8 started with Sevelamer, then switched to the high Pi diet. On the other hand, probands 2, 3, 4 and 5 consumed initially the high Pi meals and received Sevelamer in the second phase of the trial. DNA was purified and quantified from the stool samples following the protocol established in Dr Hall's lab (as indicated in 2.12.1). The exact amount of stool used for extraction and the yields of purified DNA are listed in table 6.1.

Table 6. 1: Quantification of purified DNA from the stool samples.

Sample No.	Reference code	Weight stool samples (mg)	DNA concentration in ng/µL
1	001HSV7	199	198
	001HSV12	202	191
2	005LHV7	201	146
	005LHV12	202	294
3	007MRV7	199	366
	007MRV12	200	447
4	010GRV7	198	145
	010GRV12	199	161
5	014ACV7	200	148
	014ACV12	201	273
6	019CKV7	200	570
	019CKV12	201	116
7	023RMV7	201	256
	023RMV12	197	219
8	024RGV7	200	300
	024RGV12	197	263

6.4.3. DNA sequencing library preparations and analysis strategy

The libraries for NGS sequencing were prepared and sequenced at the Wellcome Sanger Institute, Cambridge, UK using a Illumina Hi-Seq platform with a read length of 100 or 125 bp following established protocols (Forster *et al.*, 2019).

The reads were then aligned and assessed using the pipeline established in the lab of Lindsay Hall. Furthermore, for confirmation purposes, data were reassessed kindly by Dr Christopher Stewart (Newcastle University). Two of the samples which showed low read counts were submitted for re-sequencing. Data rarefaction curve was adjusted between 20,000 to 100,000 read depth. To avoid skewing in comparison tests and potential omission of bacterial species, 95200 reads was considered as the cut off level, as shown in figure 6.2.

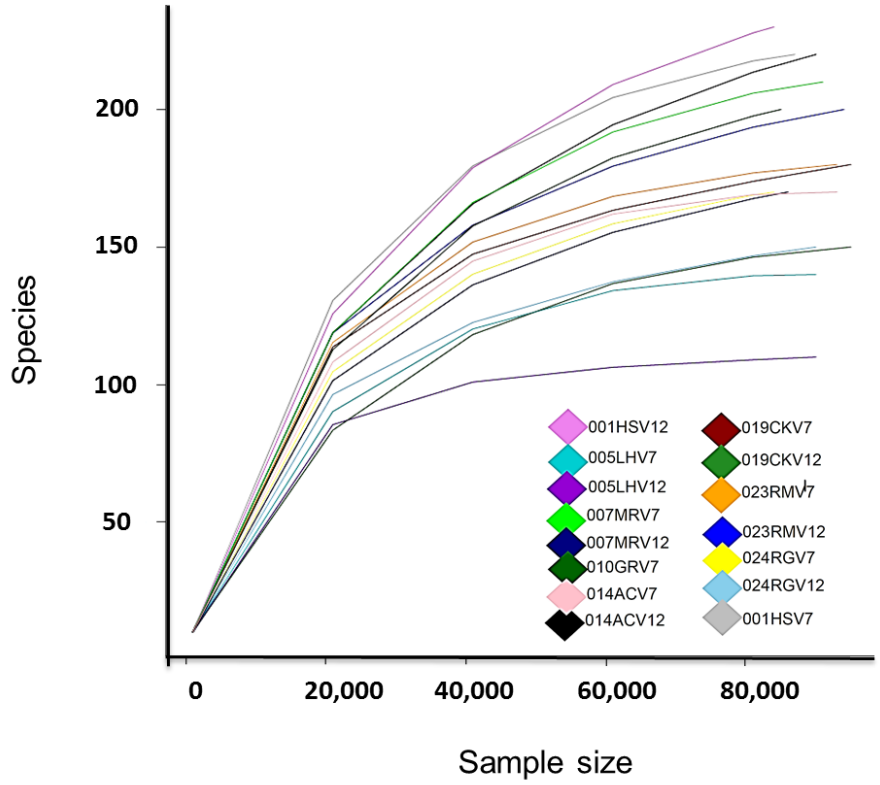

Figure 6.2: Sequencing rarefaction curves. Microbiome sequencing read counts for the 16 colour coded samples.

For data analysis, two ecological approaches were applied; alpha diversity, which measures the level of richness and evenness within samples, and beta diversity, to quantify microbiota compositions between samples. In addition, the relative abundance of bacterial phyla and species were also determined and compared between HP and Pi-binder/LP diet probands.

6.4.4. The estimated levels of α-diversity

The differences between both dietary conditions were assessed according to the groups (i.e. HP versus LP probands) and within each individual (i.e. data were examined for each person, before and after Pi intervention). Samples richness was estimated based on operational taxonomic unit (OTU) similarities and the differences in the OTU reads were estimated using Kruskal-Wallis statistical analysis. Species diversity was also assessed by calculating the Shannon diversity index.

The group comparison showed no significant difference in the observed OTU numbers between HP and LP probands (P= 0.68), as demonstrated in figure 6.3.A. Similarly, the Shannon index indicated that Pi interventions did not significantly affect bacterial composition between the two examined groups (P=0.69, Figure 6.3.B). At individual proband level, OTUs and Shannon test results showed no significant changes in richness and evenness of bacteria in the collected samples over the study period (Figures 6.3.C and D).

On the other hand, the data were also compared for each proband between the samples. Probands which were given Sevelamer at the beginning of the study experienced a consistent increase in α-diversity levels: The α-level of samples 2, 3, 4 and 5 was 8,12, 9 and 12 after Sevelamer addition, respectively. However, after the high Pi diet the α-levels decreased to 7, 9, 6 and 10, respectively. In contrast, the other group of probands which started with a high Pi diet and then switched to Sevelamer (samples 1, 6, 7, and 8) displayed a different pattern of bacterial richness. After the high Pi diet α-levels were 14, 11, 10 and 8, following Sevelamer application the α- diversity estimation levels were slightly reduced to 12, 11, 9 and 7, respectively.

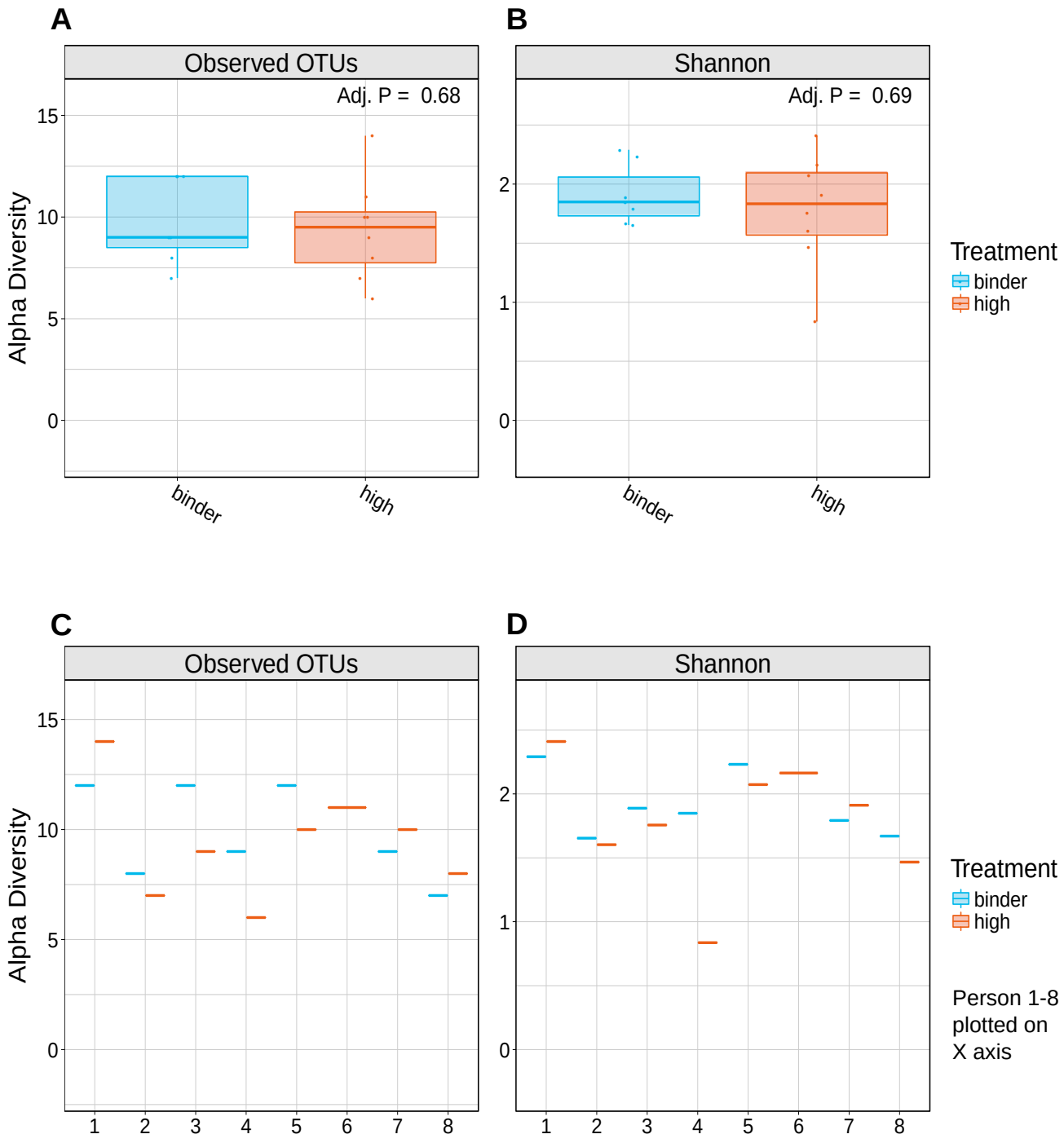

Figure 6.3: α-diversity analysis following high/low Pi dietary interventions. A) The observed operational taxonomic units (OTUs) were compared between high/low-Pi groups. B) Shannon diversity testing was applied to compare microbiome evenness in the samples of the two groups. C) OTU numbers were examined for each participant in the study and D) Shannon index.

6.4.5. The estimated levels of ß diversity

The concept behind β diversity is to compare the bacterial composition of each participant before- and after- Pi modulation in multidimensional scale measurements as compared with other participant. As a result, the microbiome of HP and LP probands become clustered in two-dimensional matrixes. The data were plotted against two principle component axes, PC1 and PC2 at 37.7 % and 20.5 % variations explained, respectively. The term 'variation explained' is used to predict the discrepancy between data variance of the particular component compared to the total variance (Rosenthal and Rosenthal, 2011).

Data dissimilarities were quantified using weighted unique fraction principle coordinate analysis (Weighted UniFrac PCoA), as previously described (Koleff *et al.*, 2003; Lozupone *et al.*, 2011). The calculations showed minor alteration in bacterial content following Pi intervention, these differences however did not reach significance levels (P=0.943, Figure 6.4).

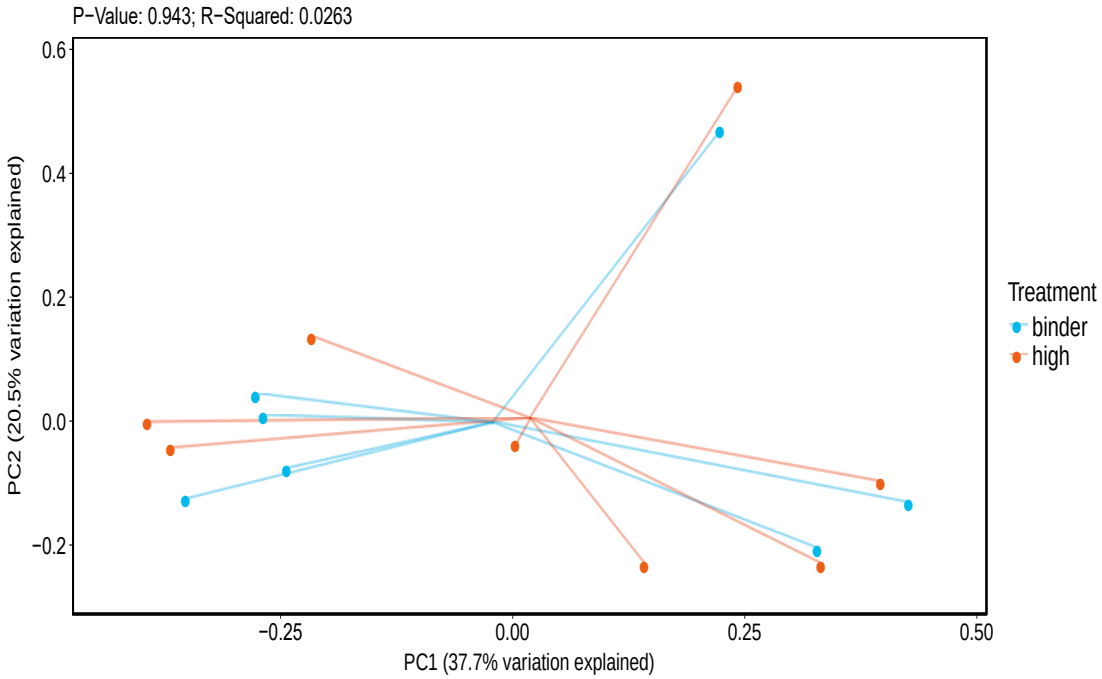

Figure 6.4: ß diversity using weighted unique fraction analysis (weighted UniFrac). Samples plotted on PC1 and PC2 variation percentages. Each sphere represents the average bacterial diversity of an individual sample. The orange cluster refers to the high Pi diet and blue to the binder treatment. The P-value was measured based on the distance between the cluster hubs (i.e. weighted Unifrac analysis).

6.4.6. Bacterial Relative abundances

Next, the abundance of bacterial phyla and species were determined. Following alignment, sequence reads were found to map predominantly to five bacterial phyla including *Bacteroidetes, Firmicutes, Actinobacteria, Proteobacteria* and *Cerrucomicrobia* , as shown in figure 6.5.A. False discovery rate (FDR) corrections were applied for multiple comparisons between phyla. Although no significant changes in abundance of bacterial phyla was recorded before and after Pi intervention, the average percentage of *Bacteroidetes* was reduced remarkably from 16 % in HP probands to 4 % following Sevelamer administration (Figure 6.5.A).

On a species level, approximately 70 bacterial species were reported. For further analysis only the 14 most abundant ones were included (Figure 6.5.B). In general, no significant changes among individual bacterial species were observed. Nevertheless, the relative abundance of *Bacteroides uniformis* and *Roseburia intestinalis* increased from 0.25 to 2.5 % and 0.19 to 2 %, respectively, in 6 HP probands. Likewise, the abundance of *Bifidobacterium adolescentis* and *Dorea formicigenerans* were also changed from 0.47 to 6 % and 0.39 to 3 %, respectively, in 5 LP probands (Figure 6.5.B).

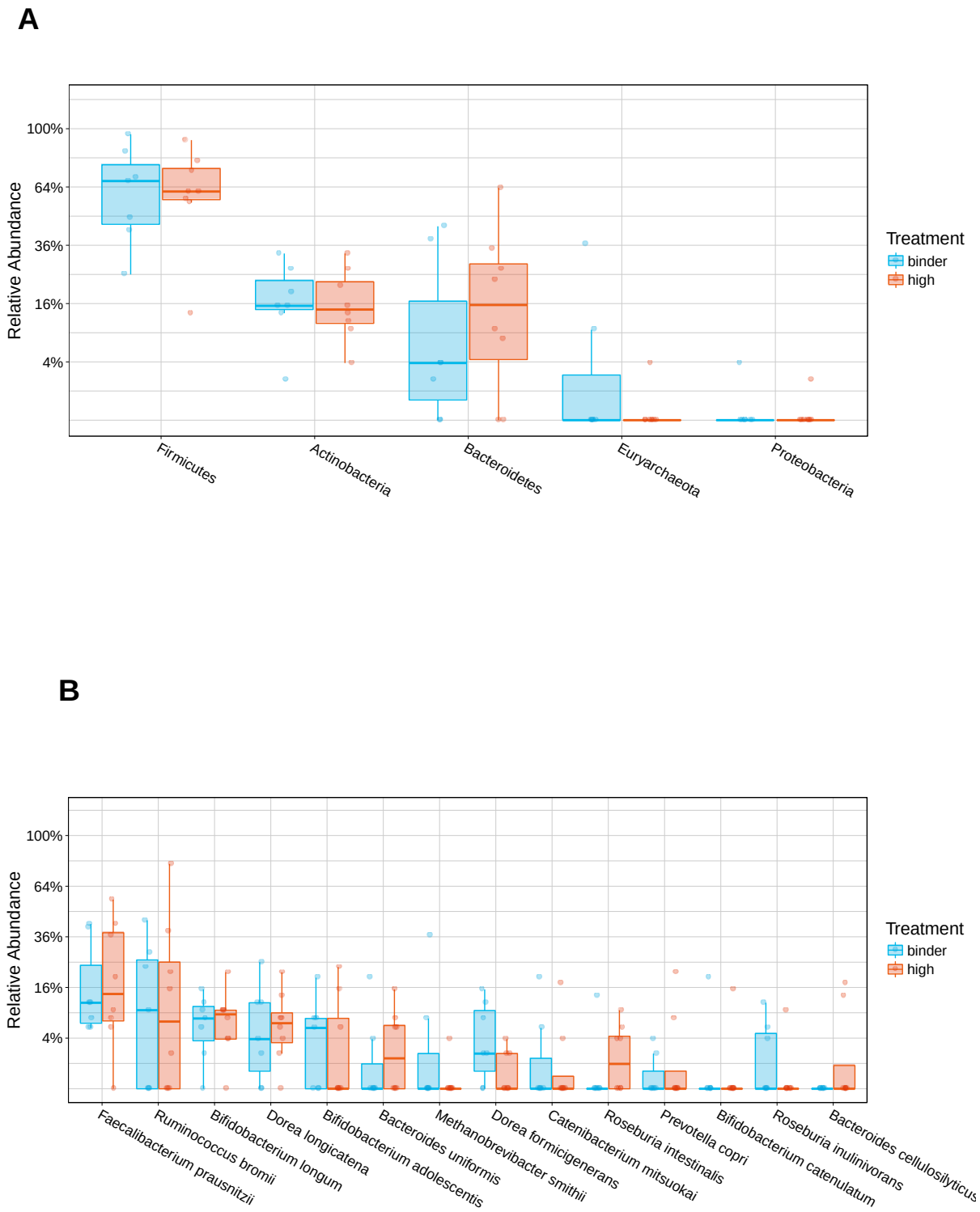

Figure 6.5: Representation of bacterial phyla (A) and species (B) in stool samples after high/low Pi diet.

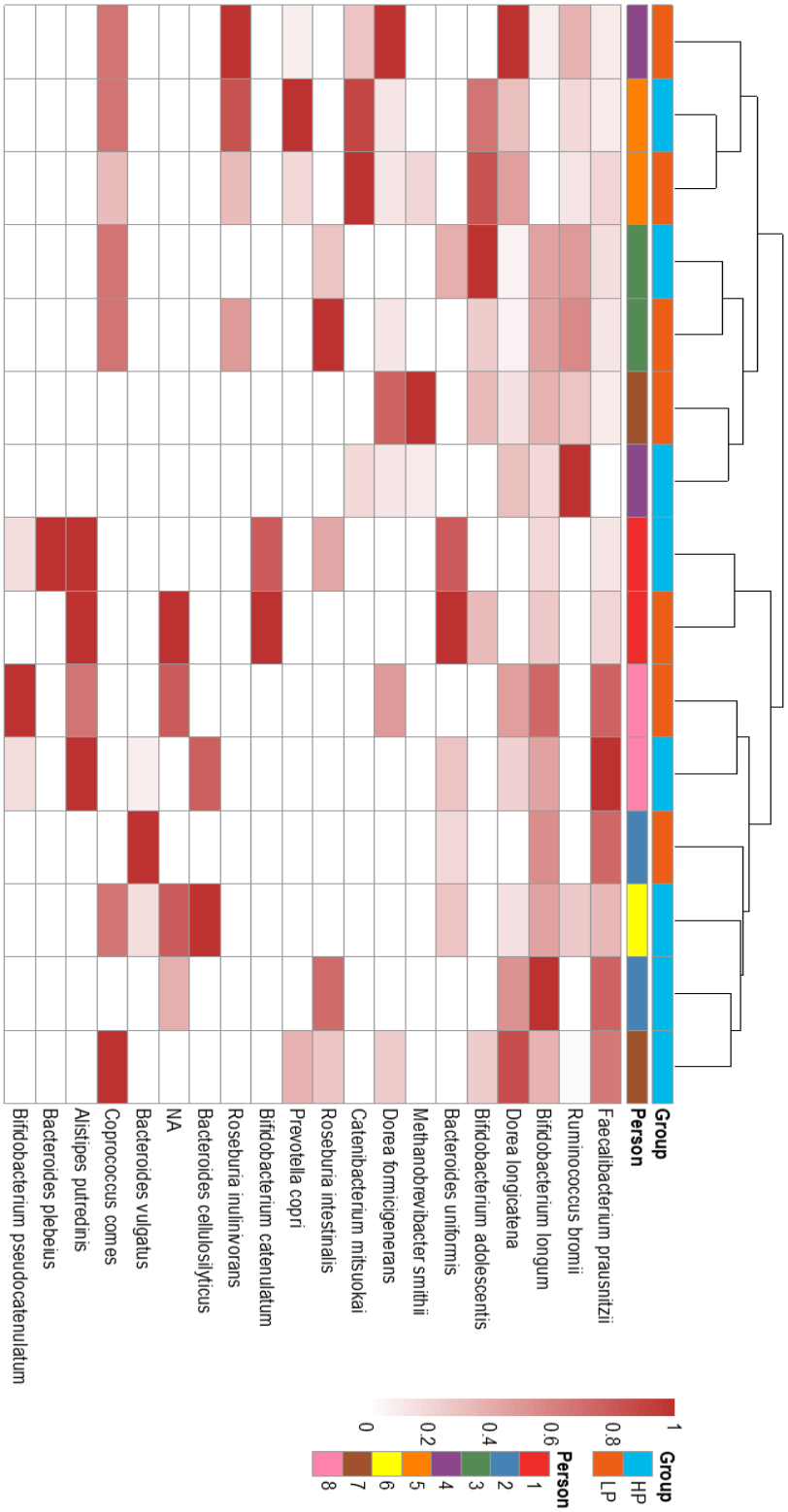

Figure 6.6: Heat-map of the most representative gut bacterial species in the examined stool samples following high/low-Pi diet interventions.

6.5. Discussion

The impact of high Pi intake on the gut microbiome has been investigated previously in both human- and animal-based models (Ditscheid *et al.*, 2005b; Borda-Molina *et al.*, 2016; Trautvetter *et al.*, 2016). It has been proposed that an excess of Pi tends to form amorphous calcium phosphate salts which adsorb fatty/bile acids in gut resulting in altered intestinal pH levels. As a consequence an increase or decrease in certain bacterial species such as *Lactobacillus paracasei* and *Clostridium XVIII* was observed (Govers and Van der Meet, 1993; Grimm *et al.*, 2001; Ditscheid *et al.*, 2005a; Trautvetter *et al.*, 2012; Metzler-Zebeli *et al.*, 2013; Trautvetter *et al.*, 2018).

The formation of amorphous salts has been investigated using pigs as a model that were feed a highly Pi enriched diet. The metagenomic data demonstrated a significant increase in strictly anaerobic bacteria particularly in small intestine, paralleled by a reduction in butyrate fermenting bacteria in large intestine (Metzler-Zebeli *et al.*, 2010). A similar study focusing on mucosa associated bacteria in the stomach of pigs showed that the abundance of *Lactobacillus* was also enriched by approximately 1.4-fold in response to a high Pi diet (Mann *et al.*, 2014).

In this study, we considered the hypothesis that the gut microbiome may contribute to maintaining host Pi homeostasis. This assumption is supported by previous evidence which showed that growth of certain bacterial species could either be enhanced or repressed in response to an altered Pi regimen. Thus, adapted bacterial species could potentially manipulate Pi levels and hence affect the intestinal absorption. The consequences of an acute switch from a high to a low-Pi diet and vice versa on the gut microbiota -to the best of my knowledge- has not been investigated in human.

6.5.1. Pi exhibited limited effect on gut microbiota diversity

To determine the effect of a high/low Pi diet on the diversity of gut microbiota, stool samples were collected in this crossover study. Lunch and dinner meals were supplemented with 1000 mg of Pi meanwhile the Pi binder Sevelamer was given to the second group of probands. At the end of the study, genomic sequencing was

performed using DNA isolated from 16 stool samples (as explained in section 6.3). To assess the impact of altered Pi levels in the diet, the sequencing data were investigated and analysed on group level and within individual probands.

When focusing on individual probands, the OTU and Shannon index indicated no enrichment of specific bacterial species following neither high nor low Pi diet interventions. Similarly, for the entire group, β diversity of the gut microbiome did not change in response to either of the dietary regimens. A number of possible interpretations may explain the absence of significant changes, as discussed below.

From experimental point of view, it is very important to involve baseline (day zero) samples and/or placebo probands. Such data could provide a reference for an individual's enterotype composition (Sinha *et al.*, 2015; Weaver and Miller, 2017). However, due to volunteer recruitment and other logistic limitations, neither pre-intervention samples nor a placebo group were incorporated in the current study. Hence the sequencing data was compared to detect differences before- and after- Pi intervention only.

The second limitation of the presented study concerns the short duration of the dietary intervention. Depending on the nature of the tested compound, previous studies have shown variations within the microbiome after both short (hours) and long (days) exposure. For example, the abundance of over 60 % of human gut microbial species was changed within 24 h of ingesting pureed human baby foods. This experiment was performed and conducted using gnotobiotic mice as a model (Turnbaugh *et al.*, 2009; Faith *et al.*, 2011). Comparable findings were reported from a human study, where 24 h of a high-fat/low-fiber or a low-fat/high-fiber diet was sufficient to induce significant changes in *Bacteroides* and *Prevotella* abundance (Wu *et al.*, 2011).

In contrast, other experiments have failed to demonstrate significant alterations in microbial composition even when human cohorts were exposed to a particular diet at an extended timescale, i.e. from weeks to months. In these experiments the microbiome only displayed minor changes that were limited to specific bacterial taxa (Ley *et al.*, 2006; Russell *et al.*, 2011; Walker *et al.*, 2011).

In this experiment, the impact of a high Pi diet and Sevelamer intake were only investigated after 5 days of intervention. However, it remains to be established how

rapidly the gut microbiota adapts to the new dietary environment. It would be highly informative to monitor microbial diversity over a time course, for instance a long intervention with sampling after 0, 1, 5, 7 days and maybe 2 and 4 weeks, for example.

The study has another potential short fall which is difficult to address and relates to anatomical considerations. Pi is mainly absorbed in the duodenum potentially by paracellular flux driven by the concentration gradient as well as by transcellular, *SLC34A2*-mediated transport. However, the stool samples reflect bacterial populations that cohabitate mainly within large intestine (Huttenhower *et al.*, 2012). An animal-based experimental strategy could provide a more precise answer with the analysis of small intestinal samples after a high/low Pi dietary intervention.

6.5.2. Sevelamer reduces Bacteroidetes abundance

The Pi binder Sevelamer is a non-absorbable polymer characterised by a high affinity for anions, particularly Pi (Garg *et al.*, 2005). Following extensive experiential trials, Sevelamer was found to reduce the levels of intestinal endotoxins (Sun *et al.*, 2009), bile acids (Braunlin *et al.*, 2002) and urate (Garg *et al.*, 2005). As a result, various gut microbiota could be affected because of the broad specificity of the drug (Guo *et al.*, 2016).

In our experiment, the probands who were given Sevelamer revealed a reduction in *Bacteroidetes* relative abundances from 16 to 4 %. However, it remains unclear whether *Bacteroidetes* were directly affected by the reduced intestinal Pi levels or as a consequence of reduced bile and ureic acid levels?

6.6. Conclusions

Cross-over intervention studies as described in the current work, particularly in humans, are strictly regulated and generally very demanding. Despite the effort, Pi had limited impact on the gut microbiome diversity, although a noticeable reduction in *Bacteroidetes* in response to Sevelamer intake was observed. This work provides a starting point and suggests possible improvements that should be considered in future work, such as increasing the number of probands, multiple sample collections at different time points, increased dietary Pi and/or binder dose, and extended duration of the experiment.

Chapter 7: General discussion

7.1. Summary of the major findings

The expression pattern of transcripts represents a key indicator for their function. The molecular structure and expression pattern of the *SLC34A1*-sense transcript has been studied extensively, however not much is known about the *SLC34A1*-antisense transcript apart from its expression in human testis. The scope of my work was to characterise the impact of the antisense transcription on the activity and the epigenetic status of the *SLC34A1* locus. (i) Expression analysis showed that only the *SLC34A1*-sense transcript was expressed in human primary renal cells, with no evidence for the presence of the antisense transcripts. (ii) In HEK293 and HKC8 cell lines, both *SLC34A1*-sense and -antisense transcripts were expressed at very low levels. (iii) In response to epigenetic modulation using dexamethasone, the *SLC34A1*-sense and -antisense transcripts were induced in HEK293 but not in HKC8, suggesting cell/tissue-context dependent expression. (iv) The *SLC34A1*-antisense transcript is concordantly co-expressed with the *SLC34A1*-sense transcript. (v) Based on the analysis of epigenetic marks, the expression of both transcripts is accompanied by H3K27Ac hyperacetylation and CpG promoter hypomethylation. (vi) CRISPR/Cas9 editing of SLC34A1-sense and SLC34A1-antisense genomic sequences corroborated previous findings that the expression of one *SLC34A1* transcript enhances the expression of the complementary RNA.

(vii) The microbiome study revealed that with the experimental Pi diet neither α- nor β -microbial diversities showed significant changes. (viii) However, the Pi binder Sevelamer negatively impacted on *Bacteroidetes*, suggesting that other bacterial species might be affected in response to a prolonged treatment regimen.

7.2. The putative role of the *SLC34A1*-antisense transcript in Pi homeostasis

The number of studies investigating the impact of NATs on gene expression and physiology has steadily increased. Researchers now agree that most of these

transcripts perform physiological functions (He *et al.*, 2008; Faghihi *et al.*, 2010; Modarresi *et al.*, 2012; Kung *et al.*, 2013), supported by studies that link differentially expressed NATs with diseases, for example *SYNGAP1*-AS, *BACE1*-AS and *H19*-AS with autism, Alzheimer's and hepatocellular bladder cancer, respectively (Matouk *et al.*, 2007; Tan *et al.*, 2013; Velmeshev *et al.*, 2013).

Specific mechanisms of action of NATs have also been proposed and investigated thoroughly. For instance, *HOTAIR*, *LUC7L* and *ANRIL* are involved in promoter methylation and histone modifications (Faghihi and Wahlestedt, 2009). *UXTAS1*, *ZEB2AS1* and *ATOXOS* form RNA duplexes and target pre-mRNA splicing sites (Beltran *et al.*, 2008; Yin *et al.*, 2017) and *ZFAS1* and *TUG1* mask miRNA binding sites (Li *et al.*, 2015; Thorenoor *et al.*, 2016). In addition, the expression pattern of most sense/antisense transcript pairs show either concordant or discordant co-expression (Wight and Werner, 2013).

The interaction between *SLC34A* –related sense/antisense transcripts has been tested in a variety of model systems. In zebrafish for example, the *Slc34a2a*-sense and *Slc34a2a*-antisense transcripts are differentially expressed during early developmental stages of zebrafish embryos. Only the *Slc34a2a*-antisense transcript is detected until 48 hpf. Thereafter, the expression of the antisense transcript decreases with increasing levels of *Slc34a2a*-sense transcript expression, hence the *Slc34a2a*-sense/antisense transcripts are discordantly expressed.

From a functional prospective, the interaction between *Slc34a2a*-sense/antisense transcripts were evaluated using *Xenopus* oocyte co-injections. Upon co-injection, *Slc34a2a*-sense/antisense transcripts form dsRNA which is cleaved into short RNAs, potentially by Dicer, within 4 h post co-injection. These findings suggested a biological role for the *Slc34a2a*-antisense transcript in zebrafish development (Carlile *et al.*, 2008).

This hypothesis was tested by Dr Monica Piatek, a former PhD student in our lab, by investigating the physiological importance of the *Slc34a2a*-antisense transcript during zebrafish embryogenesis. In situ hybridisation revealed a reciprocal relationship between *Slc34a2a*-sense/antisense transcript expression. Initially (up to 48 hpf) *Slc34a2a*-sense/antisense transcripts were detected in different tissues of

embryos including pharynx, endoderm and brain whereas at later stages the transcripts co-localised.

Ectopic expression of the *Slc34a2a*-sense transcript in early embryos led to cerebellum deformities. The phenotype could be rescued by knocking down Dicer, suggesting that the ectopically expressed *Slc34a2a* transcript hybridised to the endogenous *Slc34a2a* antisense transcript followed by processing into short RNAs (Piatek, 2016). Comparable observations were made in mice where *Slc34a1*-sense/antisense endo-siRNAs were found in testis and kidney. Dicer processing could be reproduced upon co-injection of sense/antisense transcripts into Xenopus oocytes. Endo-siRNA molecules were generated when the overlap between the sense/antisense transcripts exceeded 29 bp (Carlile *et al.*, 2009).

In this study, the human *SLC34A1*-antisense transcript could neither be detected in primary renal cells (PT) nor in HEK293, HK2 and HKC8 cell lines, it was rather abundantly expressed in testis though. Following treatment with epigenetic modifiers or CRISPR/Cas9 mediated inducement in HEK293 cells, both *SLC34A1*-sense and *SLC34A1*-antisense transcripts showed concordant expression. The expression of *SLC34A1*-sense and the antisense transcript in response to experimental stimulation confirms a regulatory role for the antisense transcript in *SLC34A1* expression. Considering the findings with human, zebrafish and murine model systems, it can be concluded that *SLC34A1*-antisense transcripts are physiologically important but mainly during the early developmental stage.

Alternatively, the concordant *SLC34A1*-sense/antisense expression could be brought about by either transcriptional activation (chromatin opener) or sense/antisense stabilisation post transcriptionally. This suggestion contrasts with the findings in zebrafish and mouse, where dsRNA is formed and endo-siRNA can be detected. Although siRNAs detection in HEK293 cells was unsuccessful due to low sensitivity northern blotting.

The co-expression of *SLC34A1*-sense and -antisense transcripts, particularly resulting from epigenetic and CRISPR/Cas9 interventions, has raised many questions that remain to be answered. For example, is the antisense expression a mere consequence of increased expression of *SLC34A1*-sense? Could *SLC34A1*-

antisense transcripts have an epigenetic impact elsewhere in the genome? Apart from mechanistic considerations, why could the *SLC34A1*-antisense transcripts not be detected in the primary renal epithelial cells? How is *SLC34A1*-sense/antisense co-expressed during the early human embryonic life? Could overexpression of the *SLC34A1*-antisense transcripts have clinical consequences? Could we use *SLC34A1*-antisense as biomarker for kidney diseases? Further research will hopefully clarify some of these questions (Paragraph 7.4).

7.3. The putative role of gut microbiome in Pi homeostasis

The investigations focusing on aspects of the gut microbiome are exponentially growing, particularly after technological advancements in metagenomic analysis tools (Ohland and Jobin, 2015). Approximately 12,900 articles have been published during the period from 2013-2017 focusing on the physiological, developmental, nutritional, and metabolic interactions of the microbiota with host systemic organs (Vandeputte *et al.*, 2017). These studies have recorded a direct relationship between the host and the diversity of the gut microbiome. An altered composition of the microbiome as a consequence of external changes, has an impact on the host's health, and vice versa. For example, in obese individuals a reduction in *Bacteroides/Prevotella* can be observed (Kong *et al.*, 2013). Moreover, an increase in *Lactobacillus* abundance occurs in patients with diabetes type 2 (Lê *et al.*, 2013), an increase in butyrate-producing bacteria such as *Roseburia intestinalis* associates with metabolic syndrome (Vrieze *et al.*, 2012; Mazidi *et al.*, 2016) and an increase in *Enterobacteria* has been found in patients with psychological disorders (Maes *et al.*, 2009).

Of interest for my work, a reverse relationship between gut microbiome or its metabolites with kidney functions has been suggested especially in patients with renal complications (Ticinesi *et al.*, 2018). For instance, in patients with end-stage renal disease the abundance of approximately 190 bacterial species were reported to be affected (Vaziri *et al.*, 2013; Rodríguez *et al.*, 2015).

Dietary components such as fibre, carbohydrates, fat, vitamins and proteins have been extensively studied and considered as main factors that shape an individual's

microbiome (Albenberg and Wu, 2014; Degnan *et al.*, 2014; Hamaker and Tuncil, 2014; Walsh *et al.*, 2014; Wegmann *et al.*, 2014). In this thesis, I investigated whether the gut microbiota could be considered as an additional regulator of Pi homeostasis. To test this hypothesis, the gut microbiome was assessed following a high Pi diet and Sevelamer, a Pi binder to mimic low Pi availability, given to healthy participants. Several studies have correlated various Pi binders with serum and urine Pi, however, limited studies have examined the relationship between Pi binders and the gut microbiome in humans.

A study by Miao *et al.,* assessed the effect of the Pi binder lanthanum carbonate on gut microbiome diversity in haemodialytic patients. The Pi binder was given for 12-weeks. Treatment caused a significant reduction in *Firmicutes*, *Bacteroidetes* and *Proteobacteria*. Moreover, no significant difference in α- and β- bacterial diversities were detected in samples collected from the healthy group and patient's samples before treatment (Miao *et al.*, 2018). These results are in line with this study.

Another study by Merino *et al.,* examined the impact of the Pi binders calcium acetate and sucroferric oxyhydroxide on gut microbiome composition in haemodialytic patients. The stool samples were collected 0, 4, 8 and 12 weeks post treatment. The analysed data revealed an increase in β diversity in response to calcium acetate, but not to sucroferric oxyhydroxide. In addition, long term treatment may not be required to affect bacterial diversity since *Bacteroides* and *Firmicutes* increased during early time-points of treatment (Merino Ribas *et al.*, 2019). In parallel, the abundance of *Clostridiaceae*, *Enterobacteriaceae* and *Verrucomicrobiaceae* significantly increased in rats with CKD that were treated with the Pi binder ferric citrate (Lau *et al.*, 2018).

To summarise, this research and other related findings provide important insights into a potential interplay between the gut microbiota and Pi homeostasis. However, it remains unclear whether the affected bacterial groups responded to a reduction in intestinal Pi level or simply to the binder itself.

7.4. Further development

The work focusing on the *SLC34A1*-antisense transcript substantially contributes to the current understanding of how sense and antisense transcripts regulate each other's expression in a cell or tissue- specific context. However, to understand the relationship comprehensively, further research needs to be accomplished.

For example, the expression pattern of *SLC34A1*-sense/antisense transcripts in HEK293 cells using CRISPR/Cas9 was induced because of transcriptional read-through. Conversely, the expression could be knocked out following inserting 4-5 repetitive termination sequences at the TSS or before the first exon sequence. In addition to transcriptional silencing, post transcriptional inhibition could be attempted using antisense oligonucleotides.

Furthermore, it would be informative to map and quantify *SLC34A1*-sense/antisense transcripts during various embryonic life stages using RNAseq and bioinformatic analysis. This approach would be performed in a mouse model.

Further insights into the mechanism of sense-antisense interactions could be obtained by determining dsRNA formation following epigenetic treatment and in CRIPSR/Cas9 edited cells using the J2 monoclonal antibody. This approach may be challenging because preliminary work in our lab found that the majority of dsRNA was not from genic loci but from mitochondrial DNA, LINE or Alu elements in cells treated with epigenetic compounds. Moreover, nuclear/cytoplasmic localisation of the *SLC34A1*-sense/antisense transcripts using in-situ hybridisation may provide further insights into the mechanism of interaction and regulation.

The latest achievements in microbiome analysis tend to use large-scale integrative multi-omics approaches. Such strategy represents a complete package of bacterial genomic, transcriptomic, epigenomic, proteomic and metabolomics analysis. A comprehensive approach would provide valuable links between the actual gut microbiota composition and a transcriptional/functional response, such as bacterial Pi transporter activity (Franzosa *et al.*, 2015). Furthermore, quantitative microbial profiling would be a useful tool alongside the sequencing techniques (Vandeputte *et al.*, 2017).

References

Adcock, I.M., Ito, K. and Barnes, P.J. (2004) 'Glucocorticoids: effects on gene transcription', *Proc Am Thorac Soc*, 1(3), pp. 247-54.

Ahloulay, M., Déchaux, M., Hassler, C., Bouby, N. and Bankir, L. (1996) 'Cyclic AMP is a hepatorenal link influencing natriuresis and contributing to glucagon-induced hyperfiltration in rats', *The Journal of clinical investigation*, 98(10), pp. 2251-2258.

Akker, S.A., Khoo, B.C.E. and Chew, S.L. (2004) 'Alternative Splicing', in Martini, L. (ed.) *Encyclopedia of Endocrine Diseases*. New York: Elsevier, pp. 173-180.

Albenberg, L.G. and Wu, G.D. (2014) 'Diet and the Intestinal Microbiome: Associations, Functions, and Implications for Health and Disease', *Gastroenterology*, 146(6), pp. 1564-1572.

Alizadeh Naderi, A.S. and Reilly, R.F. (2010) 'Hereditary disorders of renal phosphate wasting', *Nature Reviews Nephrology*, 6, p. 657.

Ambühl, P.M., Zajicek, H.K., Wang, H., Puttaparthi, K., Levi, M. and with the technical assistance of Paul, W. (1998) 'Regulation of renal phosphate transport by acute and chronic metabolic acidosis in the rat', *Kidney International*, 53(5), pp. 1288-1298.

Amini, A.R., Laurencin, C.T. and Nukavarapu, S.P. (2012) 'Bone Tissue Engineering: Recent Advances and Challenges', *Critical reviews in biomedical engineering*, 40(5), pp. 363-408.

Andergassen, D., Muckenhuber, M., Bammer, P.C., Kulinski, T.M., Theussl, H.-C., Shimizu, T., Penninger, J.M., Pauler, F.M. and Hudson, Q.J. (2019) 'The Airn lncRNA does not require any DNA elements within its locus to silence distant imprinted genes', *PLOS Genetics*, 15(7), p. e1008268.

Andersen, J.B., Factor, V.M., Marquardt, J.U., Raggi, C., Lee, Y.-H., Seo, D., Conner, E.A. and Thorgeirsson, S.S. (2010) 'An Integrated Genomic and Epigenomic Approach Predicts Therapeutic Response to Zebularine in Human Liver Cancer', *Science Translational Medicine*, 2(54), pp. 54ra77-54ra77.

Andreoli, F. and Del Rio, A. (2015) 'Computer-aided Molecular Design of Compounds Targeting Histone Modifying Enzymes', *Comput Struct Biotechnol J*, 13, pp. 358-65.

Angelini, C., Savarese, M., Fanin, M. and Nigro, V. (2016) 'Next generation sequencing detection of late onset pompe disease', *Muscle Nerve*, 53(6), pp. 981-3.

Aprea, J. and Calegari, F. (2015) 'Long non-coding RNAs in corticogenesis: deciphering the non-coding code of the brain', *The EMBO Journal*, 34(23), pp. 2865-2884.

Arumugam, M., Raes, J., Pelletier, E., Le Paslier, D., Yamada, T., Mende, D.R., Fernandes, G.R., Tap, J., Bruls, T., Batto, J.-M., Bertalan, M., Borruel, N., Casellas, F., Fernandez, L., Gautier, L., Hansen, T., Hattori, M., Hayashi, T., Kleerebezem, M., Kurokawa, K., Leclerc, M., Levenez, F., Manichanh, C., Nielsen, H.B., Nielsen, T., Pons, N., Poulain, J., Qin, J., Sicheritz-Ponten, T., Tims, S., Torrents, D., Ugarte, E., Zoetendal, E.G., Wang, J., Guarner, F., Pedersen, O., de Vos, W.M., Brunak, S., Doré, J., Meta, H.I.T.C., Antolín, M., Artiguenave, F., Blottiere, H.M., Almeida, M., Brechot, C., Cara, C., Chervaux, C., Cultrone, A., Delorme, C., Denariaz, G., Dervyn, R., Foerstner, K.U., Friss, C., van de Guchte, M., Guedon, E., Haimet, F., Huber, W., van Hylckama-Vlieg, J., Jamet, A., Juste, C., Kaci, G., Knol, J., Kristiansen, K., Lakhdari, O., Layec, S., Le Roux, K., Maguin, E., Mérieux, A., Melo Minardi, R., M'Rini, C., Muller, J., Oozeer, R., Parkhill, J., Renault, P., Rescigno, M., Sanchez, N., Sunagawa, S., Torrejon, A., Turner, K., Vandemeulebrouck, G., Varela, E., Winogradsky, Y., Zeller, G., Weissenbach, J., Ehrlich, S.D. and Bork, P. (2011) 'Enterotypes of the human gut microbiome', *Nature*, 473, p. 174.

Asemi, Z., Aarabi, M.H., Hajijafari, M., Alizadeh, S.-A., Razzaghi, R., Mazoochi, M. and Esmaillzadeh, A. (2017) 'Effects of Synbiotic Food Consumption on Serum Minerals, Liver Enzymes, and Blood Pressure in Patients with Type 2 Diabetes: A Double-blind Randomized Cross-over Controlled Clinical Trial', *International journal of preventive medicine*, 8, pp. 43-43.

Ashe, H.L., Monks, J., Wijgerde, M., Fraser, P. and Proudfoot, N.J. (1997) 'Intergenic transcription and transinduction of the human beta-globin locus', *Genes Dev*, 11(19), pp. 2494-509.

Athanasiadis, A., Rich, A. and Maas, S. (2004) 'Widespread A-to-I RNA Editing of Alu-Containing mRNAs in the Human Transcriptome', *PLOS Biology*, 2(12), p. e391.

Au - Cummings, P.J., Au - Ahmed, R., Au - Durocher, J.A., Au - Jessen, A., Au - Vardi, T. and Au - Obom, K.M. (2013) 'Pyrosequencing for Microbial Identification and Characterization', *JoVE*, (78), p. e50405.

Bacic, D., Lehir, M., Biber, J., Kaissling, B., Murer, H. and Wagner, C.A. (2006) 'The renal Na+/phosphate cotransporter NaPi-IIa is internalized via the receptor-mediated endocytic route in response to parathyroid hormone', *Kidney Int*, 69(3), pp. 495-503.

Backhed, F., Ley, R.E., Sonnenburg, J.L., Peterson, D.A. and Gordon, J.I. (2005) 'Host-bacterial mutualism in the human intestine', *Science*, 307(5717), pp. 1915-20.

Bahar Halpern, K., Caspi, I., Lemze, D., Levy, M., Landen, S., Elinav, E., Ulitsky, I. and Itzkovitz, S. (2015) 'Nuclear Retention of mRNA in Mammalian Tissues', *Cell reports*, 13(12), pp. 2653-2662.

Balbin, O.A., Malik, R., Dhanasekaran, S.M., Prensner, J.R., Cao, X., Wu, Y.M., Robinson, D., Wang, R., Chen, G., Beer, D.G., Nesvizhskii, A.I. and Chinnaiyan, A.M. (2015) 'The landscape of antisense gene expression in human cancers', *Genome Res*, 25(7), pp. 1068-79.

Bannister, A.J. and Kouzarides, T. (2011) 'Regulation of chromatin by histone modifications', *Cell Res*, 21(3), pp. 381-95.

Barman, P., Reddy, D. and Bhaumik, S.R. (2019) 'Mechanisms of Antisense Transcription Initiation with Implications in Gene Expression, Genomic Integrity and Disease Pathogenesis', *Non-coding RNA*, 5(1), p. 11.

Barrangou, R., Fremaux, C., Deveau, H., Richards, M., Boyaval, P., Moineau, S., Romero, D.A. and Horvath, P. (2007) 'CRISPR Provides Acquired Resistance Against Viruses in Prokaryotes', *Science*, 315(5819), pp. 1709-1712.

Bass, J.J., Wilkinson, D.J., Rankin, D., Phillips, B.E., Szewczyk, N.J., Smith, K. and Atherton, P.J. (2017) 'An overview of technical considerations for Western blotting applications to physiological research', *Scandinavian Journal of Medicine & Science in Sports*, 27(1), pp. 4-25.

Batt, D.B., Luo, Y. and Carmichael, G.G. (1994) 'Polyadenylation and transcription termination in gene constructs containing multiple tandem polyadenylation signals', *Nucleic Acids Research*, 22(14), pp. 2811-2816.

Baubec, T., Pecinka, A., Rozhon, W. and Mittelsten Scheid, O. (2009) 'Effective, homogeneous and transient interference with cytosine methylation in plant genomic DNA by zebularine', *The Plant Journal*, 57(3), pp. 542-554.

Beck-Nielsen, S. (2012) *Rickets in Denmark*.

Beck, L., Karaplis, A.C., Amizuka, N., Hewson, A.S., Ozawa, H. and Tenenhouse, H.S. (1998) 'Targeted inactivation of Npt2 in mice leads to severe renal phosphate wasting, hypercalciuria, and skeletal abnormalities', *Proc Natl Acad Sci U S A*, 95(9), pp. 5372-7.

Becker, D., Hirsch, A.G., Bender, L., Lingner, T., Salinas, G. and Krebber, H. (2019) 'Nuclear Pre-snRNA Export Is an Essential Quality Assurance Mechanism for Functional Spliceosomes', *Cell Reports*, 27(11), pp. 3199-3214.e3.

Beers, K.W. and Dousa, T.P. (1993) 'Thyroid hormone stimulates the Na(+)-PO4 symporter but not the Na(+)-SO4 symporter in renal brush border', *Am J Physiol*, 265(2 Pt 2), pp. F323-6.

Beltran, M., Puig, I., Pena, C., Garcia, J.M., Alvarez, A.B., Pena, R., Bonilla, F. and de Herreros, A.G. (2008) 'A natural antisense transcript regulates Zeb2/Sip1 gene expression during Snail1-induced epithelial-mesenchymal transition', *Genes Dev*, 22(6), pp. 756-69.

Bent, S.J., Pierson, J.D., Forney, L.J., Danovaro, R., Luna, G.M., Dell'anno, A. and Pietrangeli, B. (2007) 'Measuring species richness based on microbial community fingerprints: the emperor has no clothes', *Appl Environ Microbiol*, 73(7), pp. 2399-401; author reply 2399-401.

Bentley, R. and Meganathan, R. (1982) 'Biosynthesis of vitamin K (menaquinone) in bacteria', *Microbiol Rev*, 46(3), pp. 241-80.

Bercik, P., Park, A.J., Sinclair, D., Khoshdel, A., Lu, J., Huang, X., Deng, Y., Blennerhassett, P.A., Fahnestock, M., Moine, D., Berger, B., Huizinga, J.D., Kunze, W., McLean, P.G., Bergonzelli, G.E., Collins, S.M. and Verdu, E.F. (2011) 'The anxiolytic effect of Bifidobacterium longum NCC3001 involves vagal pathways for gut-brain communication', *Neurogastroenterol Motil*, 23(12), pp. 1132-9.

Bergwitz, C., Roslin, N.M., Tieder, M., Loredo-Osti, J.C., Bastepe, M., Abu-Zahra, H., Frappier, D., Burkett, K., Carpenter, T.O., Anderson, D., Garabedian, M., Sermet, I., Fujiwara, T.M., Morgan, K., Tenenhouse, H.S. and Juppner, H. (2006) 'SLC34A3 mutations in patients with hereditary hypophosphatemic rickets with hypercalciuria predict a key role for the sodium-phosphate cotransporter NaPi-IIc in maintaining phosphate homeostasis', *Am J Hum Genet*, 78(2), pp. 179-92.

Berndt, T. and Kumar, R. (2009) 'Novel mechanisms in the regulation of phosphorus homeostasis', *Physiology (Bethesda)*, 24, pp. 17-25.

Berndt, T.J. and Knox, F.G. (1984) 'Proximal tubule site of inhibition of phosphate reabsorption by calcitonin', *Am J Physiol*, 246(6 Pt 2), pp. F927-30.

Bernstein, E. and Allis, C.D. (2005) 'RNA meets chromatin', *Genes Dev*, 19(14), pp. 1635-55.

Berridge, M.V., Herst, P.M. and Tan, A.S. (2005) 'Tetrazolium dyes as tools in cell biology: new insights into their cellular reduction', *Biotechnol Annu Rev*, 11, pp. 127-52.

Biber, J., Malmström, K., Reshkin, S. and Murer, H. (1990) '[29] Phosphate transport in established renal epithelial cell lines', in *Methods in Enzymology*. Academic Press, pp. 494-505.

Billam, M., Sobolewski, M.D. and Davidson, N.E. (2010) 'Effects of a novel DNA methyltransferase inhibitor zebularine on human breast cancer cells', *Breast cancer research and treatment*, 120(3), pp. 581-592.

Bird, A. (2002) 'DNA methylation patterns and epigenetic memory', *Genes Dev*, 16(1), pp. 6-21.

Birney, E., Stamatoyannopoulos, J.A., Dutta, A., Guigo, R., Gingeras, T.R., Margulies, E.H., Weng, Z., Snyder, M., Dermitzakis, E.T., Thurman, R.E., Kuehn, M.S., Taylor, C.M., Neph, S.,

Koch, C.M., Asthana, S., Malhotra, A., Adzhubei, I., Greenbaum, J.A., Andrews, R.M., Flicek, P., Boyle, P.J., Cao, H., Carter, N.P., Clelland, G.K., Davis, S., Day, N., Dhami, P., Dillon, S.C., Dorschner, M.O., Fiegler, H., Giresi, P.G., Goldy, J., Hawrylycz, M., Haydock, A., Humbert, R., James, K.D., Johnson, B.E., Johnson, E.M., Frum, T.T., Rosenzweig, E.R., Karnani, N., Lee, K., Lefebvre, G.C., Navas, P.A., Neri, F., Parker, S.C., Sabo, P.J., Sandstrom, R., Shafer, A., Vetrie, D., Weaver, M., Wilcox, S., Yu, M., Collins, F.S., Dekker, J., Lieb, J.D., Tullius, T.D., Crawford, G.E., Sunyaev, S., Noble, W.S., Dunham, I., Denoeud, F., Reymond, A., Kapranov, P., Rozowsky, J., Zheng, D., Castelo, R., Frankish, A., Harrow, J., Ghosh, S., Sandelin, A., Hofacker, I.L., Baertsch, R., Keefe, D., Dike, S., Cheng, J., Hirsch, H.A., Sekinger, E.A., Lagarde, J., Abril, J.F., Shahab, A., Flamm, C., Fried, C., Hackermuller, J., Hertel, J., Lindemeyer, M., Missal, K., Tanzer, A., Washietl, S., Korbel, J., Emanuelsson, O., Pedersen, J.S., Holroyd, N., Taylor, R., Swarbreck, D., Matthews, N., Dickson, M.C., Thomas, D.J., Weirauch, M.T., Gilbert, J., et al. (2007) 'Identification and analysis of functional elements in 1% of the human genome by the ENCODE pilot project', *Nature*, 447(7146), pp. 799-816.

Black, J.C., Van Rechem, C. and Whetstine, J.R. (2012) 'Histone lysine methylation dynamics: establishment, regulation, and biological impact', *Mol Cell*, 48(4), pp. 491-507.

Bohn, E., Bechtold, O., Zahir, N., Frick, J.S., Reimann, J., Jilge, B. and Autenrieth, I.B. (2006) 'Host gene expression in the colon of gnotobiotic interleukin-2-deficient mice colonized with commensal colitogenic or noncolitogenic bacterial strains: common patterns and bacteria strain specific signatures', *Inflamm Bowel Dis*, 12(9), pp. 853-62.

Bolotin, A., Quinquis, B., Sorokin, A. and Ehrlich, S.D. (2005) 'Clustered regularly interspaced short palindrome repeats (CRISPRs) have spacers of extrachromosomal origin', *Microbiology*, 151(Pt 8), pp. 2551-61.

Borda-Molina, D., Vital, M., Sommerfeld, V., Rodehutscord, M. and Camarinha-Silva, A. (2016) 'Insights into Broilers' Gut Microbiota Fed with Phosphorus, Calcium, and Phytase Supplemented Diets', *Front Microbiol*, 7, p. 2033.

Bose, R., Spulber, S., Kilian, P., Heldring, N., Lönnerberg, P., Johnsson, A., Conti, M., Hermanson, O. and Ceccatelli, S. (2015) 'Tet3 mediates stable glucocorticoid-induced alterations in DNA methylation and Dnmt3a/Dkk1 expression in neural progenitors', *Cell Death &Amp; Disease*, 6, p. e1793.

Bouchard-Bourelle, P., Desjardins-Henri, C., Mathurin-St-Pierre, D., Deschamps-Francoeur, G., Fafard-Couture, É., Garant, J.-M., Elela, S.A. and Scott, M.S. (2019) 'snoDB: an interactive database of human snoRNA sequences, abundance and interactions', *Nucleic Acids Research*.

Boudal, A. and Attar, S. (2012) 'Vitamin D and Autoimmune Disease', in.

Braunlin, W., Zhorov, E., Guo, A., Apruzzese, W., Xu, Q., Hook, P., Smisek, D.L., Mandeville, W.H. and Holmes-Farley, S.R. (2002) 'Bile acid binding to sevelamer HCl', *Kidney Int*, 62(2), pp. 611-9.

Brennecke, J. and Cohen, S.M. (2003) 'Towards a complete description of the microRNA complement of animal genomes', *Genome Biol*, 4(9), p. 228.

Brown, C.D., Sayer, R., Windass, A.S., Haslam, I.S., De Broe, M.E., D'Haese, P.C. and Verhulst, A. (2008) 'Characterisation of human tubular cell monolayers as a model of proximal tubular xenobiotic handling', *Toxicol Appl Pharmacol*, 233(3), pp. 428-38.

Brown, C.J., Ballabio, A., Rupert, J.L., Lafreniere, R.G., Grompe, M., Tonlorenzi, R. and Willard, H.F. (1991) 'A gene from the region of the human X inactivation centre is expressed exclusively from the inactive X chromosome', *Nature*, 349(6304), pp. 38-44.

Brown, K., DeCoffe, D., Molcan, E. and Gibson, D.L. (2012) 'Diet-induced dysbiosis of the intestinal microbiota and the effects on immunity and disease', *Nutrients*, 4(8), pp. 1095-119.

Brown, R.B. and Razzaque, M.S. (2015) 'Dysregulation of phosphate metabolism and conditions associated with phosphate toxicity', *BoneKEy reports*, 4, pp. 705-705.

Bult, C.J., White, O., Olsen, G.J., Zhou, L., Fleischmann, R.D., Sutton, G.G., Blake, J.A., FitzGerald, L.M., Clayton, R.A., Gocayne, J.D., Kerlavage, A.R., Dougherty, B.A., Tomb, J.-F., Adams, M.D., Reich, C.I., Overbeek, R., Kirkness, E.F., Weinstock, K.G., Merrick, J.M., Glodek, A., Scott, J.L., Geoghagen, N.S.M., Weidman, J.F., Fuhrmann, J.L., Nguyen, D., Utterback, T.R., Kelley, J.M., Peterson, J.D., Sadow, P.W., Hanna, M.C., Cotton, M.D., Roberts, K.M., Hurst, M.A., Kaine, B.P., Borodovsky, M., Klenk, H.-P., Fraser, C.M., Smith, H.O., Woese, C.R. and Venter, J.C. (1996) 'Complete Genome Sequence of the Methanogenic Archaeon, Methanococcus jannaschii', *Science*, 273(5278), pp. 1058-1073.

Cabili, M.N., Trapnell, C., Goff, L., Koziol, M., Tazon-Vega, B., Regev, A. and Rinn, J.L. (2011) 'Integrative annotation of human large intergenic noncoding RNAs reveals global properties and specific subclasses', *Genes Dev*, 25(18), pp. 1915-27.

Calvo, O. and Manley, J.L. (2003) 'Strange bedfellows: polyadenylation factors at the promoter', *Genes Dev*, 17(11), pp. 1321-7.

Capuano, P., Bacic, D., Roos, M., Gisler, S.M., Stange, G., Biber, J., Kaissling, B., Weinman, E.J., Shenolikar, S., Wagner, C.A. and Murer, H. (2007) 'Defective coupling of apical PTH receptors to phospholipase C prevents internalization of the Na+-phosphate cotransporter NaPi-IIa in Nherf1-deficient mice', *Am J Physiol Cell Physiol*, 292(2), pp. C927-34.

Carlile, M., Nalbant, P., Preston-Fayers, K., McHaffie, G.S. and Werner, A. (2008) 'Processing of naturally occurring sense/antisense transcripts of the vertebrate Slc34a gene into short RNAs', *Physiol Genomics*, 34(1), pp. 95-100.

Carlile, M., Swan, D., Jackson, K., Preston-Fayers, K., Ballester, B., Flicek, P. and Werner, A. (2009) 'Strand selective generation of endo-siRNAs from the Na/phosphate transporter gene Slc34a1 in murine tissues', *Nucleic Acids Research*, 37(7), pp. 2274-2282.

Carrozza, M.J., Li, B., Florens, L., Suganuma, T., Swanson, S.K., Lee, K.K., Shia, W.J., Anderson, S., Yates, J., Washburn, M.P. and Workman, J.L. (2005) 'Histone H3 methylation by Set2 directs deacetylation of coding regions by Rpd3S to suppress spurious intragenic transcription', *Cell*, 123(4), pp. 581-92.

Caverzasio, J. and Bonjour, J.P. (1988) 'Influence of calcium on phosphate transport in cultured kidney epithelium', *Am J Physiol*, 254(2 Pt 2), pp. F217-22.

Caverzasio, J., Montessuit, C. and Bonjour, J.P. (1990) 'Stimulatory effect of insulin-like growth factor-1 on renal Pi transport and plasma 1,25-dihydroxyvitamin D3', *Endocrinology*, 127(1), pp. 453-9.

Cedar, H. and Bergman, Y. (2012) 'Programming of DNA methylation patterns', *Annu Rev Biochem*, 81, pp. 97-117.

Chan, S., Au, K., Francis, R.S., Mudge, D.W., Johnson, D.W. and Pillans, P.I. (2017) 'Phosphate binders in patients with chronic kidney disease', *Australian prescriber*, 40(1), pp. 10-14.

Chang, A.R. and Anderson, C. (2017) 'Dietary Phosphorus Intake and the Kidney', *Annual review of nutrition*, 37, pp. 321-346.

Chang, A.R., Lazo, M., Appel, L.J., Gutierrez, O.M. and Grams, M.E. (2014) 'High dietary phosphorus intake is associated with all-cause mortality: results from NHANES III', *Am J Clin Nutr*, 99(2), pp. 320-7.

Chang, J., Varghese, D.S., Gillam, M.C., Peyton, M., Modi, B., Schiltz, R.L., Girard, L. and Martinez, E.D. (2012) 'Differential response of cancer cells to HDAC inhibitors trichostatin A and depsipeptide', *British journal of cancer*, 106(1), pp. 116-125.

Chen, J., Sun, M., Kent, W.J., Huang, X., Xie, H., Wang, W., Zhou, G., Shi, R.Z. and Rowley, J.D. (2004) 'Over 20% of human transcripts might form sense-antisense pairs', *Nucleic Acids Res*, 32(16), pp. 4812-20.

Chen, W.L., Lin, C.T., Yao, C.C., Huang, Y.H., Chou, Y.B., Yin, H.S. and Hu, F.R. (2006) 'In-vitro effects of dexamethasone on cellular proliferation, apoptosis, and Na+-K+-ATPase activity of bovine corneal endothelial cells', *Ocul Immunol Inflamm*, 14(4), pp. 215-23.

Cheng, J.C., Matsen, C.B., Gonzales, F.A., Ye, W., Greer, S., Marquez, V.E., Jones, P.A. and Selker, E.U. (2003) 'Inhibition of DNA methylation and reactivation of silenced genes by zebularine', *J Natl Cancer Inst*, 95(5), pp. 399-409.

Cheng, J.C., Weisenberger, D.J., Gonzales, F.A., Liang, G., Xu, G.L., Hu, Y.G., Marquez, V.E. and Jones, P.A. (2004) 'Continuous zebularine treatment effectively sustains demethylation in human bladder cancer cells', *Mol Cell Biol*, 24(3), pp. 1270-8.

Chiruvella, K.K., Liang, Z. and Wilson, T.E. (2013) 'Repair of double-strand breaks by end joining', *Cold Spring Harb Perspect Biol*, 5(5), p. a012757.

Cho, S.W., Kim, S., Kim, J.M. and Kim, J.S. (2013) 'Targeted genome engineering in human cells with the Cas9 RNA-guided endonuclease', *Nat Biotechnol*, 31(3), pp. 230-2.

Chou, C.H., Shrestha, S., Yang, C.D., Chang, N.W., Lin, Y.L., Liao, K.W., Huang, W.C., Sun, T.H., Tu, S.J., Lee, W.H., Chiew, M.Y., Tai, C.S., Wei, T.Y., Tsai, T.R., Huang, H.T., Wang, C.Y., Wu, H.Y., Ho, S.Y., Chen, P.R., Chuang, C.H., Hsieh, P.J., Wu, Y.S., Chen, W.L., Li, M.J., Wu, Y.C., Huang, X.Y., Ng, F.L., Buddhakosai, W., Huang, P.C., Lan, K.C., Huang, C.Y., Weng, S.L., Cheng, Y.N., Liang, C., Hsu, W.L. and Huang, H.D. (2018) 'miRTarBase update 2018: a resource for experimentally validated microRNA-target interactions', *Nucleic Acids Res*, 46(D1), pp. D296-d302.

Cikos, S., Bukovská, A. and Koppel, J. (2007) 'Relative quantification of mRNA: comparison of methods currently used for real-time PCR data analysis', *BMC molecular biology*, 8, pp. 113-113.

Claesson, M.J., Wang, Q., O'Sullivan, O., Greene-Diniz, R., Cole, J.R., Ross, R.P. and O'Toole, P.W. (2010) 'Comparison of two next-generation sequencing technologies for resolving highly complex microbiota composition using tandem variable 16S rRNA gene regions', *Nucleic Acids Res*, 38(22), p. e200.

Clark, J.A. and Coopersmith, C.M. (2007) 'Intestinal crosstalk: a new paradigm for understanding the gut as the "motor" of critical illness', *Shock*, 28(4), pp. 384-93.

Corut, A., Senyigit, A., Ugur, S.A., Altin, S., Ozcelik, U., Calisir, H., Yildirim, Z., Gocmen, A. and Tolun, A. (2006) 'Mutations in SLC34A2 cause pulmonary alveolar microlithiasis and are possibly associated with testicular microlithiasis', *Am J Hum Genet*, 79(4), pp. 650-6.

Crampton, N., Bonass, W.A., Kirkham, J., Rivetti, C. and Thomson, N.H. (2006) 'Collision events between RNA polymerases in convergent transcription studied by atomic force microscopy', *Nucleic Acids Research*, 34(19), pp. 5416-5425.

Cribbs, A.P. and Perera, S.M.W. (2017) 'Science and Bioethics of CRISPR-Cas9 Gene Editing: An Analysis Towards Separating Facts and Fiction', *Yale J Biol Med*, 90(4), pp. 625-634.

Crisafulli, U., Xavier, A.M., dos Santos, F.B., Cambiaghi, T.D., Chang, S.Y., Porcionatto, M., Castilho, B.A., Malnic, B. and Glezer, I. (2018) 'Topical Dexamethasone Administration Impairs Protein Synthesis and Neuronal Regeneration in the Olfactory Epithelium', *Frontiers in Molecular Neuroscience*, 11(50).

Custer, M., Lotscher, M., Biber, J., Murer, H. and Kaissling, B. (1994a) 'Expression of Na-P(i) cotransport in rat kidney: localization by RT-PCR and immunohistochemistry', *Am J Physiol*, 266(5 Pt 2), pp. F767-74.

Custer, M., Lotscher, M., Biber, J., Murer, H. and Kaissling, B. (1994b) 'Expression of Na-P(i) cotransport in rat kidney: localization by RT-PCR and immunohistochemistry', *American Journal of Physiology-Renal Physiology*, 266(5), pp. F767-F774.

D'Argenio, V. and Salvatore, F. (2015) 'The role of the gut microbiome in the healthy adult status', *Clinica Chimica Acta*, 451, pp. 97-102.

Dasgupta, D., Wee, M.J., Reyes, M., Li, Y., Simm, P.J., Sharma, A., Schlingmann, K.P., Janner, M., Biggin, A., Lazier, J., Gessner, M., Chrysis, D., Tuchman, S., Baluarte, H.J., Levine, M.A., Tiosano, D., Insogna, K., Hanley, D.A., Carpenter, T.O., Ichikawa, S., Hoppe, B., Konrad, M., Savendahl, L., Munns, C.F., Lee, H., Juppner, H. and Bergwitz, C. (2014) 'Mutations in SLC34A3/NPT2c are associated with kidney stones and nephrocalcinosis', *J Am Soc Nephrol*, 25(10), pp. 2366-75.

David, L.A., Maurice, C.F., Carmody, R.N., Gootenberg, D.B., Button, J.E., Wolfe, B.E., Ling, A.V., Devlin, A.S., Varma, Y., Fischbach, M.A., Biddinger, S.B., Dutton, R.J. and Turnbaugh, P.J. (2014) 'Diet rapidly and reproducibly alters the human gut microbiome', *Nature*, 505(7484), pp. 559-63.

de la Horra, C., Hernando, N., Forster, I., Biber, J. and Murer, H. (2001) 'Amino acids involved in sodium interaction of murine type II Na(+)-P(i) cotransporters expressed in Xenopus oocytes', *The Journal of Physiology*, 531(Pt 2), pp. 383-391.

Deaton, A.M. and Bird, A. (2011) 'CpG islands and the regulation of transcription', *Genes & development*, 25(10), pp. 1010-1022.

Degnan, Patrick H., Barry, Natasha A., Mok, Kenny C., Taga, Michiko E. and Goodman, Andrew L. (2014) 'Human Gut Microbes Use Multiple Transporters to Distinguish Vitamin B12 Analogs and Compete in the Gut', *Cell Host & Microbe*, 15(1), pp. 47-57.

DeJong, T.M. (1975) 'A Comparison of Three Diversity Indices Based on Their Components of Richness and Evenness', *Oikos*, 26(2), pp. 222-227.

Deltcheva, E., Chylinski, K., Sharma, C.M., Gonzales, K., Chao, Y., Pirzada, Z.A., Eckert, M.R., Vogel, J. and Charpentier, E. (2011) 'CRISPR RNA maturation by trans-encoded small RNA and host factor RNase III', *Nature*, 471(7340), pp. 602-7.

Derrien, T., Johnson, R., Bussotti, G., Tanzer, A., Djebali, S., Tilgner, H., Guernec, G., Martin, D., Merkel, A., Knowles, D.G., Lagarde, J., Veeravalli, L., Ruan, X., Ruan, Y., Lassmann, T., Carninci, P., Brown, J.B., Lipovich, L., Gonzalez, J.M., Thomas, M., Davis, C.A., Shiekhattar, R., Gingeras, T.R., Hubbard, T.J., Notredame, C., Harrow, J. and Guigo, R. (2012) 'The GENCODE v7 catalog of human long noncoding RNAs: analysis of their gene structure, evolution, and expression', *Genome Res*, 22(9), pp. 1775-89.

Dewhirst, F.E., Chen, T., Izard, J., Paster, B.J., Tanner, A.C.R., Yu, W.-H., Lakshmanan, A. and Wade, W.G. (2010) 'The Human Oral Microbiome', *Journal of Bacteriology*, 192(19), pp. 5002-5017.

Ding, M., Liu, Y., Liao, X., Zhan, H., Liu, Y. and Huang, W. (2018) 'Enhancer RNAs (eRNAs): New Insights into Gene Transcription and Disease Treatment', *Journal of Cancer*, 9(13), pp. 2334-2340.

Ding, T. and Schloss, P.D. (2014) 'Dynamics and associations of microbial community types across the human body', *Nature*, 509(7500), pp. 357-60.

Ditscheid, B., Keller, S. and Jahreis, G. (2005a) 'Cholesterol Metabolism Is Affected by Calcium Phosphate Supplementation in Humans', *The Journal of Nutrition*, 135(7), pp. 1678-1682.

Ditscheid, B., Keller, S. and Jahreis, G. (2005b) 'Cholesterol metabolism is affected by calcium phosphate supplementation in humans', *J Nutr*, 135(7), pp. 1678-82.

Djebali, S., Davis, C.A., Merkel, A., Dobin, A., Lassmann, T., Mortazavi, A., Tanzer, A., Lagarde, J., Lin, W., Schlesinger, F., Xue, C., Marinov, G.K., Khatun, J., Williams, B.A., Zaleski, C., Rozowsky, J., Röder, M., Kokocinski, F., Abdelhamid, R.F., Alioto, T., Antoshechkin, I., Baer, M.T., Bar, N.S., Batut, P., Bell, K., Bell, I., Chakrabortty, S., Chen, X., Chrast, J., Curado, J., Derrien, T., Drenkow, J., Dumais, E., Dumais, J., Duttagupta, R., Falconnet, E., Fastuca, M., Fejes-Toth, K., Ferreira, P., Foissac, S., Fullwood, M.J., Gao, H., Gonzalez, D., Gordon, A., Gunawardena, H., Howald, C., Jha, S., Johnson, R., Kapranov, P., King, B., Kingswood, C., Luo, O.J., Park, E., Persaud, K., Preall, J.B., Ribeca, P., Risk, B., Robyr, D., Sammeth, M., Schaffer, L., See, L.H., Shahab, A., Skancke, J., Suzuki, A.M., Takahashi, H., Tilgner, H., Trout, D., Walters, N., Wang, H., Wrobel, J., Yu, Y., Ruan, X., Hayashizaki, Y., Harrow, J., Gerstein, M., Hubbard, T., Reymond, A., Antonarakis, S.E., Hannon, G., Giddings, M.C., Ruan, Y., Wold, B., Carninci, P., Guig, R. and Gingeras, T.R. (2012a) 'Landscape of transcription in human cells', *Nature*, 489(7414), pp. 101-108.

Djebali, S., Davis, C.A., Merkel, A., Dobin, A., Lassmann, T., Mortazavi, A., Tanzer, A., Lagarde, J., Lin, W., Schlesinger, F., Xue, C., Marinov, G.K., Khatun, J., Williams, B.A., Zaleski, C., Rozowsky, J., Roder, M., Kokocinski, F., Abdelhamid, R.F., Alioto, T., Antoshechkin, I., Baer, M.T., Bar, N.S., Batut, P., Bell, K., Bell, I., Chakrabortty, S., Chen, X., Chrast, J., Curado, J., Derrien, T., Drenkow, J., Dumais, E., Dumais, J., Duttagupta, R., Falconnet, E., Fastuca, M., Fejes-Toth, K., Ferreira, P., Foissac, S., Fullwood, M.J., Gao, H., Gonzalez, D., Gordon, A., Gunawardena, H., Howald, C., Jha, S., Johnson, R., Kapranov, P., King, B., Kingswood, C., Luo,

O.J., Park, E., Persaud, K., Preall, J.B., Ribeca, P., Risk, B., Robyr, D., Sammeth, M., Schaffer, L., See, L.H., Shahab, A., Skancke, J., Suzuki, A.M., Takahashi, H., Tilgner, H., Trout, D., Walters, N., Wang, H., Wrobel, J., Yu, Y., Ruan, X., Hayashizaki, Y., Harrow, J., Gerstein, M., Hubbard, T., Reymond, A., Antonarakis, S.E., Hannon, G., Giddings, M.C., Ruan, Y., Wold, B., Carninci, P., Guigo, R. and Gingeras, T.R. (2012b) 'Landscape of transcription in human cells', *Nature*, 489(7414), pp. 101-8.

Dominguez, J.H., Pitts, T.O., Brown, T., Puschett, D.B., Schuler, F., Chen, T.C. and Puschett, J.B. (1984) 'Prostaglandin E2 and parathyroid hormone: Comparisons of their actions on the rabbit proximal tubule', *Kidney International*, 26(4), pp. 404-410.

Dostal, A., Lacroix, C., Bircher, L., Pham, V.T., Follador, R., Zimmermann, M.B. and Chassard, C. (2015) 'Iron Modulates Butyrate Production by a Child Gut Microbiota In Vitro', *mBio*, 6(6), pp. e01453-15.

Du, J., Johnson, L.M., Jacobsen, S.E. and Patel, D.J. (2015) 'DNA methylation pathways and their crosstalk with histone methylation', *Nat Rev Mol Cell Biol*, 16(9), pp. 519-32.

Eid, A., Alshareef, S. and Mahfouz, M.M. (2018) 'CRISPR base editors: genome editing without double-stranded breaks', *The Biochemical journal*, 475(11), pp. 1955-1964.

Ernst, J., Kheradpour, P., Mikkelsen, T.S., Shoresh, N., Ward, L.D., Epstein, C.B., Zhang, X., Wang, L., Issner, R., Coyne, M., Ku, M., Durham, T., Kellis, M. and Bernstein, B.E. (2011) 'Mapping and analysis of chromatin state dynamics in nine human cell types', *Nature*, 473(7345), pp. 43-9.

Esteller, M. (2007) 'Cancer epigenomics: DNA methylomes and histone-modification maps', *Nat Rev Genet*, 8(4), pp. 286-98.

Faghihi, M.A., Kocerha, J., Modarresi, F., Engstrom, P.G., Chalk, A.M., Brothers, S.P., Koesema, E., St Laurent, G. and Wahlestedt, C. (2010) 'RNAi screen indicates widespread biological function for human natural antisense transcripts', *PLoS One*, 5(10).

Faghihi, M.A., Modarresi, F., Khalil, A.M., Wood, D.E., Sahagan, B.G., Morgan, T.E., Finch, C.E., St Laurent, G., 3rd, Kenny, P.J. and Wahlestedt, C. (2008a) 'Expression of a noncoding RNA is elevated in Alzheimer's disease and drives rapid feed-forward regulation of beta-secretase', *Nature medicine*, 14(7), pp. 723-730.

Faghihi, M.A., Modarresi, F., Khalil, A.M., Wood, D.E., Sahagan, B.G., Morgan, T.E., Finch, C.E., St Laurent, G., 3rd, Kenny, P.J. and Wahlestedt, C. (2008b) 'Expression of a noncoding RNA is elevated in Alzheimer's disease and drives rapid feed-forward regulation of beta-secretase', *Nat Med*, 14(7), pp. 723-30.

Faghihi, M.A. and Wahlestedt, C. (2009) 'Regulatory roles of natural antisense transcripts', *Nat Rev Mol Cell Biol*, 10(9), pp. 637-43.

Faith, J.J., McNulty, N.P., Rey, F.E. and Gordon, J.I. (2011) 'Predicting a human gut microbiota's response to diet in gnotobiotic mice', *Science*, 333(6038), pp. 101-4.

Fallani, M., Young, D., Scott, J., Norin, E., Amarri, S., Adam, R., Aguilera, M., Khanna, S., Gil, A., Edwards, C.A. and Dore, J. (2010) 'Intestinal microbiota of 6-week-old infants across Europe: geographic influence beyond delivery mode, breast-feeding, and antibiotics', *J Pediatr Gastroenterol Nutr*, 51(1), pp. 77-84.

Fearn, A., Allison, B., Rice, S.J., Edwards, N., Halbritter, J., Bourgeois, S., Pastor-Arroyo, E.M., Hildebrandt, F., Tasic, V., Wagner, C.A., Hernando, N., Sayer, J.A. and Werner, A. (2018) 'Clinical, biochemical, and pathophysiological analysis of SLC34A1 mutations', *Physiol Rep*, 6(12), p. e13715.

Fenollar-Ferrer, C., Forster, Ian C., Patti, M., Knoepfel, T., Werner, A. and Forrest, Lucy R. (2015a) 'Identification of the First Sodium Binding Site of the Phosphate Cotransporter NaPi-IIa (SLC34A1)', *Biophysical Journal*, 108(10), pp. 2465-2480.

Fenollar-Ferrer, C., Forster, I.C., Patti, M., Knoepfel, T., Werner, A. and Forrest, L.R. (2015b) 'Identification of the first sodium binding site of the phosphate cotransporter NaPi-IIa (SLC34A1)', *Biophys J*, 108(10), pp. 2465-2480.

Fenollar-Ferrer, C., Patti, M., Knopfel, T., Werner, A., Forster, I.C. and Forrest, L.R. (2014a) 'Structural fold and binding sites of the human Na(+)-phosphate cotransporter NaPi-II', *Biophys J*, 106(6), pp. 1268-79.

Fenollar-Ferrer, C., Patti, M., Knöpfel, T., Werner, A., Forster, Ian C. and Forrest, Lucy R. (2014b) 'Structural Fold and Binding Sites of the Human Na+-Phosphate Cotransporter NaPi-II', *Biophysical Journal*, 106(6), pp. 1268-1279.

Fischbach, F.T. and Dunning, M.B. (2009) *A manual of laboratory and diagnostic tests*. Philadelphia: Wolters Kluwer Health/Lippincott Williams & Wilkins.

Fleischmann, R., Adams, M., White, O., Clayton, R., Kirkness, E., Kerlavage, A., Bult, C., Tomb, J., Dougherty, B., Merrick, J. and al., e. (1995) 'Whole-genome random sequencing and assembly of Haemophilus influenzae Rd', *Science*, 269(5223), pp. 496-512.

Forst, T.M., Ryan, S.M., Pelle, N. and Murphy, P.J.M. (2017) 'Mutagenesis of HEK293 Cells Reveals Phenotypic and Genotypic Variants Involved in Hsp90-Mediated Glucocorticoid Signaling', *The FASEB Journal*, 31(1_supplement), pp. 591.9-591.9.

Forster, I.C., Hernando, N., Biber, J. and Murer, H. (2013) 'Phosphate transporters of the SLC20 and SLC34 families', *Molecular Aspects of Medicine*, 34(2), pp. 386-395.

Forster, S.C., Kumar, N., Anonye, B.O., Almeida, A., Viciani, E., Stares, M.D., Dunn, M., Mkandawire, T.T., Zhu, A., Shao, Y., Pike, L.J., Louie, T., Browne, H.P., Mitchell, A.L., Neville,

B.A., Finn, R.D. and Lawley, T.D. (2019) 'A human gut bacterial genome and culture collection for improved metagenomic analyses', *Nature Biotechnology*, 37(2), pp. 186-192.

Franzosa, E.A., Hsu, T., Sirota-Madi, A., Shafquat, A., Abu-Ali, G., Morgan, X.C. and Huttenhower, C. (2015) 'Sequencing and beyond: integrating molecular 'omics' for microbial community profiling', *Nature Reviews Microbiology*, 13, p. 360.

Galupa, R., Nora, E.P., Worsley-Hunt, R., Picard, C., Gard, C., van Bemmel, J.G., Servant, N., Zhan, Y., El Marjou, F., Johanneau, C., Diabangouaya, P., Le Saux, A., Lameiras, S., Pipoli da Fonseca, J., Loos, F., Gribnau, J., Baulande, S., Ohler, U., Giorgetti, L. and Heard, E. (2020) 'A Conserved Noncoding Locus Regulates Random Monoallelic Xist Expression across a Topological Boundary', *Molecular Cell*, 77(2), pp. 352-367.e8.

Garg, J.P., Chasan-Taber, S., Blair, A., Plone, M., Bommer, J., Raggi, P. and Chertow, G.M. (2005) 'Effects of sevelamer and calcium-based phosphate binders on uric acid concentrations in patients undergoing hemodialysis: a randomized clinical trial', *Arthritis Rheum*, 52(1), pp. 290-5.

Geraghty, R.J., Capes-Davis, A., Davis, J.M., Downward, J., Freshney, R.I., Knezevic, I., Lovell-Badge, R., Masters, J.R.W., Meredith, J., Stacey, G.N., Thraves, P., Vias, M. and Cancer Research, U.K. (2014) 'Guidelines for the use of cell lines in biomedical research', *British journal of cancer*, 111(6), pp. 1021-1046.

Gerritsen, J., Smidt, H., Rijkers, G.T. and de Vos, W.M. (2011) 'Intestinal microbiota in human health and disease: the impact of probiotics', *Genes Nutr*, 6(3), pp. 209-40.

Ghezzi, C., Meinild, A.K., Murer, H. and Forster, I.C. (2011) 'Voltage- and substrate-dependent interactions between sites in putative re-entrant domains of a Na(+)-coupled phosphate cotransporter', *Pflugers Arch*, 461(6), pp. 645-63.

Goffeau, A., Barrell, B.G., Bussey, H., Davis, R.W., Dujon, B., Feldmann, H., Galibert, F., Hoheisel, J.D., Jacq, C., Johnston, M., Louis, E.J., Mewes, H.W., Murakami, Y., Philippsen, P., Tettelin, H. and Oliver, S.G. (1996) 'Life with 6000 Genes', *Science*, 274(5287), pp. 546-567.

González, A., Vázquez-Baeza, Y. and Knight, R. (2014) 'SnapShot: The Human Microbiome', *Cell*, 158(3), pp. 690-690.e1.

Gorvitovskaia, A., Holmes, S.P. and Huse, S.M. (2016) 'Interpreting Prevotella and Bacteroides as biomarkers of diet and lifestyle', *Microbiome*, 4, p. 15.

Govers, M.J. and Van der Meet, R. (1993) 'Effects of dietary calcium and phosphate on the intestinal interactions between calcium, phosphate, fatty acids, and bile acids', *Gut*, 34(3), pp. 365-70.

Goyal, A., Myacheva, K., Groß, M., Klingenberg, M., Duran Arqué, B. and Diederichs, S. (2017) 'Challenges of CRISPR/Cas9 applications for long non-coding RNA genes', *Nucleic acids research*, 45(3), pp. e12-e12.

Goyal, A., Myacheva, K., Groß, M., Klingenberg, M., Duran Arqué, B. and Diederichs, S. (2016) 'Challenges of CRISPR/Cas9 applications for long non-coding RNA genes', *Nucleic Acids Research*, 45(3), pp. e12-e12.

Grice, E.A., Kong, H.H., Conlan, S., Deming, C.B., Davis, J., Young, A.C., Bouffard, G.G., Blakesley, R.W., Murray, P.R., Green, E.D., Turner, M.L. and Segre, J.A. (2009) 'Topographical and Temporal Diversity of the Human Skin Microbiome', *Science*, 324(5931), pp. 1190-1192.

Grimm, M., Muller, A., Hein, G., Funfstuck, R. and Jahreis, G. (2001) 'High phosphorus intake only slightly affects serum minerals, urinary pyridinium crosslinks and renal function in young women', *Eur J Clin Nutr*, 55(3), pp. 153-61.

Groenen, P.M., Bunschoten, A.E., van Soolingen, D. and van Embden, J.D. (1993) 'Nature of DNA polymorphism in the direct repeat cluster of Mycobacterium tuberculosis; application for strain differentiation by a novel typing method', *Mol Microbiol*, 10(5), pp. 1057-65.

Guo, Z., Zhang, J., Wang, Z., Ang, K.Y., Huang, S., Hou, Q., Su, X., Qiao, J., Zheng, Y., Wang, L., Koh, E., Danliang, H., Xu, J., Lee, Y.K. and Zhang, H. (2016) 'Intestinal Microbiota Distinguish Gout Patients from Healthy Humans', *Scientific Reports*, 6, p. 20602.

Guschin, D.Y., Waite, A.J., Katibah, G.E., Miller, J.C., Holmes, M.C. and Rebar, E.J. (2010) 'A rapid and general assay for monitoring endogenous gene modification', *Methods Mol Biol*, 649, pp. 247-56.

Gutiérrez, O.M. (2013) 'The connection between dietary phosphorus, cardiovascular disease, and mortality: where we stand and what we need to know', *Advances in nutrition (Bethesda, Md.)*, 4(6), pp. 723-729.

Gutschner, T., Baas, M. and Diederichs, S. (2011) 'Noncoding RNA gene silencing through genomic integration of RNA destabilizing elements using zinc finger nucleases', *Genome Res*, 21(11), pp. 1944-54.

Hahm, H.A., Dunn, V.R., Butash, K.A., Deveraux, W.L., Woster, P.M., Casero, R.A. and Davidson, N.E. (2001) 'Combination of standard cytotoxic agents with polyamine analogues in the treatment of breast cancer cell lines', *Clinical cancer research*, 7(2), pp. 391-399.

Hamaker, B.R. and Tuncil, Y.E. (2014) 'A Perspective on the Complexity of Dietary Fiber Structures and Their Potential Effect on the Gut Microbiota', *Journal of Molecular Biology*, 426(23), pp. 3838-3850.

Hammerman, M.R., Karl, I.E. and Hruska, K.A. (1980) 'Regulation of canine renal vesicle Pi transport by growth hormone and parathyroid hormone', *Biochim Biophys Acta*, 603(2), pp. 322-35.

Hammerman, M.R. and Rogers, S. (1987) 'Distribution of IGF receptors in the plasma membrane of proximal tubular cells', *Am J Physiol*, 253(5 Pt 2), pp. F841-7.

Han, J., Zhang, J., Chen, L., Shen, B., Zhou, J., Hu, B., Du, Y., Tate, P.H., Huang, X. and Zhang, W. (2014) 'Efficient in vivo deletion of a large imprinted lncRNA by CRISPR/Cas9', *RNA Biol*, 11(7), pp. 829-35.

Haring, M., Offermann, S., Danker, T., Horst, I., Peterhansel, C. and Stam, M. (2007) 'Chromatin immunoprecipitation: optimization, quantitative analysis and data normalization', *Plant methods*, 3, pp. 11-11.

Hartmann, C.M., Hewson, A.S., Kos, C.H., Hilfiker, H., Soumounou, Y., Murer, H. and Tenenhouse, H.S. (1996) 'Structure of murine and human renal type II Na+-phosphate cotransporter genes (Npt2 and NPT2)', *Proc Natl Acad Sci U S A*, 93(14), pp. 7409-14.

Hattenhauer, O., Traebert, M., Murer, H. and Biber, J. (1999) 'Regulation of small intestinal Na-Pi type IIb cotransporter by dietary phosphate intake', *American Journal of Physiology-Gastrointestinal and Liver Physiology*, 277(4), pp. G756-G762.

He, F. (2011) 'Laemmli-SDS-PAGE', *Bio-protocol*, 1(11), p. e80.

He, S.L. and Green, R. (2013) 'Northern blotting', *Methods in enzymology*, 530, pp. 75-87.

He, Y., Vogelstein, B., Velculescu, V.E., Papadopoulos, N. and Kinzler, K.W. (2008) 'The antisense transcriptomes of human cells', *Science*, 322(5909), pp. 1855-7.

Hediger, M.A., Romero, M.F., Peng, J.B., Rolfs, A., Takanaga, H. and Bruford, E.A. (2004) 'The ABCs of solute carriers: physiological, pathological and therapeutic implications of human membrane transport proteinsIntroduction', *Pflugers Arch*, 447(5), pp. 465-8.

Heerboth, S., Lapinska, K., Snyder, N., Leary, M., Rollinson, S. and Sarkar, S. (2014) 'Use of epigenetic drugs in disease: an overview', *Genetics & epigenetics*, 6, pp. 9-19.

Herman, J.G., Jen, J., Merlo, A. and Baylin, S.B. (1996) 'Hypermethylation-associated inactivation indicates a tumor suppressor role for p15INK4B', *Cancer Res*, 56(4), pp. 722-7.

Herman, J.G., Merlo, A., Mao, L., Lapidus, R.G., Issa, J.P., Davidson, N.E., Sidransky, D. and Baylin, S.B. (1995) 'Inactivation of the CDKN2/p16/MTS1 gene is frequently associated with aberrant DNA methylation in all common human cancers', *Cancer Res*, 55(20), pp. 4525-30.

Hermann, A., Goyal, R. and Jeltsch, A. (2004) 'The Dnmt1 DNA-(cytosine-C5)-methyltransferase methylates DNA processively with high preference for hemimethylated target sites', *J Biol Chem*, 279(46), pp. 48350-9.

Hilfiker, H., Hattenhauer, O., Traebert, M., Forster, I., Murer, H. and Biber, J. (1998a) 'Characterization of a murine type II sodium-phosphate cotransporter expressed in mammalian small intestine', *Proc Natl Acad Sci U S A*, 95(24), pp. 14564-9.

Hilfiker, H., Hattenhauer, O., Traebert, M., Forster, I., Murer, H. and Biber, J. (1998b) 'Characterization of a murine type II sodium-phosphate cotransporter expressed in mammalian small intestine', *Proceedings of the National Academy of Sciences*, 95(24), pp. 14564-14569.

Hill, D.A. and Artis, D. (2010) 'Intestinal bacteria and the regulation of immune cell homeostasis', *Annu Rev Immunol*, 28, pp. 623-67.

Hinson A.M., S.B.C. 'Parathyroid Physiology and Molecular Biology In: Stack, Jr. B., Bodenner D. (eds) Medical and Surgical Treatment of Parathyroid Diseases', *Springer, Cham*

Horrillo, A., Pezzolla, D., Fraga, M.F., Aguilera, Y., Salguero-Aranda, C., Tejedo, J.R., Martin, F., Bedoya, F.J., Soria, B. and Hmadcha, A. (2013) 'Zebularine regulates early stages of mESC differentiation: effect on cardiac commitment', *Cell Death &Amp; Disease*, 4, p. e570.

Huqun, Izumi, S., Miyazawa, H., Ishii, K., Uchiyama, B., Ishida, T., Tanaka, S., Tazawa, R., Fukuyama, S., Tanaka, T., Nagai, Y., Yokote, A., Takahashi, H., Fukushima, T., Kobayashi, K., Chiba, H., Nagata, M., Sakamoto, S., Nakata, K., Takebayashi, Y., Shimizu, Y., Kaneko, K., Shimizu, M., Kanazawa, M., Abe, S., Inoue, Y., Takenoshita, S., Yoshimura, K., Kudo, K., Tachibana, T., Nukiwa, T. and Hagiwara, K. (2007) 'Mutations in the SLC34A2 gene are associated with pulmonary alveolar microlithiasis', *Am J Respir Crit Care Med*, 175(3), pp. 263-8.

Huttenhower, C., Gevers, D., Knight, R., Abubucker, S., Badger, J.H., Chinwalla, A.T., Creasy, H.H., Earl, A.M., FitzGerald, M.G., Fulton, R.S., Giglio, M.G., Hallsworth-Pepin, K., Lobos, E.A., Madupu, R., Magrini, V., Martin, J.C., Mitreva, M., Muzny, D.M., Sodergren, E.J., Versalovic, J., Wollam, A.M., Worley, K.C., Wortman, J.R., Young, S.K., Zeng, Q., Aagaard, K.M., Abolude, O.O., Allen-Vercoe, E., Alm, E.J., Alvarado, L., Andersen, G.L., Anderson, S., Appelbaum, E., Arachchi, H.M., Armitage, G., Arze, C.A., Ayvaz, T., Baker, C.C., Begg, L., Belachew, T., Bhonagiri, V., Bihan, M., Blaser, M.J., Bloom, T., Bonazzi, V., Paul Brooks, J., Buck, G.A., Buhay, C.J., Busam, D.A., Campbell, J.L., Canon, S.R., Cantarel, B.L., Chain, P.S.G., Chen, I.M.A., Chen, L., Chhibba, S., Chu, K., Ciulla, D.M., Clemente, J.C., Clifton, S.W., Conlan, S., Crabtree, J., Cutting, M.A., Davidovics, N.J., Davis, C.C., DeSantis, T.Z., Deal, C., Delehaunty, K.D., Dewhirst, F.E., Deych, E., Ding, Y., Dooling, D.J., Dugan, S.P., Michael Dunne, W., Scott Durkin, A., Edgar, R.C., Erlich, R.L., Farmer, C.N., Farrell, R.M., Faust, K., Feldgarden, M., Felix, V.M., Fisher, S., Fodor, A.A., Forney, L.J., Foster, L., Di Francesco, V., Friedman, J., Friedrich, D.C., Fronick, C.C., Fulton, L.L., Gao, H., Garcia, N., Giannoukos, G., Giblin, C.,

Giovanni, M.Y., Goldberg, J.M., Goll, J., Gonzalez, A., Griggs, A., et al. (2012) 'Structure, function and diversity of the healthy human microbiome', *Nature*, 486(7402), pp. 207-214.

Ishino, Y., Shinagawa, H., Makino, K., Amemura, M. and Nakata, A. (1987) 'Nucleotide sequence of the iap gene, responsible for alkaline phosphatase isozyme conversion in Escherichia coli, and identification of the gene product', *Journal of Bacteriology*, 169(12), pp. 5429-5433.

Itoh, N. and Ornitz, D.M. (2011) 'Fibroblast growth factors: from molecular evolution to roles in development, metabolism and disease', *The Journal of Biochemistry*, 149(2), pp. 121-130.

Jacquillet, G. and Unwin, R.J. (2019) 'Physiological regulation of phosphate by vitamin D, parathyroid hormone (PTH) and phosphate (Pi)', *Pflugers Arch*, 471(1), pp. 83-98.

Jaenisch, R. and Bird, A. 'Epigenetic regulation of gene expression: how the genome integrates intrinsic and environmental signals', *Nat Genet*.

Jansen, R., Embden, J.D., Gaastra, W. and Schouls, L.M. (2002) 'Identification of genes that are associated with DNA repeats in prokaryotes', *Mol Microbiol*, 43(6), pp. 1565-75.

Jenuwein, T. and Allis, C.D. (2001) 'Translating the histone code', *Science*, 293(5532), pp. 1074-80.

Jeon, Y. and Lee, J.T. (2011) 'YY1 tethers Xist RNA to the inactive X nucleation center', *Cell*, 146(1), pp. 119-33.

Ji, Z., Song, R., Regev, A. and Struhl, K. (2015) 'Many lncRNAs, 5'UTRs, and pseudogenes are translated and some are likely to express functional proteins', *eLife*, 4, p. e08890.

Jinek, M., Chylinski, K., Fonfara, I., Hauer, M., Doudna, J.A. and Charpentier, E. (2012) 'A programmable dual-RNA-guided DNA endonuclease in adaptive bacterial immunity', *Science*, 337(6096), pp. 816-21.

Jones, A., Tzenova, J., Frappier, D., Crumley, M., Roslin, N., Kos, C., Tieder, M., Langman, C., Proesmans, W., Carpenter, T., Rice, A., Anderson, D., Morgan, K., Fujiwara, T. and Tenenhouse, H. (2001) 'Hereditary hypophosphatemic rickets with hypercalciuria is not caused by mutations in the Na/Pi cotransporter NPT2 gene', *J Am Soc Nephrol*, 12(3), pp. 507-14.

Jorjani, H., Kehr, S., Jedlinski, D.J., Gumienny, R., Hertel, J., Stadler, P.F., Zavolan, M. and Gruber, A.R. (2016) 'An updated human snoRNAome', *Nucleic Acids Res*, 44(11), pp. 5068-82.

Kang, M.-J., Abdelmohsen, K., Hutchison, E.R., Mitchell, S.J., Grammatikakis, I., Guo, R., Noh, J.H., Martindale, J.L., Yang, X., Lee, E.K., Faghihi, M.A., Wahlestedt, C., Troncoso, J.C., Pletnikova, O., Perrone-Bizzozero, N., Resnick, S.M., de Cabo, R., Mattson, M.P. and Gorospe, M. (2014) 'HuD regulates coding and noncoding RNA to induce APP→Aβ processing', *Cell reports*, 7(5), pp. 1401-1409.

Karimi, Z., Ahmadi, A., Najafi, A. and Ranjbar, R. (2018) 'Bacterial CRISPR Regions: General Features and their Potential for Epidemiological Molecular Typing Studies', *The open microbiology journal*, 12, pp. 59-70.

Kashi, K., Henderson, L., Bonetti, A. and Carninci, P. (2016) 'Discovery and functional analysis of lncRNAs: Methodologies to investigate an uncharacterized transcriptome', *Biochimica et Biophysica Acta (BBA) - Gene Regulatory Mechanisms*, 1859(1), pp. 3-15.

Katayama, S., Tomaru, Y., Kasukawa, T., Waki, K., Nakanishi, M., Nakamura, M., Nishida, H., Yap, C.C., Suzuki, M., Kawai, J., Suzuki, H., Carninci, P., Hayashizaki, Y., Wells, C., Frith, M., Ravasi, T., Pang, K.C., Hallinan, J., Mattick, J., Hume, D.A., Lipovich, L., Batalov, S., Engstrom, P.G., Mizuno, Y., Faghihi, M.A., Sandelin, A., Chalk, A.M., Mottagui-Tabar, S., Liang, Z., Lenhard, B. and Wahlestedt, C. (2005a) 'Antisense transcription in the mammalian transcriptome', *Science*, 309(5740), pp. 1564-6.

Katayama, S., Tomaru, Y., Kasukawa, T., Waki, K., Nakanishi, M., Nakamura, M., Nishida, H., Yap, C.C., Suzuki, M., Kawai, J., Suzuki, H., Carninci, P., Hayashizaki, Y., Wells, C., Frith, M., Ravasi, T., Pang, K.C., Hallinan, J., Mattick, J., Hume, D.A., Lipovich, L., Batalov, S., Engström, P.G., Mizuno, Y., Faghihi, M.A., Sandelin, A., Chalk, A.M., Mottagui-Tabar, S., Liang, Z., Lenhard, B. and Wahlestedt, C. (2005b) 'Molecular biology: Antisense transcription in the mammalian transcriptome', *Science*, 309(5740), pp. 1564-1566.

Kato, S., Takeyama, K., Kitanaka, S., Murayama, A., Sekine, K. and Yoshizawa, T. (1999) 'In vivo function of VDR in gene expression-VDR knock-out mice', *J Steroid Biochem Mol Biol*, 69(1-6), pp. 247-51.

Kaur, G. and Dufour, J.M. (2012) 'Cell lines: Valuable tools or useless artifacts', *Spermatogenesis*, 2(1), pp. 1-5.

Kc, R., Srivastava, A., Wilkowski, J.M., Richter, C.E., Shavit, J.A., Burke, D.T. and Bielas, S.L. (2016) 'Detection of nucleotide-specific CRISPR/Cas9 modified alleles using multiplex ligation detection', *Scientific Reports*, 6, p. 32048.

Kempson, S.A., Lotscher, M., Kaissling, B., Biber, J., Murer, H. and Levi, M. (1995) 'Parathyroid hormone action on phosphate transporter mRNA and protein in rat renal proximal tubules', *Am J Physiol*, 268(4 Pt 2), pp. F784-91.

Kendrick, J., Kestenbaum, B. and Chonchol, M. (2011) 'Phosphate and Cardiovascular Disease', *Advances in Chronic Kidney Disease*, 18(2), pp. 113-119.

Kent, W.J., Sugnet, C.W., Furey, T.S., Roskin, K.M., Pringle, T.H., Zahler, A.M. and Haussler, D. (2002) 'The human genome browser at UCSC', *Genome Res*, 12(6), pp. 996-1006.

Kiss, T. (2002) 'Small nucleolar RNAs: an abundant group of noncoding RNAs with diverse cellular functions', *Cell*, 109(2), pp. 145-8.

Kiyosawa, H., Yamanaka, I., Osato, N., Kondo, S. and Hayashizaki, Y. (2003) 'Antisense transcripts with FANTOM2 clone set and their implications for gene regulation', *Genome Res*, 13(6b), pp. 1324-34.

Knöpfel, T. (2016) 'Mechanisms of Intestinal Phosphate Absorption', Ph.D. thesis, pp. 45-48.

Knopfel, T., Pastor-Arroyo, E.M., Schnitzbauer, U., Kratschmar, D.V., Odermatt, A., Pellegrini, G., Hernando, N. and Wagner, C.A. (2017) 'The intestinal phosphate transporter NaPi-IIb (Slc34a2) is required to protect bone during dietary phosphate restriction', *Sci Rep*, 7(1), p. 11018.

Knöpfel, T., Pastor-Arroyo, E.M., Schnitzbauer, U., Kratschmar, D.V., Odermatt, A., Pellegrini, G., Hernando, N. and Wagner, C.A. (2017) 'The intestinal phosphate transporter NaPi-IIb (Slc34a2) is required to protect bone during dietary phosphate restriction', *Scientific Reports*, 7(1), p. 11018.

Kobayashi, H., Sakurai, T., Imai, M., Takahashi, N., Fukuda, A., Yayoi, O., Sato, S., Nakabayashi, K., Hata, K., Sotomaru, Y., Suzuki, Y. and Kono, T. (2012) 'Contribution of intragenic DNA methylation in mouse gametic DNA methylomes to establish oocyte-specific heritable marks', *PLoS Genet*, 8(1), p. e1002440.

Kohli, R.M. and Zhang, Y. (2013) 'TET enzymes, TDG and the dynamics of DNA demethylation', *Nature*, 502(7472), pp. 472-9.

Koleff, P., Gaston, K.J. and Lennon, J.J. (2003) 'Measuring beta diversity for presence–absence data', *Journal of Animal Ecology*, 72(3), pp. 367-382.

Kong, L.C., Wuillemin, P.-H., Bastard, J.-P., Sokolovska, N., Gougis, S., Fellahi, S., Darakhshan, F., Bonnefont-Rousselot, D., Bittar, R., Doré, J., Zucker, J.-D., Clément, K. and Rizkalla, S. (2013) 'Insulin resistance and inflammation predict kinetic body weight changes in response to dietary weight loss and maintenance in overweight and obese subjects by using a Bayesian network approach', *The American Journal of Clinical Nutrition*, 98(6), pp. 1385-1394.

Kong, W.Y., Yee, Z.Y., Mai, C.W., Fang, C.-M., Abdullah, S. and Ngai, S.C. (2019) 'Zebularine and trichostatin A sensitized human breast adenocarcinoma cells towards tumor necrosis factor-related apoptosis inducing ligand (TRAIL)-induced apoptosis', *Heliyon*, 5(9), p. e02468.

Kortman, G.A., Raffatellu, M., Swinkels, D.W. and Tjalsma, H. (2014) 'Nutritional iron turned inside out: intestinal stress from a gut microbial perspective', *FEMS Microbiol Rev*, 38(6), pp. 1202-34.

Kowalczyk, M.S., Higgs, D.R. and Gingeras, T.R. (2012a) 'Molecular biology: RNA discrimination', *Nature*, 482(7385), pp. 310-311.

Kowalczyk, M.S., Higgs, D.R. and Gingeras, T.R. (2012b) 'RNA discrimination', *Nature*, 482(7385), pp. 310-311.

Kozomara, A., Birgaoanu, M. and Griffiths-Jones, S. (2019) 'miRBase: from microRNA sequences to function', *Nucleic Acids Res*, 47(D1), pp. D155-d162.

Kruskal, W.H. and Wallis, W.A. (1952) 'Use of Ranks in One-Criterion Variance Analysis', *Journal of the American Statistical Association*, 47(260), pp. 583-621.

Kumar, R. and Thompson, J.R. (2011) 'The regulation of parathyroid hormone secretion and synthesis', *J Am Soc Nephrol*, 22(2), pp. 216-24.

Kung, J.T., Colognori, D. and Lee, J.T. (2013) 'Long noncoding RNAs: past, present, and future', *Genetics*, 193(3), pp. 651-69.

Kunze, W.A., Mao, Y.K., Wang, B., Huizinga, J.D., Ma, X., Forsythe, P. and Bienenstock, J. (2009) 'Lactobacillus reuteri enhances excitability of colonic AH neurons by inhibiting calcium-dependent potassium channel opening', *J Cell Mol Med*, 13(8b), pp. 2261-70.

Laboratories, B.-R. (2014) 'Gel Doc EZ Imaging System with Image Lab Software', (Version 5.1), pp. 91-99.

Laird, P.W. (2010) 'Principles and challenges of genomewide DNA methylation analysis', *Nat Rev Genet*, 11(3), pp. 191-203.

Latos, P.A., Pauler, F.M., Koerner, M.V., Şenergin, H.B., Hudson, Q.J., Stocsits, R.R., Allhoff, W., Stricker, S.H., Klement, R.M., Warczok, K.E., Aumayr, K., Pasierbek, P. and Barlow, D.P. (2012) 'Airn Transcriptional Overlap, But Not Its lncRNA Products, Induces Imprinted Igf2r Silencing', *Science*, 338(6113), pp. 1469-1472.

Lau, W.L., Vaziri, N.D., Nunes, A.C.F., Comeau, A.M., Langille, M.G.I., England, W., Khazaeli, M., Suematsu, Y., Phan, J. and Whiteson, K. (2018) 'The Phosphate Binder Ferric Citrate Alters the Gut Microbiome in Rats with Chronic Kidney Disease', *J Pharmacol Exp Ther*, 367(3), pp. 452-460.

Laurent, L., Wong, E., Li, G., Huynh, T., Tsirigos, A., Ong, C.T., Low, H.M., Kin Sung, K.W., Rigoutsos, I., Loring, J. and Wei, C.L. (2010) 'Dynamic changes in the human methylome during differentiation', *Genome Res*, 20(3), pp. 320-31.

Lavorgna, G., Dahary, D., Lehner, B., Sorek, R., Sanderson, C.M. and Casari, G. (2004) 'In search of antisense', *Trends Biochem Sci*, 29(2), pp. 88-94.

Law, J.A. and Jacobsen, S.E. (2010) 'Establishing, maintaining and modifying DNA methylation patterns in plants and animals', *Nat Rev Genet*, 11(3), pp. 204-20.

Lê, K.-A., Li, Y., Xu, X., Liu, T., Yang, W., He, F., Su, K., Cai, D.H., Go, V.L.W., Pandol, S. and Hui, H. (2013) 'Alterations in fecal Lactobacillus and Bifidobacterium species in type 2 diabetic patients in Southern China population', *Frontiers in Physiology*, 3(496).

Lederer, E. (2014) 'Regulation of serum phosphate', *The Journal of Physiology*, 592(Pt 18), pp. 3985-3995.

Lee, H.C., Jenner, A.M., Low, C.S. and Lee, Y.K. (2006) 'Effect of tea phenolics and their aromatic fecal bacterial metabolites on intestinal microbiota', *Res Microbiol*, 157(9), pp. 876-84.

Lesser, D., Young, L.R. and Hagood, J.S. (2019) '55 - Rare Childhood Lung Disorders', in Wilmott, R.W., Deterding, R., Li, A., Ratjen, F., Sly, P., Zar, H.J. and Bush, A. (eds.) *Kendig's Disorders of the Respiratory Tract in Children (Ninth Edition)*. Philadelphia: Content Repository Only!, pp. 817-824.e2.

Levi, M., Lotscher, M., Sorribas, V., Custer, M., Arar, M., Kaissling, B., Murer, H. and Biber, J. (1994) 'Cellular mechanisms of acute and chronic adaptation of rat renal P(i) transporter to alterations in dietary P(i)', *Am J Physiol*, 267(5 Pt 2), pp. F900-8.

Levi, M., Shayman, J.A., Abe, A., Gross, S.K., McCluer, R.H., Biber, J., Murer, H., Lötscher, M. and Cronin, R.E. (1995) 'Dexamethasone modulates rat renal brush border membrane phosphate transporter mRNA and protein abundance and glycosphingolipid composition', *The Journal of clinical investigation*, 96(1), pp. 207-216.

Ley, R.E., Turnbaugh, P.J., Klein, S. and Gordon, J.I. (2006) 'Microbial ecology: human gut microbes associated with obesity', *Nature*, 444(7122), pp. 1022-3.

Li, L.C. and Dahiya, R. (2002) 'MethPrimer: designing primers for methylation PCRs', *Bioinformatics*, 18(11), pp. 1427-31.

Li, T., Xie, J., Shen, C., Cheng, D., Shi, Y., Wu, Z., Deng, X., Chen, H., Shen, B., Peng, C., Li, H., Zhan, Q. and Zhu, Z. (2015) 'Amplification of Long Noncoding RNA ZFAS1 Promotes Metastasis in Hepatocellular Carcinoma', *Cancer Res*, 75(15), pp. 3181-91.

Li, Y.Y., Qin, L., Guo, Z.M., Liu, L., Xu, H., Hao, P., Su, J., Shi, Y., He, W.Z. and Li, Y.X. (2006) 'In silico discovery of human natural antisense transcripts', *BMC Bioinformatics*, 7, p. 18.

Liang, F., Han, M., Romanienko, P.J. and Jasin, M. (1998) 'Homology-directed repair is a major double-strand break repair pathway in mammalian cells', *Proceedings of the National Academy of Sciences*, 95(9), pp. 5172-5177.

Lister, R., Pelizzola, M., Dowen, R.H., Hawkins, R.D., Hon, G., Tonti-Filippini, J., Nery, J.R., Lee, L., Ye, Z., Ngo, Q.M., Edsall, L., Antosiewicz-Bourget, J., Stewart, R., Ruotti, V., Millar, A.H., Thomson, J.A., Ren, B. and Ecker, J.R. (2009) 'Human DNA methylomes at base resolution show widespread epigenomic differences', *Nature*, 462(7271), pp. 315-22.

Liu, Y., Dou, M., Song, X., Dong, Y., Liu, S., Liu, H., Tao, J., Li, W., Yin, X. and Xu, W. (2019) 'The emerging role of the piRNA/piwi complex in cancer', *Molecular Cancer*, 18(1), p. 123.

Liu, Y., Han, X., Yuan, J., Geng, T., Chen, S., Hu, X., Cui, I.H. and Cui, H. (2017) 'Biallelic insertion of a transcriptional terminator via the CRISPR/Cas9 system efficiently silences expression of protein-coding and non-coding RNA genes', *J Biol Chem*, 292(14), pp. 5624-5633.

Lo, C.-A., Greben, A.W. and Chen, B.E. (2017) 'Generating stable cell lines with quantifiable protein production using CRISPR/Cas9-mediated knock-in', *BioTechniques*, 62(4), pp. 165-174.

López-Barragán, M.J., Quiñones, M., Cui, K., Lemieux, J., Zhao, K. and Su, X.-z. (2011) 'Effect of PCR extension temperature on high-throughput sequencing', *Molecular and biochemical parasitology*, 176(1), pp. 64-67.

Lorenz-Depiereux, B., Benet-Pages, A., Eckstein, G., Tenenbaum-Rakover, Y., Wagenstaller, J., Tiosano, D., Gershoni-Baruch, R., Albers, N., Lichtner, P., Schnabel, D., Hochberg, Z.e. and Strom, T.M. (2006) 'Hereditary hypophosphatemic rickets with hypercalciuria is caused by mutations in the sodium-phosphate cotransporter gene SLC34A3', *American journal of human genetics*, 78(2), pp. 193-201.

Lozupone, C., Lladser, M.E., Knights, D., Stombaugh, J. and Knight, R. (2011) 'UniFrac: an effective distance metric for microbial community comparison', *The ISME journal*, 5(2), pp. 169-172.

Luger, K., Mader, A.W., Richmond, R.K., Sargent, D.F. and Richmond, T.J. (1997) 'Crystal structure of the nucleosome core particle at 2.8 A resolution', *Nature*, 389(6648), pp. 251-60.

Luo, S., Lu, J.Y., Liu, L., Yin, Y., Chen, C., Han, X., Wu, B., Xu, R., Liu, W., Yan, P., Shao, W., Lu, Z., Li, H., Na, J., Tang, F., Wang, J., Zhang, Yong E. and Shen, X. (2016) 'Divergent lncRNAs

Regulate Gene Expression and Lineage Differentiation in Pluripotent Cells', *Cell Stem Cell*, 18(5), pp. 637-652.

Lv, Q., Lai, L., Yuan, L., Song, Y., Sui, T. and Li, Z. (2016) 'Tandem repeat knockout utilizing the CRISPR/Cas9 system in human cells', *Gene*, 582(2), pp. 122-7.

Ma, L., Chua, M.-S., Andrisani, O. and So, S. (2014) 'Epigenetics in hepatocellular carcinoma: an update and future therapy perspectives', *World journal of gastroenterology*, 20(2), pp. 333-345.

Ma, Y., Kanakousaki, K. and Buttitta, L. (2015) 'How the cell cycle impacts chromatin architecture and influences cell fate', *Frontiers in genetics*, 6, pp. 19-19.

Macfarlane, G.T. and Cummings, J.H. (1999) 'Probiotics and prebiotics: can regulating the activities of intestinal bacteria benefit health?', *Bmj*, 318(7189), pp. 999-1003.

Macfarlane, S., Steed, H. and Macfarlane, G.T. (2009) 'Intestinal bacteria and inflammatory bowel disease', *Crit Rev Clin Lab Sci*, 46(1), pp. 25-54.

Maes, M., Yirmyia, R., Noraberg, J., Brene, S., Hibbeln, J., Perini, G., Kubera, M., Bob, P., Lerer, B. and Maj, M. (2009) 'The inflammatory & neurodegenerative (I&ND) hypothesis of depression: leads for future research and new drug developments in depression', *Metab Brain Dis*, 24(1), pp. 27-53.

Magagnin, S., Werner, A., Markovich, D., Sorribas, V., Stange, G., Biber, J. and Murer, H. (1993) 'Expression cloning of human and rat renal cortex Na/Pi cotransport', *Proc Natl Acad Sci U S A*, 90(13), pp. 5979-83.

Magen, D., Berger, L., Coady, M.J., Ilivitzki, A., Militianu, D., Tieder, M., Selig, S., Lapointe, J.Y., Zelikovic, I. and Skorecki, K. (2010) 'A loss-of-function mutation in NaPi-IIa and renal Fanconi's syndrome', *N Engl J Med*, 362(12), pp. 1102-9.

Makarova, K.S., Grishin, N.V., Shabalina, S.A., Wolf, Y.I. and Koonin, E.V. (2006) 'A putative RNA-interference-based immune system in prokaryotes: computational analysis of the predicted enzymatic machinery, functional analogies with eukaryotic RNAi, and hypothetical mechanisms of action', *Biol Direct*, 1, p. 7.

Mali, P., Yang, L., Esvelt, K.M., Aach, J., Guell, M., DiCarlo, J.E., Norville, J.E. and Church, G.M. (2013) 'RNA-Guided Human Genome Engineering via Cas9', *Science*, 339(6121), pp. 823-826.

Mann, E., Schmitz-Esser, S., Zebeli, Q., Wagner, M., Ritzmann, M. and Metzler-Zebeli, B.U. (2014) 'Mucosa-associated bacterial microbiome of the gastrointestinal tract of weaned pigs and dynamics linked to dietary calcium-phosphorus', *PLoS One*, 9(1), p. e86950.

Marchal, J.A., Lopez, G.J., Peran, M., Comino, A., Delgado, J.R., García-García, J.A., Conde, V., Aranda, F.M., Rivas, C., Esteban, M. and Garcia, M.A. (2014) 'The impact of PKR activation: from neurodegeneration to cancer', *The FASEB Journal*, 28(5), pp. 1965-1974.

Marks, J., Debnam, E.S. and Unwin, R.J. (2010) 'Phosphate homeostasis and the renal-gastrointestinal axis', *American Journal of Physiology-Renal Physiology*, 299(2), pp. F285-F296.

Martin, A., David, V. and Quarles, L.D. (2012) 'Regulation and function of the FGF23/klotho endocrine pathways', *Physiological reviews*, 92(1), pp. 131-155.

Masek, T., Vopalensky, V., Suchomelova, P. and Pospisek, M. (2005) 'Denaturing RNA electrophoresis in TAE agarose gels', *Analytical Biochemistry*, 336(1), pp. 46-50.

Masi, L. (2011) 'Phosphatonins: new hormones involved in numerous inherited bone disorders', *Clinical cases in mineral and bone metabolism : the official journal of the Italian Society of Osteoporosis, Mineral Metabolism, and Skeletal Diseases*, 8(3), pp. 9-13.

Matouk, I.J., DeGroot, N., Mezan, S., Ayesh, S., Abu-lail, R., Hochberg, A. and Galun, E. (2007) 'The H19 non-coding RNA is essential for human tumor growth', *PLoS One*, 2(9), p. e845.

Matsuda, A., Asada, Y., Takakuwa, K., Sugita, J., Murakami, A. and Ebihara, N. (2015) 'DNA Methylation Analysis of Human Trabecular Meshwork Cells During Dexamethasone Stimulation', *Invest Ophthalmol Vis Sci*, 56(6), pp. 3801-9.

Mayer, W., Niveleau, A., Walter, J., Fundele, R. and Haaf, T. (2000) 'Demethylation of the zygotic paternal genome', *Nature*, 403(6769), pp. 501-2.

Mazidi, M., Rezaie, P., Kengne, A.P., Mobarhan, M.G. and Ferns, G.A. (2016) 'Gut microbiome and metabolic syndrome', *Diabetes Metab Syndr*, 10(2 Suppl 1), pp. S150-7.

McNamara, J. and Worthley, L.I. (2001) 'Acid-base balance: part I. Physiology', *Crit Care Resusc*, 3(3), pp. 181-7.

Mercer, T.R. and Mattick, J.S. (2013) 'Structure and function of long noncoding RNAs in epigenetic regulation', *Nat Struct Mol Biol*, 20(3), pp. 300-307.

Merino Ribas, A., Bancu, I., Graterol, F., Vergara, A., Noguera-Julian, M., Paredes, R. and Bonal, J. (2019) 'FO047GUT MICROBIOME IN HEMODIALYSYS PATIENTS TREATED WITH DIFFERENT TYPES OF PHOSPHATE BINDERS', *Nephrology Dialysis Transplantation*, 34(Supplement_1).

Metzler-Zebeli, B.U., Mann, E., Schmitz-Esser, S., Wagner, M., Ritzmann, M. and Zebeli, Q. (2013) 'Changing dietary calcium-phosphorus level and cereal source selectively alters

abundance of bacteria and metabolites in the upper gastrointestinal tracts of weaned pigs', *Appl Environ Microbiol*, 79(23), pp. 7264-72.

Metzler-Zebeli, B.U., Vahjen, W., Baumgartel, T., Rodehutscord, M. and Mosenthin, R. (2010) 'Ileal microbiota of growing pigs fed different dietary calcium phosphate levels and phytase content and subjected to ileal pectin infusion', *J Anim Sci*, 88(1), pp. 147-58.

Miao, Y.-Y., Xu, C.-M., Xia, M., Zhu, H.-Q. and Chen, Y.-Q. (2018) 'Relationship between Gut Microbiota and Phosphorus Metabolism in Hemodialysis Patients: A Preliminary Exploration', *Chinese medical journal*, 131(23), pp. 2792-2799.

Miyamoto, K., Ito, M., Kuwahata, M., Kato, S. and Segawa, H. (2005) 'Inhibition of intestinal sodium-dependent inorganic phosphate transport by fibroblast growth factor 23', *Ther Apher Dial*, 9(4), pp. 331-5.

Modarresi, F., Faghihi, M.A., Lopez-Toledano, M.A., Fatemi, R.P., Magistri, M., Brothers, S.P., van der Brug, M.P. and Wahlestedt, C. (2012) 'Inhibition of natural antisense transcripts in vivo results in gene-specific transcriptional upregulation', *Nat Biotechnol*, 30(5), pp. 453-9.

Mojica, F.J., Diez-Villasenor, C., Garcia-Martinez, J. and Soria, E. (2005) 'Intervening sequences of regularly spaced prokaryotic repeats derive from foreign genetic elements', *J Mol Evol*, 60(2), pp. 174-82.

Mojica, F.J., Ferrer, C., Juez, G. and Rodriguez-Valera, F. (1995) 'Long stretches of short tandem repeats are present in the largest replicons of the Archaea Haloferax mediterranei and Haloferax volcanii and could be involved in replicon partitioning', *Mol Microbiol*, 17(1), pp. 85-93.

Mojica, F.J., Juez, G. and Rodriguez-Valera, F. (1993) 'Transcription at different salinities of Haloferax mediterranei sequences adjacent to partially modified PstI sites', *Mol Microbiol*, 9(3), pp. 613-21.

Morange, M. (2015a) 'What history tells us XXXIX. CRISPR-Cas: From a prokaryotic immune system to a universal genome editing tool', *Journal of biosciences*, 40(5), pp. 829-832.

Morange, M. (2015b) 'What history tells us XXXVII. CRISPR-Cas: The discovery of an immune system in prokaryotes', *Journal of biosciences*, 40(2), pp. 221-223.

Mueller, C. and Macpherson, A.J. (2006) 'Layers of mutualism with commensal bacteria protect us from intestinal inflammation', *Gut*, 55(2), pp. 276-84.

Murani, E., Trakooljul, N., Hadlich, F., Ponsuksili, S. and Wimmers, K. (2019) 'Transcriptome Responses to Dexamethasone Depending on Dose and Glucocorticoid Receptor Sensitivity in the Liver', *Frontiers in Genetics*, 10(559).

Myakala, K., Motta, S., Murer, H., Wagner, C.A., Koesters, R., Biber, J. and Hernando, N. (2014) 'Renal-specific and inducible depletion of NaPi-IIc/Slc34a3, the cotransporter mutated in HHRH, does not affect phosphate or calcium homeostasis in mice', *Am J Physiol Renal Physiol*, 306(8), pp. F833-43.

Nakamura, K., Nakabayashi, K., Htet Aung, K., Aizawa, K., Hori, N., Yamauchi, J., Hata, K. and Tanoue, A. (2015) 'DNA methyltransferase inhibitor zebularine induces human cholangiocarcinoma cell death through alteration of DNA methylation status', *PLoS One*, 10(3), p. e0120545.

Nakamura, Y., Murai, T. and Ogawa, Y. (1996) 'Effect of in vitro and in vivo administration of dexamethasone on rat macrophage functions: comparison between alveolar and peritoneal macrophages', *Eur Respir J*, 9(2), pp. 301-6.

Newbury, S.F., Smith, N.H., Robinson, E.C., Hiles, I.D. and Higgins, C.F. (1987) 'Stabilization of translationally active mRNA by prokaryotic REP sequences', *Cell*, 48(2), pp. 297-310.

Newton, R. (2000) 'Molecular mechanisms of glucocorticoid action: what is important?', *Thorax*, 55(7), pp. 603-613.

Nielsen, S., Yuzenkova, Y. and Zenkin, N. (2013) 'Mechanism of Eukaryotic RNA Polymerase III Transcription Termination', *Science*, 340(6140), pp. 1577-1580.

Noh, J.H., Kim, K.M., McClusky, W.G., Abdelmohsen, K. and Gorospe, M. (2018) 'Cytoplasmic functions of long noncoding RNAs', *Wiley interdisciplinary reviews. RNA*, 9(3), pp. e1471-e1471.

Noronha-Blob, L. and Sacktor, B. (1986) 'Inhibition by glucocorticoids of phosphate transport in primary cultured renal cells', *J Biol Chem*, 261(5), pp. 2164-9.

Ohland, C.L. and Jobin, C. (2015) 'Microbial Activities and Intestinal Homeostasis: A Delicate Balance Between Health and Disease', *Cellular and Molecular Gastroenterology and Hepatology*, 1(1), pp. 28-40.

Ohnishi, M. and Razzaque, M.S. (2010) 'Dietary and genetic evidence for phosphate toxicity accelerating mammalian aging', *Faseb j*, 24(9), pp. 3562-71.

Okano, M., Bell, D.W., Haber, D.A. and Li, E. (1999) 'DNA methyltransferases Dnmt3a and Dnmt3b are essential for de novo methylation and mammalian development', *Cell*, 99(3), pp. 247-57.

Okano, M., Xie, S. and Li, E. (1998) 'Cloning and characterization of a family of novel mammalian DNA (cytosine-5) methyltransferases', *Nat Genet*, 19(3), pp. 219-20.

Olaharski, A.J., Ji, Z., Woo, J.-Y., Lim, S., Hubbard, A.E., Zhang, L. and Smith, M.T. (2006) 'The Histone Deacetylase Inhibitor Trichostatin A Has Genotoxic Effects in Human Lymphoblasts In Vitro', *Toxicological Sciences*, 93(2), pp. 341-347.

Olsen, G.J., Lane, D.J., Giovannoni, S.J., Pace, N.R. and Stahl, D.A. (1986) 'Microbial ecology and evolution: a ribosomal RNA approach', *Annu Rev Microbiol*, 40, pp. 337-65.

Osato, N., Suzuki, Y., Ikeo, K. and Gojobori, T. (2007) 'Transcriptional interferences in cis natural antisense transcripts of humans and mice', *Genetics*, 176(2), pp. 1299-306.

Pascussi, J.M., Drocourt, L., Fabre, J.M., Maurel, P. and Vilarem, M.J. (2000) 'Dexamethasone induces pregnane X receptor and retinoid X receptor-alpha expression in human hepatocytes: synergistic increase of CYP3A4 induction by pregnane X receptor activators', *Molecular pharmacology*, 58(2), pp. 361-372.

Pasini, D., Malatesta, M., Jung, H.R., Walfridsson, J., Willer, A., Olsson, L., Skotte, J., Wutz, A., Porse, B., Jensen, O.N. and Helin, K. (2010) 'Characterization of an antagonistic switch between histone H3 lysine 27 methylation and acetylation in the transcriptional regulation of Polycomb group target genes', *Nucleic Acids Res*, 38(15), pp. 4958-69.

Patti, M., Fenollar-Ferrer, C., Werner, A., Forrest, L.R. and Forster, I.C. (2016) 'Cation Interactions and Membrane Potential Induce Conformational Changes in NaPi-IIb', *Biophys J*, 111(5), pp. 973-88.

Pennacchio, L.A., Bickmore, W., Dean, A., Nobrega, M.A. and Bejerano, G. (2013) 'Enhancers: five essential questions', *Nat Rev Genet*, 14(4), pp. 288-95.

Penny, G.D., Kay, G.F., Sheardown, S.A., Rastan, S. and Brockdorff, N. (1996) 'Requirement for Xist in X chromosome inactivation', *Nature*, 379(6561), pp. 131-7.

Perez, E.E., Wang, J., Miller, J.C., Jouvenot, Y., Kim, K.A., Liu, O., Wang, N., Lee, G., Bartsevich, V.V., Lee, Y.L., Guschin, D.Y., Rupniewski, I., Waite, A.J., Carpenito, C., Carroll, R.G., Orange, J.S., Urnov, F.D., Rebar, E.J., Ando, D., Gregory, P.D., Riley, J.L., Holmes, M.C. and June, C.H. (2008) 'Establishment of HIV-1 resistance in CD4+ T cells by genome editing using zinc-finger nucleases', *Nat Biotechnol*, 26(7), pp. 808-16.

Perwad, F., Zhang, M.Y., Tenenhouse, H.S. and Portale, A.A. (2007) 'Fibroblast growth factor 23 impairs phosphorus and vitamin D metabolism in vivo and suppresses 25-hydroxyvitamin D-1alpha-hydroxylase expression in vitro', *Am J Physiol Renal Physiol*, 293(5), pp. F1577-83.

Petersen, A., Carlsson, T., Karlsson, J.O., Jonhede, S. and Zetterberg, M. (2008) 'Effects of dexamethasone on human lens epithelial cells in culture', *Mol Vis*, 14, pp. 1344-52.

Pfister, M.F., Lederer, E., Forgo, J., Ziegler, U., Lotscher, M., Quabius, E.S., Biber, J. and Murer, H. (1997) 'Parathyroid hormone-dependent degradation of type II Na+/Pi cotransporters', *J Biol Chem*, 272(32), pp. 20125-30.

Pfister, M.F., Ruf, I., Stange, G., Ziegler, U., Lederer, E., Biber, J. and Murer, H. (1998) 'Parathyroid hormone leads to the lysosomal degradation of the renal type II Na/Pi cotransporter', *Proc Natl Acad Sci U S A*, 95(4), pp. 1909-14.

Piatek, M.J. (2016) 'The biological role of natural antisense transcripts in zebrafish development ', *PhD thesis*.

Piatek, M.J., Henderson, V., Zynad, H.S. and Werner, A. (2016) 'Natural antisense transcription from a comparative perspective', *Genomics*, 108(2), pp. 56-63.

Picard, N., Capuano, P., Stange, G., Mihailova, M., Kaissling, B., Murer, H., Biber, J. and Wagner, C.A. (2010) 'Acute parathyroid hormone differentially regulates renal brush border membrane phosphate cotransporters', *Pflugers Arch*, 460(3), pp. 677-87.

Platt, T. (1986) 'Transcription termination and the regulation of gene expression', *Annu Rev Biochem*, 55, pp. 339-72.

Pourcel, C., Salvignol, G. and Vergnaud, G. (2005) 'CRISPR elements in Yersinia pestis acquire new repeats by preferential uptake of bacteriophage DNA, and provide additional tools for evolutionary studies', *Microbiology*, 151(Pt 3), pp. 653-63.

Powers, C.J., McLeskey, S.W. and Wellstein, A. (2000) 'Fibroblast growth factors, their receptors and signaling', *Endocr Relat Cancer*, 7(3), pp. 165-97.

Prasad, N. and Bhadauria, D. (2013) 'Renal phosphate handling: Physiology', *Indian journal of endocrinology and metabolism*, 17(4), pp. 620-627.

Prescott, E.M. and Proudfoot, N.J. (2002) 'Transcriptional collision between convergent genes in budding yeast', *Proc Natl Acad Sci U S A*, 99(13), pp. 8796-801.

Proudfoot, N.J. (2016) 'Transcriptional termination in mammals: Stopping the RNA polymerase II juggernaut', *Science*, 352(6291), p. aad9926.

Pufall, M.A., Fang, M., Bradley, R.K., Guo-Liang, C., Lanier, R. and Tasian, S.K. (2019) 'Glucocorticoids Regulate the Splicing Factor MBNL1, a Potential Control Point for B-Cell Specification', *Blood*, 134(Supplement_1), pp. 2478-2478.

Quann, E.E., Fulgoni, V.L. and Auestad, N. (2015) 'Consuming the daily recommended amounts of dairy products would reduce the prevalence of inadequate micronutrient

intakes in the United States: diet modeling study based on NHANES 2007–2010', *Nutrition Journal*, 14, p. 90.

Quinn, J.J. and Chang, H.Y. (2015) 'Unique features of long non-coding RNA biogenesis and function', *Nature Reviews Genetics*, 17, p. 47.

Rajagopal, A., Braslavsky, D., Lu, J.T., Kleppe, S., Clément, F., Cassinelli, H., Liu, D.S., Liern, J.M., Vallejo, G., Bergadá, I., Gibbs, R.A., Campeau, P.M. and Lee, B.H. (2014) 'Exome Sequencing Identifies a Novel Homozygous Mutation in the Phosphate Transporter SLC34A1 in Hypophosphatemia and Nephrocalcinosis', *The Journal of Clinical Endocrinology & Metabolism*, 99(11), pp. E2451-E2456.

Ramezani, A. and Raj, D.S. (2014) 'The gut microbiome, kidney disease, and targeted interventions', *J Am Soc Nephrol*, 25(4), pp. 657-70.

Ran, F.A., Hsu, Patrick D., Lin, C.-Y., Gootenberg, Jonathan S., Konermann, S., Trevino, Alexandro E., Scott, David A., Inoue, A., Matoba, S., Zhang, Y. and Zhang, F. (2013a) 'Double Nicking by RNA-Guided CRISPR Cas9 for Enhanced Genome Editing Specificity', *Cell*, 155(2), pp. 479-480.

Ran, F.A., Hsu, P.D., Wright, J., Agarwala, V., Scott, D.A. and Zhang, F. (2013b) 'Genome engineering using the CRISPR-Cas9 system', *Nature Protocols*, 8, p. 2281.

Ranch, D., Zhang, M.Y., Portale, A.A. and Perwad, F. (2011) 'Fibroblast growth factor 23 regulates renal 1,25-dihydroxyvitamin D and phosphate metabolism via the MAP kinase signaling pathway in Hyp mice', *J Bone Miner Res*, 26(8), pp. 1883-90.

Ransohoff, J.D., Wei, Y. and Khavari, P.A. (2018) 'The functions and unique features of long intergenic non-coding RNA', *Nature reviews. Molecular cell biology*, 19(3), pp. 143-157.

Raubenheimer, E. and Noffke, C. (2011) 'Vitamin D and health: a historical overview', *SA Orthopaedic Journal*, 10, pp. 39-43.

Rio, D.C., Ares, M., Jr., Hannon, G.J. and Nilsen, T.W. (2010) 'Nondenaturing agarose gel electrophoresis of RNA', *Cold Spring Harb Protoc*, 2010(6), p. pdb.prot5445.

Ritz, E., Hahn, K., Ketteler, M., Kuhlmann, M.K. and Mann, J. (2012a) 'Phosphate additives in food--a health risk', *Deutsches Arzteblatt international*, 109(4), pp. 49-55.

Ritz, E., Hahn, K., Ketteler, M., Kuhlmann, M.K. and Mann, J. (2012b) 'Phosphate additives in food--a health risk', *Dtsch Arztebl Int*, 109(4), pp. 49-55.

Robertson, K.D. (2002) 'DNA methylation and chromatin - unraveling the tangled web', *Oncogene*, 21(35), pp. 5361-79.

Rodríguez, J.M., Murphy, K., Stanton, C., Ross, R.P., Kober, O.I., Juge, N., Avershina, E., Rudi, K., Narbad, A., Jenmalm, M.C., Marchesi, J.R. and Collado, M.C. (2015) 'The composition of the gut microbiota throughout life, with an emphasis on early life', *Microbial ecology in health and disease*, 26, pp. 26050-26050.

Rogers, S.A. and Hammerman, M.R. (1989) 'Growth hormone activates phospholipase C in proximal tubular basolateral membranes from canine kidney', *Proceedings of the National Academy of Sciences of the United States of America*, 86(16), pp. 6363-6366.

Romanoski, C.E., Glass, C.K., Stunnenberg, H.G., Wilson, L. and Almouzni, G. (2015) 'Epigenomics: Roadmap for regulation', *Nature*, 518(7539), pp. 314-6.

Rosenthal, G. and Rosenthal, J.A. (2011) *Statistics and Data Interpretation for Social Work*. Springer Publishing Company.

Rossignol, F., de Laplanche, E., Mounier, R., Bonnefont, J., Cayre, A., Godinot, C., Simonnet, H. and Clottes, E. (2004) 'Natural antisense transcripts of HIF-1α are conserved in rodents', *Gene*, 339, pp. 121-130.

Rouse, D. and Suki, W.N. (1985) 'Modulation of phosphate absorption by calcium in the rabbit proximal convoluted tubule', *J Clin Invest*, 76(2), pp. 630-6.

Rueden, C.T., Schindelin, J., Hiner, M.C., DeZonia, B.E., Walter, A.E., Arena, E.T. and Eliceiri, K.W. (2017) 'ImageJ2: ImageJ for the next generation of scientific image data', *BMC Bioinformatics*, 18(1), p. 529.

Ruefli, A.A., Ausserlechner, M.J., Bernhard, D., Sutton, V.R., Tainton, K.M., Kofler, R., Smyth, M.J. and Johnstone, R.W. (2001) 'The histone deacetylase inhibitor and chemotherapeutic agent suberoylanilide hydroxamic acid (SAHA) induces a cell-death pathway characterized by cleavage of Bid and production of reactive oxygen species', *Proceedings of the National Academy of Sciences of the United States of America*, 98(19), pp. 10833-10838.

Russell, W.R., Gratz, S.W., Duncan, S.H., Holtrop, G., Ince, J., Scobbie, L., Duncan, G., Johnstone, A.M., Lobley, G.E., Wallace, R.J., Duthie, G.G. and Flint, H.J. (2011) 'High-protein, reduced-carbohydrate weight-loss diets promote metabolite profiles likely to be detrimental to colonic health', *The American Journal of Clinical Nutrition*, 93(5), pp. 1062-1072.

Ruta, M., Burgess, W., Givol, D., Epstein, J., Neiger, N., Kaplow, J., Crumley, G., Dionne, C., Jaye, M. and Schlessinger, J. (1989) 'Receptor for acidic fibroblast growth factor is related to the tyrosine kinase encoded by the fms-like gene (FLG)', *Proc Natl Acad Sci U S A*, 86(22), pp. 8722-6.

Sabbagh, Y., Giral, H., Caldas, Y., Levi, M. and Schiavi, S.C. (2011) 'Intestinal phosphate transport', *Adv Chronic Kidney Dis*, 18(2), pp. 85-90.

Sahay, M. and Sahay, R. (2012) 'Rickets-vitamin D deficiency and dependency', *Indian journal of endocrinology and metabolism*, 16(2), pp. 164-176.

Sanchez, G.J., Richmond, P.A., Bunker, E.N., Karman, S.S., Azofeifa, J., Garnett, A.T., Xu, Q., Wheeler, G.E., Toomey, C.M., Zhang, Q., Dowell, R.D. and Liu, X. (2018) 'Genome-wide dose-dependent inhibition of histone deacetylases studies reveal their roles in enhancer remodeling and suppression of oncogenic super-enhancers', *Nucleic acids research*, 46(4), pp. 1756-1776.

Santiago, Y., Chan, E., Liu, P.-Q., Orlando, S., Zhang, L., Urnov, F.D., Holmes, M.C., Guschin, D., Waite, A., Miller, J.C., Rebar, E.J., Gregory, P.D., Klug, A. and Collingwood, T.N. (2008) 'Targeted gene knockout in mammalian cells by using engineered zinc-finger nucleases', *Proceedings of the National Academy of Sciences*, 105(15), pp. 5809-5814.

Santos-Reboucas, C.B. and Pimentel, M.M. (2007) 'Implication of abnormal epigenetic patterns for human diseases', *Eur J Hum Genet*, 15(1), pp. 10-7.

Sapiro, A.L., Shmueli, A., Henry, G.L., Li, Q., Shalit, T., Yaron, O., Paas, Y., Billy Li, J. and Shohat-Ophir, G. (2019) 'Illuminating spatial A-to-I RNA editing signatures within the Drosophila brain', *Proceedings of the National Academy of Sciences*, 116(6), pp. 2318-2327.

Sapranauskas, R., Gasiunas, G., Fremaux, C., Barrangou, R., Horvath, P. and Siksnys, V. (2011) 'The Streptococcus thermophilus CRISPR/Cas system provides immunity in Escherichia coli', *Nucleic Acids Res*, 39(21), pp. 9275-82.

Savić, N. and Schwank, G. (2016) 'Advances in therapeutic CRISPR/Cas9 genome editing', *Translational Research*, 168, pp. 15-21.

Schoenfelder, S. and Fraser, P. (2019) 'Long-range enhancer–promoter contacts in gene expression control', *Nature Reviews Genetics*, 20(8), pp. 437-455.

Segawa, H., Onitsuka, A., Furutani, J., Kaneko, I., Aranami, F., Matsumoto, N., Tomoe, Y., Kuwahata, M., Ito, M., Matsumoto, M., Li, M., Amizuka, N. and Miyamoto, K. (2009a) 'Npt2a and Npt2c in mice play distinct and synergistic roles in inorganic phosphate metabolism and skeletal development', *Am J Physiol Renal Physiol*, 297(3), pp. F671-8.

Segawa, H., Onitsuka, A., Kuwahata, M., Hanabusa, E., Furutani, J., Kaneko, I., Tomoe, Y., Aranami, F., Matsumoto, N., Ito, M., Matsumoto, M., Li, M., Amizuka, N. and Miyamoto, K. (2009b) 'Type IIc sodium-dependent phosphate transporter regulates calcium metabolism', *J Am Soc Nephrol*, 20(1), pp. 104-13.

Segawa, H., Shiozaki, Y., Kaneko, I. and Miyamoto, K. (2015) 'The Role of Sodium-Dependent Phosphate Transporter in Phosphate Homeostasis', *J Nutr Sci Vitaminol (Tokyo)*, 61 Suppl, pp. S119-21.

Sender, R., Fuchs, S. and Milo, R. (2016) 'Revised Estimates for the Number of Human and Bacteria Cells in the Body', *PLoS biology*, 14(8), pp. e1002533-e1002533.

Serman, A., Vlahovic, M., Serman, L. and Bulic-Jakus, F. (2006) 'DNA methylation as a regulatory mechanism for gene expression in mammals', *Coll Antropol*, 30(3), pp. 665-71.

Shanahan, F. (2002) 'The host-microbe interface within the gut', *Best Pract Res Clin Gastroenterol*, 16(6), pp. 915-31.

Shen, T., Li, H., Song, Y., Yao, J., Han, M., Yu, M., Wei, G. and Ni, T. (2018) 'Antisense transcription regulates the expression of sense gene via alternative polyadenylation', *Protein & cell*, 9(6), pp. 540-552.

Sherman, R.A. and Mehta, O. (2009) 'Phosphorus and potassium content of enhanced meat and poultry products: implications for patients who receive dialysis', *Clin J Am Soc Nephrol*, 4(8), pp. 1370-3.

Sims, J.K., Houston, S.I., Magazinnik, T. and Rice, J.C. (2006) 'A trans-tail histone code defined by monomethylated H4 Lys-20 and H3 Lys-9 demarcates distinct regions of silent chromatin', *J Biol Chem*, 281(18), pp. 12760-6.

Sinha, R., Abnet, C.C., White, O., Knight, R. and Huttenhower, C. (2015) 'The microbiome quality control project: baseline study design and future directions', *Genome biology*, 16, pp. 276-276.

Sinturel, F., Navickas, A., Wery, M., Descrimes, M., Morillon, A., Torchet, C. and Benard, L. (2015) 'Cytoplasmic Control of Sense-Antisense mRNA Pairs', *Cell Reports*, 12(11), pp. 1853-1864.

Skrypnik, K. and Suliburska, J. (2018) 'Association between the gut microbiota and mineral metabolism', *J Sci Food Agric*, 98(7), pp. 2449-2460.

Sleutels, F., Zwart, R. and Barlow, D.P. (2002) 'The non-coding Air RNA is required for silencing autosomal imprinted genes', *Nature*, 415(6873), pp. 810-3.

Smallwood, S.A. and Kelsey, G. (2012) 'De novo DNA methylation: a germ cell perspective', *Trends Genet*, 28(1), pp. 33-42.

So, A.Y., Chaivorapol, C., Bolton, E.C., Li, H. and Yamamoto, K.R. (2007) 'Determinants of cell- and gene-specific transcriptional regulation by the glucocorticoid receptor', *PLoS Genet*, 3(6), p. e94.

Strahl, B.D. and Allis, C.D. (2000) 'The language of covalent histone modifications', *Nature*, 403(6765), pp. 41-5.

Su, X.-z., Wu, Y., Sifri, C.D. and Wellems, T.E. (1996) 'Reduced Extension Temperatures Required for PCR Amplification of Extremely A+T-rich DNA', *Nucleic Acids Research*, 24(8), pp. 1574-1575.

Sullivan, C., Sayre, S.S., Leon, J.B., Machekano, R., Love, T.E., Porter, D., Marbury, M. and Sehgal, A.R. (2009) 'Effect of food additives on hyperphosphatemia among patients with end-stage renal disease: a randomized controlled trial', *Jama*, 301(6), pp. 629-35.

Sun, P.P., Perianayagam, M.C. and Jaber, B.L. (2009) 'Endotoxin-binding affinity of sevelamer: a potential novel anti-inflammatory mechanism', *Kidney Int Suppl*, (114), pp. S20-5.

Supharattanasitthi, W., Carlsson, E., Sharif, U. and Paraoan, L. (2019) 'CRISPR/Cas9-mediated one step bi-allelic change of genomic DNA in iPSCs and human RPE cells in vitro with dual antibiotic selection', *Scientific reports*, 9(1), pp. 174-174.

Tachon, S., Lee, B. and Marco, M.L. (2014) 'Diet alters probiotic Lactobacillus persistence and function in the intestine', *Environ Microbiol*, 16(9), pp. 2915-26.

Talmage, R.V. and Mobley, H.T. (2008) 'Calcium homeostasis: Reassessment of the actions of parathyroid hormone', *General and Comparative Endocrinology*, 156(1), pp. 1-8.

Tamburini, S., Shen, N., Wu, H.C. and Clemente, J.C. (2016) 'The microbiome in early life: implications for health outcomes', *Nat Med*, 22(7), pp. 713-22.

Tan, L., Yu, J.T., Hu, N. and Tan, L. (2013) 'Non-coding RNAs in Alzheimer's disease', *Mol Neurobiol*, 47(1), pp. 382-93.

Tang, W.H., Kitai, T. and Hazen, S.L. (2017) 'Gut Microbiota in Cardiovascular Health and Disease', *Circ Res*, 120(7), pp. 1183-1196.

Tessarz, P., Santos-Rosa, H., Robson, S.C., Sylvestersen, K.B., Nelson, C.J., Nielsen, M.L. and Kouzarides, T. (2014) 'Glutamine methylation in histone H2A is an RNA-polymerase-I-dedicated modification', *Nature*, 505(7484), pp. 564-8.

Thomas, S., Maynard, N.D. and Gill, J. (2015) 'DNA library construction using Gibson Assembly®', *Nature Methods*, 12, p. 1098.

Thomassin, H., Flavin, M., Espinás, M.L. and Grange, T. (2001) 'Glucocorticoid-induced DNA demethylation and gene memory during development', *The EMBO journal*, 20(8), pp. 1974-1983.

Thorenoor, N., Faltejskova-Vychytilova, P., Hombach, S., Mlcochova, J., Kretz, M., Svoboda, M. and Slaby, O. (2016) 'Long non-coding RNA ZFAS1 interacts with CDK1 and is involved in

p53-dependent cell cycle control and apoptosis in colorectal cancer', *Oncotarget*, 7(1), pp. 622-37.

Ticinesi, A., Milani, C., Guerra, A., Allegri, F., Lauretani, F., Nouvenne, A., Mancabelli, L., Lugli, G.A., Turroni, F., Duranti, S., Mangifesta, M., Viappiani, A., Ferrario, C., Dodi, R., Dall'Asta, M., Del Rio, D., Ventura, M. and Meschi, T. (2018) 'Understanding the gut–kidney axis in nephrolithiasis: an analysis of the gut microbiota composition and functionality of stone formers', *Gut*, 67(12), pp. 2097-2106.

Tomasello, S. (2008) 'Secondary Hyperparathyroidism and Chronic Kidney Disease', *Diabetes Spectrum*, 21(1), pp. 19-25.

Tomizawa, S., Kobayashi, H., Watanabe, T., Andrews, S., Hata, K., Kelsey, G. and Sasaki, H. (2011) 'Dynamic stage-specific changes in imprinted differentially methylated regions during early mammalian development and prevalence of non-CpG methylation in oocytes', *Development*, 138(5), pp. 811-20.

Tonelli, M. (2013) 'Serum phosphorus in people with chronic kidney disease: you are what you eat', *Kidney Int*, 84(5), pp. 871-3.

Tonelli, M., Curhan, G., Pfeffer, M., Sacks, F., Thadhani, R., Melamed, M.L., Wiebe, N. and Muntner, P. (2009) 'Relation between alkaline phosphatase, serum phosphate, and all-cause or cardiovascular mortality', *Circulation*, 120(18), pp. 1784-92.

Torres, A.G., Reina, O., Stephan-Otto Attolini, C. and Ribas de Pouplana, L. (2019) 'Differential expression of human tRNA genes drives the abundance of tRNA-derived fragments', *Proceedings of the National Academy of Sciences*, 116(17), pp. 8451-8456.

Tost, J. and Gut, I.G. (2007) 'DNA methylation analysis by pyrosequencing', *Nat Protoc*, 2(9), pp. 2265-75.

Trautvetter, U., Camarinha-Silva, A., Jahreis, G., Lorkowski, S. and Glei, M. (2018) 'High phosphorus intake and gut-related parameters – results of a randomized placebo-controlled human intervention study', *Nutrition Journal*, 17(1), p. 23.

Trautvetter, U., Ditscheid, B., Kiehntopf, M. and Jahreis, G. (2012) 'A combination of calcium phosphate and probiotics beneficially influences intestinal lactobacilli and cholesterol metabolism in humans', *Clin Nutr*, 31(2), pp. 230-7.

Trautvetter, U., Jahreis, G., Kiehntopf, M. and Glei, M. (2016) 'Consequences of a high phosphorus intake on mineral metabolism and bone remodeling in dependence of calcium intake in healthy subjects - a randomized placebo-controlled human intervention study', *Nutr J*, 15, p. 7.

Tufarelli, C., Stanley, J.A.S., Garrick, D., Sharpe, J.A., Ayyub, H., Wood, W.G. and Higgs, D.R. (2003) 'Transcription of antisense RNA leading to gene silencing and methylation as a novel cause of human genetic disease', *Nature Genetics*, 34(2), pp. 157-165.

Turnbaugh, P.J. and Gordon, J.I. (2009) 'The core gut microbiome, energy balance and obesity', *The Journal of Physiology*, 587(17), pp. 4153-4158.

Turnbaugh, P.J., Ridaura, V.K., Faith, J.J., Rey, F.E., Knight, R. and Gordon, J.I. (2009) 'The effect of diet on the human gut microbiome: a metagenomic analysis in humanized gnotobiotic mice', *Sci Transl Med*, 1(6), p. 6ra14.

Ubeda, C., Djukovic, A. and Isaac, S. (2017) 'Roles of the intestinal microbiota in pathogen protection', *Clinical & translational immunology*, 6(2), pp. e128-e128.

Ungerstedt, J.S., Sowa, Y., Xu, W.-S., Shao, Y., Dokmanovic, M., Perez, G., Ngo, L., Holmgren, A., Jiang, X. and Marks, P.A. (2005a) 'Role of thioredoxin in the response of normal and transformed cells to histone deacetylase inhibitors', *Proceedings of the National Academy of Sciences of the United States of America*, 102(3), pp. 673-678.

Ungerstedt, J.S., Sowa, Y., Xu, W.S., Shao, Y., Dokmanovic, M., Perez, G., Ngo, L., Holmgren, A., Jiang, X. and Marks, P.A. (2005b) 'Role of thioredoxin in the response of normal and transformed cells to histone deacetylase inhibitors', *Proc Natl Acad Sci U S A*, 102(3), pp. 673-8.

Uribarri, J. (2007) 'Phosphorus homeostasis in normal health and in chronic kidney disease patients with special emphasis on dietary phosphorus intake', *Semin Dial*, 20(4), pp. 295-301.

Vandeputte, D., Kathagen, G., D'hoe, K., Vieira-Silva, S., Valles-Colomer, M., Sabino, J., Wang, J., Tito, R.Y., De Commer, L., Darzi, Y., Vermeire, S., Falony, G. and Raes, J. (2017) 'Quantitative microbiome profiling links gut community variation to microbial load', *Nature*, 551, p. 507.

Vaziri, N.D., Wong, J., Pahl, M., Piceno, Y.M., Yuan, J., DeSantis, T.Z., Ni, Z., Nguyen, T.H. and Andersen, G.L. (2013) 'Chronic kidney disease alters intestinal microbial flora', *Kidney Int*, 83(2), pp. 308-15.

Velmeshev, D., Magistri, M. and Faghihi, M.A. (2013) 'Expression of non-protein-coding antisense RNAs in genomic regions related to autism spectrum disorders', *Mol Autism*, 4(1), p. 32.

Vrieze, A., Van Nood, E., Holleman, F., Salojärvi, J., Kootte, R.S., Bartelsman, J.F.W.M., Dallinga–Thie, G.M., Ackermans, M.T., Serlie, M.J., Oozeer, R., Derrien, M., Druesne, A., Van Hylckama Vlieg, J.E.T., Bloks, V.W., Groen, A.K., Heilig, H.G.H.J., Zoetendal, E.G., Stroes, E.S., de Vos, W.M., Hoekstra, J.B.L. and Nieuwdorp, M. (2012) 'Transfer of Intestinal Microbiota

From Lean Donors Increases Insulin Sensitivity in Individuals With Metabolic Syndrome', *Gastroenterology*, 143(4), pp. 913-916.e7.

Wagner, C.A., Hernando, N., Forster, I.C. and Biber, J. (2014) 'The SLC34 family of sodium-dependent phosphate transporters', *Pflugers Arch*, 466(1), pp. 139-53.

Walker, A.W., Ince, J., Duncan, S.H., Webster, L.M., Holtrop, G., Ze, X., Brown, D., Stares, M.D., Scott, P., Bergerat, A., Louis, P., McIntosh, F., Johnstone, A.M., Lobley, G.E., Parkhill, J. and Flint, H.J. (2011) 'Dominant and diet-responsive groups of bacteria within the human colonic microbiota', *Isme j*, 5(2), pp. 220-30.

Walsh, C.J., Guinane, C.M., O'Toole, P.W. and Cotter, P.D. (2014) 'Beneficial modulation of the gut microbiota', *FEBS Letters*, 588(22), pp. 4120-4130.

Wang, H., Chung, P.J., Liu, J., Jang, I.-C., Kean, M.J., Xu, J. and Chua, N.-H. (2014) 'Genome-wide identification of long noncoding natural antisense transcripts and their responses to light in Arabidopsis', *Genome research*, 24(3), pp. 444-453.

Wang, X.J., Gaasterland, T. and Chua, N.H. (2005) 'Genome-wide prediction and identification of cis-natural antisense transcripts in Arabidopsis thaliana', *Genome Biol*, 6(4), p. R30.

Wang, Y., Hao, L., Wang, H., Santostefano, K., Thapa, A., Cleary, J., Li, H., Guo, X., Terada, N., Ashizawa, T. and Xia, G. (2018) 'Therapeutic Genome Editing for Myotonic Dystrophy Type 1 Using CRISPR/Cas9', *Molecular Therapy*, 26(11), pp. 2617-2630.

Washietl, S., Kellis, M. and Garber, M. (2014) 'Evolutionary dynamics and tissue specificity of human long noncoding RNAs in six mammals', *Genome Res*, 24(4), pp. 616-28.

Weaver, C.M. and Miller, J.W. (2017) 'Challenges in conducting clinical nutrition research', *Nutrition reviews*, 75(7), pp. 491-499.

Webster, S.K., Haramati, A. and Knox, F.G. (1986) 'Effect of dexamethasone on segmental phosphate reabsorption in phosphate-deprived rats', *Am J Physiol*, 251(4 Pt 2), pp. F576-80.

Wegmann, U., Louis, P., Goesmann, A., Henrissat, B., Duncan, S.H. and Flint, H.J. (2014) 'Complete genome of a new Firmicutes species belonging to the dominant human colonic microbiota ('Ruminococcus bicirculans') reveals two chromosomes and a selective capacity to utilize plant glucans', *Environmental Microbiology*, 16(9), pp. 2879-2890.

Weinstock, G.M. (2012) 'Genomic approaches to studying the human microbiota', *Nature*, 489(7415), pp. 250-6.

Wen, S.F., Boynar, J.W., Jr. and Stoll, R.W. (1978) 'Effect of phosphate deprivation on renal phosphate transport in the dog', *Am J Physiol*, 234(3), pp. F199-206.

Werner, A. (2013) 'Biological functions of natural antisense transcripts', *BMC Biology*, 11(1), p. 31.

Whisner, C.M., Martin, B.R., Nakatsu, C.H., Story, J.A., MacDonald-Clarke, C.J., McCabe, L.D., McCabe, G.P. and Weaver, C.M. (2016) 'Soluble Corn Fiber Increases Calcium Absorption Associated with Shifts in the Gut Microbiome: A Randomized Dose-Response Trial in Free-Living Pubertal Females', *J Nutr*, 146(7), pp. 1298-306.

Wight, M. and Werner, A. (2013) 'The functions of natural antisense transcripts', *Essays in biochemistry*, 54, pp. 91-101.

Wood, E., Chin-Inmanu, K., Jia, H. and Lipovich, L. (2013) 'Sense-antisense gene pairs: sequence, transcription, and structure are not conserved between human and mouse', *Frontiers in Genetics*, 4(183).

Woodmansey, E.J. (2007) 'Intestinal bacteria and ageing', *J Appl Microbiol*, 102(5), pp. 1178-86.

Wu, G.D., Chen, J., Hoffmann, C., Bittinger, K., Chen, Y.Y., Keilbaugh, S.A., Bewtra, M., Knights, D., Walters, W.A., Knight, R., Sinha, R., Gilroy, E., Gupta, K., Baldassano, R., Nessel, L., Li, H., Bushman, F.D. and Lewis, J.D. (2011) 'Linking long-term dietary patterns with gut microbial enterotypes', *Science*, 334(6052), pp. 105-8.

Wu, H., Mao, C., Duenstl, G., Su, W. and Qian, S. (2013) 'Assay development of inducible human renal phosphate transporter Npt2A (SLC34A1) in Flp-In-Trex-HEK293 cells', *Eur J Pharmacol*, 721(1-3), pp. 332-40.

Wu, S.C. and Zhang, Y. (2010) 'Active DNA demethylation: many roads lead to Rome', *Nat Rev Mol Cell Biol*, 11(9), pp. 607-20.

Xiao, H., Wen, Y., Pan, Z., Shangguan, Y., Qin, J., Tan, Y., Jiang, H., Li, B., Zhang, Q., Chen, L. and Wang, H. (2018) 'Increased H3K27ac level of ACE mediates the intergenerational effect of low peak bone mass induced by prenatal dexamethasone exposure in male offspring rats', *Cell Death & Disease*, 9(6), p. 638.

Xiao, Q., Guo, D. and Chen, S. (2019) 'Application of CRISPR/Cas9-Based Gene Editing in HIV-1/AIDS Therapy', *Frontiers in Cellular and Infection Microbiology*, 9(69).

Xie, Y.B., Li, J.P., Shen, K., Meng, F., Wang, L., Han, G.X., Ai, G., Jiang, B.L., Zhao, Q.Q., Hou, Y., Yang, H.Y. and Li, W.Q. (2019) '[Effect of HIF-1alpha on Angiogenesis-Related Factors in K562 Cells]', *Zhongguo Shi Yan Xue Ye Xue Za Zhi*, 27(5), pp. 1476-1481.

Xu, Z., Wei, W., Gagneur, J., Clauder-Munster, S., Smolik, M., Huber, W. and Steinmetz, L.M. (2011) 'Antisense expression increases gene expression variability and locus interdependency', *Mol Syst Biol*, 7, p. 468.

Yamamoto, T., Michigami, T., Aranami, F., Segawa, H., Yoh, K., Nakajima, S., Miyamoto, K. and Ozono, K. (2007) 'Hereditary hypophosphatemic rickets with hypercalciuria: a study for the phosphate transporter gene type IIc and osteoblastic function', *J Bone Miner Metab*, 25(6), pp. 407-13.

Yamashita, T., Yoshioka, M. and Itoh, N. (2000) 'Identification of a Novel Fibroblast Growth Factor, FGF-23, Preferentially Expressed in the Ventrolateral Thalamic Nucleus of the Brain', *Biochemical and Biophysical Research Communications*, 277(2), pp. 494-498.

Yang, H., Wei, W., Menconi, M. and Hasselgren, P.O. (2007) 'Dexamethasone-induced protein degradation in cultured myotubes is p300/HAT dependent', *Am J Physiol Regul Integr Comp Physiol*, 292(1), pp. R337-4.

Yang, H., Zhong, Y., Xie, H., Lai, X., Xu, M., Nie, Y., Liu, S. and Wan, Y.-J.Y. (2013) 'Induction of the liver cancer-down-regulated long noncoding RNA uc002mbe.2 mediates trichostatin-induced apoptosis of liver cancer cells', *Biochemical pharmacology*, 85(12), pp. 1761-1769.

Yelin, R., Dahary, D., Sorek, R., Levanon, E.Y., Goldstein, O., Shoshan, A., Diber, A., Biton, S., Tamir, Y., Khosravi, R., Nemzer, S., Pinner, E., Walach, S., Bernstein, J., Savitsky, K. and Rotman, G. (2003) 'Widespread occurrence of antisense transcription in the human genome', *Nature Biotechnology*, 21(4), pp. 379-386.

Yin, J., Luo, W., Zeng, X., Zeng, L., Li, Z., Deng, X., Tan, X. and Hu, W. (2017) 'UXT-AS1-induced alternative splicing of UXT is associated with tumor progression in colorectal cancer', *Am J Cancer Res*, 7(3), pp. 462-472.

Yoder, J.A., Walsh, C.P. and Bestor, T.H. (1997) 'Cytosine methylation and the ecology of intragenomic parasites', *Trends Genet*, 13(8), pp. 335-40.

Yoo, C.B., Cheng, J.C. and Jones, P.A. (2004) 'Zebularine: a new drug for epigenetic therapy', *Biochem Soc Trans*, 32(Pt 6), pp. 910-2.

Yoo, C.B., Valente, R., Congiatu, C., Gavazza, F., Angel, A., Siddiqui, M.A., Jones, P.A., McGuigan, C. and Marquez, V.E. (2008) 'Activation of p16 gene silenced by DNA methylation in cancer cells by phosphoramidate derivatives of 2'-deoxyzebularine', *J Med Chem*, 51(23), pp. 7593-601.

Yoshiko, Y., Wang, H., Minamizaki, T., Ijuin, C., Yamamoto, R., Suemune, S., Kozai, K., Tanne, K., Aubin, J.E. and Maeda, N. (2007) 'Mineralized tissue cells are a principal source of FGF23', *Bone*, 40(6), pp. 1565-73.

Yu, W., Gius, D., Onyango, P., Muldoon-Jacobs, K., Karp, J., Feinberg, A.P. and Cui, H. (2008) 'Epigenetic silencing of tumour suppressor gene p15 by its antisense RNA', *Nature*, 451(7175), pp. 202-6.

Zannas, A.S., Arloth, J., Carrillo-Roa, T., Iurato, S., Röh, S., Ressler, K.J., Nemeroff, C.B., Smith, A.K., Bradley, B., Heim, C., Menke, A., Lange, J.F., Brückl, T., Ising, M., Wray, N.R., Erhardt, A., Binder, E.B. and Mehta, D. (2015) 'Lifetime stress accelerates epigenetic aging in an urban, African American cohort: relevance of glucocorticoid signaling', *Genome biology*, 16, pp. 266-266.

Zhang, K. and Tang, H. (2003) 'Analysis of core histones by liquid chromatography-mass spectrometry and peptide mapping', *J Chromatogr B Analyt Technol Biomed Life Sci*, 783(1), pp. 173-9.

Zhang, X., Zhang, D., Jia, H., Feng, Q., Wang, D., Liang, D., Wu, X., Li, J., Tang, L., Li, Y., Lan, Z., Chen, B., Li, Y., Zhong, H., Xie, H., Jie, Z., Chen, W., Tang, S., Xu, X., Wang, X., Cai, X., Liu, S., Xia, Y., Li, J., Qiao, X., Al-Aama, J.Y., Chen, H., Wang, L., Wu, Q.J., Zhang, F., Zheng, W., Li, Y., Zhang, M., Luo, G., Xue, W., Xiao, L., Li, J., Chen, W., Xu, X., Yin, Y., Yang, H., Wang, J., Kristiansen, K., Liu, L., Li, T., Huang, Q., Li, Y. and Wang, J. (2015a) 'The oral and gut microbiomes are perturbed in rheumatoid arthritis and partly normalized after treatment', *Nat Med*, 21(8), pp. 895-905.

Zhang, Y. and Reinberg, D. (2001) 'Transcription regulation by histone methylation: interplay between different covalent modifications of the core histone tails', *Genes Dev*, 15(18), pp. 2343-60.

Zhang, Y.J., Li, S., Gan, R.Y., Zhou, T., Xu, D.P. and Li, H.B. (2015b) 'Impacts of gut bacteria on human health and diseases', *Int J Mol Sci*, 16(4), pp. 7493-519.

Zhao, Y., Hou, Y., Zhao, C., Liu, F., Luan, Y., Jing, L., Li, X., Zhu, M. and Zhao, S. (2016) 'Cis-Natural Antisense Transcripts Are Mainly Co-expressed with Their Sense Transcripts and Primarily Related to Energy Metabolic Pathways during Muscle Development', *International journal of biological sciences*, 12(8), pp. 1010-1021.

Zhao, Y., Zuo, Y., Huo, H., Xiao, Y., Yang, X. and Xin, D. (2014) 'Dexamethasone reduces ATDC5 chondrocyte cell viability by inducing autophagy', *Mol Med Rep*, 9(3), pp. 923-7.

Zheng, Q., Cai, X., Tan, M.H., Schaffert, S., Arnold, C.P., Gong, X., Chen, C.-Z. and Huang, S. (2014) 'Precise gene deletion and replacement using the CRISPR/Cas9 system in human cells', *BioTechniques*, 57(3), pp. 115-124.

Zhou, L., Cheng, X., Connolly, B.A., Dickman, M.J., Hurd, P.J. and Hornby, D.P. (2002) 'Zebularine: a novel DNA methylation inhibitor that forms a covalent complex with DNA methyltransferases', *J Mol Biol*, 321(4), pp. 591-9.

Zinad, H.S., Natasya, I. and Werner, A. (2017) 'Natural Antisense Transcripts at the Interface between Host Genome and Mobile Genetic Elements', *Frontiers in microbiology*, 8, p. 2292 [Online]. Available at: http://europepmc.org/abstract/MED/29209299

http://europepmc.org/articles/PMC5701935?pdf=render

http://europepmc.org/articles/PMC5701935

https://doi.org/10.3389/fmicb.2017.02292 DOI: 10.3389/fmicb.2017.02292 (Accessed: 2017).

Appendix A

Real time qPCR primer pairs sequences for *SLC34A1-sense* transcripts.

Primer ID	*SLC34A1-sense* sequence (5'-3')	Melting Temp (°C)	Product length
S1F	ATGTTGTCCTACGGAGAGAGGCTGG	71.1	170
S1R	GCCCAGGCTGGGGAAGGCATAG	75.1	
S2F	TGTGGCCCTTGCTGAGCA	69.6	209
S2R	CGAGGTAGAGGAAGGTGAGCATCA	69.5	
S3F	TGCTGGAGGTGAGCTCTGCCAT	72.6	186
S3R	GTGCAGGTAGCCAGTGGCA	67.6	
S4F	AAGGGCCAAGTGGCCAAGGTCAT	74	198
S4R	GATGTTGGAACCCAGTGTGAGCGG	74.4	
S5F	CAGCCCTCAGGTCCTACACA	65.3	163
S5R	CTCTGGCTTCTGCTCCTCCT	65.1	
S6F	CGTTGCTGAGACCCACTGAC	66.1	165
S6R	TGTGTAGGACCTGAGGGCTG	65.3	
S7F	ACCTCTTCGTCTGCTCCCTG	65.9	171
S7R	TGGATGTGGAGGTGCTGGAG	68.8	
S8F	GATAACGCCATCCTGTCCA	63.6	179
S8R	GACAGAGGTGCCGATGTTG	64.5	
S9F	CCAAGTGGCCAAGGTCAT	63.7	200
S9R	GATGTTGGAACCCAGTGTGA	63.6	
S10F	CATGACTAGGATAGGCAGGAGTAAGG	65.7	85
S10R	GTAACGCAGGCACCAACATCT	66.1	
S11F	AGGATATCTGGGTATGATTTCAGGT	63.5	102
S11R	CACAAACAGCTGCACAGTCATATAC	64.4	

Appendix B

Real time qPCR primer pairs sequences for *SLC34A1-antisense* transcripts.

Primer Name	SLC34A1-antisense sequence (5'-3')	*Melting Temp (°C)*	*Product length*
AS1F	GCGTGGCGCCTCTATATTTCCC	71.1	178
AS1R	CTCCTGCGGCGAGATGGC	71.9	
AS2F	ATGAGCACCACGAAGGCCAG	69.8	150
AS2R	CAAGGCGCTGGGGAAACGCA	76.4	
AS3F	ATGGGCAGGCGTGTGCAG	71.2	170
AS3R	GGAAACTTTCCTGCTGCCCAGA	70.5	
AS4F	GTTGGGAAGGGAATTAATTGTGG	66	150
AS4R	CATGGTAGGTGTGGGCACG	67.6	
AS5F	GTTGGGAAGGGAATTAATTGTGG	66	172
AS5R	CAAGGCGCTGGGGAAACGCA	76.4	
AS6F	TGGAAGGTCTACATCAGTGCAG	64.2	187
AS6R	CATCCTAACCCAGGTCTTCGG	66.6	
AS7F	GATGGGCGACTGGAAGGTCTA	67.4	182
AS7R	CTTCGGCACCACCACAATTA	65.7	
AS8F	GACTGGAAGGTCTACATCAGTGC	63.9	170
AS8R	GCACCACCACAATTAATTCCCT	65.7	
AS9F	TGGGCGACTGGAAGGTCTACA	69	182
AS9R	GTCTTCGGCACCACCACAATTA	67.9	
AS10F	CTGCGTGTGGGCTTCGC	69.7	79
AS10R	ATTAATTCCCTTCCCAACACTTGC	66.7	
AS11F	GGCCATGCGGACAACAG	66.8	112
AS11R	TAATTGTGGTGGTGCCGAAG	65.7	

Publications and abstracts

1- Publications

Zinad, H.S., Natasya, I. and Werner, A. (2017) 'Natural Antisense Transcripts at the Interface between Host Genome and Mobile Genetic Elements', *Front Microbiol*, 8, p. 2292.

Piatek, M.J., Henderson, V., Zinad, H.S. and Werner, A. (2016) 'Natural antisense transcription from a comparative perspective', Genomics, 108(2), pp. 56-63.

Werner, A., Patti, M., Zinad, H.S., Fearn, A., Laude, A. and Forster, I. (2016) 'Molecular determinants of transport function in zebrafish Slc34a Na-phosphate transporters', Am J Physiol Regul Integr Comp Physiol, 311(6), pp. R1213-r1222.

2- Confrences attended

June 2019	84th Symposium: RNA Control and Regulation	New York, USA
Feb 2019	Long Noncoding RNA: From Molecular Mechanism to Functional Genetics- published abstract	British Columbia, Canada
Oct 2018	Genomic Parasites and noncoding RNA in Evolution and Disease	Baeza, Spain
Jan 2018	RNA UK meeting	Lake District, UK
June 2017	Non-Coding RNA: Recent Insights into the Mechanisms of Action	Edinburgh, UK